University of Calgary

PRISM Repository **https://prism.ucalgary.ca**

The Vault Open Theses and Dissertations

2016

A Detailed Chemical Kinetics Mechanism for Biogas and Syngas Combustion

Lee, Hsu Chew

Lee, H. C. (2016). A Detailed Chemical Kinetics Mechanism for Biogas and Syngas Combustion (Doctoral thesis, University of Calgary, Calgary, Canada). Retrieved from https://prism.ucalgary.ca. doi:10.11575/PRISM/24711

http://hdl.handle.net/11023/3381

Downloaded from PRISM Repository, University of Calgary

UNIVERSITY OF CALGARY

A Detailed Chemical Kinetics Mechanism for Biogas and Syngas Combustion

by

Hsu Chew Lee

A THESIS

SUBMITTED TO THE FACULTY OF GRADUATE STUDIES

IN PARTIAL FULFILLMENT OF THE REQUIREMENTS FOR THE

DEGREE OF DOCTOR OF PHILOSOPHY

GRADUATE PROGRAM IN MECHANICAL AND MANUFACTURING ENGINEERING

CALGARY, ALBERTA

SEPTEMBER, 2016

© Hsu Chew Lee 2016

Abstract

The interests in alternative renewable fuels such as syngas and biogas have intensified the search for an accurate chemical kinetics model to describe the combustion of syngas and biogas fuels. Unfortunately, a generally accepted mechanism for the fuels of interest remains elusive. Therefore, this thesis is aimed at developing the most up-to-date chemistry model for syngas and biogas combustion. Based on comprehensive comparison between several notable mechanisms available in the literature, the NUIG2013 mechanism [1] was found to have the closest agreement with the experimental data for $H_2 - CO - CH_4 - CO_2$ fuel mixtures diluted with N_2 and H_2O. However, the NUIG2013 mechanism failed to predict accurately the ignition delay time at several experimental conditions and the NUIG2013 consists of too many irrelevant species and reactions for syngas and biogas combustion purpose. Therefore, sensitivity analysis were conducted to identify the cause of discrepancies observed between the predicted results and experimental data, and Genetic Algorithm (GA) approach was proposed and validated to optimally extract relevant reactions for $H_2/CO/CH_4/CO_2$ mixtures from the detailed NUIG2013 chemical kinetics mechanism. Two new rate constants for $H + O_2(+CO_2) = HO_2(+CO_2)$ and $CH_4 + OH = CH_3 + H_2O$ reactions were proposed based on the sensitivity analysis, and it was found that the modified rate constants reconciled the observed discrepancies between the predicted and the measured results. The GA eliminated 1777 insensitive reactions in the NUIG2013 mechanism [1], where the final detailed chemical kinetics model presented in this thesis for biogas/syngas fuel mixtures comprised of 290 reactions and 72 species. The final detailed chemical kinetics model with the incorpo-

ration of the two modified rate constants was validated against a large set of experimental data, and excellent agreements were found between the predicted and experimental data. Consequently, the final mechanism presented in this thesis is currently the most up-to-date detailed chemical kinetics mechanism that is suitable for predicting the combustion properties of biogas/syngas accurately.

Preface

This thesis provides an updated detailed chemical kinetics mechanism for the purpose of biogas and syngas combustion. The introductory part (Chapter 1) is not a general review of the subject but rather a summary of the works contained in the three papers. The thesis is based on and contains the following papers.

Paper 1. H.C. Lee, A.A. Mohamad, L.Y. Jiang. 2014. A review on the laminar flame speed and ignition delay time of syngas mixtures. *International Journal of Hydrogen Energy*, **39(2)**, 1105–1121.

Paper 2. H.C. Lee, A.A. Mohamad, L.Y. Jiang. 2015. Comprehensive comparison of chemical kinetics mechanisms for syngas/biogas mixtures. *Energy & Fuel*, **29(9)**, 6126–6145.

Paper 3. H.C. Lee, L.Y. Jiang, A.A. Mohamad. 2016. An updated chemical kinetics mechanism for biogas and syngas combustion. Submitted to *Fuel*

Acknowledgements

I am extremely grateful and indebted to my graduate advisors, Professor A.A. Mohamad and Dr. L.Y. Jiang, who were abundantly helpful and offered invaluable assistance, support and guidance. They are always there to encourage me and have been patience with me over the last three and a half years. My dissertation would not have been possible and complete without the supports of Prof. Mohamad and Dr. Jiang.

I would also like to thank my family for their unconditional support and love, especially my father and my mother for their understanding throughout the duration of my studies at the University of Calgary. They have kept me going against all odds.

Last but not least, I would like to dedicate this dissertation to ShihJye, for her continuous support and encouragement. In addition, she endured countless nights of burning the midnight oil reading most of my works to give me valuable feedback. Most importantly, she has always believed in me, even when I didn't believe in myself.

Table of Contents

Abstract ii

Preface iv

Acknowledgements v

Table of Contents vi

List of Tables ix

List of Figures xi

1 Introduction 1

2 Combustion Characteristics of Syngas 4

2.1 Background 5

2.2 Laminar Flame Speed 11

2.2.1 Dilute effects on flame speeds 19

2.3 Ignition Delay Time 23

2.4 Concluding Remarks 36

3 Comprehensive Comparison of Chemical Kinetics Mechanisms 38

3.1 Background 39

3.2 Modeling Approach 41

3.3 Results and discussion 46

3.3.1 Laminar flame speed 46

3.3.2 Ignition delay time 62

3.4 Sensitivity Analysis 77

3.4.1 $H_2/CO/CO_2$ 78

3.4.2 $H_2/CO/CH_4$ 83

3.5 Concluding remarks 90

4 Reduced mechanism for biogas and syngas combustion . . . 94
4.1 Background . . . 95
4.2 Methodology . . . 97
4.2.1 Modeling approach . . . 97
4.2.2 Genetic algorithm . . . 98
4.3 Results and discussion . . . 103
4.3.1 Reduced mechanism . . . 103
4.3.2 Validations . . . 112
4.4 Concluding remarks . . . 124
5 Conclusions . . . 127
Bibliography . . . 130
A Supporting Materials for Chapter 3 . . . 149
A.1 Relative error values - Laminar flame speed . . . 159
A.1.1 Mixture Combination: H_2/CO . . . 159
A.1.2 Mixture Combination: $H_2/CO/CO_2$ . . . 162
A.1.3 Mixture Combination: $H_2/CO/H_2O$ . . . 166
A.1.4 Mixture Combination: $H_2/CO/N_2$ . . . 168
A.1.5 Mixture Combination: $H_2/CO/CH_4$ . . . 169
A.2 Relative error values – Ignition delay time . . . 172
A.2.1 Mixture Combination: H_2/CO . . . 172
A.2.2 Mixture Combination: $H_2/CO/H_2O$ . . . 173
A.2.3 Mixture Combination: $H_2/CO/CO_2$ . . . 175
A.2.4 Mixture Combination: $H_2/CO/CH_4$ . . . 177
A.3 Sensitivity Analysis . . . 184
A.4 Rate constant expressions and sensitivity analysis . . . 184
B Supporting Materials for Chapter 4 . . . 193
B.1 Comparison with experimental data - Ignition delay time . . . 202
B.1.1 Mixture combination: H_2/CO . . . 202
B.1.2 Mixture combination: $H_2/CO/H_2O$ . . . 203
B.1.3 Mixture combination: $H_2/CO/CO_2$ . . . 204

B.1.4 Mixture combination: $H_2/CO/CH_4$ . . . 205
B.1.5 Mixture combination: $H_2/CO/CO_2/H_2O/CH_4$ . . . 206
B.1.6 Mixture combination: H_2/CH_4 . . . 207
B.1.7 Mixture combination: CH_4 . . . 208
B.1.8 Mixture combination: CH_4/H_2O . . . 209
B.1.9 Mixture combination: $CH_4/C_2H_6/H_2$ . . . 210
B.1.10 Mixture combination: CH_4/C_3H_8 . . . 211
B.1.11 Mixture combination: $CH_4/C_2H_6/C_3H_8$ . . . 213
B.2 Comparison with experimental data - Flame speed . . . 216
B.2.1 Mixture combination: H_2/CO . . . 216
B.2.2 Mixture combination: $H_2/CO/CO_2$ . . . 218
B.2.3 Mixture combination: $H_2/CO/H_2O$ . . . 220
B.2.4 Mixture combination: $H_2/CO/N_2$ . . . 221
B.2.5 Mixture combination: H_2/CH_4 . . . 222
B.2.6 Mixture combination: $H_2/CO/CH_4/CO_2$ . . . 223
B.2.7 Mixture combination: CH_4 . . . 226
C Code Snippets . . . 227
C.1 Sensitivity Analysis for Ignition Delay Time - Parallelized Version . . . 227
C.2 Genetic Algorithm - Parallelized Version . . . 230
D 290Rxn Mechanism . . . 241
Bibliography . . . 262

List of Tables

2.1 Available experimental kinetic data for the combustion of syngas fuel(Ignition delay time) 6

3.1 Summary of the mixture combinations and the experimental conditions considered. 42

3.2 Chemical kinetics mechanisms considered. All mechanisms can handle N_2 bath gas and the table indicates the capability of the mechanism to handle Ar and He bath gases. The grand mean for all mechanisms are provided for the flame speed and the ignition delay time cases: [A] - Laminar flame speed of syngas, all diluents except He and CH_4; [B] - Laminar flame speed of syngas, all diluents except CH_4; [C] - Laminar flame speed of syngas, all diluents except He; [D] - Laminar flame speed of syngas, all diluents; [E] - Ignition delay time of syngas, all diluents except CH_4; [F] - Ignition delay time of syngas, all diluents. The minimum value in each column is indicated in bold. 44

4.1 Overview of the fuel mixtures and experimental conditions included as optimization targets to guide the genetic algorithm in finding an optimized sub-mechanism for biogas/syngas fuel mixtures. 101

4.2 Genetic algorithm parameters and genetic operators used in this study. 103

4.3 Summary of the mixture combinations and the experimental conditions used for mechanism validation. Refer to Supplementary Table B.1 for more detailed information on the fuel compositions and experimental conditions used in each case. . . 112

A.1 The average absolute relative error values between the measured and simulated flame speed for all the mechanisms investigated in this study. The grand mean for all the mechanisms sare given for four cases: [A] Flame speed of syngas with all diluents, except He and CH_4; [B] - Flame speed of syngas with all diluents, except CH_4; [C] - Flame speed of syngas with all diluents, except He; [D] - Flame speed of syngas with all diluents. Min value in each category is colored red (modified NUIG mechanisms are not included). Blue colored values indicate the variants of NUIG2013 mechanism; please see Chapter 3 for more information.) 152

A.2 The average relative error values between the measured and simulated ignition delay time for all the mechanisms investigated in this study. The grand mean for all the mechanisms are given for two cases: [E] Ignition delay time of syngas with all diluents, except CH_4; [F] - Ignition delay time of syngas with all diluents. NUIG_V1, NUIG_V2, and NUIG_V3 are the variants of NUIG2013 mechanism with one or more rate constants being replaced; see manuscript for more information. Min value in each category is colored red (modified NUIG mechanisms are not included). 156

B.1 Fuel matrix and experimental conditions used in this study for the validation of the reduced mechanism. The highest relative error (E_{max}) in each case is computed and tabulated. 195

List of Figures and Illustrations

2.1 Laminar flame speed of H_2:CO-50:50 at atmospheric pressure and 298K. 12

2.2 Laminar flame speed of various H_2:CO mixture at atmospheric pressure and 298K. 12

2.3 Laminar flame speed of H_2:CO with O_2 as the oxidizer diluted in He with a ratio of He:O_2-7:1 at T=298 K. (a) P=5 atm, (b) P=10 atm and T=298 K; Filled Symbol: H_2:CO-5:95; Open Symbol: H_2:CO-50:50. 16

2.4 Laminar flame speed of H_2:CO-5:95 with O_2 as the oxidizer diluted in He with a ratio of He:O_2-7:1 at P=20-40 atm and T=298 K. 16

2.5 Laminar flame speed of H_2/CO-air mixture at P=1 atm and T=300,400,500,600,700 K. (a) H_2:CO-50:50, (b) H_2:CO-5:95. Filled symbol: measured by [42], open symbol: measured by [35]. 17

2.6 Variation of temperature exponent (α) for H_2:CO-5:95 and H_2:CO-50:50 at P=1 atm. The lines show the second degree polynomial fitted to both experimental data. 18

2.7 Laminar flame speed of $H_2/CO/H_2O$/air mixture at P=1 atm and T=323 and 400 K. Filled symbol: measured by [42], open symbol: measured by [45]. 20

2.8 Laminar flame speed of H_2/CO-50:50 air mixture diluted with N_2 T=298 K at P= 1 atm. Filled symbol: measured by [37], open symbol: measured by [40]. 21

2.9 Laminar flame speed of H_2/CO-50:50 air mixture diluted with CO_2 at P=1 atm and T=298 K. Filled symbol: measured by [35], open symbol: measured by [40]. . 21

2.10 Laminar flame speed of $H_2/CO/CO_2/O_2$ mixture (T=300 K, ϕ=0.4) at P=1 and 2 atm. $Z = XCO_2/(XCO_2 + XO_2)$ and $ZH_2 = XH_2/(XCO + XH_2)$. X refers to the mole fraction of the specific species in the mixtures. Measured by [34]. 22

2.11 Measured ignition delay time of various H_2/CO mixture as a function of temperature at around P=1.6, 7.9, 12, 15, 15.8, 30, 32, and 50 atm. (a) Mixture: $1.00\%(\alpha H_2 + (1-\alpha)CO) + 1.00\%O_2 + 98.00\%Ar$, measured in a shock tube facility by [43], (b) Mixture: $17.36\%(\alpha H_2 + (1-\alpha)CO) + 17.36\%O_2 + 32.64\%N_2 + 32.64\%Ar$, measured in a RCM facility by [44], (c) Mixture: $1.00\%(\alpha H_2 + (1-\alpha)CO) + 1.00\%O_2 + 98.00\%Ar$, measured in a shock tube facility by [43], (d) Black symbol: Mixture: $12.5\%(\alpha H_2 + (1-\alpha)CO) + 6.25\%O_2 + 18.25\%N_2 + 63.125\%Ar$, measured in a RCM facility by [47]; Grey symbol: Mixture: $17.5\%(\alpha H_2 + (1-\alpha)CO) + 17.5\%O_2 + 65.2\%N_2$, measured in a shock tube facility [48]. α refers to the mole fraction of H_2. 26

2.12 Effect of pressure on the ignition delay time for H_2:CO-50:50 at ϕ=0.5. Measured in shock tube [43] and RCM facility [44]. 28

2.13 Measured ignition delay time of H_2/CO mixture diluted with methane at ϕ=0.5. Filled symbol: Grey-experiments conducted by [50]; Black-experiments conducted by [49]. Open symbol: experiments conducted by [49]. 29

2.14 Measured ignition delay time of H_2/CO mixture diluted with H_2O at ϕ=0.5. Filled symbol: Grey-experiments conducted by [50]; Black-experiments conducted by [49]. Blue symbol: experiments conducted by [55]. 32

2.15 Measured ignition delay time of H_2/CO mixture diluted with CO_2 at ϕ=0.5. Filled symbol: Grey-experiments conducted by [50]; Black-experiments conducted by [49]. Blue symbol: experiments conducted by [51]. 34

2.16 Measured ignition delay time of H_2/CO mixture diluted with NH_3 at ϕ=0.5. Filled symbol: Grey-experiments conducted by [50]; Black-experiments conducted by [49]. 35

2.17 Measured ignition delay time of practical Syngas mixture at ϕ=0.5 diluted with and without NH_3. Black symbol: H_2:CO-50:50 without any dilution; Grey symbol: mixture-H_2:CO:CH_4:CO_2:H_2O-28.5:28.5:8.57:15.13:19.3 without NH_3 addition; Blue symbol: mixture-H_2:CO:CH_4:CO_2:H_2O:NH_3-27.95:27.95:8.5:14.85:18.95:1.8 with NH_3 addition. Measurements conducted by [50]. 36

3.1 Measured and calculated laminar flame speed versus equivalence ratio for H_2/CO fuel mixture at P = 1 atm and T = 300 K. Symbols represent the experimental data: (□) - Burke et al. [39], (△) - Sun et al. [36], (◯) - Hassan et al. [92], (⋆) - McLean [93], (▷) - Prathap et al. [94]. Lines show predictions from the different kinetics models, see Table 3.2 for legend. 46

3.2 Measured and calculated laminar flame speed versus equivalence ratio for H_2:CO-50:50 fuel mixture with He:O_2= 7 by 1 mole at T = 300 K. Symbols represent experimental data: (□) - Kerji et al. [43], (△) - Natarajan et al. [35], (◯) - Sun et al. [36]. Lines show predictions from the different kinetics models, see Table 3.2 for legend. 47

3.3 Measured and calculated laminar flame speed versus equivalence ratio for H_2:CO-5:95 with He:O_2= 7 by 1 mole at elevated pressures (T = 300 K). Symbols represent experimental data. Lines show predictions from the different kinetics models, see Table 3.2 for legend. 47

3.4 Measured and calculated laminar burning velocities of $H_2/CO/CO_2$-35:35:30 fuel mixture at P = 1-3 atm and T = 303-373 K. The experimental data were obtained from Hu et al. [91]. Lines show predictions from the different kinetics models, see Table 3.2 for legend. 49

3.5 Measured and predicted adiabatic laminar burning velocity as a function of equivalence ratio for H_2/CO/CO_2 fuel mixture with H_2/CO ratios 80:20, 50:50 and 20:80 at 1 atm and 303 K. CO_2 is kept constant at 50% by volume. Experimental data were obtained from Kishore et al. [95]. Lines show predictions from the different kinetics models, see Table 3.2 for legend. 50

3.6 Measured and predicted laminar burning velocity (cm/s) as hydrogen concentration ratio of H_2/CO/CO_2 fuel mixture with CO_2 varying from Z_{CO_2}=0.4-0.7 at T=300 K and ϕ=0.4. The experimental data were obtained from Wang et al. [96]. Lines show predictions from the different kinetics models, see Table 3.2 for legend. . . . 51

3.7 Measured and calculated laminar burning velocities of $H_2/CO/H_2O$ fuel mixture at P=1 atm and T=323 K. (a) ϕ = 0.9 and T = 323 K, (b) ϕ=0.4, 0.5, and 0.6 and T = 323 K. The experimental data were obtained from Das et al. [97]. Lines show predictions from the different kinetics models, see Table 3.2 for legend. 53

3.8 Laminar flame speed for $H_2/CO/H_2O$ fuel mixture at P = 1 atm, T = 400 K, and ϕ = 1.0. The experimental data were obtained from Singh et al. [42]. Lines show predictions from the different kinetics models, see Table 3.2 for legend. 53

3.9 Measured and calculated laminar flame speed of $H_2/CO/N_2$-11:31:58 fuel mixture at P=1 - 5 atm and T=303-373 K. The experimental data were obtained from Hu et al. [91]. Lines show predictions from the different models. See Table 3.2 for legend. 55

3.10 Measured and calculated laminar flame speed of H_2/CH_4 fuel mixture as a function of CH_4 concentration at ϕ=1.0. Symbols represent experimental data: ($\Diamond$) - Law et al. [98], ($\bigtriangledown$) - Yu et al. [99], ($\square$) - Donohoe et al. [100]. Lines show predictions from the different models. See Table 3.2 for legend. 56

3.11 Measured and calculated laminar flame speed of H_2/CH_4 fuel mixture at P = 1 atm and T=298 K. Symbols represent experimental data: ($\bigtriangledown$) - Yu et al. [99], ($\bigtriangleup$) - Halter et al. [101],($\bigcirc$) - Dirrenberger et al. [102] ,($\square$) - Hermanns et al. [103],($\star$) - Donohoe et al. [100]. Lines show predictions from the different kinetics models, see Table 3.2 for legend. 57

3.12 Measured and calculated flame speed of $H_2/CO/CH_4/CO_2$ fuel mixture at P = 1 atm and T=300 K. The experimental data were obtained from [90]. Lines show predictions from the different kinetics models, see Table 3.2 for legend. 59

3.12 Measured and calculated flame speed of $H_2/CO/CH_4/CO_2$ fuel mixture at P = 1 atm and T=300 K. The experimental data were obtained from [90]. Lines show predictions from the different kinetics models, see Table 3.2 for legend (continued). 60

3.13 Performance of the mechanisms for laminar flame speed based on the overall mean value ($\bar{\bar{\varepsilon}}$). 61

3.14 Measured and calculated ignition delay time for H_2:CO-50:50 fuel mixture diluted in 98% of Argon (ϕ = 0.5). The experimental data were obtained from Mathieu et al. [104]. Lines show predictions from the different kinetics models, see Table 3.2 for legend. 62

3.15 Comparison among detailed chemical kinetics models and ignition delay time determined from H_2/CO/H_2O fuel mixture diluted in 98% of Argon. The experimental data were obtained from Mathieu et al. [104]. Lines show predictions from the different kinetics models, see Table 3.2 for legend. 64

3.16 Comparison among detailed chemical kinetics models and ignition delay time determined from H_2/H_2O fuel mixtures. The experimental data were obtained from [105]. Lines show predictions from the different kinetics models, see Table 3.2 for legend. 65

3.17 Comparison among detailed chemical kinetics models and ignition delay time determined from $H_2/CO/CO_2$ fuel mixture diluted in 98% of Argon. The experimental data were obtained from [104]. Lines show predictions from the different kinetics models, see Table 3.2 for legend. 68

3.18 Comparisons of measured and predicted ignition delay time of $H_2/CO/CO_2$ fuel mixture at P = 1.24 - 2.36 atm. The experimental data were obtained from [51]. Lines show predictions from the different kinetics models, see Table 3.2 for legend. 70

3.19 Comparisons of measured and predicted ignition delay time of $H_2/CO/CO_2/CH_4/H_2O$ fuel mixture diluted in 98% of Argon. The experimental data were obtained from [104]. Lines show predictions from the different kinetics models, see Table 3.2 for legend. 71

3.20 Comparisons of measured and predicted ignition delay time of $H_2/CO/CH_4$ fuel mixture (ϕ=0.5). The experimental data were obtained from [104]. Lines show predictions from the different kinetics models, see Table 3.2 for legend. 73

3.21 Comparisons of measured and predicted ignition delay time of H_2/CH_4 fuel mixtures (ϕ = 0.5). The experimental data were obtained from [28]. Lines show predictions from the different kinetics models, see Table 3.2 for legend. 74

3.22 Performance of the mechanisms for ignition delay time based on the overall mean value ($\bar{\bar{\varepsilon}}$). 77

3.23 Logarithmic sensitivity analysis on the ignition delay time of $H_2/CO/CO_2$ mixture at P = 2.36 atm for NUIG2013 mechanism. Only the ten most sensitive reactions are included, for clarity. 78

3.24 Ignition delay time of $H_2/CO/CO_2$ with various low-pressure limiting expression of $H + O_2 + CO_2 = HO_2 + CO_2$ implemented in the NUIG2013 mechanism. . . . 82

3.25 Low-pressure limiting expression of $H + O_2 + CO_2 = HO_2 + CO_2$ reaction compared to experimental data. The experimental data were obtained from Vasu et al. [51] and Ashman and Haynes [121]. 83

3.26 Logarithmic sensitivity analysis on the ignition delay time of $H_2/CO/CH_4$ and $H_2/CO/CO_2/CH_4/H_2O$ at P = 32 atm for NUIG2013 mechanism. Only the ten most sensitive reactions are included, for clarity. 85

3.27 Arrhenius plot for $CH_4 + OH = CH_3 + H_2O$. Solid line represents newly fitted rate constant expression and dash-line represents the rate constant expression used in NUIG2013 mechanism. The experimental data were procured from Felder and Madronich [127], Srinivasan et al. [128], and Hong et al. [129]. 87

3.28 Comparisons of measured and predicted ignition delay time. Solid-line: NUIG2013 mechanism; dash-line: NUIG_V3 mechanism. The experimental data were procured from [104]. 88

4.1 Flow chart of the genetic algorithm. [143] 99

4.2 Overall fitness and the maximum relative error value among the 90 optimization targets of the reduced mechanism (277Rxn) in 3000 generations. 104

4.3 The maximum relative error values between the 290Rxn mechanism and the NUIG2013 mechanism for Cases 1 to 32 (Ignition Delay Time). The number above the bar represents the case number and its respective fuel compositions and experimental conditions can be found in Table B or Supplementary Table B.1. 106

4.4 Comparisons of measured and predicted ignition delay time of $H_2/CO/CO_2$ fuel mixture (ϕ = 1.0). The experimental data were obtained from ref. [51]. Lines show predictions from the different kinetics models. 108

4.5 Comparisons of measured and predicted ignition delay time of $H_2/CO/CH_4$ fuel mixture (ϕ = 0.5). The experimental data were obtained from ref. [104]. Lines show predictions from the different kinetics models. 109

4.6 Comparisons of measured and predicted ignition delay time of $H_2/CO/CH_4/CO_2/H_2O$ fuel mixture (ϕ = 0.5). The experimental data were obtained from ref. [104]. Lines show predictions from the different kinetics models. 110

4.7 Comparisons of measured and predicted ignition delay time of H_2/CH_4 fuel mixtures (ϕ = 0.5) at various pressure conditions. The experimental data were obtained from ref. [28]. Lines show predictions from the different kinetics models. 111

4.8 The maximum relative error values between the 290Rxn mechanism and the NUIG2013 mechanism for Cases 33 to 57 (Ignition Delay Time). The number above the bar represents the case number and its respective fuel compositions and experimental conditions can be found in Table 4.3 or Supplementary Table B.1. 114

4.9 Comparisons of measured and predicted ignition delay time of $H_2/CH_4/C_2H_6$ fuel mixtures (ϕ = 0.5). The experimental data were obtained from ref. [152] . Lines show predictions from the different kinetics models. 115

4.10 The maximum relative error values between the 290Rxn mechanism and the NUIG2013 mechanism for Cases 58 to 94 (Ignition Delay Time). The number above the bar represents the case number and its respective fuel compositions and experimental conditions can be found in Table 4.3 or Supplementary Table B.1. 117

4.11 Comparisons of measured and predicted ignition delay time of CH_4/C_3H_8 fuel mixtures. The experimental data were obtained from ref. [148]. Lines show predictions from the different kinetics models. 118

4.12 Comparisons of measured and predicted ignition delay time of $CH_4/C_2H_6/C_3H_8$ fuel mixtures (ϕ = 0.5). The experimental data were obtained from ref. [147]. Lines show predictions from the different kinetics models. 119

4.13 The maximum relative error values between the 290Rxn mechanism and the NUIG2013 mechanism for Case 95 to Case 149 (Laminar Flame Speed). The number above the bar represents the case number and its respective fuel compositions and experimental conditions can be found in Table 4.3 or Supplementary Table B.1. 121

4.14 Measured and calculated flame speed of $H_2/CO/CH_4/CO_2$ fuel mixture at P = 1 atm and T = 300 K. The experimental data were obtained from ref. [90] and the lines show the predictions from the different kinetics models. The δS_u represents the relative error between the predicted flame speed and the measured flame speed. The E represents the relative error between the 290Rxn mechanism and the NUIG2013 mechanism. 122

4.15 Measured and calculated flame speed of CH_4/H_2 at P = 1 atm and T = 300 K. The experimental data were obtained from [100] and the lines show the predictions from the different kinetics models. 122

4.16 Measured and calculated flame speed of $H_2/CO/CO_2$. The experimental data were obtained from ref. [95, 96] and the lines show the predictions from the different kinetics models. 124

A.1 The relative error between the simulated and measured laminar flame speed for H_2/CO mixtures, as shown in Fig. 3.1. The values next to the mechanism name represent the average relative error for the experimental condition shown in the sub-caption. 159

A.2 The relative error between the simulated and measured laminar flame speed for H_2/CO mixtures, as shown in Fig. 3.2. The values next to the mechanism name represent the average relative error for the experimental condition shown in the sub-caption. 160

A.3 The relative error between the simulated and measured laminar flame speed for H_2/CO mixtures, as shown in Fig. 3.3. The values next to the mechanism name represent the average relative error for the experimental condition shown in the sub-caption. 161

A.4 The relative error between the simulated and measured laminar flame speed for $H_2/CO/CO_2$ mixtures, as shown in Fig. 3.4. The values next to the mechanism name represent the average relative error for the experimental condition shown in the sub-caption. 162

A.5 The relative error between the simulated and measured laminar flame speed for $H_2/CO/CO_2$ mixtures, as shown in Fig. 3.5. The values next to the mechanism name represent the average relative error for the experimental condition shown in the sub-caption. 163

A.6 The relative error between the simulated and measured laminar flame speed for $H_2/CO/CO_2$ mixtures, as shown in Fig. 3.6(a). The values next to the mechanism name represent the average relative error for the experimental condition shown in the sub-caption. 164

A.7 The relative error between the simulated and measured laminar flame speed for $H_2/CO/CO_2$ mixtures, as shown in Fig. 3.6(b). The values next to the mechanism name represent the average relative error for the experimental condition shown in the sub-caption. 165

A.8 The relative error between the simulated and measured laminar flame speed for $H_2/CO/H_2O$ mixtures, as shown in Fig. 3.7. The values next to the mechanism name represent the average relative error for the experimental condition shown in the sub-caption. 166

A.9 The relative error between the simulated and measured laminar flame speed for $H_2/CO/H_2O$ mixtures, as shown in Fig. 3.8. The values next to the mechanism name represent the average relative error for the experimental condition shown in the sub-caption. 167

A.10 The relative error between the simulated and measured laminar flame speed for $H_2/CO/N_2$ mixtures, as shown in Fig. 3.9. The values next to the mechanism name represent the average relative error for the experimental condition shown in the sub-caption. 168

A.11 The relative error between the simulated and measured laminar flame speed for H_2/CH_4 mixtures, as shown in Fig. 3.10. The values next to the mechanism name represent the average relative error for the experimental condition shown in the sub-caption. 169

A.12 The relative error between the simulated and measured laminar flame speed for H_2/CH_4 mixtures, as shown in Fig. 3.11. The values next to the mechanism name represent the average relative error for the experimental condition shown in the sub-caption. 170

A.13 The relative error between the simulated and measured reference flame speed ($S_{u,ref}$) for $H_2/CO/CH_4/CO_2$ mixtures with air, as shown in Fig. 3.12. The values next to the mechanism name represent the average relative error for the experimental condition shown in the sub-caption. 171

A.14 The relative error between the simulated and measured ignition delay time for H_2/CO - 50:50 mixture, as shown in Fig. 3.14. The values next to the mechanism name represent the average relative error for the experimental condition shown in the sub-caption. 172

A.15 The relative error between the simulated and measured ignition delay time for $H_2/CO/H_2O/O_2$ - 0.444:0.444:0.223:0.889 mixture, as shown in Fig. 3.15. The values next to the mechanism name represent the average relative error for the experimental condition shown in the sub-caption. 173

A.16 The relative error between the simulated and measured ignition delay time for H_2/H_2O mixture, as shown in Fig. 3.16. The values next to the mechanism name represent the average relative error for the experimental condition shown in the sub-caption. 174

A.17 The relative error between the simulated and measured ignition delay time for $H_2/CO/CO_2/O_2$ - 0.46:0.46:0.15:0.93 mixture, as shown in Fig. 3.17. The values next to the mechanism name represent the average relative error for the experimental condition shown in the sub-caption. 175

A.18 The relative error between the simulated and measured ignition delay time for $H_2/CO/CO_2$ mixture, as shown in Fig. 3.18. The values next to the mechanism name represent the average relative error for the experimental condition shown in the sub-caption. 176

A.19 The relative error between the simulated and measured ignition delay time for $H_2/CO/CO_2/CH_4/H_2O$ mixture, as shown in Fig. 3.19. The values next to the mechanism name represent the average relative error for the experimental condition shown in the sub-caption. 177

A.20 The relative error between the simulated and measured ignition delay time for $H_2/CO/CH_4$ mixture, as shown in Fig. 3.20. The values next to the mechanism name represent the average relative error for the experimental condition shown in the sub-caption. 178

A.21 The relative error between the simulated and measured ignition delay time for H_2/CH_4 mixtures, as shown in Fig. 3.21(a) and 3.21(b). The values next to the mechanism name represent the average relative error for the experimental condition shown in the sub-caption. 179

A.22 The relative error between the simulated and measured ignition delay time for H_2/CH_4 mixtures, as shown in Fig. 3.21(c) and 3.21(d). The values next to the mechanism name represent the average relative error for the experimental condition shown in the sub-caption. 180

A.23 The relative error between the simulated and measured ignition delay time for H_2/CH_4 mixtures, as shown in Fig. 3.21(e) and 3.21(f). The values next to the mechanism name represent the average relative error for the experimental condition shown in the sub-caption. 181

A.24 Logarithmic sensitivity analysis on the laminar flame speed of syngas mixtures diluted with CO_2 at experimental conditions shown in Fig. 3.4, 3.5, and 3.6 for NUIG2013 mechanism. Only the ten most sensitive reactions are included, for clarity. 182

A.25 The rate constants of reaction $CH_4 + OH = CH_3 + H_2O$ at T = 1000 2000 K. Lines show the rate constant of $CH_4 + OH = CH_3 + H_2O$ incorporated in the kinetics mechanisms investigated in this study and the red dotted line represents the newly fitted rate constant expression. Symbols represent data taken from [**?**, **?**, **?**] 183

A.26 The rate constants of reaction $CH_4 + OH = CH_3 + H_2O$ at T = 200 2000 K. Solid line represents $k = 5.83 \times 10^4 \times T^{2.60} \times exp[(-1152K)/T]$ from NUIG2013; dashed line represents $k = 2.30 \times 10^8 \times T^{1.40} \times exp[(-2850K)/T]$ from Current Study. Symbols represent data taken from [**?**, **?**, **?**, **?**, **?**, **?**, **?**, **?**, **?**, **?**] 184

A.27 Sensitivity analysis for $CH_4 + OH = CH_3 + H_2O$ reaction at several different pressures and temperatures. 185

A.28 Comparisons of measured and predicted ignition delay time of H_2/CH_4 mixtures computed using NUIG_V3 mechanism. Symbols represent experimental data; please refer to Fig. 3.21 in manuscript for more information. Solid-line: NUIG2013 mechanism; dash-line: USC2007; dash-dot-line: NUIG_V3. 186

A.29 The rate constants of reaction $C_2H_6 = CH_3 + CH_3$. Symbol patterns represent the temperatures and colors of the symbol represent where the experimental data were obtained. Blue colored symbols, Du et al. [**?**]; green colored symbols, Hwang et al. [**?**]; red colored symbols, Davison et al. [**?**]; black colored symbols, Oehlschlaeger et al. [**?**]. ($\Diamond$) : T = 1425 K; (O): T = 1503; ($\triangledown$): T = 1720 K; ($\bigstar$): T = 1924 K. The lines denote the rate constant of $C_2H_6 = CH_3 + CH_3$ incorporated in the kinetics mechanisms investigated in this study. 187

A.30 Sensitivity analysis for $CH_3 + CH_3(+M) = C_2H_6(+M)$ reaction at several different pressures and temperatures. 188

A.31 The rate constants of reaction $CH_3 + HO_2 = CH_3O + OH$. The pink lines denote the rate constant determined from theoretical studies. Solid pink line, Jasper et al. [**?**]; dash pink line, Lin and Zhu [**?**]. The rate constant of $CH_3 + HO_2 = CH_3O + OH$ employed in NUIG2013 is identical to the rate constant proposed by Jasper et al. [**?**], which explains why the line is masked by the solid pink line. . . . 189

A.32 Sensitivity analysis for $CH_3 + HO_2 = CH_3O + OH$ reaction at several different pressures and temperatures. 190

A.33 The rate constants of reaction $CH_4 + O = CH_3 + OH$. The lines denote the rate constant of $CH_4 + O = CH_3 + OH$ incorporated in the kinetics mechanisms investigated in this study. 191

A.34 Sensitivity analysis for $CH_4 + O = CH_3 + OH$ reaction at several different pressures and temperatures. 192

B.1 Comparisons of measured and predicted ignition delay time of H_2/CO mixtures computed using Aramco-1.3, 290Rxn, and 290Rxn-V1 mechanisms. Symbols represent experimental data; please refer to Table B.1 for references and more information on the fuel compositions and the experimental conditions. 202

B.2 Comparisons of measured and predicted ignition delay time of $H_2/CO/H_2O$ mixtures computed using Aramco-1.3, 290Rxn, and 290Rxn-V1 mechanisms. Symbols represent experimental data; please refer to Table B.1 for references and more information on the fuel compositions and the experimental conditions. 203

B.3 Comparisons of measured and predicted ignition delay time of $H_2/CO/CO_2$ mixtures computed using Aramco-1.3, 290Rxn, and 290Rxn-V1 mechanisms. Symbols represent experimental data; please refer to Table B.1 for references and more information on the fuel compositions and the experimental conditions. 204

B.4 Comparisons of measured and predicted ignition delay time of $H_2/CO/CH_4$ mixtures computed using Aramco-1.3, 290Rxn, and 290Rxn-V1 mechanisms. Symbols represent experimental data; please refer to Table B.1 for references and more information on the fuel compositions and the experimental conditions. 205

B.5 Comparisons of measured and predicted ignition delay time of $H_2/CO/CO_2/H_2O/CH_4$ mixtures computed using Aramco-1.3, 290Rxn, and 290Rxn-V1 mechanisms. Symbols represent experimental data; please refer to Table B.1 for references and more information on the fuel compositions and the experimental conditions. 206

B.6 Comparisons of measured and predicted ignition delay time of H_2/CH_4 mixtures computed using Aramco-1.3, 290Rxn, and 290Rxn-V1 mechanisms. Symbols represent experimental data; please refer to Table B.1 for references and more information on the fuel compositions and the experimental conditions. 207

B.7 Comparisons of measured and predicted ignition delay time of CH_4 mixtures computed using Aramco-1.3, 290Rxn, and 290Rxn-V1 mechanisms. Symbols represent experimental data; please refer to Table B.1 for references and more information on the fuel compositions and the experimental conditions. 208

B.8 Comparisons of measured and predicted ignition delay time of CH_4/H_2O mixtures computed using Aramco-1.3, 290Rxn, and 290Rxn-V1 mechanisms. Symbols represent experimental data; please refer to Table B.1 for references and more information on the fuel compositions and the experimental conditions. 209

B.9 Comparisons of measured and predicted ignition delay time of $CH_4/C_2H_6/H_2$ mixtures computed using Aramco-1.3, 290Rxn, and 290Rxn-V1 mechanisms. Symbols represent experimental data; please refer to Table B.1 for references and more information on the fuel compositions and the experimental conditions. 210

B.10 Comparisons of measured and predicted ignition delay time of CH_4/C_3H_8 mixtures computed using Aramco-1.3, 290Rxn, and 290Rxn-V1 mechanisms. Symbols represent experimental data; please refer to Table B.1 for references and more information on the fuel compositions and the experimental conditions. 211

B.11 Comparisons of measured and predicted ignition delay time of $CH_4/C_2H_6/C_3H_8$ mixtures computed using Aramco-1.3, 290Rxn, and 290Rxn-V1 mechanisms. Symbols represent experimental data; please refer to Table B.1 for references and more information on the fuel compositions and the experimental conditions. 213

B.12 Comparisons of measured and predicted laminar flame speed of H_2/CO mixtures computed using Aramco-1.3, 290Rxn, and 290Rxn-V1 mechanisms. Symbols represent experimental data; please refer to Table B.1 for references and more information on the fuel compositions and the experimental conditions. 216

B.13 Comparisons of measured and predicted laminar flame speed of $H_2/CO/CO_2$ mixtures computed using Aramco-1.3, 290Rxn, and 290Rxn-V1 mechanisms. Symbols represent experimental data; please refer to Table B.1 for references and more information on the fuel compositions and the experimental conditions. 218

B.14 Comparisons of measured and predicted laminar flame speed of $H_2/CO/H_2O$ mixtures computed using Aramco-1.3, 290Rxn, and 290Rxn-V1 mechanisms. Symbols represent experimental data; please refer to Table B.1 for references and more information on the fuel compositions and the experimental conditions. 220

B.15 Comparisons of measured and predicted laminar flame speed of $H_2/CO/N_2$ mixtures computed using Aramco-1.3, 290Rxn, and 290Rxn-V1 mechanisms. Symbols represent experimental data; please refer to Table B.1 for references and more information on the fuel compositions and the experimental conditions. 221

B.16 Comparisons of measured and predicted laminar flame speed of H_2/CH_4 mixtures computed using Aramco-1.3, 290Rxn, and 290Rxn-V1 mechanisms. Symbols represent experimental data; please refer to Table B.1 for references and more information on the fuel compositions and the experimental conditions. 222

B.17 Comparisons of measured and predicted laminar flame speed of $H_2/CO/CH_4/CO_2$ mixtures computed using Aramco-1.3, 290Rxn, and 290Rxn-V1 mechanisms. Symbols represent experimental data; please refer to Table B.1 for references and more information on the fuel compositions and the experimental conditions. 223

B.19 Comparisons of measured and predicted laminar flame speed of CH_4 mixtures computed using Aramco-1.3, 290Rxn, and 290Rxn-V1 mechanisms. Symbols represent experimental data; please refer to Table B.1 for references and more information on the fuel compositions and the experimental conditions. 226

Chapter 1

Introduction

The fluctuation in crude oil price and harmful pollutants emitted from fossil fuels combustion have led gas turbine manufacturers to search for renewable, environmental friendly and secure fuel supplies that will meet the ever stringent emission regulations. Syngas, an alternative fuel has recently drawn considerable amount of interest to gas turbines manufacturers because hydrogen is known to burn without emitting unburned hydrocarbon, CO_2, and CO [2]. Integrated Gasification Combined Cycle (IGCC) power plants that combust syngas have been in commercial operation for more than a decade [3] and they have proved to be capable of offering better energy efficiency and environmental performance compared to conventional coal fired power generators [4, 5]. In addition, there is a potential to realize zero CO_2 emissions from IGCC power plants by implementing carbon capture and storage (CCS) techniques [6]. Furthermore, the gasification technology employed in the IGCC power plant allows a wide range of feedstocks such as municipal solid waste [7], agriculture residues [8, 9, 10], herbaceous energy crops [11, 12, 13], and others to be converted into syngas.

The high reactivity of syngas and the inherent risks for the gas turbines' hardwares have prompted the use of diffusion flame combustion technique [14, 15] in IGCC systems. This approach typically generates regions of near-stoichiometric condition, where the temperature in the combustor is considerably high. High temperature is favorable for the formation of NO_x through thermal NO_x

pathway. Thus, diluents such as N_2 or steam are required for NO_x abatement. These will reduce the plant efficiency due to the additional energy required to inject the diluent into the combustion zone [16]. In order to further lower the NO_x emissions to 3 ppm (parts per million), the diffusion flame combustor is required to be equipped with selective catalyst reduction system (SCR) that removes the NO_x emissions. The efficacy of this technique in mitigating NO_X emissions is very high, but is expensive due to the catalyst [17].

Alternative approach to reduce emissions is the state of the art Lean-Premixed or Dry Low NO_x combustion technology. This approach has been gaining momentum since 1980s because of their inherent advantages over emissions reduction and higher efficiency compared to the former technology [18, 19]. In lean premixed combustion, fuel and air are thoroughly mixed in the primary stage. The mixture will subsequently be transfered to a secondary stage where the combustion reaction takes place. The fuel/air ratio typically approaches one-half of the stoichiometric condition [20], where the air supplied is approximately twice the amount required to completely burn the fuel. The available excess air will reduce the residence time at peak temperature inside the combustor area and subsequently decrease the NO_x formation. In the past decades, this technology has been optimized and demonstrated for natural gas combustion, where the NO_x emission is able to reach a single digit ppm and the CO emission is able to reach $<$20 ppm [19].

Converting current Lean Premixed combustion systems that have been optimized to operate on natural gas for high hydrogen content fuel is not feasible because syngas has high flashback propensity and high gas flow rate issues [21]. Higher gas flow rate of syngas than natural gas is required to maintain similar gas turbine power output because hydrogen has a lower Lower Heating Value (LHV). The higher flow rate might lead to blow-off, instability of compressor, and insufficient cooling of turbine blade [22, 21], if proper measures are not taken. Therefore, syngas-/methane-based fuel blends are of great interest to gas turbine manufacturers [23]. In addition, previous studies have demonstrated that the addition of hydrogen to methane-based fuel could further mitigate both CO and NO_x emissions [24, 25, 26, 27]. This outcome is most likely caused by the high

concentration of radicals in the presence of H_2, where it increases the reactivity of the methane mixture [28]. Methane-based fuels such as natural gas emit low levels of pollutants relative to conventional coal combustion; they are not, however, a sustainable source of energy. Moreover, the long-term demand for natural gas has intensified the need for sustainable sources. Biogas derived from the decomposition of living matter, which consists primarily of CH_4 and CO_2, is a promising replacement for natural gas and, more importantly, it is a renewable energy source. Therefore, this thesis is aimed at understanding the limitations in current kinetics models for syngas and biogas combustion purpose and develop an accurate chemical kinetics model that can be used to study and understand syngas and biogas combustion numerically.

The thesis is sectioned into 5 chapters, where Chapter 2 discusses the fundamental combustion properties of syngas mixtures, and how impurities such as CO_2 or H_2O affect the reactivity of the fuel mixtures. In addition, Chapter 2 summarized and categorized all available experimental data in literature on syngas mixture accordingly to the type of measurement techniques and fuel mixtures. The experimental data compiled in Chapter 2 were used in Chapter 3 to compare and evaluate currently available chemical kinetics mechanisms. Since there is a limited study on the combustion characteristics on biogas fuel mixtures, and biogas consists mainly of CH_4 and CO_2, combustion properties of CH_4 mixtures found in literature were used in Chapter 3 to compare several notable chemical kinetics mechanism to identify the most accurate kinetics scheme for syngas and biogas combustion. The chemical kinetics mechanism identified in Chapter 3 that has the best agreement with the experimental data, consists of too many irrelevant species and reactions for syngas and biogas combustion purpose. Therefore, Chapter 4 introduces an approach known as the Genetic Algorithm to search optimally for a sub-mechanism within the large mechanism for syngas and biogas combustion purpose. Finally, Chapter 5 summarizes the findings from this dissertation and future works are addressed.

Chapter 2

Combustion Characteristics of Syngas

Abstract

Syngas has shown great success in Integrated Gasification Combined Cycle (IGCC) technology for providing cleaner and higher efficiency energy production with minimal environment impact. Thus, it sounds promising that syngas is able to replace the conventional fossil fuel resources, while at the same time minimizing pollutants. The drawback of traditional gas turbines that burn syngas is that they use diffusion flame combustion technology that suffers from low efficiency and high emissions. Recently, Lean-Premixed combustion technique has emerged as a promising solution, but the variation of hydrogen fraction in syngas has prohibited its usage. Besides, other gases such as CO_2, N_2, H_2O, NH_3, and CH_4 found in syngas mixtures have adverse effects on the combustion characteristics. To address these issues, better understanding of the syngas's fundamental combustion properties are vital. Hence, recent works published on syngas combustion at lean-premixed and gas turbine relevant conditions are reviewed, classified according to their objectives, and remarks were concluded.

2.1 Background

Hydrogen concentration in syngas mixture varies vastly, depending on the gasification technique and also the feedstock used during the conversion process. Typically, syngas composition from various gasifier processes ranges from 6.8% - 50.4% H_2, 8.1% - 60.5% CO, 1.3% - 29.6% CO_2, 0% - 20.4% H_2O, 0% - 9.3% CH_4, and contains traces of other contaminates [29]. H_2 and CO pose a very unique combustion characteristic which differs significantly from hydrocarbon fuel. Recent studies showed that the variation of hydrogen composition in syngas introduces substantial adverse effects on the flame shape, emissions, blow-off and flashback limit, and most importantly combustion instability [30, 31, 32]. Fu et al. [33] revealed that even at the same equivalence ratio and pressure, the flame structure of different syngas mixtures with different hydrogen compositions vary significantly. In addition, the triatomic molecules (CO_2 and H_2O) that contain in the Syngas mixture are strong radiation species. If large fractions of CO_2 and H_2O exist in the fuel mixture, it will have a drastic impact on the flame radiation and will influence the combustion temperature as well as the flame dynamics [34]. This chapter aims to present a comprehensive summary of recent experimental results on the laminar flame speed and ignition delay time of syngas mixtures at gas turbine conditions, and address the importance of studying the dilutes that exists in syngas mixture. Table 2.1 summarized the recent available experimental data on syngas mixture combustion at has turbine conditions for validation and optimization of chemical kinetics mechanism.

Table 2.1: Available experimental kinetic data for the combustion of syngas fuel(Ignition delay time)

Technique	**Mixture**	**Conditions**	**Data type and comments**	**Ref.**
Bunsen burner	H_2/CO/air	The laminar flame speed of H_2:CO (ratios from 0.25-4.0) were measured at atmospheric pressure and uncontrolled burner temperature, for equivalence ratios of 0.5-1.2.	Flame speed measured versus equivalence ratios (0.5-1.2) for H_2:CO ratios varied from 0.25-4.0.	[33]
Cylindrical chamber	$H_2/CO/CO_2$/ O_2	The laminar flame speed of $H_2/CO/CO_2$ with ZH_2=0.1-0.7 ($ZH_2 = XH_2/(XCO + XH_2)$) and Z=0.4-0.7 ($Z = XCO_2/(XCO_2 + XO_2)$) were measured at P=1 and 2 atm and T=300 K, for equivalence ratio of 0.4.	Flame speed measured versus H concentrations (0.1-0.7) for Z=0.4-0.7.	[34]
Bunsen burner & Wall Stagnation Flame	$H_2/CO/CO_2$/ air	The laminar flame speed of H_2:CO-50:50 and 5:95 diluted with 0% and 20% of CO_2 were measured at P=1 and 5 atm and T=300-700 K, for equivalence ratios of 0.6-1.0.	Flame speed measured versus equivalence ratios (0.6-1.0) at atmospheric condition using bunsen method. Flame speed measured versus strain rate for equivalence ratios of 0.59, 0.6, 0.68, 0.78, and 0.8 using wall stagnation flame method.	[35]
Cylindrical bomb	H_2/CO/air and $H_2/CO/O_2/He$	The laminar flame speed of H_2:CO-50:50, 25:75, 5:95, and 1:99 were measured at P=1, 2, 5, 10, 20, and 40 atm, and T=298 K, for equivalence ratios of 0.5-5.0.	Flame speed measured versus equivalence ratios (0.5-5.0) at six different pressures.	[36]
Cylindrical Chamber	$H_2/CO/N_2$/air	The laminar flame speed of H_2:CO-50:50 diluted with 0% to 60% of N_2 were measured at P=1 atm and T=302 K, for equivalence ratios of 0.6-3.5.	Flame speed measured versus equivalence ratios (0.6-3.5) at atmospheric condition for 0% to 60% of N_2	[37]
Bunsen burner	H_2/CO/air	The laminar flame speed of H_2:CO ratios varied from 0 to 1 with increment of 0.1 were measured at atmospheric and ambient conditions, for equivalence ratios of 0.4-2.1.	Flame speed measured versus equivalence ratios (0.4-2.1) at standard conditions for 0% to 100% of H_2. Flame speed correlation derived from the laminar flame speed data.	[38]

Continued on next page

Table 2.1 – *Continued on next page*

Technique	**Mixture**	**Conditions**	**Data type and comments**	**Ref.**
Cylindrical Chamber	H_2/CO/air	The laminar flame speed of H_2:CO-50:50 , 25:75, 10:90, and 5:95 were measured at atmospheric and ambient conditions, for equivalence ratios of 0.4-5.0.	Flame speed measured versus equivalence ratios (0.5-5.0) at standard conditions. Flame speed deduced using linear and non-linear extrapolation methodologies.	[39]
Bunsen Burner	$H_2/CO/CO_2/N_2$/air	The laminar flame speed of H_2:CO-50:50 diluted with 0-20% of CO_2 and 0-60% of N_2 were measured at atmospheric pressure and ambient temperature (303 K), for equivalence ratios of 0.6-4.25.	Flame speed measured versus equivalence ratios (0.6-4.25) at atmospheric conditions.	[40]
Cylindrical bomb	$H_2/CO/H_2O/O_2/He$	The laminar flame speed of H_2:CO-100:0 and 50:50 diluted with 0-15% of H_2O were measured at atmospheric pressure and T=323-423 K, for equivalence ratios of 0.5-5.0.	Flame speed measured versus equivalence ratios (0.5-5.0) at atmospheric pressure.	[41]
Cylindrical chamber	$H_2/CO/H_2O$/ air	The laminar flame speed of H_2:CO-50:50 and 5:95 diluted with 0-20% of H_2O were measured at atmospheric pressure and T=298, 400, and 500 K, for equivalence ratios of 0.6-3.0.	Flame speed measured versus equivalence ratios (0.6-3.0) for H_2:CO-50:50 and 5:95 at atmospheric pressure, and T=298, 400, and 500 K. Flame speed measured versus $\%H_2O$ in fuel mixture (0%-40%) for equimolar H_2:CO and 5:95 at P=1 atm and T=400 K.	[42]
Shock tube	$H_2/CO/O_2/Ar$	H_2:CO-10:90, 20:80, 40:60, 50:50, and 80:20 diluted in 98% of Ar were ignited at ϕ=0.5, P=1.6, 12, and 32 atm, and T=960-2000 K	Ignition delay measured versus temperature (960-2000 K) at one equivalence ratio. Pressure profile recorded versus time for T=1375 K at 1.65 atm	[43]
Cylindrical bomb	$H_2/CO/O_2/He$	The laminar flame speed of H_2:CO-100:0 and 50:50 mixtures diluted with 7He:O_2 were measured at P=1,5, and 10atm, and T=298-443 K, for equivalence ratios of 0.3-4.0.	Flame speed measured versus equivalence ratios (0.3-4.0) at three different pressures.	[43]

Continued on next page

Table 2.1 – *Continued on next page*

Technique	**Mixture**	**Conditions**	**Data type and comments**	**Ref.**
Rapid compression machine	$H_2/CO/O_2/N_2$	H_2:CO-100:0, 50:50, 25:75, and 10:90 diluted in 81.25% of N_2 were ignited at ϕ=0.5, P=69 atm, T=914-1068 K.	Ignition delay measured versus temperature (914-1068 K) at one equivalence ratio.	[44]
Shock tube	$H_2/CO/O_2/N_2$/ Ar	H_2:CO-100:0, 85:15, 50:50, and 5:95 diluted with N_2 and Ar were ignited at ϕ=0.1, 0.5, and 4.0, P=1, 4, 16 atm, T=870-2100 K.	Ignition delay measured versus temperature (870-2100 K) at one equivalence ratio (ϕ=0.5).	[44]
Rapid compression machine	$H_2/CO/O_2/N_2$/ Ar	H_2:CO-100:0, 85:15, 50:50, and 25:75 diluted in 50:50-N_2:Ar were ignited at ϕ=0.5, P=7.8, 15.8, and 31.5 atm, T=929-1049 K.	Ignition delay measured versus temperature (929-1049 K) at one equivalence ratio.	[44]
Spherical bomb	$H_2/CO/O_2$/He	The laminar flame speed of H_2:CO-50:50, 20:80, 15:85, and 10:90 diluted with helium with an O_2:He-1:7 were measured at P=5 and 10 atm and T=298 K, for equivalence ratio of 0.5-3.5.	Flame speed measured versus equivalence ratios (0.5-3.5) for P=5 and 10 atm.	[44]
Counterflow twin-flame	$H_2/CO/H_2O$/ air	The laminar flame speed of H_2:CO-50:50, 20:80, 15:85, and 10:90 diluted with H_2O were measured at P=1 atm and T=323 K, for equivalence ratio of 0.3-0.9.	Flame speed measured versus $\%H_2O$ in fuel mixtures (0%-35%) for ϕ=0.4, 0.5, 0.6, 0.7, 0.8 and 0.9.	[45]
Constant volume bomb	$H_2/CO/N_2/CO_2$/air	The laminar flame speed of H_2:CO-70:30 and 33:67, H_2:CO:N_2-11:31:58, and H_2:CO:CO_2-35:35:30 were measured at P=1 and 5 atm and T=303 and 373 K, for equivalence ratio of 0.4-1.0.	Flame speed measured versus equivalence ratios (0.4-1.0) for P=1 and 5 atm.	[46]

Continued on next page

Table 2.1 – *Continued on next page*

Technique	**Mixture**	**Conditions**	**Data type and comments**	**Ref.**
Rapid compression machine	$H_2/CO/O_2/N_2/Ar$	H_2:CO-100:0, 75:25, 50:50, 35:65, and 20:80 diluted in approximately 63% Ar were ignited at ϕ=0.3-1.6, P=14.9-49 atm, and T=950-1100 K.	Ignition delay measured versus temperature (950-1100 K) at one equivalence ratios (ϕ=1.0) for P=14.9, 29.6, and 49 atm.	[47]
Shock tube	$H_2/CO/O_2/N_2$	H_2:CO-5:95, 10:90, 20:80, 40:60, 60:40 and 80:20 were ignited at ϕ=0.5, P=1-15 atm, T=890-1300 K.	Ignition delay measured versus temperature (890-1300 K) at one equivalence ratio. Pressure profile recorded versus time for P=1.2 and 2.5 atm and T=985 and 929 K, respectively.	[48]
Rapid compression machine	$H_2/CO/CH_4/O_2/N_2/Ar$	H_2:CO-70:30 and H_2:CO:CH_4-50:30:20 were ignited at ϕ=0.5 and 1.0, P=19.8-79 atm,and T=900-1100 K.	Ignition delay measured versus temperature (900-1100 K) at two equivalence ratios for P=49 and 39 atm. Ignition delay measured versus pressures (19.8-79 atm) at ϕ=0.5 and T=1010 K.	[49]
Shock tube	$H_2/CO/CO_2/CH_4/H_2O/NH_3/O_2/Ar$	H_2:CO-50:50 with addition of CO_2, H_2O, CH_4, and NH_3 in the fuel mixtures diluted in 98% of Ar were ignited at ϕ=0.5, P=1.65, 12.5, and 32 atm,and T=1005-2030 K.	Ignition delay measured versus temperature (1005-2030 K) at one equivalence ratio for the three pressures.	[50]
Shock tube	$H_2/CO/CO_2/O_2/N_2$	8.91% H_2 + 11.58% CO + 24.44% CO_2 + 10.25% O_2 + 44.83% N_2, by volume was ignited in stoichiometric condition at P=1.1-2.6 atm ,and T=974-1160 K.	Ignition delay measured versus temperature (974-1160 K) at one equivalence ratio. Pressure profile recorded versus time.	[51]
Rapid compression machine	$H_2/CO/$ air	H_2:CO ratios varied from 0.25 to 4.0 were ignited at ϕ=0.1 -1.0, P=7.1-26.4 atm, and T=849-1051 K	Ignition delay measured versus temperature (849-1051 K) for a wide range of equivalence ratios (0.1-1.0). Ignition delay correlation derived from the data.	[52]

Continued on next page

Table 2.1 – *Continued on next page*

Technique	**Mixture**	**Conditions**	**Data type and comments**	**Ref.**
Shock tube	$H_2/CO/CO_2$/ air	7.33% H_2 + 9.71% CO + 1.98% CO_2 + 17.01% O_2 + 63.97% N_2 was ignited at ϕ=0.5, P≈21 atm, T=943-1148 K	Ignition delay measured versus temperature (943-1148 K) at one equivalence ratio.	[53]
Flow reactor	H_2/CO/ air	H_2:CO-50:50 was ignited at ϕ ≈0.5, P≈5 atm, T=760-783 K	Ignition delay measured versus temperature (760-783 K) at approximately equivalence ratio of 0.5.	[53]
Continuous flow reactor	$H_2/CO/CO_2$/ air	38.6% H_2 + 51.1% CO + 10.3% CO_2, by volume was ignited at ϕ=0.5, P=11.9-23 atm, T=633-781 K	Ignition delay measured versus temperature (633-781 K) at one equivalence ratio.	[54]
Rapid compression machine	$H_2/CO/H_2O/O_2/N_2/Ar$	H_2:CO-50:50 and 5:95 with 0%, 5%, and 10% of H_2O addition were ignited in stoichiometric condition at P=29.5 atm, and T=930-1050 K	Ignition delay measured versus temperature (930-1050 K) at one equivalence ratio. Pressure profile recorded versus time.	[55]
Shock tube	$H_2/CO/O_2/Ar$	H_2:CO-5:95 and 50:50 with dilution of 1:2, 1:5, 1:10 were ignited at ϕ=0.5, P=15.8 atm, and T=1019-1259 K.	Ignition delay measured versus temperature (1019-1259 K) at one equivalence ratio. Pressure profile recorded versus time for 50:50 and 5:95 at P=15.38, 16, and 15.8 atm and T=1054, 1107, and T=1223 K, respectively.	[56]
Bunsen Burner	$H_2/CO/CO_2/N_2$/air	The laminar flame speed of H_2:CO-50:50 and 25:75 diluted with 20% of CO_2 and 40% of N_2 were measured at sub atmospheric pressures (0.947, 0.838, and 0.767) and ambient temperatures (303, 297, 294 K), for equivalence ratios of 0.6-3.4.	Flame speed measured versus equivalence ratios (0.6-3.4) at sub-atmospheric conditions.	[40]

2.2 Laminar Flame Speed

Among flame properties, the laminar flame speed is regarded as an important parameter because it serves as a basis to turbulent combustion, and it also contains the fundamental information on the reactivity, diffusivity, and exothermicity. In addition, the value of the flame speed has important impacts on the propensity of a flame to flashback and blowoff. It also controls other key combustion characteristics, such as the flame's spatial distribution [35]. In the combustion community, laminar flame speed is also one of the fundamental parameters that helps validate chemical kinetics models and aids the design of combustors. Figure 2.1 shows an extensive literature comparison for atmospheric Syngas (H_2/CO) air mixture at room temperature utilizing different techniques by McLean et al. [57], Hassan et al. [58], Sun et al. [36], Natarajan et al. [35], Prathap et al. [37], Dong et al. [38], Bouvet et al. [39],Burbano et al. [40], Krejci et al. [41], and Singh et al. [42]. Since the H_2/CO/air chemical kinetic system has been well studied at atmospheric and ambient conditions for the past decades, it is expected that the agreement would be quite good between the experimental data found in literature for Syngas mixture with H_2/CO-50:50 composition, as depicted in Fig. 2.1. However, unified agreement only appears in the fuel-lean side and it begins to deviate at an equivalence ratio of approximately 2.0 and above.

The observed disparities at rich condition (ϕ >2.0) can be explained by the different approaches and processing procedures adopted by the authors, especially the choice of useful experimental data range used for the flame speed extrapolation [39]. Another potential source of anomaly among the flame speed data sets at rich condition could be explained by the presence of unwanted carbonyl compounds in the H_2/CO blend of interest [59]. Bouvet et al. [39] reported that these compounds tended to have strong inhibition effects on flames and were essentially effective on the rich side of the flame speed curve. More recently, Burke et al. [60] proposed a new correlation for correcting laminar flame speed measurements due to confinement effects when the experimental data used for extrapolation was lower than half of the radius of the cylindrical chamber, r_w. If this correction is

not applied, results obtained may be lower by 15-20%. Since most of the researchers did not report the flame radii chosen for extrapolation to non-stretch flame speed, it is not possible to analyze the differences.

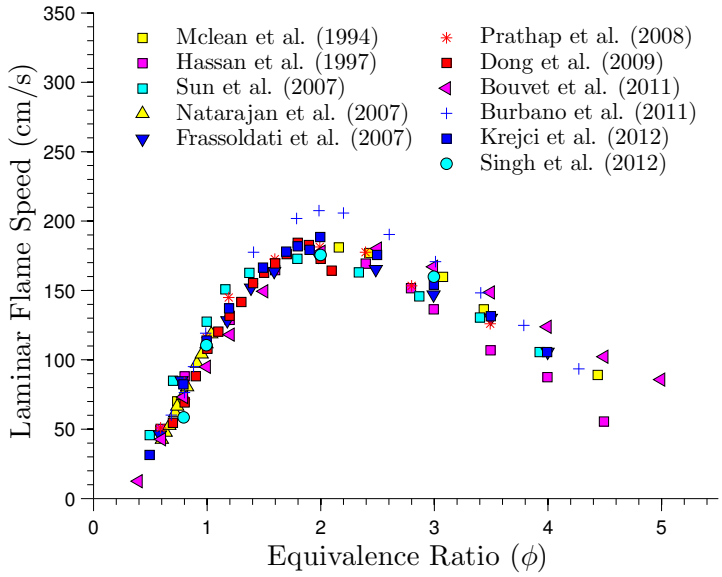

Figure 2.1: Laminar flame speed of H_2:CO-50:50 at atmospheric pressure and 298K.

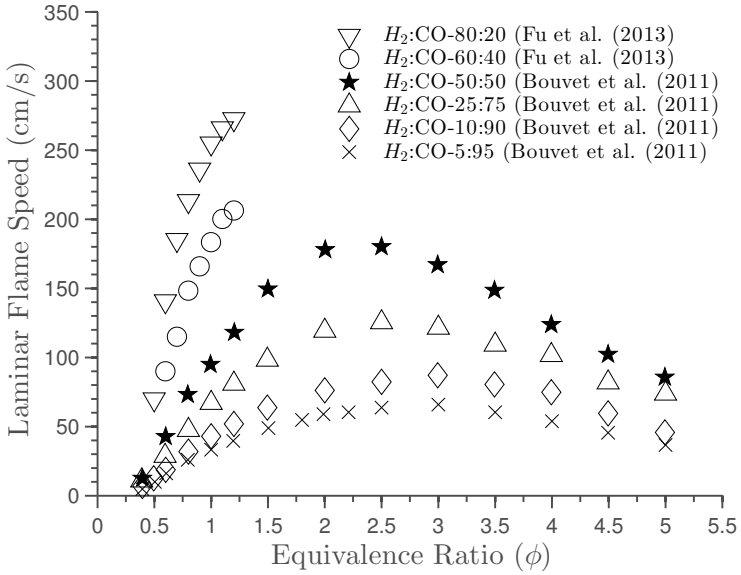

Figure 2.2: Laminar flame speed of various H_2:CO mixture at atmospheric pressure and 298K.

The laminar flame speed of Syngas flames at various H_2:CO ratios were investigated by Fu et al. [33], Sun et al. [36], Dong et al. [38], and Bouvet et al. [39] at standard conditions. Only the measured flame speed by Bouvet et al. [39] and Fu et al. [33] are shown in Fig. 2.2 for brevity purpose. These data are in line with earlier measurements reported by Sun et al. [36] and Dong et al. [38]. It can be seen from Fig. 2.2 that the flame speed increases simultaneously with H_2 concentration in the fuel mixture. Fu et al. [33] work differs slightly from the above literature as they investigated the flame speed in an uncontrolled temperature burner. However, their work is worth to be mentioned because they investigated the leanest condition for hydrogen concentration of 60% and 80% in H_2/CO mixture and measured the blow-off limit particular to the employed burner, while others did not study the blow-off limit of Syngas. The blow-off limit becomes leaner with the increase of H_2 concentration because the flame is more stable at high H_2 concentration (see Fig. 2.2). Besides, the flame speed of H_2/CO exhibits a non-linear relationship with the equivalence ratio. The observed behavior is related to the variation of flame height due to air/fuel ratio [33].

Measurements at elevated pressure for high hydrogen ($>$50%) concentration in Syngas is missing, and at low hydrogen concentration, the database is somewhat limited. Sun et al. [36], Krejci et al. [43], and Kéromnès et al. [44] were the only researches that explored the effects of elevated pressure. For P$>$ 5 atm, the Syngas mixtures are burned with O_2 as the oxidizer highly diluted with helium at a ratio of He:O_2-7:1. Helium, instead of nitrogen is used in all of the studies as the diluent for pressure measurement beyond 5 atm because the combustion of Syngas/air mixture becomes cellularly unstable. Helium substitution will not affect the fundamental chemistry of the phenomena [61], but will increase the mixture Lewis number due to higher thermal conductivity than nitrogen, thereby suppressing the onset of these diffusive-thermal cells [62]. Aside from the thermal-diffusive effect, hydrodynamic instability and body forces are also responsible for the flame instabilities [63, 64, 65]. Body forces effect is not significant and can be neglected when compared with hydrodynamic and thermal-diffusive effects [66]. Furthermore, body forces effect

only appears when laminar flame speed is small and equivalence ratio is near the flammability limits [40, 66]. In contrary, hydrodynamic instability in Syngas-air flame is due to the density jump in the flame front and depends on the thermal expansion ratio and also the flame thickness, where thicker flame will decrease the hydrodynamic instability [63, 64, 65, 66, 40]. Interestingly, the hydrodynamic instability is restrained by the thermal-diffusive effect when Lewis number is greater than unity [67, 68]. However, if the Lewis number is below unity, the thermal diffusive effect will surface and be compounded onto the hydrodynamic instability [67]. Vu et al. [66] studied the dilution effect of CO_2, N_2, and He on the cellular instabilities in Syngas-air mixture. They reported that the addition of CO_2, N_2, and He will decrease the thermal expansion ratio and increase the flame thickness. Hence, the effect of hydrodynamic instability can be diminished with the addition of CO_2, N_2, and He. However, they observed that the Lewis number decrease with the increase of CO_2 and N_2 addition in the Syngas-air mixture, instigating the effect of thermal-diffusive instability. He, on the other hand, increases the Lewis number and limited the cellular instability of Syngas-air mixture [62, 66].

It is still possible to obtain the laminar flame speed of Syngas-air mixture without any dilution that is independent of the cellular flames and flame instabilities effect. This can be accomplished by restricting the flame speed measurement before the occurrence of the cellular structure [69]. However, for lean and elevated pressure conditions, it is nearly impossible to obtain accurate laminar flame speed before the onset of the flame instabilities without taking into consideration of the effect of flame instabilities. Bradly et al. [69] developed a method to calculate the instability free laminar flame speed in an unstable flame region by taking into account of the instabilities that caused the rapid increase in flame speed. However, this method requires high speed camera with up to 30,000 fps (frame per second) and the accuracy of the laminar flame speed is questionable because only three data points could be obtained using such high speed camera at P=10 atm. Moreover, the laminar flame speed is increasingly dependent on the large corrections to the measured unstable flame speeds [69]. Hence, the authors [69] questioned the purpose of deriving virtual values of the

laminar flame speed if there exits no measurable stable regime. Therefore, Syngas-air mixture that is highly diluted with Helium to increase the Lewis Number at elevated pressure for measuring the laminar flame speed remains favorable approach among Combustion community.

With limited literature available at elevated pressure conditions, overall agreement at both pressures tested is quite good for both fuel mixtures. Only minor discrepancy between the work of Kerjci et al. [43] and Sun et al. [36] is observed around the peak flame speed of H_2:CO-50-50 mixture (P=10 atm, see Fig. 2.3b). This discrepancy remains unclear and is still under their investigation [43]. Sun et al.[36] further extended their work to study the flame speed at P=20 and 40 atm for 5:95-H_2/CO mixture, as depicted in Fig. 2.4. Scrutinizing Fig. 3-2.4, it reveals that the measured flame speed increases with increasing H_2 concentration, while they decrease with increasing pressure for the helium-diluted mixture. Liu et al. [70] plotted (refer therein [70]) the variations of laminar flame speed with pressure, varying from P=1-10 atm for H_2:CO-35:65 mixture at ϕ=0.5 and 0.7. They then curve fitted their data and discovered that the flame speed data of lean Syngas mixture at two different equivalence ratio have almost the same pressure dependence, that was $S_L \approx p^{-0.15}$ at ϕ=0.7 and $S_L \approx p^{-0.17}$ at ϕ=0.5. Such weak pressure dependence found for lean Syngas flames could be understood from the consideration of chemical kinetics.

Studies on the effect of preheated temperature on flame speed are as limited as the studies on elevated pressure, only Singh et al. [42], Krejci et al. [43, 41], and Natarajan et al. [35] extended their flame speed measurements of various H_2-CO mixture ratios (H_2/CO-5:95 and 50:50) to investigate the effect of preheated temperature. The effect of preheated temperature ranging from 300 K to 700 K on flame speed for H_2:CO-50:50 and H_2:CO-5:95 are shown in Fig. 2.5a and 2.5b, respectively. Interestingly, Singh et al. [42] used a non-linear extrapolation instead of conventional approach (linear extrapolation) to procure the flame speed, where they discovered that the flame speed obtained by linear and non-linear extrapolation were very similar. Their finding is similar to Bouvet et al. [39] studies, where they reported that there was no significant disparity between linear and non-linear extrapolation for these set of experimental conditions. As expected, the preheated

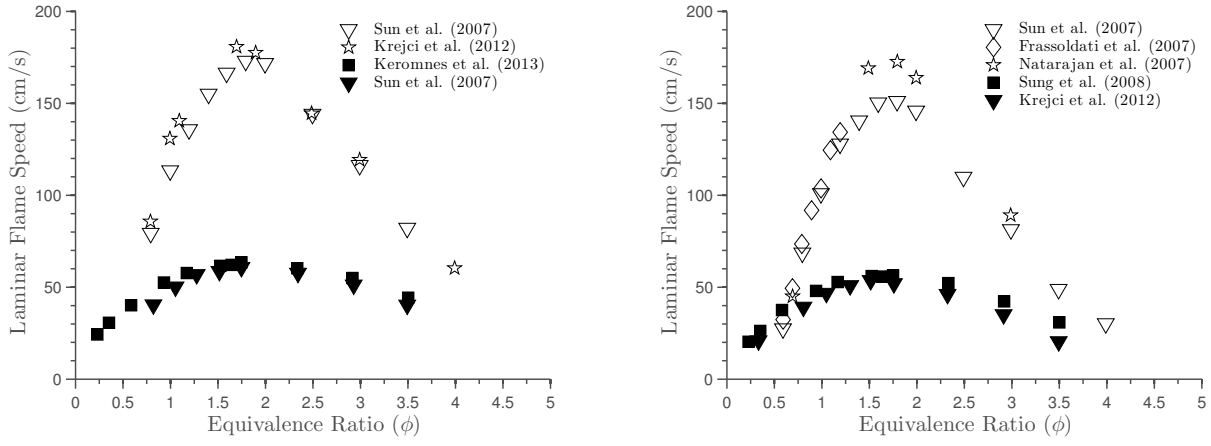

(a) (b)

Figure 2.3: Laminar flame speed of H_2:CO with O_2 as the oxidizer diluted in He with a ratio of He:O_2-7:1 at T=298 K. (a) P=5 atm, (b) P=10 atm and T=298 K; Filled Symbol: H_2:CO-5:95; Open Symbol: H_2:CO-50:50.

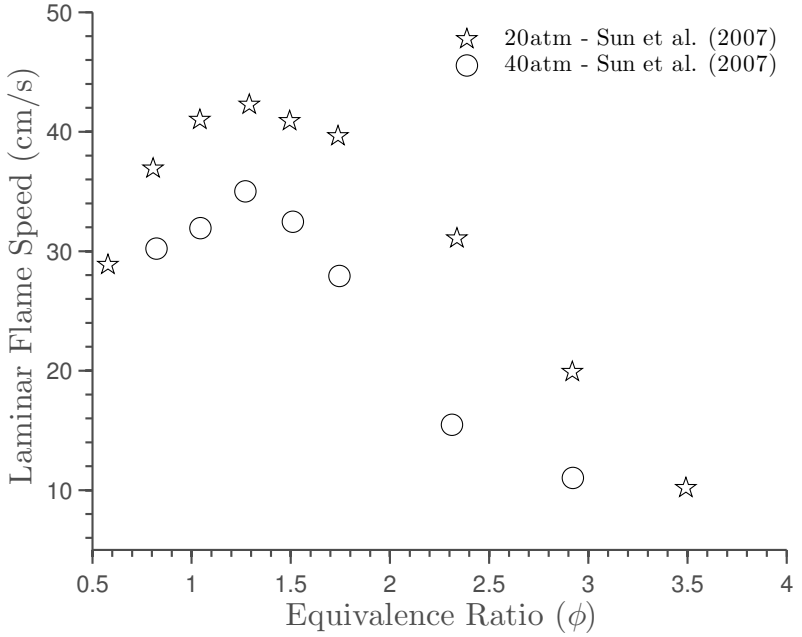

Figure 2.4: Laminar flame speed of H_2:CO-5:95 with O_2 as the oxidizer diluted in He with a ratio of He:O_2-7:1 at P=20-40 atm and T=298 K.

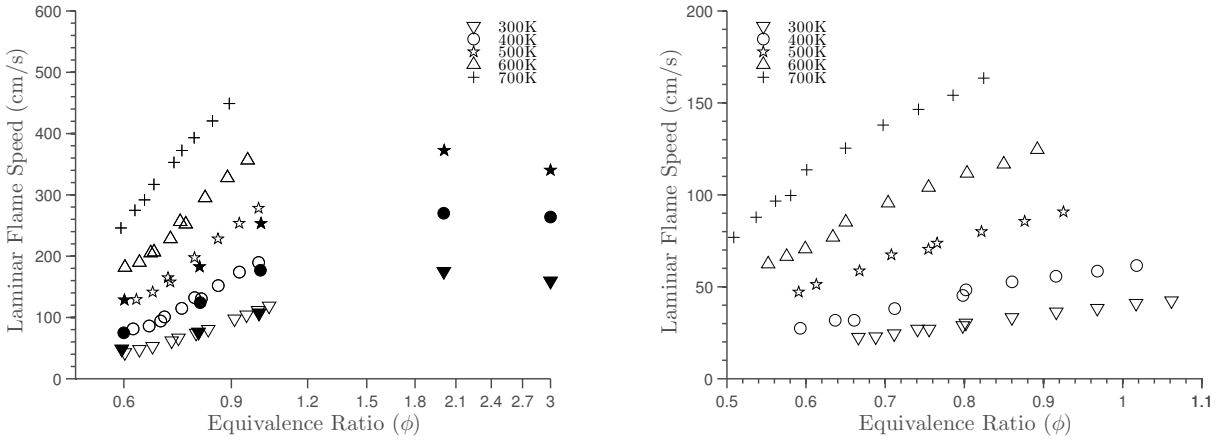

Figure 2.5: Laminar flame speed of H_2/CO-air mixture at P=1 atm and T=300,400,500,600,700 K. (a) H_2:CO-50:50, (b) H_2:CO-5:95. Filled symbol: measured by [42], open symbol: measured by [35].

temperature (300-700 K) increases the flame speed substantially, as depicted in Fig. 2.5a and 2.5b. The data showed in Fig. 2.5a and 2.5b are fitted using a power law correlation for different equivalence ratio, where the laminar flame speed at higher temperatures for given conditions of mixture equivalence ratio can be obtained by Eq. (1).

$$\mathrm{S_u} = \mathrm{S_{u,o}} \times \left(\frac{\mathrm{T_u}}{\mathrm{T_{u,o}}} \right)^{\alpha} \tag{2.1}$$

$\mathrm{S_{u,o}}$ is the laminar flame speed at temperature of 300 K, $\mathrm{T_{u,o}}$ is the initial temperature of the unburned mixture, $\mathrm{T_u}$ is the temperature of unburned mixture, and α is the temperature exponent. For brevity, only the variation of the temperature exponent (α) with the mixture equivalence ratio are shown in Fig. 2.6. Second degree polynomials were fitted to the two experimental data for better visualization of the trend. The temperature exponent decreases with an increase in the equivalence ratio for both Syngas mixtures (H_2:CO - 5:95 and 50:50). The trend observed in Fig. 2.6 is somewhat similar to the temperature exponent trend for H_2 diluted with N_2 and CO_2 [71].

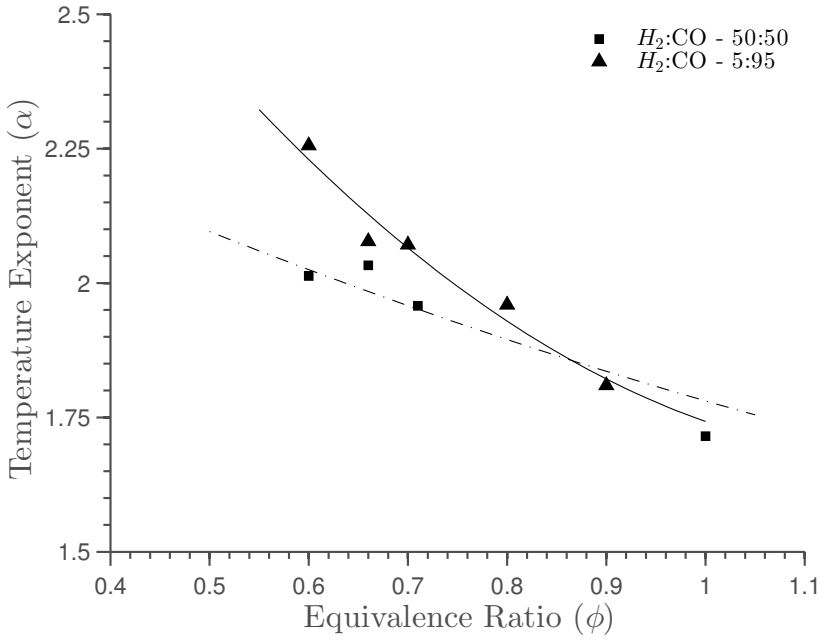

Figure 2.6: Variation of temperature exponent (α) for H_2:CO-5:95 and H_2:CO-50:50 at P=1 atm. The lines show the second degree polynomial fitted to both experimental data.

However, Paidi et al. [71] reported that the temperature exponent attained a minimum value at approximately 1.1 $<\phi<$1.2 and increases again for pure H_2 diluted with N_2 and CO_2. The aforementioned trend can not be seen in Fig. 2.6 is because of the range of our analysis is kept at ϕ $<$1.0. Besides, the cross-over of the two polynomial fits observed in Fig. 2.6 at $\phi \approx 0.85$ is not reported in the work of Paidi et al. [71] for pure H_2 diluted with N_2 and CO_2. This might be due to the range of their investigation (ϕ = 0.8-1.3) and fuel mixtures are different from our analysis. The mean value for α at ϕ = 0.6-1.0 for H_2:CO-50:50 is 1.813, and at ϕ =0.6-0.9 for H_2:CO-5:95 is 2.035. As mentioned previously, the experimental data on elevated temperature is limited and more flame speed at elevated temperature and lean condition for various H_2:CO ratios are required to elucidate the cross-over of the temperature exponent trend.

2.2.1 Dilute effects on flame speeds

Syngas derived from coal through gasifications typically contains moisture content ranging from 6-20% [72]. Hence, it is important to take into account the effect of H_2O dilution. Singh et al. [42] and Das et al. [45] studied the effect of water addition (0%-40% of H_2O, by volume) on the flame speed. Singh et al. [42] performed their experiments in a spherical combustion chamber with stoichiometric fuel mixtures (H_2:CO-5:95 and 50:50) at elevated temperatures (298, 400, and 500 K) and atmospheric pressure, while Das et al. [55] conducted their experiments using counterflow burner with lean (ϕ=0.4, 0.5, and 0.6) fuel mixture (H_2:CO-50:50) at T=323 K and atmospheric pressure. Figure 2.7 shows the experimental results from both studies at various percentages of water dilution to the fuel mixture. For high hydrogen concentration (50% H_2), the flame speed decreases monotonically with H_2O addition in the fuel mixture. However, at low hydrogen fraction ($< 50\%$), the laminar flame speed increases with small amount of water addition ($< 20\%$), then decreases gradually when water dilution is higher ($> 20\%$). The flame speed decreases in low hydrogen concentration (H_2:CO-5:95) mixture could be due to the dominance of chemical effect (e.g., chemical reaction involving H_2O to produce H, O, and OH radicals). The measured flame speed from both studies for H_2:CO-50:50 mixture depicted in Fig. 2.7 are not congruent due to the different conditions (Equivalence ratio and Preheated Temperature) adopted. Nevertheless, both studies exhibit similar trend for equimolor H_2/CO mixture with water dilution at ϕ=0.5 and 1.0.

The dilution effect of N_2 and CO_2 on the flame speed of H_2/CO mixtures at atmospheric and ambient conditions were studied by Burbano et al. [40], Prathap et al. [37], Wang et al. [34], and Hu et al. [46]. Prathap et al. [37] and Burbano et al. [40] investigated the laminar flame speed of equimolar H_2/CO mixture diluted with 20, 40 and 60% of N_2 by volume at standard conditions, as depicted in Fig. 2.8. Excellent agreement between the two studies can be observed at lean condition, but it starts to deviate at $\phi > 1.5$, especially at equivalence ratio where the maximum

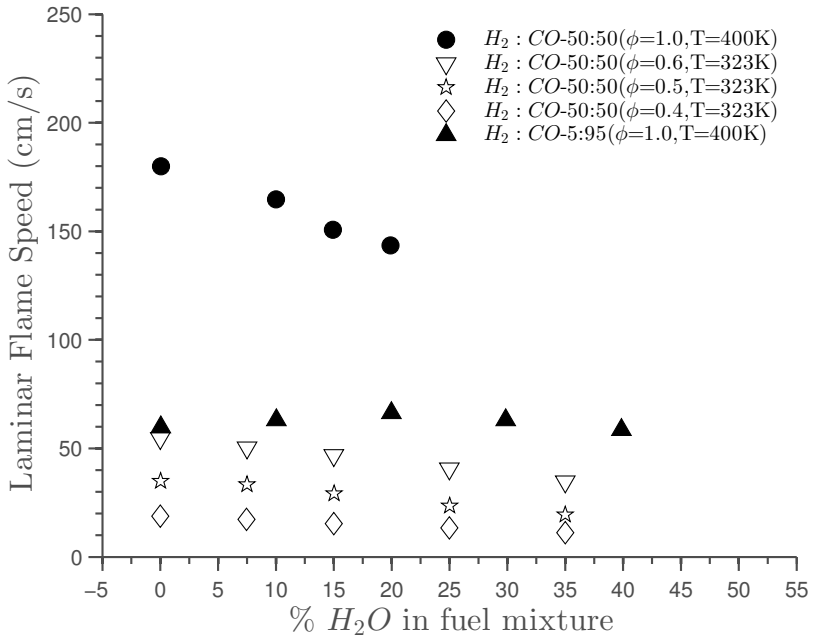

Figure 2.7: Laminar flame speed of $H_2/CO/H_2O$/air mixture at P=1 atm and T=323 and 400 K. Filled symbol: measured by [42], open symbol: measured by [45].

value of flame speed is obtained. However, at very rich condition (ϕ >2.5), the disparity among the two studies decreases. Burbano et al. [40] argued that the anomaly observed was simply because Pranthap et al. [37] used a cylindrical chamber and did not correct their measured flame speed with the methodology proposed by Burke et al. [60]. Moreover, Prathap et al. [37] used flame radii between 0.02 and 0.21 times r_w, which may generate erroneous data due to the small flame radii considered. Nevertheless, the two studies illustrate similar trend, which the addition of N_2 substantially reduces the peak flame speed and shifts the peak to the lean side. The observed phenomenon is also due to the extra heat capacity provided by N_2 dilution. It increases the heat capacity of the combustion products and decreases the rates of reaction of H_2 and CO_2.

For CO_2 dilution, experimental results of Burbano et al. [40] are in good agreement with those of Natarajan et al. [35] work. It is because they both used the same experimental approach (Bunsen burner) for measuring the flame speed (see Fig. 2.9). Furthermore, Natarajan et al. [35] compared the Bunsen burner approach with jet wall stagnation approach in procuring the flame speed, and

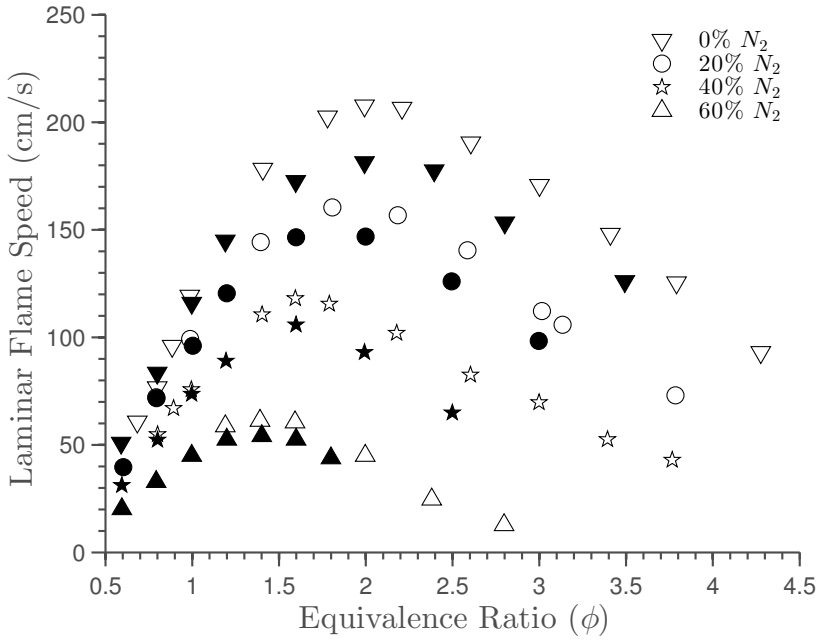

Figure 2.8: Laminar flame speed of H_2/CO-50:50 air mixture diluted with N_2 T=298 K at P= 1 atm. Filled symbol: measured by [37], open symbol: measured by [40].

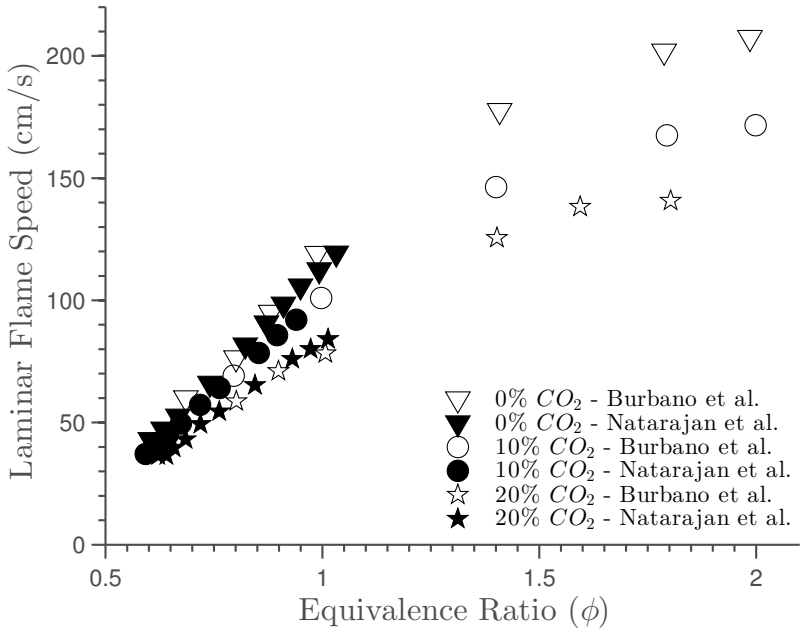

Figure 2.9: Laminar flame speed of H_2/CO-50:50 air mixture diluted with CO_2 at P=1 atm and T=298 K. Filled symbol: measured by [35], open symbol: measured by [40].

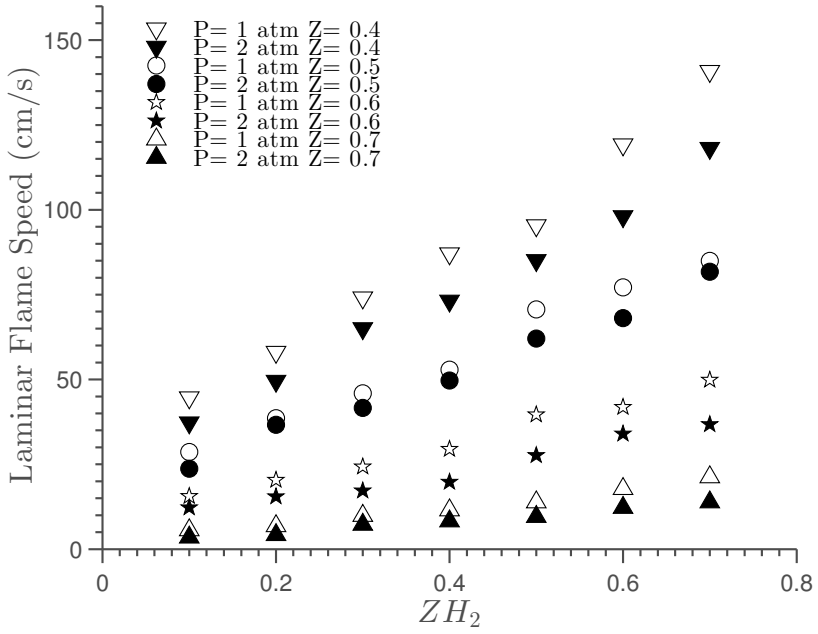

Figure 2.10: Laminar flame speed of $H_2/CO/CO_2/O_2$ mixture (T=300 K, ϕ=0.4) at P=1 and 2 atm. $Z = XCO_2/(XCO_2 + XO_2)$ and $ZH_2 = XH_2/(XCO + XH_2)$. X refers to the mole fraction of the specific species in the mixtures. Measured by [34].

discovered that the easy implement Bunsen flame approach agreed well with the wall stagnation flame results for a wide range of H_2/CO mixtures. Similarly, CO_2 dilution considerably reduces the laminar flame speed as depicted in Fig. 2.9. However, CO_2 dilution decreases the flame speed in a higher proportion compared to N_2. This is because CO_2 exhibits higher heat capacity than N_2. The dissociation of CO_2 during combustion helps further reduces the flame speed [40]. Moreover, the data presented in Fig. 2.8 and 2.9 are in line with the recent measurements performed by Hu et al. [46]. Natarajan et al. [35] extended their study to investigate the effect of 40% CO_2 dilution at high preheated temperature (700 K) for equimolar H_2/CO mixture using stagnation flame technique. They reported that CO_2 dilution at preheated temperature behaved analogously with those at ambient temperature for lean condition (ϕ=0.6 and 0.8), where the leaner mixture demonstrated higher strain sensitivity.

Instead of using air as the oxidizer, Wang et al. [34] used O_2 diluted with CO_2 as the oxidizer to

investigate the laminar flame speed of $CO/H_2/CO_2/O_2$ mixture over a wide range of H_2 and CO_2 fractions. The mixture selection by the authors is to extend the dataset of Syngas oxyfuel combustion. This combustion concept has attractive features such as enhanced radiation heat transfer, downsizing of combustors, zero NO_x emission, and it is expected to be applicable to various highly efficient combustion systems. However, there is not much study on Syngas oxyfuel combustion as most of the researchers are focused on technology feasibility and/or system analysis [34]. Their experimental results are depicted in Fig. 2.10, where the flame speed decreases with increasing pressure across the entire range of hydrogen fraction ($ZH_2 = XH_2/(XCO + XH_2)$). This observation is identical to Syngas-air mixture discussed earlier. Besides, Fig. 2.10 shows that the effect of H_2 concentration in fuel mixture on the flame speed is weakened with the increase of CO_2. At Z=0.7 ($Z = XCO_2/(XCO_2 + XO_2)$), the flame speed increases marginally with the increase of ZH_2. It is because CO_2 behaves as an inhibitor on the flame speed through the competition of the reactions of $H + O_2 = O + OH$, $CO + OH = CO_2 + H$, and $H + O_2(+M) = HO_2(+M)$ on H radical. In addition, they discovered that the radiation loss of Syngas-air mixture is much weaker compared to Syngas oxyfuel combustion due to the large amount of CO_2 that is present in the flame.

2.3 Ignition Delay Time

In operational aspects, variation in the autoignition delay time of the fuel can results in pre-ignition in lean premixed Gas Turbines, which could physically damage the equipment and it is crucial to avoid such phenomena. Therefore, understanding the autoignition behavior of Syngas is an integral aspect of the development and benchmarking of chemical mechanisms of Syngas, since H_2/O_2 mechanism forms an essential subset of any hydrocarbon and oxygenate oxidation mechanism. Earlier studies on the ignition delay time of H_2/CO were mostly based on shock tube experiments in the temperature range of 1160-1900 K and pressure range of 1-2 atm. Since most of the studies

were performed at atmospheric or sub-atmospheric conditions, their works will not be discussed in this review, and most of them have been summarized in 2005 by Davis et al. [73].

Figure 2.11 shows the measured ignition delay time of Syngas mixtures at various H_2:CO ratios with pressure ranging from 1.6-49 atm collected from Krejci et al. [43], Mathieu et al. [31], Mathieu et al.[50], Vasu et al. [51] using shock tube, and Kéromnès et al. [44], Gersen et al. [49], Mittal et al. [47] using rapid compression machine (RCM). Scrutinizing Fig. 2.11 reveals that the ignition delay time decreases with increasing compressed temperature and pressure. The is due to higher pressure leads to an increase in the concentration of the reactants, hence, an acceleration in the reactivity. Figure 2.11(d), (f), and (h) are scaled such that they congruent to exhibit the effect of CO addition with pressure on the ignition delay time at ϕ=1.0. At P=15 atm, the ignition delay time for increasing amount of CO addition are closer to each other compared to P=29.6 and 49 atm. The ignition delay lines become progressively more apart at higher pressure for increasing amount of CO addition at P=49 atm (see Fig. 2.11(h)). This implies that the CO oxidation is retarded at elevated pressures [61]. However, the observation is in contrast to what have been reported by Kèromnés et al. [44] for high hydrogen concentration ($\geq$50%) and low temperature ($<$1025 K). The ignition delay time were almost indistinguishable from each other and also to pure hydrogen across the entire pressure range investigated (P= 7.9, 15.8, and 32 atm; see Fig. 2.11(b), (e), and (f)). Kerjci et al. [58] also studied the effect of CO concentration on ignition delay time at elevated pressure and intermediate to high temperature (1000 K $<$ T $<$ 2000 K) in a shock tube. Their results are presented in Fig. 2.11(a), (c), and (g), where at relatively low pressure (1.6 atm), the ignition delay time of high hydrogen concentration ($\geq$ 40%) are very similar for the entire range of temperature (975-1670 K). At P=12 and 32 atm, the ignition delay time of high hydrogen mixture ($\geq$50%) are identical at only lower temperature ($<$1140 K), as depicted in Fig. 2.11. Besides, Gersen et al. [49] also measured the ignition delay time at similar condition as of Mittal et al. [47] and found that addition of CO to H_2 did not result in a substantial increase in the ignition delay time for high hydrogen concentration ($\geq$ 50%). The origin of the discrepancy between the studies

is at present unclear. It could be due to the dilution adopted by both studies are different as Gersen et al. [49] used 27.1% of Ar and 30% of $\mathrm{N_2}$ as dilution while Mittal et al. [47] diluted the mixture in 67% Ar. However, it requires further evaluation to identify the origin of this disparity.

The effect of high CO concentration (>60%) on ignition delay time are also amplified and clearly visible in Fig. 2.11. The decrease in the reactivity with addition of CO is due to the decrease of H atoms available. In addition, Fig. 2.11(b) shows that leaner mixture exhibit lower reactivity (longer ignition delay time), where the ignition delay time are longer for ϕ=0.35 than ϕ=0.5, and this applies to all pressures (7.9, 15.8, and 32 atm), mixture ratios, and temperature (900-1050 K) [44]. Furthermore, Fig. 2.11 shows that $\mathrm{H_2}$ is much more reactive than CO and is driving the ignition of Syngas mixtures, even if only 5% of $\mathrm{H_2}$ is presence in the fuel mixture. The addition of carbon monoxide in the mixture leads to a decrease in the activation energy in comparison with the $\mathrm{H_2/O_2}$ mxiture, especially at higher pressure [43]. Figure 2.11(e) and (g) shows the comparison of the measured ignition delay time of the Syngas mixtures at 15.8 atm and ϕ=0.5 across a wide range of temperature (880-1280 K). Lower activation energy can be observed at high temperature region, followed by a very steep increase at about 1000 K.

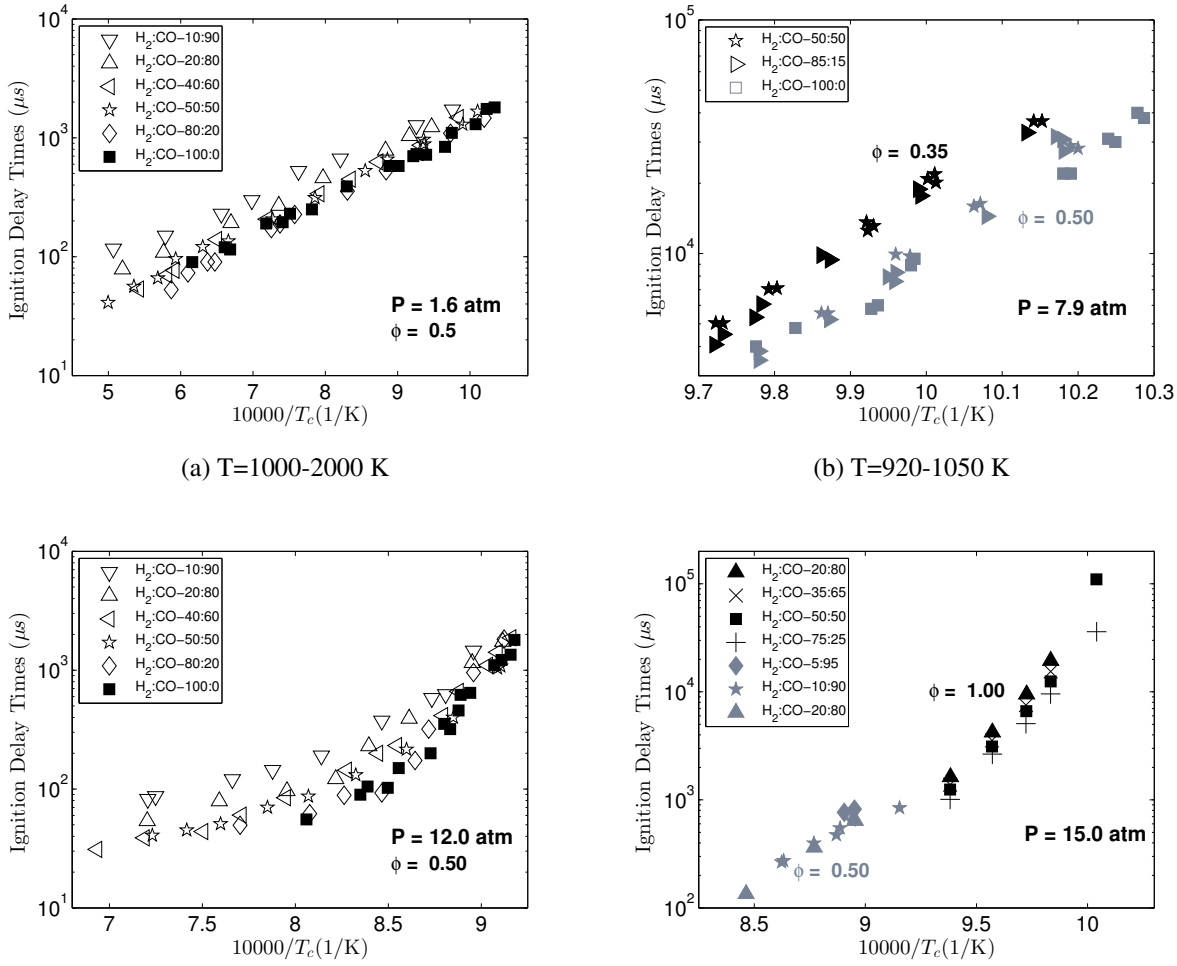

(a) T=1000-2000 K

(b) T=920-1050 K

(c) T=1080-1450 K

(d) T=980-1200 K

Figure 2.11: Measured ignition delay time of various H_2/CO mixture as a function of temperature at around P=1.6, 7.9, 12, 15, 15.8, 30, 32, and 50 atm. (a) Mixture: $1.00\%(\alpha H_2 + (1-\alpha)CO) + 1.00\%O_2 + 98.00\%Ar$, measured in a shock tube facility by [43], (b) Mixture: $17.36\%(\alpha H_2 + (1-\alpha)CO) + 17.36\%O_2 + 32.64\%N_2 + 32.64\%Ar$, measured in a RCM facility by [44], (c) Mixture: $1.00\%(\alpha H_2 + (1-\alpha)CO) + 1.00\%O_2 + 98.00\%Ar$, measured in a shock tube facility by [43], (d) Black symbol: Mixture: $12.5\%(\alpha H_2 + (1-\alpha)CO) + 6.25\%O_2 + 18.25\%N_2 + 63.125\%Ar$, measured in a RCM facility by [47]; Grey symbol: Mixture: $17.5\%(\alpha H_2 + (1-\alpha)CO) + 17.5\%O_2 + 65.2\%N_2$, measured in a shock tube facility [48]. α refers to the mole fraction of H_2.

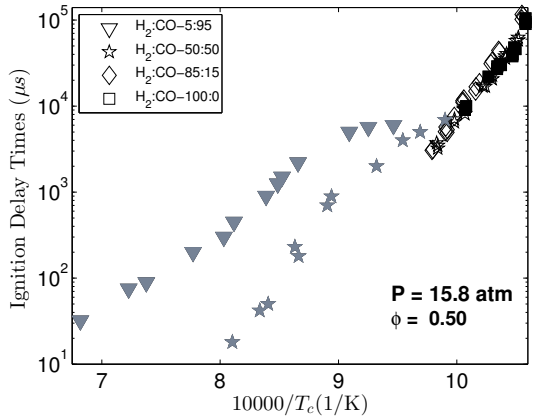

(e) T=900-1050 K

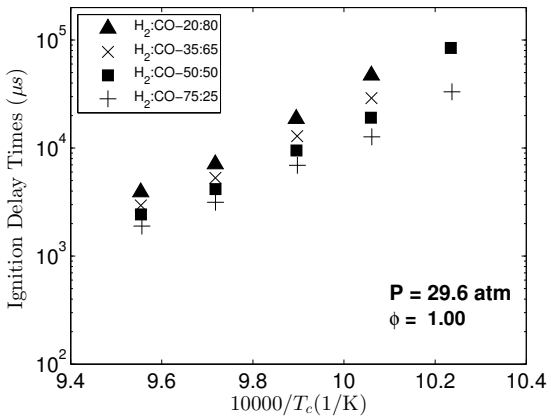

(f) T=975-1040 K

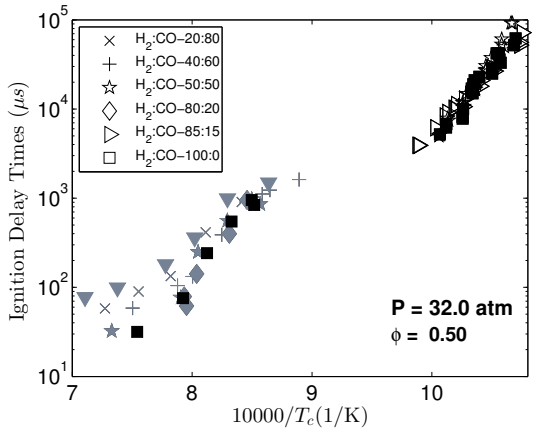

(g) T=880-1280 K

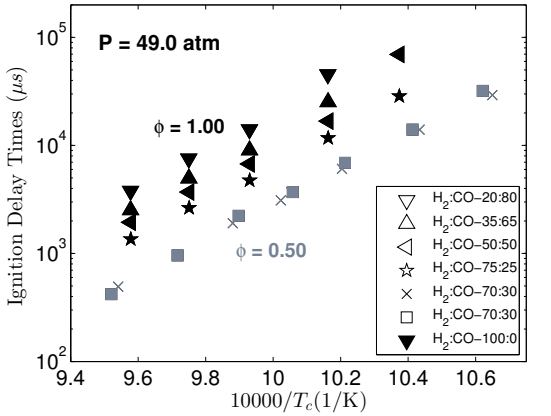

(h) T=950-1050 K

Figure 2.11: (e) Grey symbol: Mixture: $3.48\%(\alpha\mathrm{H_2}+(1-\alpha)\mathrm{CO})+3.47\%\mathrm{O_2}+93.06\%\mathrm{Ar}$, measured in a shock tube facility by [44]; Black symbol: Mixture: $17.36\%(\alpha\mathrm{H_2}+(1-\alpha)\mathrm{CO})+17.36\%\mathrm{O_2}+32.64\%\mathrm{N_2}+32.64\%\mathrm{Ar}$, measured in a RCM facility [44], (f) Mixture: $12.50\%(\alpha\mathrm{H_2}+(1-\alpha)\mathrm{CO})+6.25\%\mathrm{O_2}+18.25\%\mathrm{N_2}+63.125\%\mathrm{Ar}$, measured in a RCM facility by [47], (g) Grey symbol: Mixture: $1.00\%(\alpha\mathrm{H_2}+(1-\alpha)\mathrm{CO})+1.00\%\mathrm{O_2}+98.00\%\mathrm{Ar}$, measured in a shock tube facility by [43]; Open symbol: Mixture: $17.36\%(\alpha\mathrm{H_2}+(1-\alpha)\mathrm{CO})+17.36\%\mathrm{O_2}+32.64\%\mathrm{N_2}+32.64\%\mathrm{Ar}$, measured in a RCM facility by [44], (h) Black symbol: $12.50\%(\alpha\mathrm{H_2}+(1-\alpha)\mathrm{CO})+6.25\%\mathrm{O_2}+18.25\%\mathrm{N_2}+63.125\%\mathrm{Ar}$, measured in a RCM facility by [47]; Grey symbol: Mixture: $16.70\%(\alpha\mathrm{H_2}+(1-\alpha)\mathrm{CO})+16.70\%\mathrm{O_2}+30.00\%\mathrm{N_2}+36.70\%\mathrm{Ar}$, measured in a RCM facility by [49]. α refers to the mole fraction of $\mathrm{H_2}$ (continued).

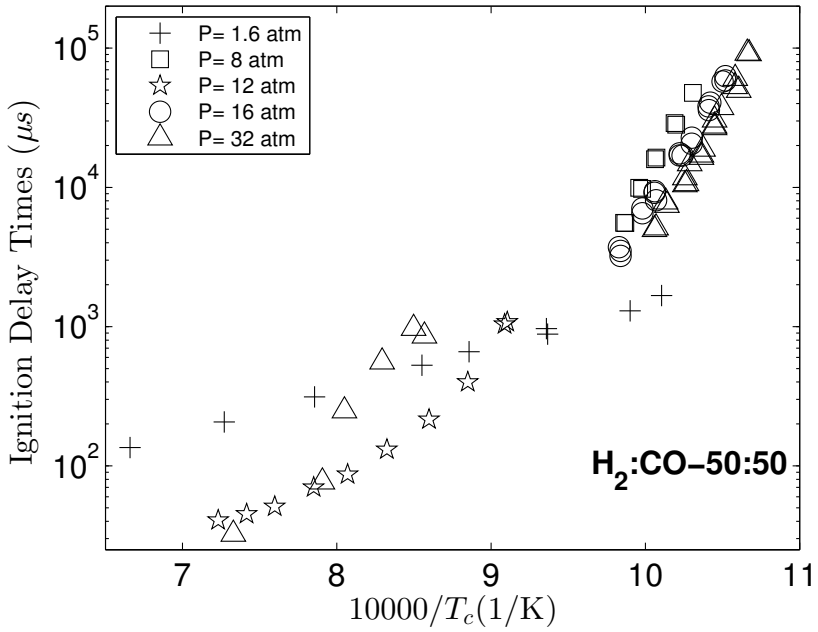

Figure 2.12: Effect of pressure on the ignition delay time for H_2:CO-50:50 at ϕ=0.5. Measured in shock tube [43] and RCM facility [44].

To better visualize the effect of pressure, the ignition delay time of H_2:CO-50:50 at P=1.6, 8, 12, and 32 atm are plotted in the same graph as depicted in Fig. 2.12. It shows that the measured ignition delay time of Syngas exhibits a very complex pressure dependence at high temperature (> 1050K). The ignition delay time at 1110 K<T<1250 K are shorter for 12 atm compared to 32 atm. At T $>$ 1250 K, the ignition delay time is shorter for 32 atm than 12 atm. Similar trend is also observed by Kèromnés et al. [44] for H_2:CO-5:95. The cross-over behavior is due to the competition between the chain branching reaction of $H + O_2 \rightarrow O + OH$ and the pressure dependent propagation reaction of $H + O_2(+M) \rightarrow HO_2(+M)$. The former reaction dominates in the high temperature region while the latter reaction dominates in the low temperature region. Besides, the latter reaction is pressure dependent and is more favorable to elevate pressure. Hence, the latter reaction inhibits the chain branching via the former reaction and leads to longer ignition delay time at high pressure.

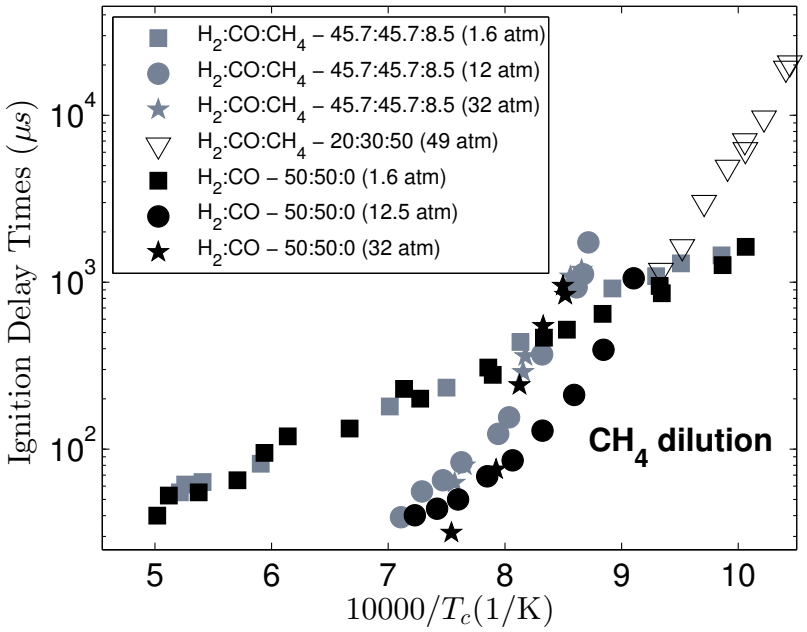

Figure 2.13: Measured ignition delay time of H_2/CO mixture diluted with methane at ϕ=0.5. Filled symbol: Grey-experiments conducted by [50]; Black-experiments conducted by [49]. Open symbol: experiments conducted by [49].

The data of Walton et al. [52] were collected from RCM facility, and they followed the trend established by the shock tube and flow reactors measurements reported by Petersen et al. [53]. However, the data of Walton et al. [52] appeared to be rather scatter, even after the data were normalized (refer therein [53]). Furthermore, the data of Walton et al. [52] remarkably deviated from the Mittal et al. [47] data trend at low temperatures. This might be due to the presence of reaction fronts during the ignition process [52]. Besides, presence of particles in the test volume was observed in the photographic image sequences showed in the studies of Walton et al. [52]. The presence of particles has been reported to have significant effect on the ignition process in rapid compression machine studies [74, 75]. The measured ignition delay time of Walton et al. [52] were normalized by assuming proportionality to P^{-1} and they were plotted along with the ignition delay time procured from high pressure flow reactor and shock tube facility by Peschke and Spadaccini [54] and Petersen et al. [53], respectively in Petersen et al. [53] paper. Interestingly,

the measured data began to substantially depart from the zero-dimensional, homogeneous constant internal energy (U) and volume (V) or constant enthalpy (H) and pressure (P) assumptions at temperature below 1050 K. The ignition delay time increased with the decreased of temperature, followed by reaching a plateau value at T<800 K (refer therein [53]). Nevertheless, Petersen et al. [53] and Walton et al. [52] studied the fuel-air mixtures without any dilution at low temperature and high pressure conditions which have led to non-ideal ignition behavior.

Mansfield and Wooldridge [76] analyzed the ignition studies conducted by Walton et al. [52] in a RCM facility for Syngas fuel blends at P=7.1-26.4 atm, temperature from T= 855-1051 K, and equivalence ratio spanning 0.1 to 1.0. They found that the high speed imaging of chemiluminescence captured by Walton et al. [52] showed spatial features to the ignition of the test gas mixtures in majority of their experiments. This implies that the ignition delay time for T= 855 - 1051 K are in the weak ignition regime for the Syngas fuel blend considered by Walton et al. [52]. Chaos and Dryer [59] also substantiated that there existed a weak ignition region at low reflected shock temperature, and their findings are in line with the work of Mansfield and Wooldridge [76]. Weak ignition occurs when localized ignition sites are formed, and eventually merging and transitioning to a contiguous combustion front. It is categorized as multidimensional and non-uniform process [77, 78]. Furthermore, the existence of weak and strong ignition was substantiated by Blumenthal et al. [79] and Wang et al. [80] by capturing the ignition process of 15% H_2 + 85% air mixture in a shock tube using Shadowgraphs and Schlieren techniques, respectively. Chaos and Dryer [59] also showed that at sufficiently high reflected shock temperature ($>$ 1050 K), there was a strong ignition and the reaction initiation started at a single locus point in the reflected region near the end-wall, rapidly transitioning to a uniform detonation wave. In addition, Davidson et al. [81] identified the presence of preignition pressure rise that caused the disparities between the measured and the predicted ignition delay time at low temperature region. The pressure rise in the shock tube experiments generally grow with time and is acute at low temperature [82]. These coupled effects will compress the test mixture prior to ignition leading to shorter ignition delay time [83]. To rec-

oncile the discrepancy between measurements and predictions at low temperature range, ignition delay time along with the pressure-time histories needed to be reported and modeled if the studies encompass weak and weak-strong regimes.

Figure 2.13 shows the effect of methane addition into Syngas mixture at P=1.6, 12, and 32 atm. It can be seen that at relatively low pressure (1.6 atm), the ignition delay time are almost identical with Syngas. However, noticeable effect can be seen for temperature below 1230 K, where addition of CH_4 tends to increase the ignition delay time. At P=12 atm, the ignition delay time increases by a factor of 6 with CH_4 addition at T=1150 K. The effect of CH_4 dilution at P=32 atm is only visible at temperature above 1220 K, and there is no appreciable difference at low temperature. Gersen et al. [49] also studied the effect of CH_4 addition on the ignition delay time of Syngas. They observed that the ignition delay time of $H_2/CO/CH_4$ mixture and H_2/CO mixture were almost indistinguishable for P= 20-70 bar at T=1010 K. The findings of Gersen et al. [49] contradicted the conclusion drawn from Fig. 2.13, where the ignition delay time increases with the addition of CH_4 at P=12 atm across the entire temperature tested by Mathieu et al. [50]. This is due to the temperature range adopted by the two studies are different. Gersen et al. [49] performed the experiments at temperature ranging from 950-1070 K while Mathieu et al. [50] conducted their experiments at temperature ranging from 1100-1430 K. In addition, Mathieu et al. [50] discovered that the effect of CH_4 addition vanished at temperature below 1220 K for high pressure (P=32 atm). Furthermore, Gersen et al. [49] reported an interesting observation that the ignition delay time of $H_2/CO/CH_4$-30:20:50 was identical to CH_4/H_2-70:30 for both rich and lean conditions. This indicates that CH_4 behaves similarly to CO as an inhibitor in the fuel mixture.

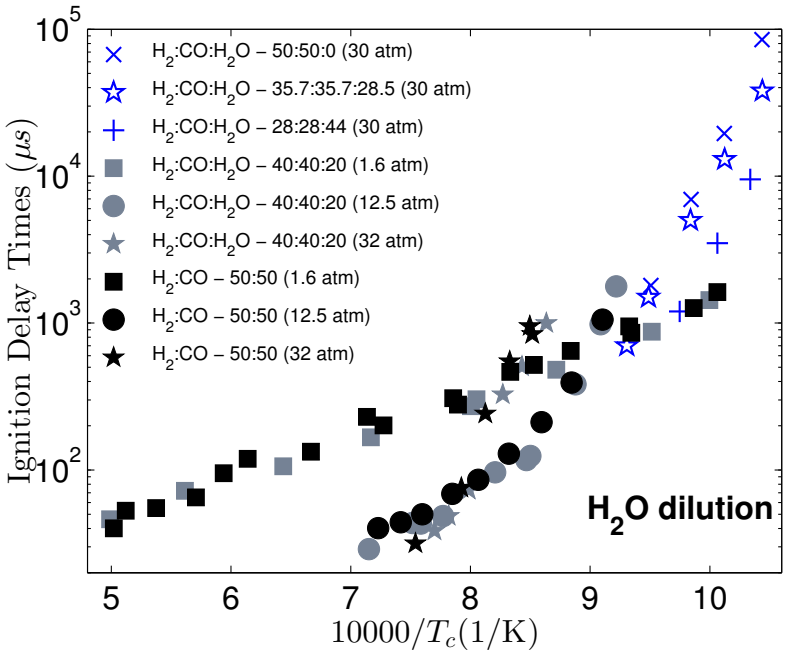

Figure 2.14: Measured ignition delay time of H_2/CO mixture diluted with H_2O at ϕ=0.5. Filled symbol: Grey-experiments conducted by [50]; Black-experiments conducted by [49]. Blue symbol: experiments conducted by [55].

In contrary, the ignition delay time of Syngas with and without CO_2 addition are identical from low (1.6 atm) to high (32 atm) pressure and across the entire range of temperature, as depicted in Fig. 2.15. However, the conclusion that CO_2 dilution has no impact on the ignition delay time can not be drawn from the Fig. 2.15 because Mathieu et al. [50] diluted their fuel mixture with only 14% of CO_2. Hence, Syngas diluted with higher CO_2 concentration at high pressure is at present ambiguous. Although Vasu et al. [51] diluted their fuel mixture with 54.4% of CO_2, they only investigated low pressure range (1.1-2.59 atm) and did not compare their results with Syngas. Therefore, specific conclusions can not be drawn between these two studies and more studies on CO_2 dilution is warranted as the CO_2 mole fraction in actual Syngas can be as high as 29% [29].

Das et al. [55] and Mathieu et al. [50] studied the ignition delay time of moist Syngas at elevated

pressure. Das et al. [55] performed their experiments at P=30 atm and T=980-1110 K, while Mathieu conducted their measurements at various pressure ranging from 1.6-32 atm and at higher temperature (10050-2030 K) than of Das et al. [55]. Their measured ignition delay time are depicted in Fig. 2.14. Similar to CO_2, H_2O dilution does not have much impact on the ignition delay time at low pressure ($<$12.5 atm). However, at P=32 atm, water addition exhibits a small, promoting effect and shorten the ignition delay time compared to Syngas. This indicates that water dilution increases the reactivity of the mixture at P=30 atm and at low temperature. The observed behavior is due to HO_2/H_2O_2 reactions become very important [47, 63]. Besides, the important chain branching reaction of $H_2O_2(+M) \rightarrow OH + OH(+M)$ has considerable effect on the reactivity of the mixture at these conditions. Previous studies [80, 55] showed that the ignition delay time of moist pure H_2 mixture at T$<$ 1330 K and P$<$9.8 atm exhibited opposite effect than the observed trend in Fig. 2.14, where the addition of H_2O increased the ignition delay time at low pressure and temperature. Therefore, additional of water has two opposite effects under different conditions; under high pressure and low temperature, the water addition increases the reactivity and decreases the ignition delay time, and at low temperature and at low pressure, water addition results in longer ignition delay time. Furthermore, water effect is only profound at low temperature regime and has negligible effect at high temperature.

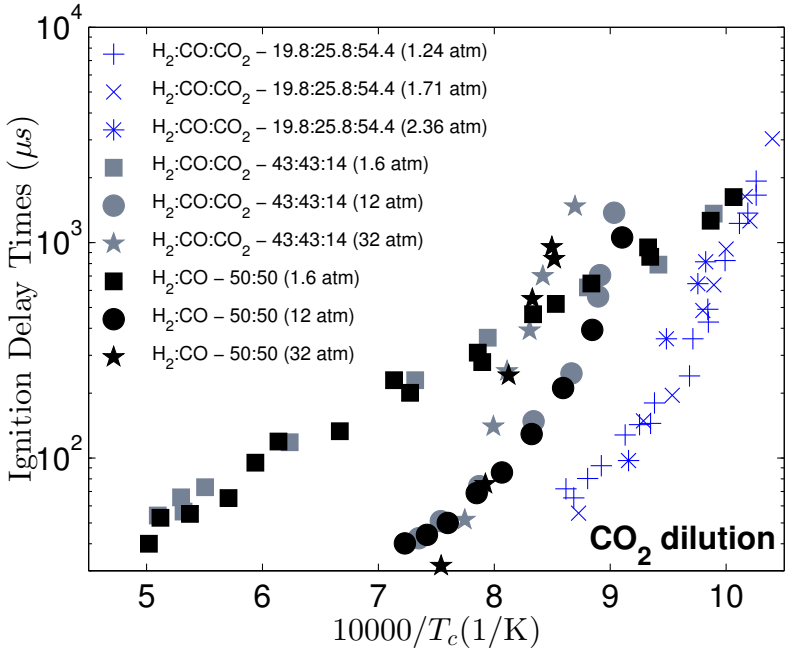

Figure 2.15: Measured ignition delay time of H_2/CO mixture diluted with CO_2 at ϕ=0.5. Filled symbol: Grey-experiments conducted by [50]; Black-experiments conducted by [49]. Blue symbol: experiments conducted by [51].

Since impurities such as ammonia (NH_3) can also be presence in Syngas mixture through gasification process [84], Mathieu et al. [50] investigated the impact of NH_3 dilution on the ignition delay time of Syngas. Figure 2.16 shows the ignition delay time of $H_2/CO/NH_3$ mixture with 200 ppm of ammonia at P=1.6, 12.5, and 32 atm. At low pressure (1.6 atm), NH_3 addition slightly increases the reactivity of the fuel mixture compared to Syngas across the entire range of temperature tested. However, at P=12 atm, there is no visible influence on the ignition delay time for temperature below 1315 K. Negligible effect of NH_3 addition can also be observed at P=32 atm over the entire range of temperature tested. Mathieu et al. [50] further analyzed the observed behavior and discovered that NH_3 did not react before the ignition started nor did it interacted with the radical pool. In addition, they found that ammonia has low reactivity, hence, NH_3 did not have direct impact on ignition delay time. However, they discovered that approximately 1/3 to 1/2 of NH_3 that was presence in the fuel mixture was converted to NO during the ignition process.

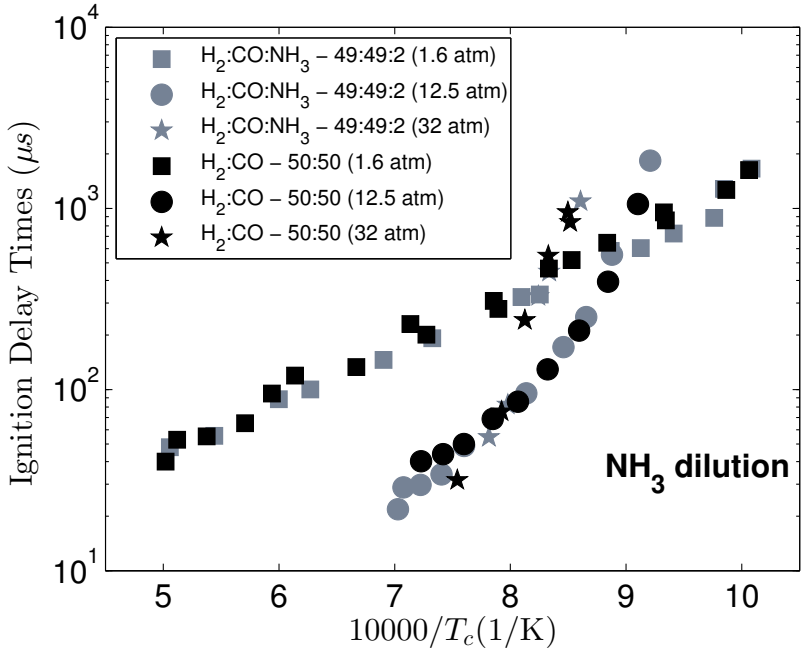

Figure 2.16: Measured ignition delay time of H_2/CO mixture diluted with NH_3 at ϕ=0.5. Filled symbol: Grey-experiments conducted by [50]; Black-experiments conducted by [49].

CO_2, CH_4, and H_2O addition effects on the ignition delay time have been investigated over the past few years, but these effects are mostly studied individually, as discussed above. To date, Mathieu et al. [50] is the only one that studied the ignition delay time of actual Syngas mixture that takes into account all the dilution (CO_2, H_2O, CH_4, and NH_3) that might exist in actual Syngas chemical composition, as depicted in Fig. 2.17. The composition of the actual Syngas used in their studied was determined by averaging the components of 23 actual Syngas mixtures found in literature [85, 86, 87, 88]. It can be seen from Fig. 2.17 that the addition of CO_2, CH_4, and H_2O dramatically shorten the ignition delay time compared to Syngas, especially at higher pressure and temperature below 1230 K. In addition, with the CO_2, CH_4, and H_2O presence in the fuel mixture, NH_3 addition has negligible effect on the ignition delay time across the entire range of temperature and pressure investigated, as depicted in Fig. 2.17. This strongly implies that the simple Syngas mixture is not fully adequate to represent a practical Syngas chemical kinetics.

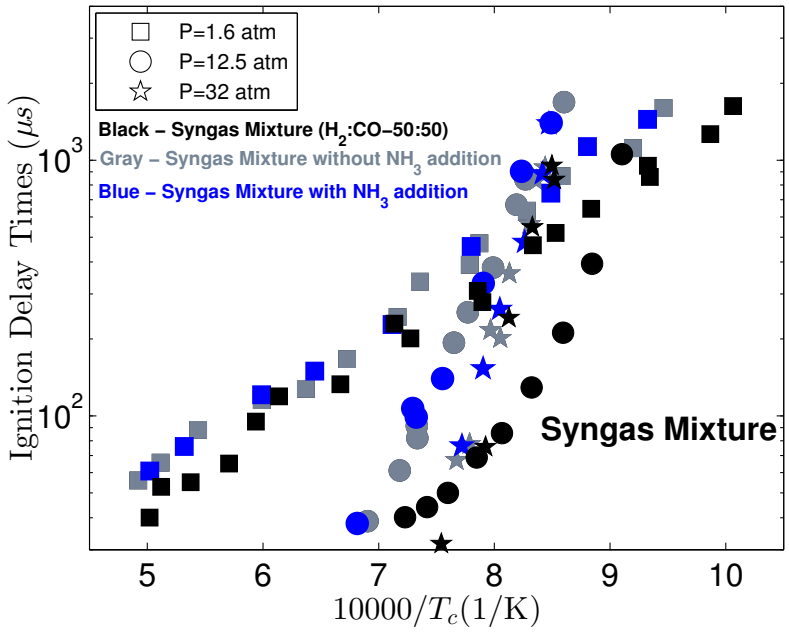

Figure 2.17: Measured ignition delay time of practical Syngas mixture at ϕ=0.5 diluted with and without NH_3. Black symbol: H_2:CO-50:50 without any dilution; Grey symbol: mixture-H_2:CO:CH_4:CO_2:H_2O-28.5:28.5:8.57:15.13:19.3 without NH_3 addition; Blue symbol: mixture-H_2:CO:CH_4:CO_2:H_2O:NH_3-27.95:27.95:8.5:14.85:18.95:1.8 with NH_3 addition. Measurements conducted by [50].

2.4 Concluding Remarks

A large data set of experimental data is available for the combustion of Syngas (H_2/CO) with various H_2/CO concentration. However, studies on Syngas mixed with other gases such as CO_2 and H_2O are still very limited. Besides, there is no experimental data available for the study of laminar flame speed of Syngas diluted with CH_4 and/or NH_3. New measurements on the laminar flame speed of Syngas diluted with other gaseous compositions at elevated pressure would helps us further understand Syngas combustion kinetics. Ignition delay time of H_2/CO diluted with higher percentage of CO_2 ($> 14\%$) at elevated pressure is warranted to draw a conclusion that

the addition of CO_2 has no impact on the ignition delay time. More data that represents practical Syngas mixtures are needed to further validate and improve current kinetics models, although lots of progress have been made throughout these years.

Chapter 3

Comprehensive Comparison of Chemical Kinetics Mechanisms

Abstract

The performance of the most commonly used chemical kinetics mechanisms is compared against a large set of experimental data, accumulated for syngas mixtures diluted with other gases such as CO_2, H_2O, N_2, and CH_4. These dilutes are pertinent to syngas/biogas mixtures and could have significant effects on the combustion characteristics. The laminar flame speed and ignition delay are used as quantitative metrics to compare the simulation predictions with the experimental data. The experimental data include ignition measurements obtained from shock tubes and rapid compressions, and flame speed measurements obtained from spherical bombs as well as counterflow configurations covering a wide range of temperature, pressure, and equivalence ratios. The mixture compositions are systematically categorized in this study. After an exhaustive comparisons, it is found that the NUIG2013 mechanism is in closest agreement with the measured ignition delay and laminar flame speed for the investigated mixtures. However, the predictions deviated significantly from the measured ignition delays for the $H_2/CO/CO_2$, $H_2/CO/CH_4$, and $H_2/CO/CH_4/CO_2/H_2O$

mixtures. We performed a sensitivity analysis on the ignition delay time of the $H_2/CO/CO_2$, $H_2/CO/CH_4$, and $H_2/CO/CH_4/CO_2/H_2O$ mixtures, using the NUIG2013 mechanism to identify the reactions that are responsible for the deviations. We found that by adopting a much lower rate constant expression [$k_0(CO_2) = 8.82 \times 10^{19} \times T[K]^{-1.40}(cm^6/mol^2/s)$] for $H + O_2(+CO_2) = HO_2(+CO_2)$ (R2), the NUIG2013 mechanism could accurately predict the ignition delay time of the $H_2/CO/CO_2$ mixture at low pressures (P = 1.24 - 2.36 atm) and low temperatures ($<$ 1025 K) range. A new rate constant expression [$k_3 = 2.3 \times 10^8 \times T[K]^{1.40}\, exp(-2850/T)(cm^3/mol/s)$] for the $CH_4 + OH = CH_3 + H_2O$ (R3) reaction in the NUIG2013 mechanism is required to reconcile the discrepancy observed between the measured and simulated ignition delay time of the $H_2/CO/CH_4$ and $H_2/CO/CH_4/CO_2/H_2O$ mixtures at P = 32 atm. In addition, the newly fitted rate constant expression for (R3) improved the performance of the NUIG2013 mechanism in predicting the ignition delay of H_2/CH_4 at P = 5, 10, and 20 atm. More importantly, the modifications made to the reactions (R2) and (R3) did not substantially affect the NUIG2013 mechanism's excellent predictions of the flame speed. Hence, it is recommended that the rate constant expressions for (R2) and (R3) be incorporated into the NUIG2013 mechanism for any study of the combustion characteristics of biogas/syngas mixtures.

3.1 Background

As mentioned in Chapter 2, the hydrogen concentration in a syngas mixture is highly sensitive to the types of feedstock and the gasification processes used, such that it can vary from 25% to over 80% [89]. This variation adversely affects the flame shape, emissions, blow-off and flashback limits, and most importantly, the combustion instability. This has posed a great challenge to gas turbine manufacturers in that combustion chambers must be able to support a fuel with such a variation in its hydrogen content. Therefore, syngas-/methane-based fuel blends are of great interest to gas turbine manufacturers [23]. In addition, previous studies have demonstrated that the

addition of hydrogen to methane-based fuel could further mitigate both CO and NO_x emissions [24, 25, 26, 27]. This outcome is most likely caused by the high concentration of radicals in the presence of H_2, where it increases the reactivity of the methane mixture [28].

To the best knowledge of the authors, there has been only one study [90] that has investigated the flame speed of syngas/biogas blends ($H_2/CO/CH_4/CO_2$). Hence, in this chapter, we included most of the experimental data discussed in Chapter 2 for syngas mixtures and collected several fuel mixtures that are pertinent to biogas mixtures, and summarized them in Table 3.1, to evaluate the capabilities of several of the most commonly used kinetics mechanisms in simulating the ignition delay time and the laminar flame speed. Diluents such as CO_2, H_2O, CH_4, and N_2 were also addressed by this study, because syngas derived through gasification technique not only contains H_2 and CO, but also other species.

The flame speed is a critical parameter affecting combustion because it is dependent on the fundamental information related to the reactivity, diffusivity, and exothermicity of the fuel [91]. Therefore, for this study, the laminar flame speed was used as a quantitative metric to compare the simulation prediction with the experimental data. In addition, it serves as a basis for determining the turbulent flame speed, which is directly related to the flashback and blowoff issues. Therefore, it is very important to obtain an accurate prediction of the laminar burning velocities of biogas/syngas mixtures when designing and optimizing combustion chambers [91]. Similarly, the auto-ignition delay is another crucial parameter that is chosen to evaluate the performance of kinetics schemes because it has been widely used for benchmarking the validity of combustion chemistry models. Moreover, it provides a useful insight into the self-ignition threshold and the flashback propensity, which could have drastic effects on the design of the gas turbine combustors and also the hazard assessments, due to the rapid flame propagation of hydrogen.

The main objective of this chapter was to identify potential chemical kinetics mechanism that could be used to accurately predict the combustion characteristics of biogas/syngas fuel blends. This comparison was made using a very comprehensive set of published experiments that used

techniques such as jet-wall stagnation configurations, rapid compression machines, shock tubes, and different types of measurements. This chapter also systematically categorized all of the measured flame speeds and ignition delays for each of the tabulated fuel mixtures, as depicted in Table 3.1. Nonetheless, results of this chapter will help researchers in the selection of a mechanism that is best suited to the chosen initial conditions and fuel mixture compositions. Furthermore, a sensitivity analysis was conducted whenever there was a large discrepancy between the measured and simulated laminar flame speed and/or ignition delay resulting from a potential chemical kinetics mechanism to further elucidate which reaction(s) was/were responsible for the discrepancy. New rate constants expression were proposed for the said reaction to reconcile the observed discrepancy.

3.2 Modeling Approach

Numerical simulations were performed using the CANTERA reacting flow package [106]. Shock tube experiments were simulated by assuming a constant volume and adiabatic conditions. The simulated ignition delay time results were computed as described in the respective publications, e.g., based on the maximum slope of the pressure profile or based on the measurement of the chemiluminescence of $OH*$. There have been several studies that have measured the ignition delay time based on the maximum concentration of the excited radical OH*. Hence, the OH* sub mechanism developed by Kathrotia et al. [107] is incorporated into all the mechanisms considered in this study except for the NUIG2013 mechanism, so as to match the experimental results. Unfortunately, for this study, the published experimental data did not have the pressure trace profile published along with the measured ignition delay time; therefore, the facility effects could not be taken into consideration in this study. Nevertheless, the facility effects only affect those long ignition delays above 1 - 2 ms. For short ignition delays ($<$ 1 ms), the constant volume and adiabatic assumptions remain relevant. For completeness, the ignition delay time data points above 1 - 2

Table 3.1: Summary of the mixture combinations and the experimental conditions considered.

Figure Number	Mixture	Experimental conditions			Ref.
		ϕ	P [atm]	T [K]	
		Laminar Flame Speed			
1 - 3	H_2/CO	0.5 - 5.0	1	300	[39, 36, 92, 93, 94]
		0.6 - 4.0	5 - 10	300	[43, 35, 36]
		0.7 - 3.5	5 - 40	300	[36, 44]
4 - 6	$H_2/CO/CO_2$	0.4 - 1.0	1 - 3	303 - 373	[91]
		0.8 - 2.0	1	303	[95]
		0.4	1 - 2	300	[96]
7 - 8	$H_2/CO/H_2O$	0.4 - 0.9	1	323	[97]
		1.0	1	400	[42]
9	$H_2/CO/N_2$	0.5 - 1.0	1 - 5	303 - 373	[91]
10 - 11	H_2/CH_4	1.0	1	300	[98, 99, 100]
		0.6 - 2.0	1 - 5	298 - 450	[99, 101, 102, 103, 100]
12	$H_2/CO/CH_4/CO_2$	0.7 - 1.0	1	300	[90]
		Ignition Delay Time			
14	H_2/CO	0.5	1.6 - 32.0	990 - 2000	[104]
15	$H_2/CO/H_2O$	0.5	1.6 - 32.0	995 - 2010	[104]
16	H_2/H_2O	1.0	10.0 - 70.0	907 - 1048	[105]
17 - 18	$H_2/CO/CO_2$	0.5	1.6 - 32.0	1005 - 1965	[104]
		1.0	1.24 - 2.36	952 - 1091	[51]
19	$H_2/CO/CO_2/CH_4/H_2O$	0.5	1.6 - 32.0	1050 - 2030	[104]
20	$H_2/CO/CH_4$	0.5	1.6 - 32.0	1010 - 1920	[104]
21	H_2/CH_4	0.5	5.0 - 20.0	1050 - 2000	[28]

ms are also simulated using the constant volume and adiabatic assumptions without correcting the results for the facility effects. Rapid compression machine experiments were simulated using the wall velocity function in CANTERA [106], to account for the effects of compression and heat loss. Das et al. [97] are the only authors to have published their volume-time histories along with the measured ignition delay time for H_2/H_2O mixtures.

Laminar flames were simulated using the FreeFlame class included in the CANTERA package [106]. The FreeFlame class is similar to the PREMIX code [112] of the CHEMKIN-II package. One of the main differences between the PREMIX [112] and FreeFlame of CANTERA [106] is the discretization schemes. The jet-wall stagnation flames were simulated using the premixed stagnation flame code of the CANTERA reacting flow software package [106], which is also identical to the CHEMKIN-II package [113]. The boundary conditions specified in the simulation of the jet-wall stagnation flame are taken directly from the experimental measurements, allowing a direct comparison of the measured and simulated profiles. For more information on the stagnation flames simulation methodology, refer to [90]. In all of the laminar flame speed simulations, multicomponent diffusion and Soret effects are included, as we have found that these effects have a significant impact on the calculated laminar flame speed, especially for H_2/CO mixtures without any dilution at P = 1 atm. The converged solution is obtained for a large number of grid points (approximately 400) by considering a gradient and curvature of 0.1 (see Appendix D.4 in [114]). The standard definition of equivalence ratio (ϕ) is adopted in this work and it is defined as follows:

$$\phi = \frac{(n_{fuel}/n_{oxygen})_{act}}{(n_{fuel}/n_{oxygen})_{st}}$$

where *n* represents the number of moles, and the suffix *act* and *st* represent actual mixture and stoichiometric mixture, respectively.

The combustion mechanisms considered in this study are listed in Table 3.2 and the composition of the mixtures is expressed in molar percentage unless otherwise specified. Only the most re-

Table 3.2: Chemical kinetics mechanisms considered. All mechanisms can handle N_2 bath gas and the table indicates the capability of the mechanism to handle Ar and He bath gases. The grand mean for all mechanisms are provided for the flame speed and the ignition delay time cases: [A] - Laminar flame speed of syngas, all diluents except He and CH_4; [B] - Laminar flame speed of syngas, all diluents except CH_4; [C] - Laminar flame speed of syngas, all diluents except He; [D] - Laminar flame speed of syngas, all diluents; [E] - Ignition delay time of syngas, all diluents except CH_4; [F] - Ignition delay time of syngas, all diluents. The minimum value in each column is indicated in bold.

ID	Species # (reaction #)	Ar/He	Ref	Legend	Grand mean value ($\bar{\psi}$) for each case [%]					
					[A]	[B]	[C]	[D]	[E]	[F]
GRI1999	53 (325)	x/-	[108]		12.96	-	10.86	-	126.10	84.78
Li2007	21(93)	x/x	[109]		**10.13**	**10.47**	9.46	9.67	158.93	121.72
Davis2005	14 (38)	x/x	[73]		11.02	11.03	-	-	66.99	-
USC2007	111(784)	x/-	[110]		10.66	-	9.95	-	70.69	**49.21**
UCSD2014	50(30)	x/x	[111]		13.75	13.82	11.37	11.61	**52.73**	50.37
Sun2007	15 (48)	x/x	[36]		11.01	10.85	-	-	122.76	-
NUIG2013	325(2067)	x/x	[1]		11.30	11.19	**9.39**	**9.40**	81.00	76.86
NUIG_V1	325(2068)	x/x	Current study		11.15	11.24	9.86	9.91	32.13	54.19
NUIG_V2	325(2068)	x/x	Current study		9.26	9.42	8.41	8.52	32.81	55.48
NUIG_V3	325(2068)	x/x	Current study		11.15	11.24	9.74	9.86	32.11	28.32

cent mechanism was considered, when several mechanisms had been devised by the same research group. For instance, the research group at the University of California, had devised several mechanisms, but only the most recent and updated mechanism (UCSD2014) was considered in this study. The NUIG_V1, NUIG_V2, and NUIG_V3 mechanisms are all variants of the NUIG2013 mechanism (see the section explaining the sensitivity analysis for a detailed explanation of the modifications made to the NUIG2013 mechanism). The agreement between experimental results and simulation results is investigated using the following objective functions:

$$\bar{\mathrm{E}}_{\mathrm{i}} = \frac{1}{\mathrm{N_i}} \sum_{\mathrm{j=1}}^{\mathrm{N_j}} \left| \frac{\mathrm{Y_{sim,ij}} - \mathrm{Y_{exp,ij}}}{\mathrm{Y_{exp,ij}}} \right| \times 100\%$$

$$\bar{\bar{\boldsymbol{\varepsilon}}} = \frac{1}{\mathrm{N}} \sum_{\mathrm{i=1}}^{\mathrm{N}} \bar{\mathrm{E}}_{\mathrm{i}}$$

$$\bar{\bar{\boldsymbol{\psi}}} = \frac{1}{\mathrm{G}} \sum_{\mathrm{i=1}}^{\mathrm{G}} \bar{\mathrm{E}}_{\mathrm{i}}$$

Here, $\bar{\mathrm{E}}_{\mathrm{i}}$ is the average absolute relative error values, $\bar{\bar{\boldsymbol{\varepsilon}}}$ is the overall mean, and $\bar{\bar{\boldsymbol{\psi}}}$ is the grand mean. N represents the number of datasets in a figure, $\mathrm{N_i}$ denotes the number of data points in the ith dataset, and G represents the number of datasets in a considered case. The values $\mathrm{Y_{sim,ij}}$ and $\mathrm{Y_{exp,ij}}$ correspond to the calculated and the measured result for the jth data point, respectively, in the ith dataset. If there was more than one measured value for a given data point, the mean of the experimental data ($\bar{\mathrm{Y}}_{\mathrm{exp,ij}}$) was used instead of $\mathrm{Y_{exp,ij}}$. For brevity, the average absolute relative error ($\bar{\mathrm{E}}_{\mathrm{i}}$) and the overall mean ($\bar{\bar{\boldsymbol{\varepsilon}}}$) are graphed and tabulated in the supplementary information. Only the grand mean ($\bar{\bar{\boldsymbol{\psi}}}$) values for the six cases considered in this study are tabulated in the Table 3.2.

3.3 Results and discussion

3.3.1 Laminar flame speed

H_2/CO mixtures

Figure 3.1 compares the simulation results with the measured laminar flame speed of H_2:CO-5:95 and H_2:CO-50:50 mixtures under standard conditions. Under lean conditions ($\phi < 1.0$), all of the mechanisms' predictions are in reasonably good agreement with one another and with the experimental data. However, the UCSD2014 mechanism predicts a slightly higher flame speed compared to the other mechanisms for $\phi < 2.5$. The predicted flame speed results differ substantially from one another at fuel rich conditions ($\phi > 1.0$), with recent mechanisms such as NUIG2013 and UCSD2014 predicting the highest flame speed at ϕ = 1.5 – 3.0. By computing the overall mean

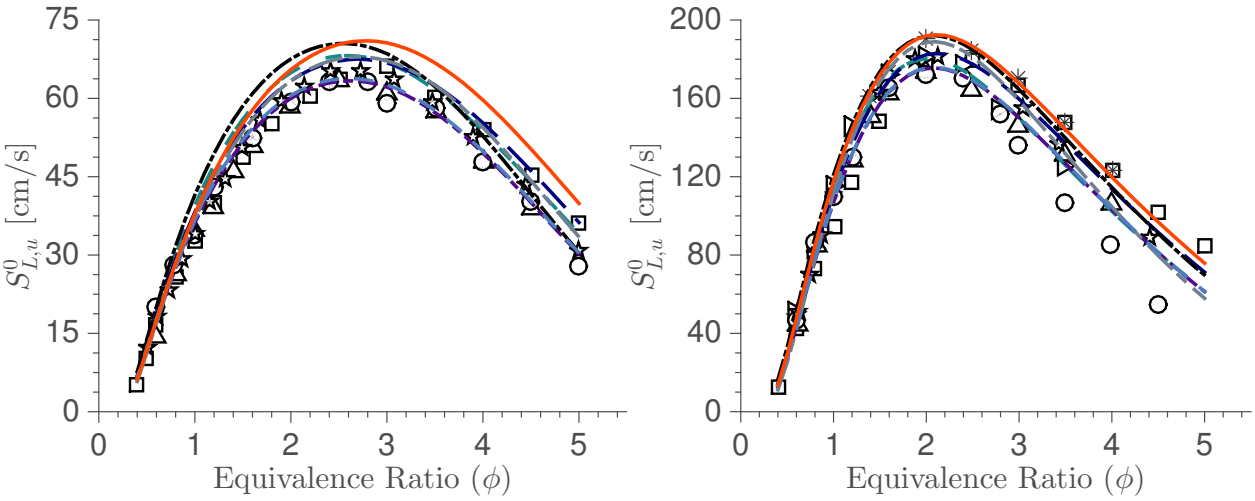

(a) H_2:CO - 5:95 (b) H_2:CO - 50:50

Figure 3.1: Measured and calculated laminar flame speed versus equivalence ratio for H_2/CO fuel mixture at P = 1 atm and T = 300 K. Symbols represent the experimental data: (□) - Burke et al. [39], (△) - Sun et al. [36], (◯) - Hassan et al. [92], (⋆) - McLean [93], (▷) - Prathap et al. [94]. Lines show predictions from the different kinetics models, see Table 3.2 for legend.

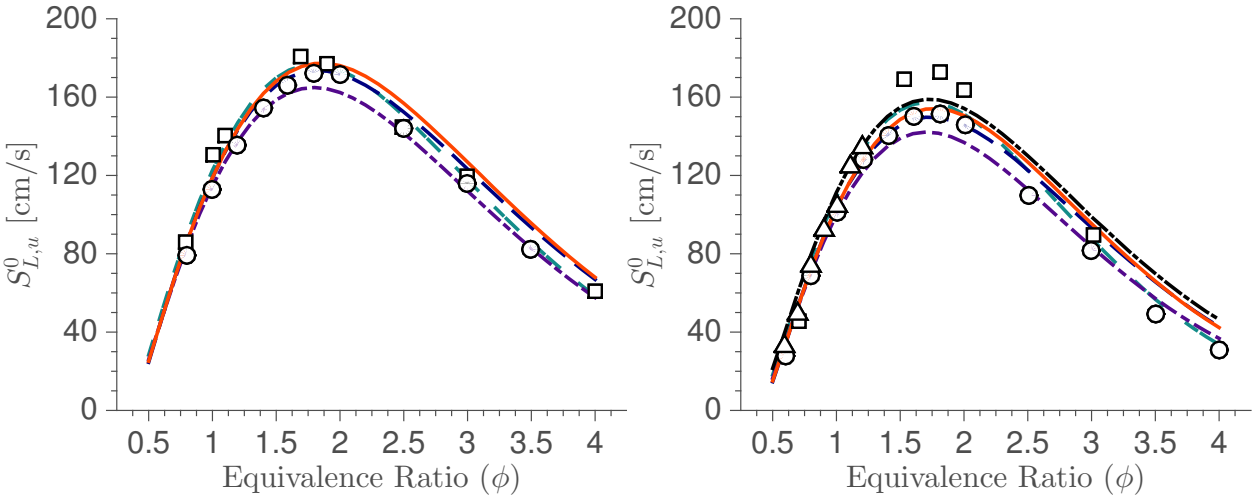

(a) P = 5 atm

(b) P = 10 atm

Figure 3.2: Measured and calculated laminar flame speed versus equivalence ratio for H_2:CO-50:50 fuel mixture with He:O_2= 7 by 1 mole at T = 300 K. Symbols represent experimental data: (□) - Kerji et al. [43], (△) - Natarajan et al. [35], (◯) - Sun et al. [36]. Lines show predictions from the different kinetics models, see Table 3.2 for legend.

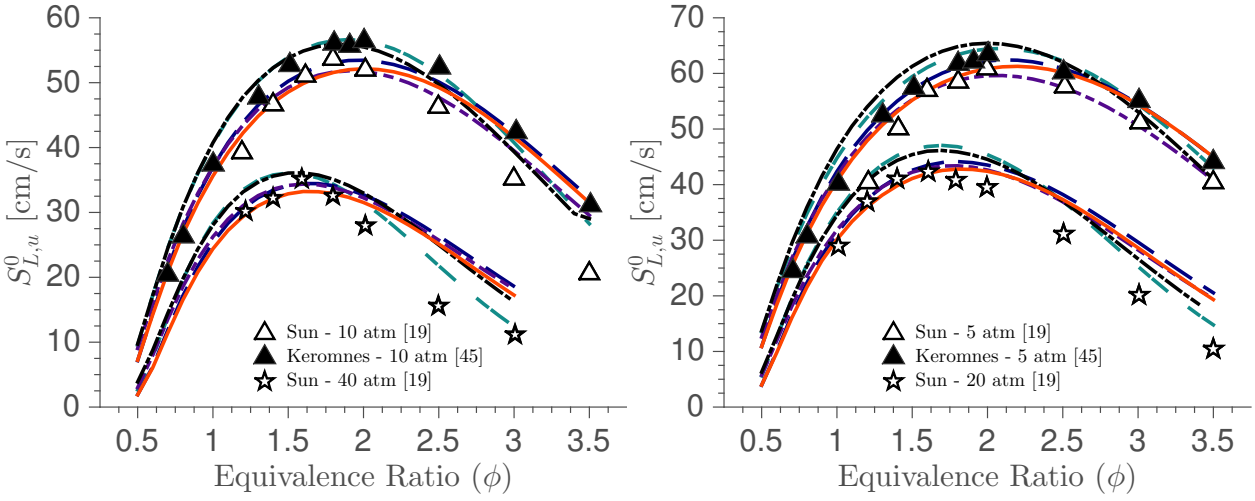

(a) P = 10 and 40 atm

(b) P = 5 and 20 atm

Figure 3.3: Measured and calculated laminar flame speed versus equivalence ratio for H_2:CO-5:95 with He:O_2= 7 by 1 mole at elevated pressures (T = 300 K). Symbols represent experimental data. Lines show predictions from the different kinetics models, see Table 3.2 for legend.

for each mechanism, the Davis2005 and USC2007 mechanisms were found to yield the lowest overall mean value of approximately 5%, while the GRI1999, Li2007, and Sun2007 mechanisms have overall mean values ranging from 7% to 8% (see Supplementary Table A.1). Interestingly, the recently published chemical kinetics mechanisms such as the NUIG2013 and UCSD2014 mechanisms give the highest overall mean values of 10.04% and 12.61%, respectively, for Fig. 3.1. Nevertheless, it is worth noting here that the experimental data shown in Fig. 3.1 appears rather scattered; therefore, the flame speed predicted by all the mechanisms are well within limit of experimental uncertainty.

At elevated pressures, all of the mechanisms were found to be able to capture the effect of pressure on the laminar flame speed of H_2/CO - 50:50 and 5:95, as shown in Figs. 3.2 and 3.3. In terms of accuracy, the Sun2007 mechanism has the best performance for H_2/CO - 50:50 mixture at P = 5 and 10 atm (see Figs. 3.2(a) and 3.2(b)), as it yields the lowest average relative error values, as evidenced in supplementary Figs. A.2(a) and A.2(b). However, for the H_2/CO - 5:95 mixture shown in Fig. 3.3, the Sun2007 mechanism's performance deteriorates slightly while the NUIG2013 mechanism gives the lowest overall mean value of 12.05%, indicating that the NUIG2013 mechanism offers the highest level of performance (see Supplementary Table A.1). The simulation results for the GRI1999 and USC2007 mechanisms are not included in Figs. 3.2 and 3.3 because the helium bath gas was not incorporated into their models. Therefore, all of the models considered in this study are recommended for the study of the flame speed of H_2/CO at atmospheric pressure, and only the Sun2007 and NUIG2013 mechanisms are recommended for the study of the flame speed of H_2/CO at elevated pressures.

$H_2/CO/CO_2$ mixtures

Figure 3.4 shows the flame speed calculated using the chemical kinetics mechanisms for $H_2/CO/CO_2$ - 35:35:30 mixture at elevated pressures and temperatures. Under the standard conditions (P = 1 atm, T = 303 K; Fig. 3.4(a)) and elevated conditions (P = 3 atm, T = 373 K; Fig. 3.4(c)), the

UCSD2014 mechanism performs remarkably well at predicting the laminar flame speed across all of the equivalence ratios investigated by Hu et al. [91], as evidenced in Figs. 3.4(a), 3.4(c), supplementary Figs. A.4(a), and A.4(c). However, at elevated temperatures (P = 1 atm, T = 373 K; Fig. 3.4(b)), the performance of the UCSD2014 mechanism deteriorates slightly, and the Li2007 and Sun2007 mechanisms produce the lowest average relative errors of approximately 6.5%, in-

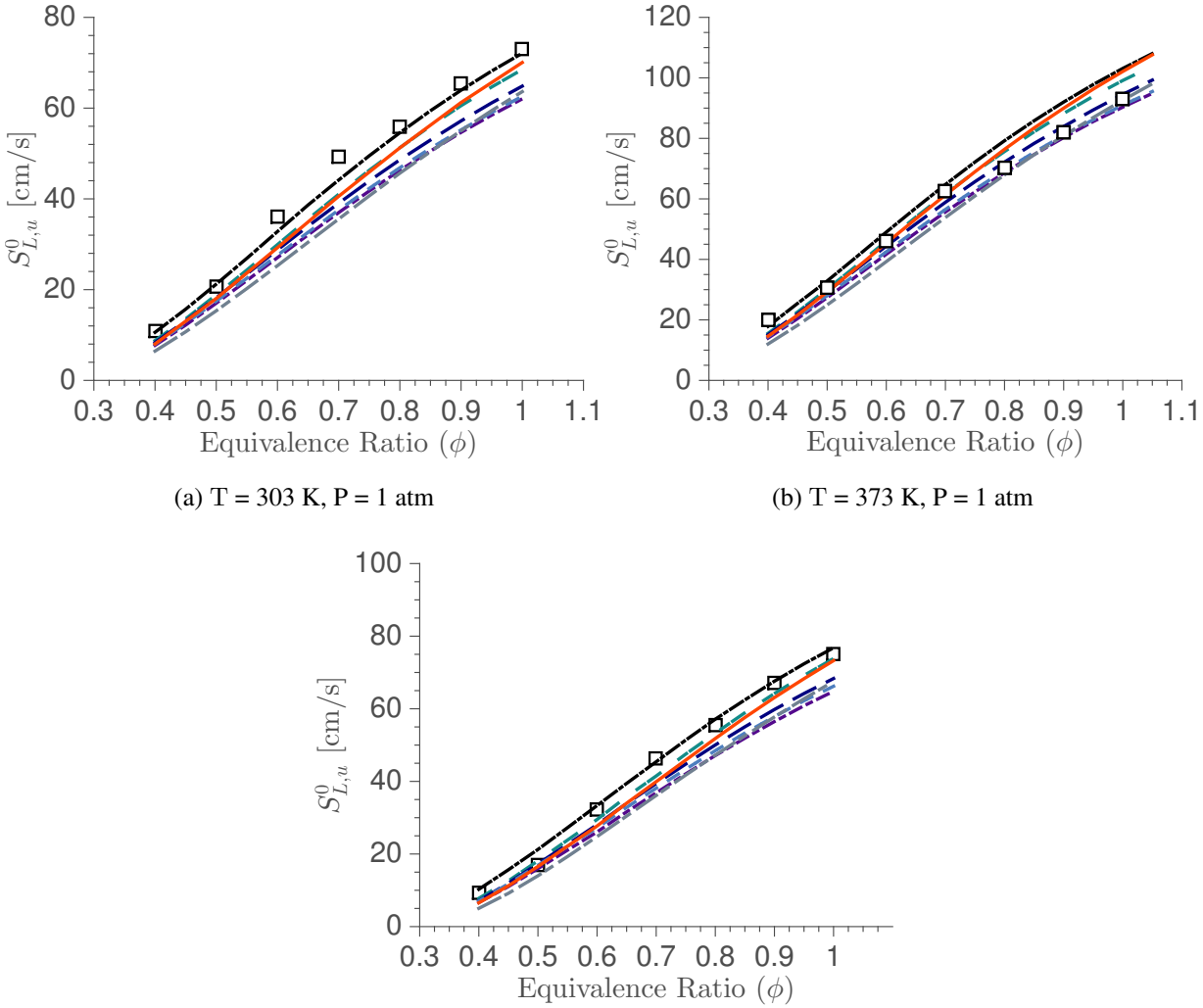

(a) T = 303 K, P = 1 atm

(b) T = 373 K, P = 1 atm

(c) T = 373 K, P = 3 atm

Figure 3.4: Measured and calculated laminar burning velocities of $H_2/CO/CO_2$-35:35:30 fuel mixture at P = 1-3 atm and T = 303-373 K. The experimental data were obtained from Hu et al. [91]. Lines show predictions from the different kinetics models, see Table 3.2 for legend.

dicating that the Li2007 and Sun2007 mechanisms offer the best performance for the respective experimental conditions.

Interestingly, for a higher CO_2 content (50%; Fig 3.5), the NUIG2013 mechanism performs extremely well when predicting the flame speed of the H_2/CO/CO_2 - 10:40:50 mixture at standard conditions, producing an average relative error of only 1.47% (see supplementary Fig. A.5(c)) across all of the equivalence ratios investigated by Kishore et al. [95], as shown in Fig. 3.5. However, for mixtures with a higher hydrogen content (H_2/CO/CO_2 - 25:25:50 and 40:10:50), the performance of the NUIG2013 mechanism declines significantly, while the Li2007 mechanism instead offers the best performance, as shown in supplementary Figs. A.5(a) and A.5(b).

Instead of using air as the oxidizer, Wang et al. [96] used pure oxygen as the oxidizer to study the oxyfuel combustion of $H_2/CO/CO_2$ mixtures at ϕ = 0.4, as depicted in Fig. 3.6. The percentage

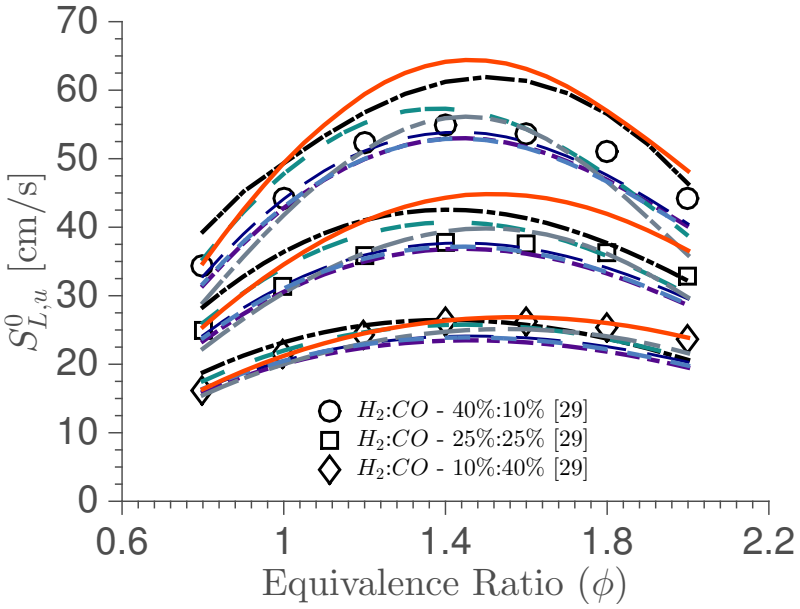

Figure 3.5: Measured and predicted adiabatic laminar burning velocity as a function of equivalence ratio for H_2/CO/CO_2 fuel mixture with H_2/CO ratios 80:20, 50:50 and 20:80 at 1 atm and 303 K. CO_2 is kept constant at 50% by volume. Experimental data were obtained from Kishore et al. [95]. Lines show predictions from the different kinetics models, see Table 3.2 for legend.

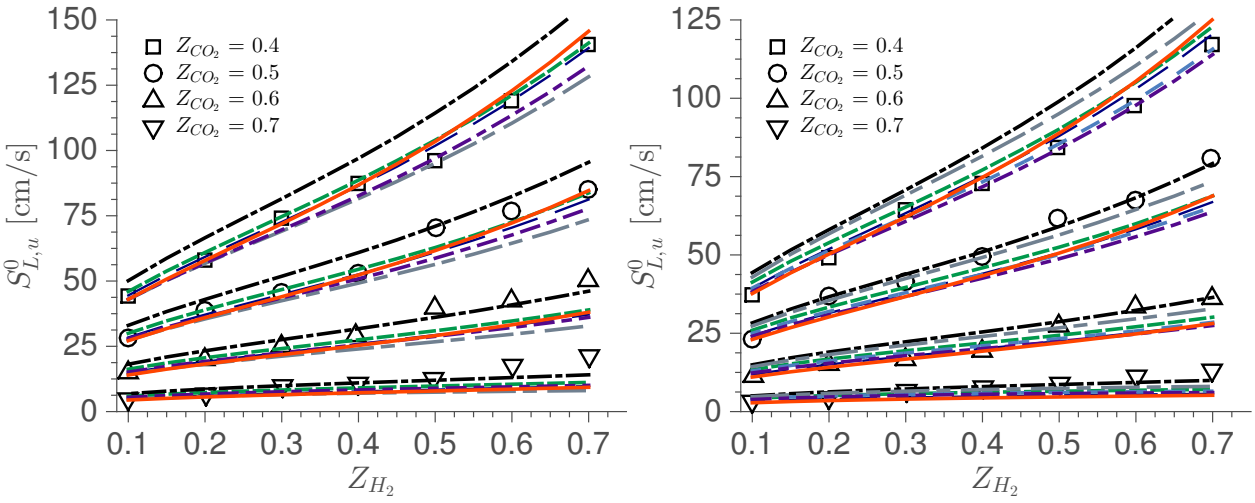

(a) P = 1 atm

(b) P = 2 atm

Figure 3.6: Measured and predicted laminar burning velocity (cm/s) as hydrogen concentration ratio of H_2/CO/CO_2 fuel mixture with CO_2 varying from Z_{CO_2}=0.4-0.7 at T=300 K and ϕ=0.4. The experimental data were obtained from Wang et al. [96]. Lines show predictions from the different kinetics models, see Table 3.2 for legend.

of CO_2 in the oxidizer and the percentage of H_2 in the fuel are given by:

$$Z_{CO_2} = XCO_2/(XCO_2 + XO_2)$$

$$Z_{H_2} = XH_2/(XH_2 + XCO)$$

where Z_{CO_2} varies from 40% to 70% and Z_{H_2} varies from 10% to 70%. It was found that the Li2007, Sun2007, and NUIG2013 mechanisms were in closest agreement with the experimental data for Z_{CO_2}= 0.4 and 0.5 at P = 1 and 2 atm with average relative error values of less than 5%, as shown in Figs. 3.6(a), 3.6(b), and supplementary Table A.1. Contrary to the results presented in Figs. 3.4(a) and 3.4(c), the UCSD2014 mechanism constantly over-predicts the laminar flame speed produces the highest average relative error values of 13.12% and 10.90% for Z_{CO_2} = 0.4 and

0.5 at P = 1 atm, respectively. However, for fuel mixtures with a high CO_2 content (Z_{CO_2} = 0.6) and high H_2 content ($Z_{H_2} > 0.6$) at P = 1 and 2 atm, all of the mechanisms except the UCSD2014 mechanisms significantly under-predicted the laminar flame speed (see Figs. 3.6(a) and 3.6(b)). At Z_{CO_2} = 0.7 and $Z_{H_2} > 0.5$, none of the mechanisms were able to accurately predict the laminar flame speed with relative error values ranging from 20% to 60% (see Supplementary Figs. A.6(d) and A.7(d)). Although all of the mechanisms were able to capture the effect of CO_2 addition on the laminar flame speed of syngas mixtures at elevated temperatures and pressures, as shown in Figs. 3.4, 3.5, and 3.6, the accuracy of each mechanism at predicting the flame speed of $H_2/CO/CO_2$ varies considerably and depends greatly on the experimental conditions (see Supplementary Table A.1). Therefore, in the next section, we describe a sensitivity analysis that was conducted for the $H_2/CO/CO_2$ mixtures to identify the important reaction(s) that could further improve the accuracy of the mechanism.

$H_2/CO/H_2O$ mixtures

Syngas derived from coal through gasification technique typically has a moisture content of 6 to 20% [115]. Hence, it is important for chemical kinetics mechanisms to be able to accurately predict the laminar flame speed of moist syngas. Figure 3.7 shows the predicted and measured laminar flame speed of moist H_2/CO mixtures at elevated temperatures, under atmospheric pressure. The UCSD2014 and Sun2007 mechanisms significantly over-predict the laminar flame speed of moist syngas (H_2/CO - 5:95) at an equivalence ratio of 0.9, as shown in Fig. 3.7(a). Although the Davis2005, GRI1999, USC2007, NUIG2013 and Li2007 mechanisms exhibit different degrees of agreement with the experimental data (see Fig. 3.7(a)), their average relative error values vary insignificantly ($\approx$ 2.0% to 3.6%; see Supplementary Fig. A.8(a)), indicating excellent agreement with the measured laminar flame speed. Under leaner conditions (ϕ = 0.4 - 0.6) and for a mixture with a hydrogen content (H_2/CO - 50:50), the Li2007 and NUIG2013 mechanisms offer the best level of agreement with the experimental data, while also exhibiting the lowest overall mean value

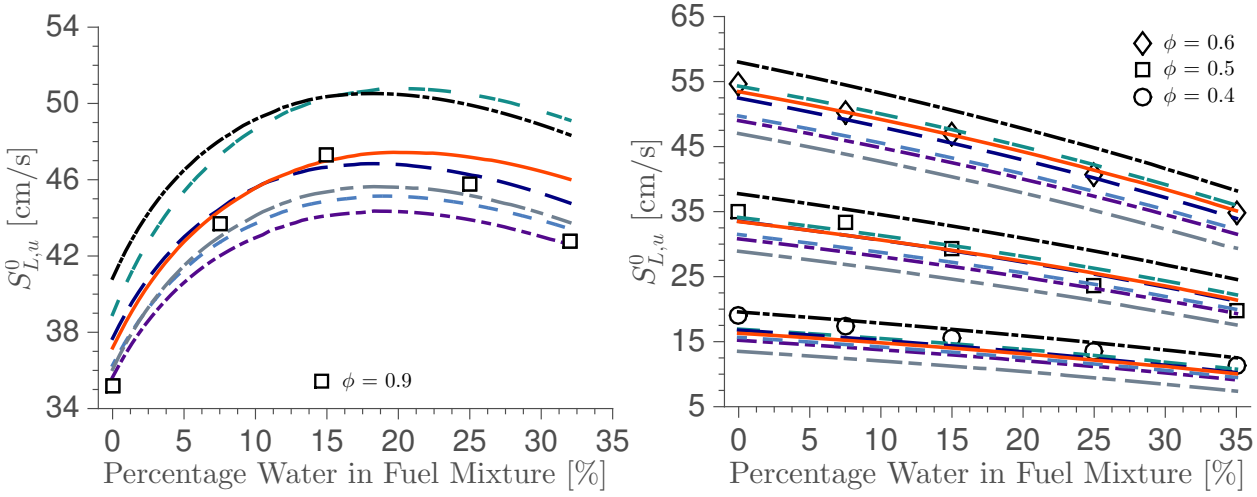

(a) H_2:CO-5:95 (b) H_2:CO-50:50

Figure 3.7: Measured and calculated laminar burning velocities of $H_2/CO/H_2O$ fuel mixture at P=1 atm and T=323 K. (a) ϕ = 0.9 and T = 323 K, (b) ϕ=0.4, 0.5, and 0.6 and T = 323 K. The experimental data were obtained from Das et al. [97]. Lines show predictions from the different kinetics models, see Table 3.2 for legend.

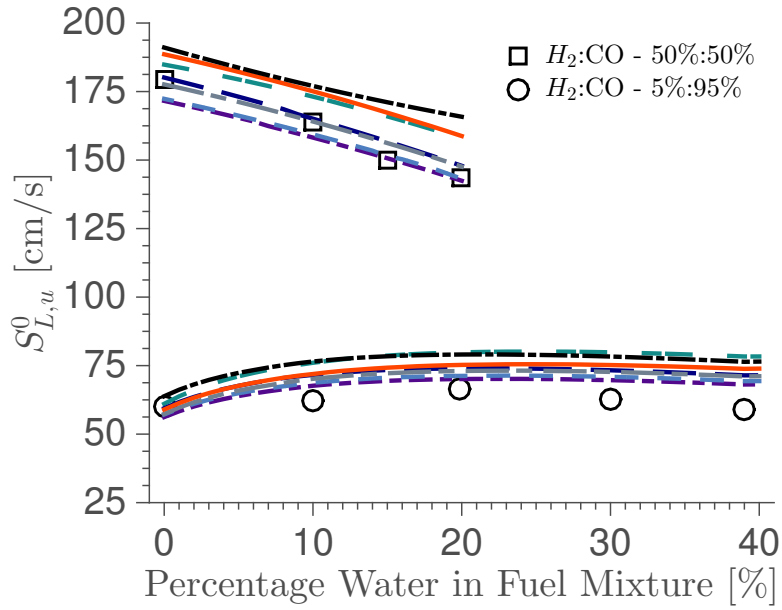

Figure 3.8: Laminar flame speed for $H_2/CO/H_2O$ fuel mixture at P = 1 atm, T = 400 K, and ϕ = 1.0. The experimental data were obtained from Singh et al. [42]. Lines show predictions from the different kinetics models, see Table 3.2 for legend.

of approximately 5% (see Supplementary Table A.1).

Under stoichiometric condition and for a mixture with a low hydrogen content (H_2/CO - 5:95), all of the mechanisms considered in this study were found to be able to capture the effect of water addition on the flame speed of H_2/CO mixtures at T = 400 K, as shown in Fig. 3.8. However, the UCSD2014 and Sun2007 mechanisms are not recommended for the study of the flame speed of the H_2/CO - 5:95 mixture under stoichiometric and elevated temperature conditions, as these two mechanisms yield the highest average relative error values of 20.19% and 20.49%, respectively. Interestingly, the performance of more recent mechanisms such as the NUIG2013 and UCSD2014 mechanisms is worse than that of older mechanisms (GRI1999, Li2007, Davis2005, and USC2007) in predicting the flame speed for H_2/CO - 50:50 mixture at ϕ = 1.0 and T = 400 K, for which the average relative error value produced by the older mechanisms is well below 2.3% and the average relative error values for the NUIG2013 and UCSD2014 mechanisms are 8.51% and 11.01%, respectively (see Supplementary Fig. A.9(b)). Hence, under the lean and standard conditions ($\phi <$ 0.9), only the Li2007, Davis2005, Sun2007, and NUIG2013 mechanisms are recommended for the study of the flame speed of moist syngas. However, at elevated temperatures and stoichiometric conditions, the UCSD2014 and Sun2007 mechanisms should be avoided.

$H_2/CO/N_2$ mixtures

Figure 3.9 shows the measured laminar flame speed when nitrogen is mixed into the H_2/CO mixture at elevated pressures (P = 1 to 5 atm) and temperatures (T = 303 to 373 K) across a wide range of equivalence ratios. At ambient temperature and under atmospheric conditions, the GRI1999 mechanism exhibits the worst performance while the UCSD2014 mechanism is in the closest agreement with the experimental data (see Figs. 3.9(a) and Supplementary Fig. A.10(a)). However, at elevated temperature and/or pressure, the results produced by the GRI1999 mechanism are in closest agreement with the experimental data, while the UCSD2014, Sun2007, and Li2007 mechanisms exhibit the poorest performance and therefore should be avoided. Although the UCSD2014,

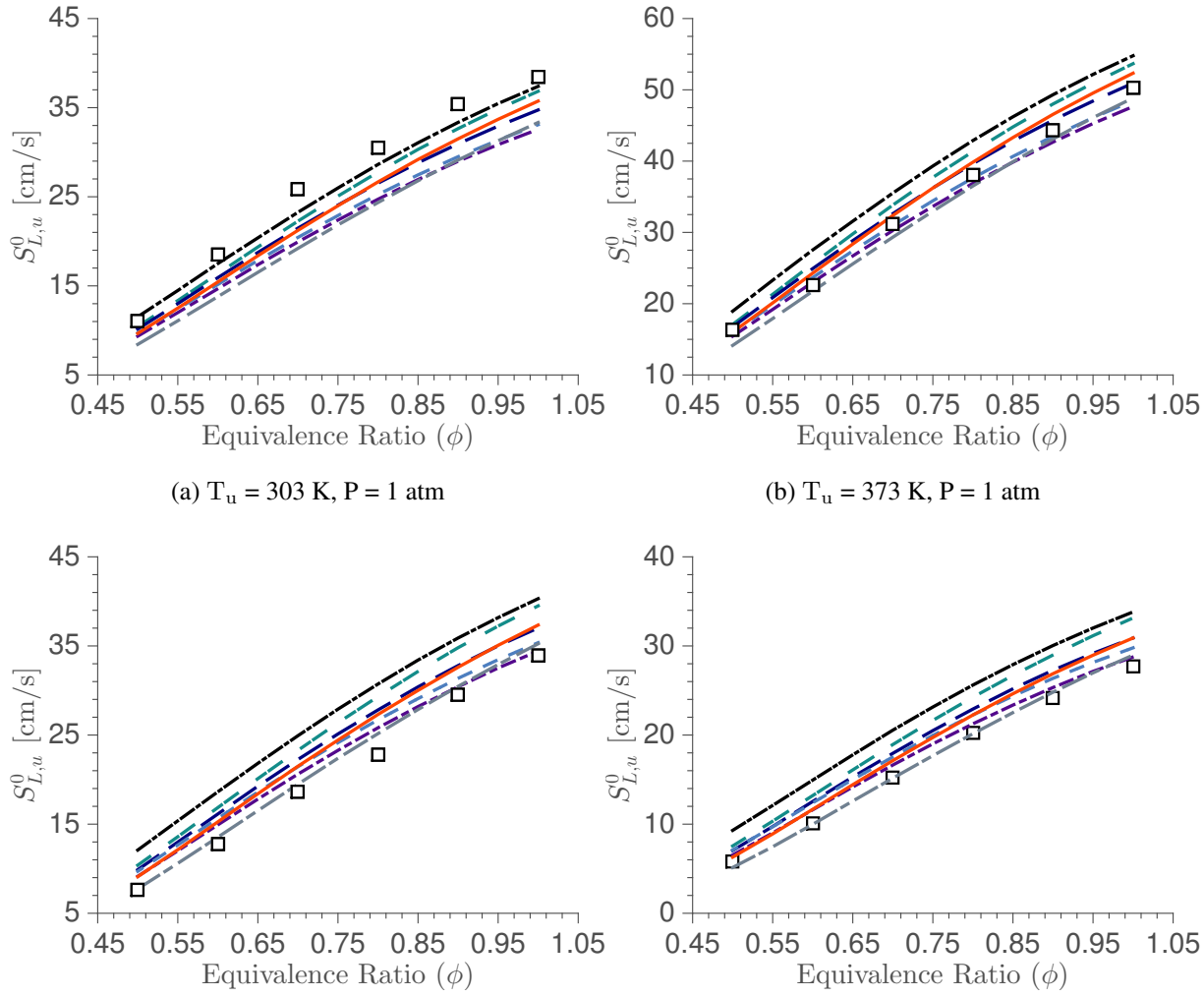

(a) T_u = 303 K, P = 1 atm

(b) T_u = 373 K, P = 1 atm

(c) T_u = 373 K, P = 3 atm

(d) T_u = 373 K, P = 5 atm

Figure 3.9: Measured and calculated laminar flame speed of $H_2/CO/N_2$-11:31:58 fuel mixture at P=1 - 5 atm and T=303-373 K. The experimental data were obtained from Hu et al. [91]. Lines show predictions from the different models. See Table 3.2 for legend.

Sun2007, and Li2007 mechanisms are not capable of predicting the flame speed of $H_2/CO/N_2$ accurately, they are still capable of predicting the effects of N_2 addition to H_2/CO mixture at elevated pressure and temperature. Hence, under the standard conditions, the UCSD2014 mechanism is highly recommended for the study of the flame speed of $H_2/CO/N_2$ mixtures, while the GRI1999, Davis2005, and NUIG2013 mechanisms are recommended for the study of the flame speed of syngas diluted with N_2 at elevated pressures and temperatures.

H_2/CH_4 mixtures

To date, there has been only one study that investigated the flame speed of syngas/biogas mixtures. However, the authors [90] were only interested in the NO formed from the syngas/biogas mixture. They did not investigate the effect of the equivalence ratios on the laminar flame speed of the syngas/biogas mixtures. Therefore, there is a need for more experimental data on the laminar flame speed of syngas/biogas mixtures at different unburned temperatures and equivalence ratios. Hence, the laminar flame speed of H_2/CH_4 at a range of CH_4 ratios and equivalence ratio is also considered in this study to evaluate the mechanisms. Figure 3.10 shows the measured and predicted laminar flame speed of H_2/CH_4 as a function of the CH_4 concentration under stoichiometric conditions. The predictions produced with the Sun2007 and Davis2005 mechanisms are not included because they are not equipped with C_1 chemistry. Generally, all of the models considered

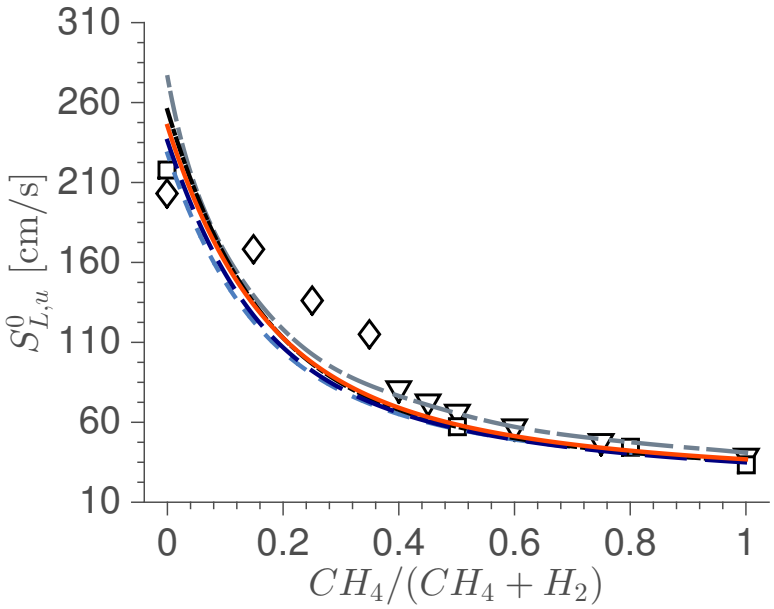

Figure 3.10: Measured and calculated laminar flame speed of H_2/CH_4 fuel mixture as a function of CH_4 concentration at ϕ=1.0. Symbols represent experimental data: (◊) - Law et al. [98], (▽) - Yu et al. [99], (□) - Donohoe et al. [100]. Lines show predictions from the different models. See Table 3.2 for legend.

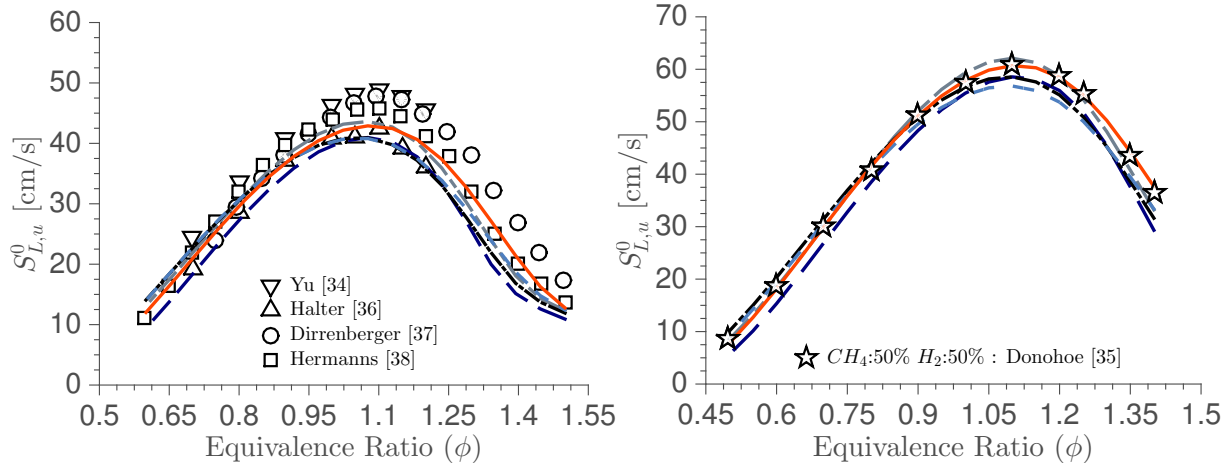

(a) P = 1 atm; T = 298 K; H_2/CH_4 - 20:80

(b) P = 1 atm; T = 300 K;H_2/CH_4 - 50:50

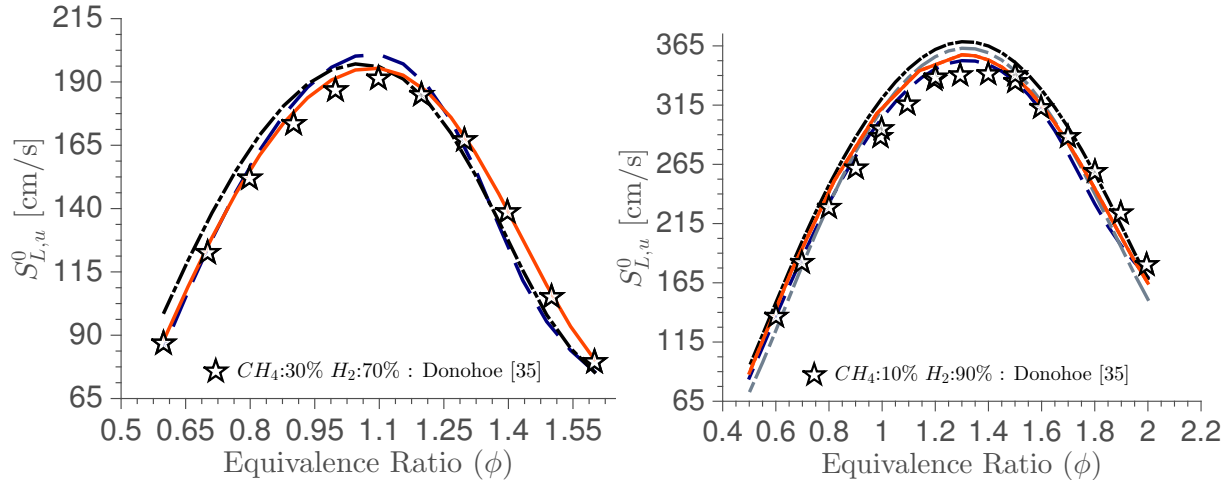

(c) P = 5 atm; T = 450 K; H_2/CH_4 - 70:30

(d) P = 1 atm; T = 450 K;H_2/CH_4 - 90:10

Figure 3.11: Measured and calculated laminar flame speed of H_2/CH_4 fuel mixture at P = 1 atm and T=298 K. Symbols represent experimental data: ($\bigtriangledown$) - Yu et al. [99], ($\bigtriangleup$) - Halter et al. [101],($\bigcirc$) - Dirrenberger et al. [102] ,($\square$) - Hermanns et al. [103],($\star$) - Donohoe et al. [100]. Lines show predictions from the different kinetics models, see Table 3.2 for legend.

in this study produce an almost identical prediction of the laminar flame speed and are all capable of predicting the effect of the addition of methane to the hydrogen mixture under standard and stoichiometric conditions with average relative error values varying from 15% to 20% (see Fig. 3.10 and Supplementary Table A.1) . Figure 3.11 shows the laminar flame speed for various H_2:CH_4 ratios at elevated pressure and temperature, and at equivalence ratio ranging from 0.5 to 2.0. The simulation results for the GRI1999 and USC2007 mechanisms are not shown in Fig. 3.11(c) as neither of these mechanisms incorporate the helium bath gas. For the H_2/CH_4 mixtures shown in Fig. 3.11, the results obtained with the NUIG2013 mechanism exhibit the best agreement with the experimental data relative to the other mechanisms, by producing the lowest overall mean value of 5.73% for Fig. 3.11.

$H_2/CO/CH_4/CO_2$ mixtures

The parameter used to compare the results obtained with the mechanisms with the experimental data obtained from jet-wall stagnation flames is the reference flame speed, $S_{u,ref}$. The reference flame speed is defined as the minimum upstream velocity of the flow, prior to the temperature rise. This velocity also represents the local mass burning rate of the flame at the inlet temperature, composition, and hydrodynamic strain rate. Generally, the NUIG2013 and UCSD2014 mechanisms offer the most accurate prediction of the flame speed of the biogas/syngas mixtures at equivalence ratio ranging from 0.7 to 1.0. However, it is worth mentioning that the NUIG2013 mechanism incurs a maximum relative error value of only 8.56% for all of the syngas/biogas mixtures (ϕ = 0.7 to 1.0) considered by Watson et al. [90], while the UCSD2014 mechanism has a maximum relative error value of 14.70%.

To better visualize the performances of the mechanisms at different initial conditions and fuel mixture compositions for laminar flame speed, the overall mean value ($\bar{\bar{\varepsilon}}$) for the laminar flame speed results is graphed in Fig. 3.13, where the experimental conditions for each figure are summarized in Table 3.1. Since the hydrogen content of syngas varies substantially and syngas mixtures can

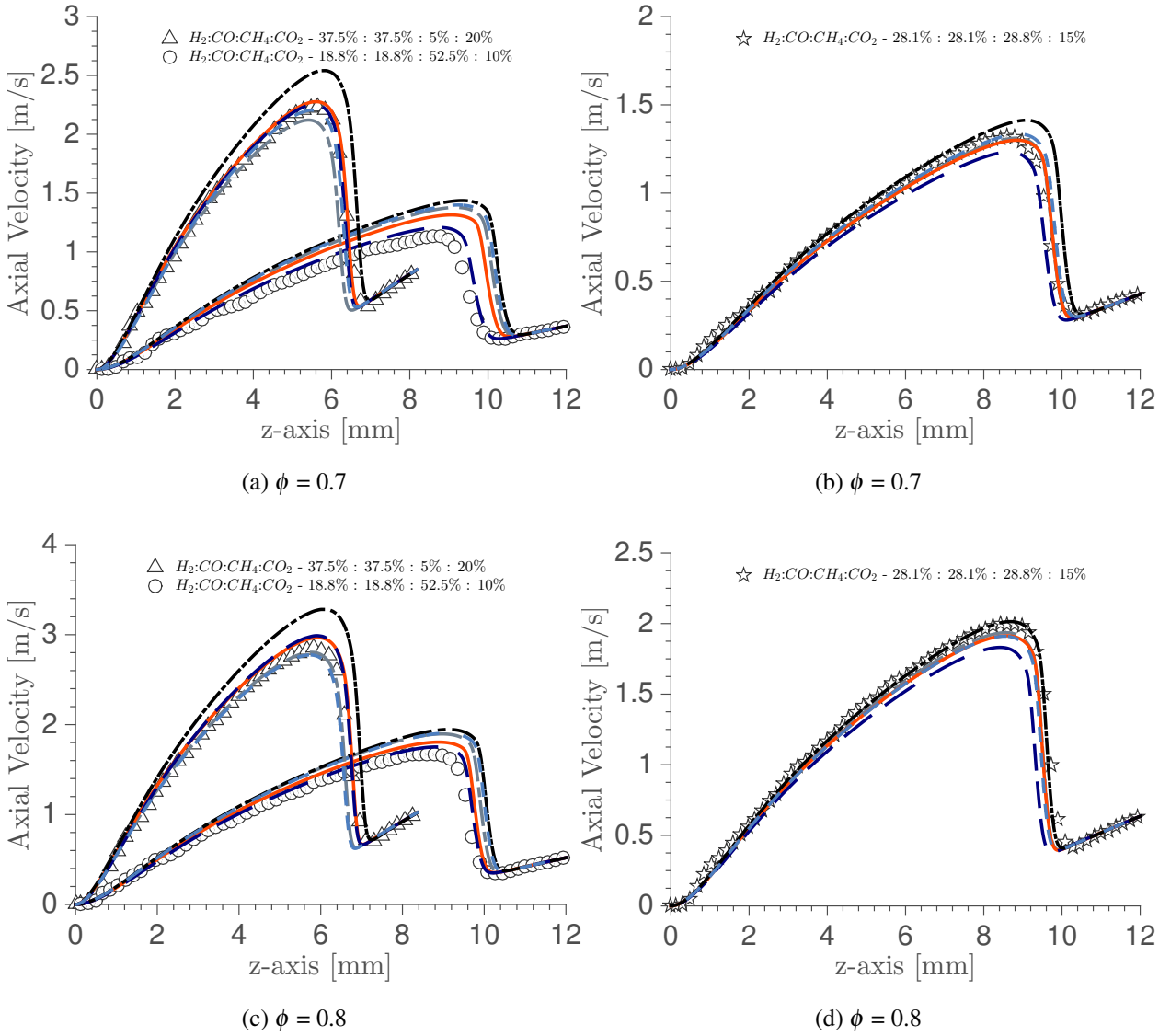

(a) ϕ = 0.7

(b) ϕ = 0.7

(c) ϕ = 0.8

(d) ϕ = 0.8

Figure 3.12: Measured and calculated flame speed of $H_2/CO/CH_4/CO_2$ fuel mixture at P = 1 atm and T=300 K. The experimental data were obtained from [90]. Lines show predictions from the different kinetics models, see Table 3.2 for legend.

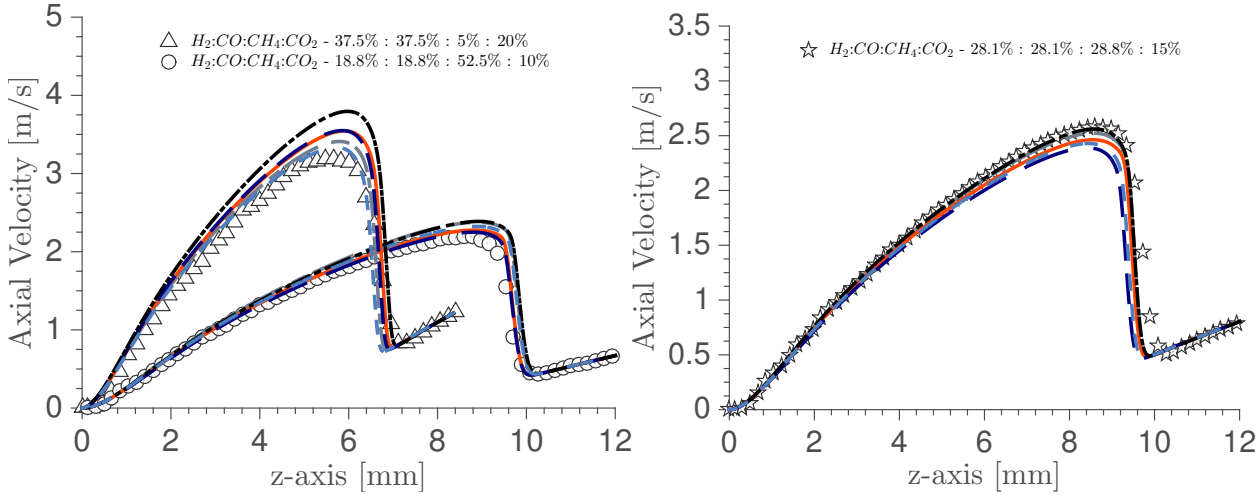

(e) ϕ = 0.9

(f) ϕ = 0.9

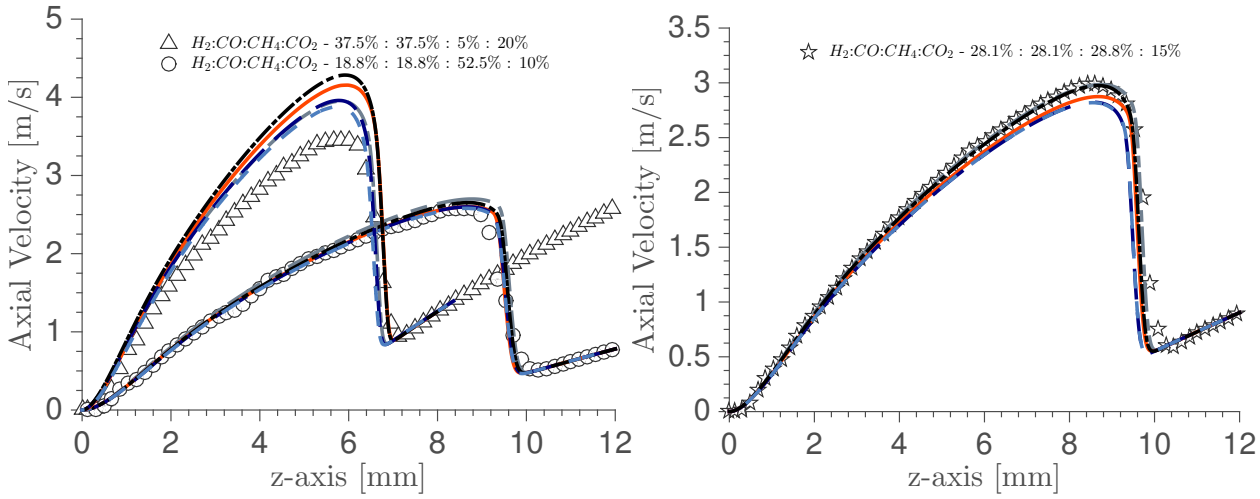

(g) ϕ = 1.0

(h) ϕ = 1.0

Figure 3.12: Measured and calculated flame speed of $H_2/CO/CH_4/CO_2$ fuel mixture at P = 1 atm and T=300 K. The experimental data were obtained from [90]. Lines show predictions from the different kinetics models, see Table 3.2 for legend (continued).

incorporate impurities such as N_2 and H_2O, the ideal mechanism should be able to describe all of the fuel mixtures listed in Table 3.1. Hence, four different types of grand mean are computed and listed in Table 3.2 for flame speed calculation. The NUIG2013 mechanism is found to yield the lowest grand mean values for the [C] and [D] categories. Interestingly, the performance of the Li2007 mechanism (with grand mean values for [C] and [D] of 9.46% and 9.67%, respectively), which has only 21 species and 93 reactions, is comparable to that of the NUIG2013 mechanism in predicting the flame speed of syngas with every diluent. The GRI1999 and UCSD2014 mechanisms are not recommended for studying the flame speed of syngas and syngas/biogas mixtures. Hence, both the NUIG2013 and Li2007

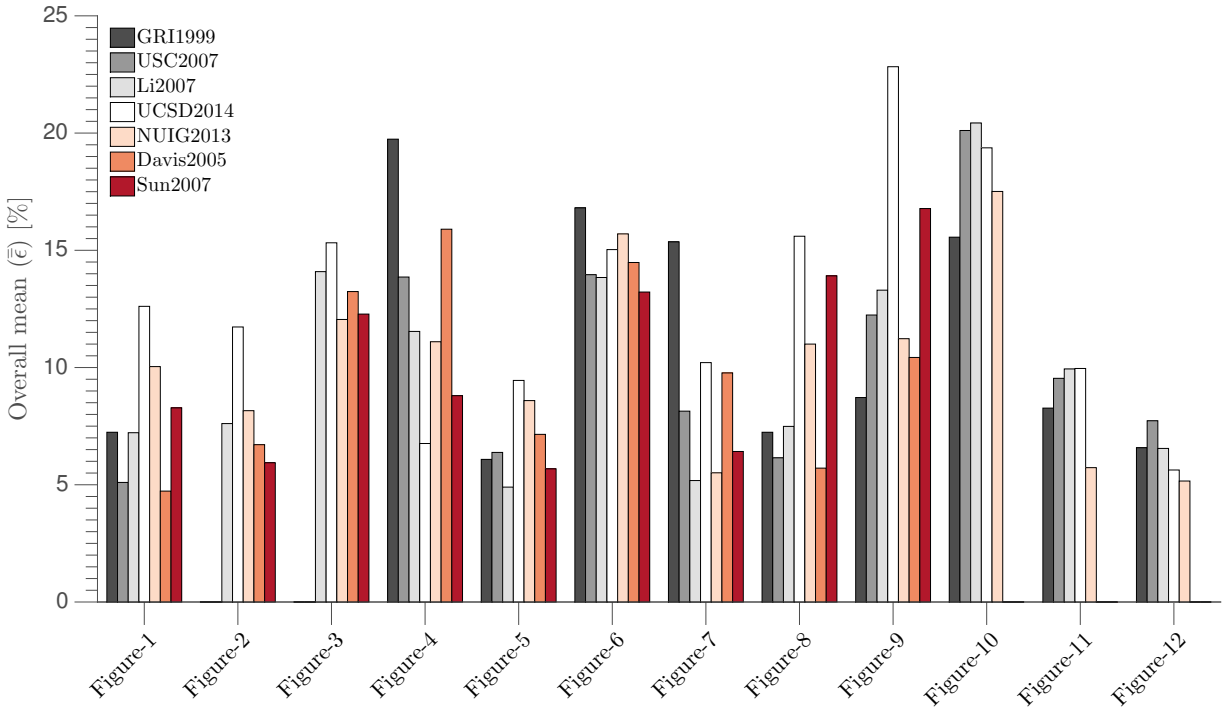

Figure 3.13: Performance of the mechanisms for laminar flame speed based on the overall mean value ($\bar{\bar{\epsilon}}$).

3.3.2 Ignition delay time

H_2/CO mixtures

The measured and predicted ignition delay time for H_2/CO mixture as a function of temperature is shown in Fig. 3.14. As depicted in Figs. 3.14(a) to 3.14(c) for equimolar H_2/CO under

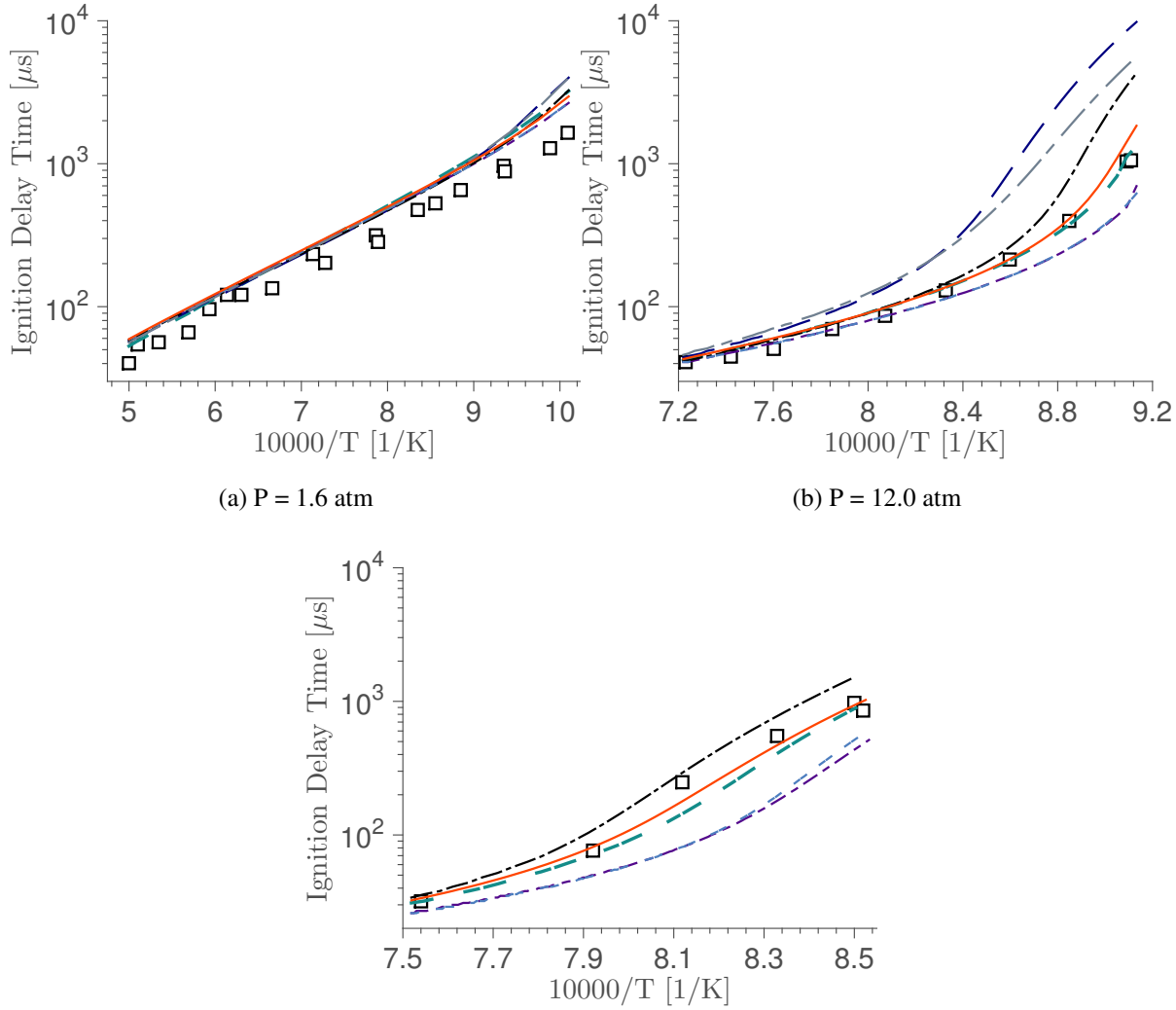

(a) P = 1.6 atm

(b) P = 12.0 atm

(c) P = 32.0 atm

Figure 3.14: Measured and calculated ignition delay time for H_2:CO-50:50 fuel mixture diluted in 98% of Argon (ϕ = 0.5). The experimental data were obtained from Mathieu et al. [104]. Lines show predictions from the different kinetics models, see Table 3.2 for legend.

atmospheric and elevated pressures, the measured trends are captured well by the mechanisms of NUIG2013 and Sun2007 mechanisms, and to some extent by the UCSD2014, USC2007, and Davis2005 mechanisms. All of the mechanisms predict a longer ignition delay time in the low-temperature region for P = 1.6 atm, but differ substantially from the experimental data. This is due to the measured ignition delay time results in the low temperature region being artificially shortened by non-ideal facility effects. It is worth noting here that Gersen et al. [116] measured the ignition delay time of H_2:CO-70:30 (ϕ = 0.5 = 1.0) in a rapid compression machine at pressures ranging from 45 to 70 atm and temperatures of approximately 960 to 1010 K. They reported that the predictions for the NUIG2013 mechanism were in extremely good agreement with their measured ignition delay time. However, the experimental data obtained by Gersen et al. [116] could not be reproduced because of the missing pressure trace profiles. Based on the overall mean values computed for Fig. 3.14, the NUIG2013 and Sun2007 mechanisms exhibit the lowest overall mean values of approximately 20%, while the GRI1999 and Li2007 mechanisms produce significantly higher overall mean values of approximately 100% (see Supplementary Table A.2). These high overall mean values are due to the failure of the mechanisms to accurately predict the ignition delay time at elevated pressures, as evidenced in Figs. 3.14(b) and 3.14(c). Hence, the NUIG2013 and Sun2007 mechanisms are recommended for the study of the ignition delay time of H_2/CO mixtures.

$H_2/CO/H_2O$ mixtures

As mentioned above, syngas contains not only H_2/CO, but also some other inert gases such as nitrogen, carbon dioxide, and water vapor. The inert gases may have a substantial effect on the reactivity of a syngas fuel mixture, in that they may exacerbate the ignition delay time of H_2/CO mixture. Figure 3.15 shows the ignition delay time for $H_2/CO/H_2O$ at atmospheric and elevated pressures. The Li2007 and GRI1999 mechanisms are not able to capture the effect of water addition or the pressure-dependent effects with significantly high overall mean values of 229.95%

and 160.25%, respectively (see Figs. 3.15(b), 3.15(c), and Supplementary Table A.2). Although the UCSD2014 mechanism is able to predict the effect of water vapor addition, it over-predicts the ignition delay time. On the other hand, the NUIG2013, Sun2007, USC2007, and Davis2005

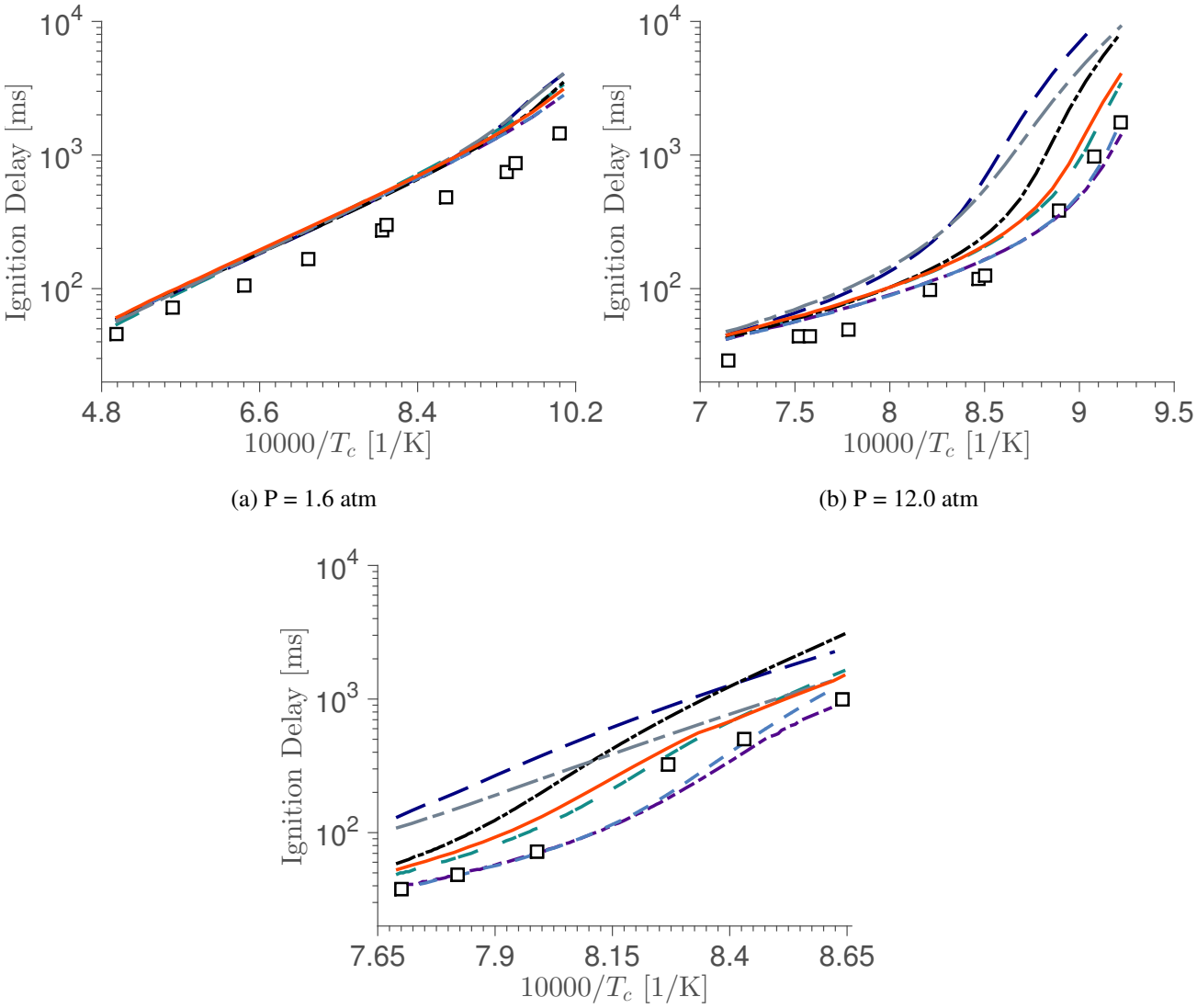

(a) P = 1.6 atm

(b) P = 12.0 atm

(c) P = 32 atm

Figure 3.15: Comparison among detailed chemical kinetics models and ignition delay time determined from $H_2/CO/H_2O$ fuel mixture diluted in 98% of Argon. The experimental data were obtained from Mathieu et al. [104]. Lines show predictions from the different kinetics models, see Table 3.2 for legend.

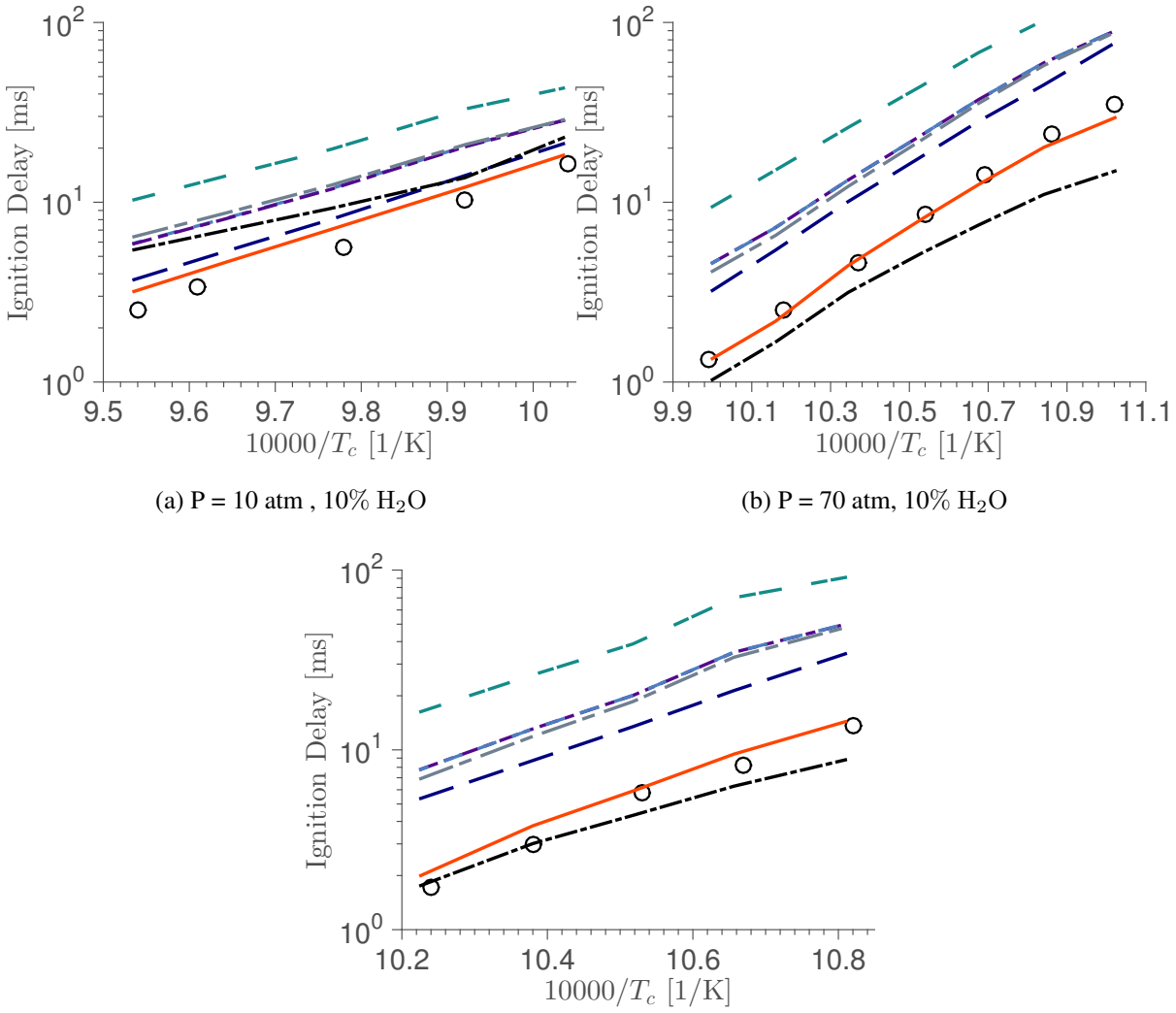

(a) P = 10 atm , 10% H_2O

(b) P = 70 atm, 10% H_2O

(c) P = 70 atm, 40% H_2O

Figure 3.16: Comparison among detailed chemical kinetics models and ignition delay time determined from H_2/H_2O fuel mixtures. The experimental data were obtained from [105]. Lines show predictions from the different kinetics models, see Table 3.2 for legend.

mechanisms are able to accurately predict the ignition delay time resulting from water addition to the syngas mixture with overall mean values ranging from 37% to 60% (see Supplementary Table A.2).

Mathieu et al. [104] conducted their experiments with 20% by volume of H_2O addition; as such, it would be insufficient to evaluate the performance of the mechanisms at predicting the ignition delay time of moist syngas. To the best knowledge of the authors, only Mathieu et al. [104] studied the effect of H_2O addition on the ignition delay time of syngas mixture. Therefore, the measured ignition delay time results for $H_2/H_2O/N_2$ from Das et al. [105] are included in this study to further evaluate the performance of the kinetics mechanisms, as depicted in Fig. 3.16. Das et al. [105] conducted ignition delay time experiments under stoichiometric conditions with 0% to 40% mole percentage water addition to the fuel mixture (H_2:O_2:N_2-12.5:6.25:81.250) at T = 907 to 1048 K and P = 10 to 70 atm. Compared to the work of Mathieu et al. [104] (T = 1025 to 2000 K and P = 1.6 to 32 atm), Das et al. [105] measured the ignition delay time of $H_2/CO/H_2O$ at a lower temperature range and at higher pressures. The results were similar to those shown in Fig. 3.15, where the Li2007 and GRI1999 mechanisms are not able to capture the effect of water addition or predict the pressure-dependent effect (see Figs. 3.16(a) to 3.16(d)). Furthermore, both mechanisms have overall mean values of over 100%, indicating that the mechanisms fail to accurately predict the ignition delay time of the $H_2/H_2O/N_2$. This is also consistent with the conclusion drawn by Das et al. [55], where they discovered that the Li2007 mechanism was not able to predict the ignition delay time of a moist hydrogen mixture. Interestingly, the Davis2005, USC2007, and Sun2007 mechanisms significantly over-predict the ignition delay time for all the conditions considered by Das et al. [105]. Hence, these three mechanisms are only suitable for predicting the ignition delay time of moist syngas that is highly diluted in argon at higher temperatures and lean condition (ϕ = 0.5), much like the conditions adopted for the work of Mathieu et al. [104]. Recent mechanisms such as the UCSD2014 and NUIG2013 mechanisms are able to capture the effect of the addition of water on the ignition delay time of hydrogen. However, only the NUIG2013

mechanism is able to accurately predict the ignition delay time of moist hydrogen mixture with an overall mean value of only 15.73%, as shown in Fig. 3.16 and Supplementary Fig. A.16. Therefore, the NUIG2013 mechanism is the only mechanism that is highly recommended for the study of the ignition delay time of moist syngas mixtures under both atmospheric conditions and at elevated pressures.

$H_2/CO/CO_2$ mixtures

The measured and predicted ignition delay time resulting from the addition of CO_2 to the H_2/CO mixtures are shown in Figs. 3.17 and 3.18. All of the mechanisms considered in this study produce almost identical predictions of the ignition delay time for $H_2/CO/CO_2$ at a low pressure (P = 1.6 atm) and high temperatures. At elevated pressures, only the Sun2007 and NUIG2013 mechanisms are able to accurately predict the ignition delay time and they yield the lowest average relative error values, as depicted in Figs. 3.17(b), 3.17(c), and Supplementary Fig. A.17. Other mechanisms such as the Li2007 and GRI1999 over-predict the ignition delay time, while the USC2007 and Davis2005 mechanisms under-predict the ignition delay time (see Figs. 3.17(b) and 3.17(c)).

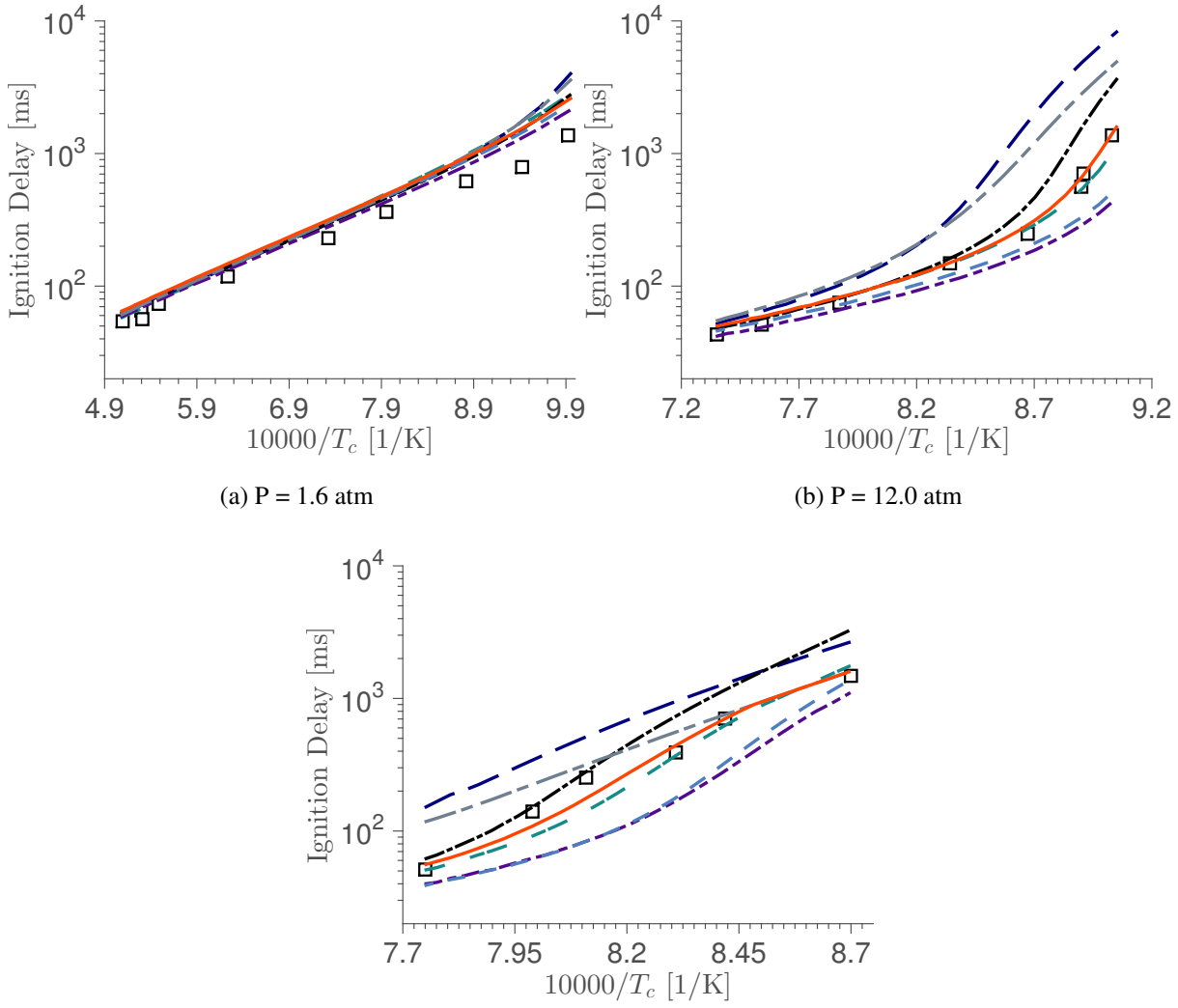

(a) P = 1.6 atm

(b) P = 12.0 atm

(c) P = 32 atm

Figure 3.17: Comparison among detailed chemical kinetics models and ignition delay time determined from $H_2/CO/CO_2$ fuel mixture diluted in 98% of Argon. The experimental data were obtained from [104]. Lines show predictions from the different kinetics models, see Table 3.2 for legend.

The ignition delay time of the $H_2/CO/CO_2$ at near atmospheric conditions is shown in Fig. 3.18, where the pressure varies from 1.24 atm to 2.36 atm. Under the experimental conditions considered by Vasu et al. [51], the mechanisms attain varying degrees of success in matching the experimental data, while the Davis2005 mechanism offers the best level of agreement with the measured ignition

delay time. One of the reasons why the NUIG2013 mechanism is seen to perform remarkably well in Fig. 3.17 but not in Fig. 3.18, is because the fuel mixture in the study conducted by Mathieu et al. [105] was diluted with 98% of argon, while the syngas mixture in the study conducted by Vasu et al. [51] was diluted with 44.84% of N_2. To date, no definitive results have been obtained for syngas diluted with higher CO_2 concentrations at high pressures. Although Vasu et al. [51] diluted their fuel mixture with 54.4% of CO2, their study addressed only relatively low pressures (P = 1.1 to 2.59 atm). Therefore, further studies of H_2/CO diluted with CO_2 at high pressures are warranted as the CO_2 mole fraction in actual syngas can be as high as 29% [117]. Contrary to the results presented in the previous sub-sections, the ignition delay time results produced by the NUIG2013 mechanism for $H_2/CO/CO_2$ deviate significantly from the experimental data, having an overall mean value of 285.54% at the experimental conditions shown in Fig. 3.18 (see Supplementary Table A.2). Hence, sensitivity analysis was conducted for the fuel mixture and experimental conditions adopted for the study conducted by Vasu et al. [51]. The results of the sensitivity analysis are further discussed in the subsequent section.

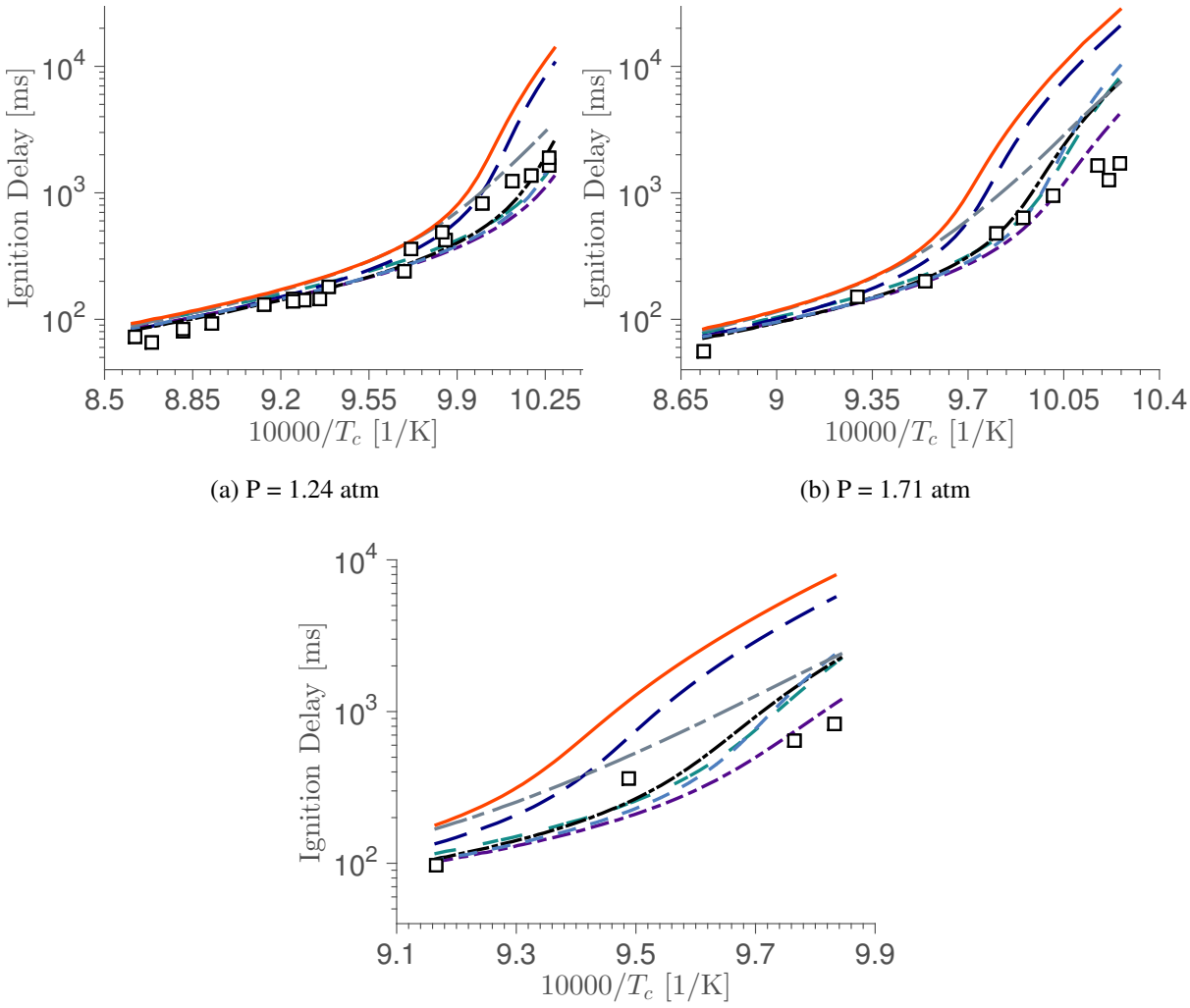

(a) P = 1.24 atm

(b) P = 1.71 atm

(c) P = 2.36 atm

Figure 3.18: Comparisons of measured and predicted ignition delay time of $H_2/CO/CO_2$ fuel mixture at P = 1.24 - 2.36 atm. The experimental data were obtained from [51]. Lines show predictions from the different kinetics models, see Table 3.2 for legend.

$H_2/CO/CO_2/CH_4/H_2O$ mixtures

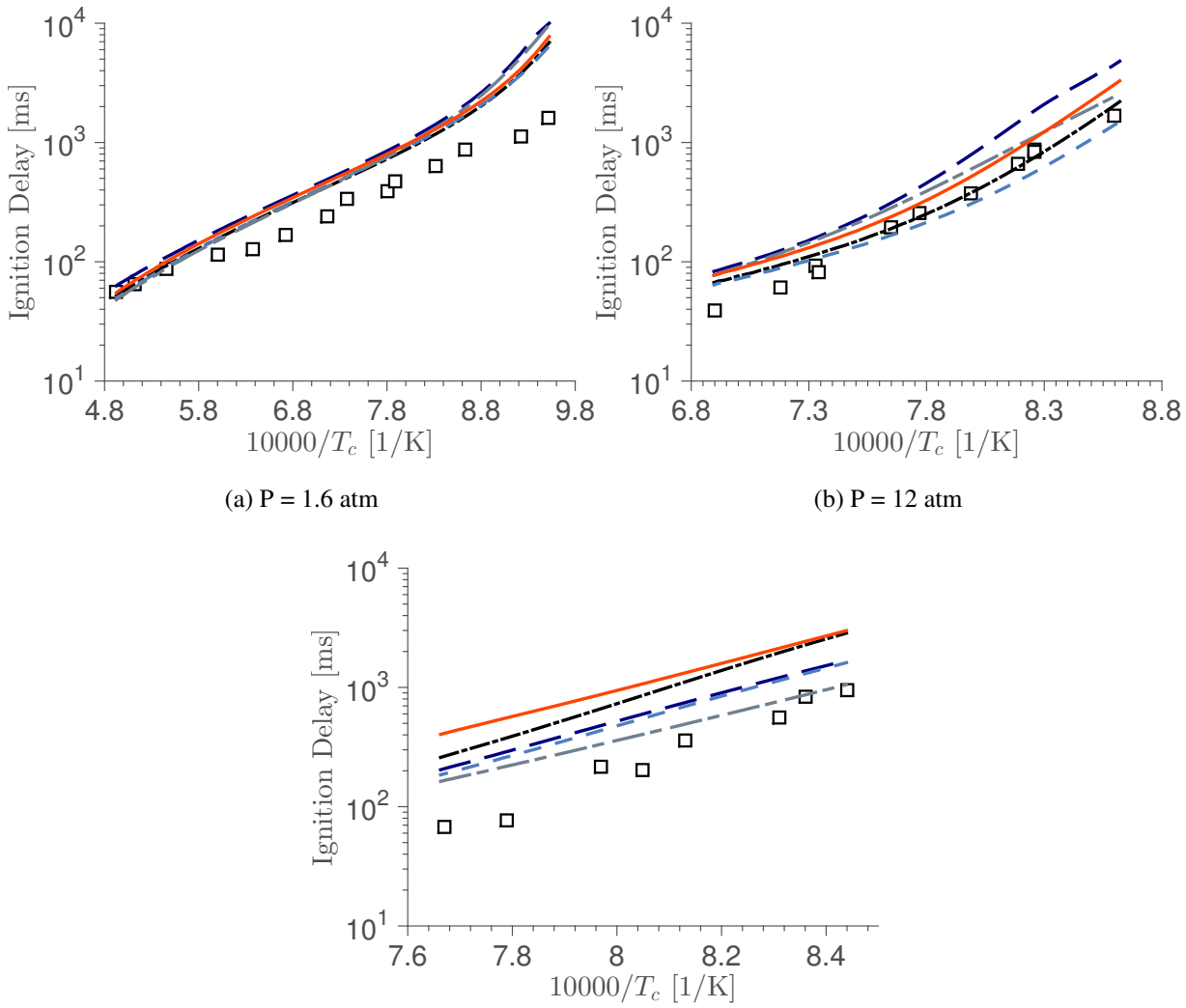

(a) P = 1.6 atm

(b) P = 12 atm

(c) P = 32 atm

Figure 3.19: Comparisons of measured and predicted ignition delay time of $H_2/CO/CO_2/CH_4/H_2O$ fuel mixture diluted in 98% of Argon. The experimental data were obtained from [104]. Lines show predictions from the different kinetics models, see Table 3.2 for legend.

Syngas may contain a small amount of impurities, as mentioned above. They are normally found to be homogeneously mixed in the actual syngas fuel mixture. Therefore, it is crucial that the

mechanism be able to accurately predict the effects of most of the impurities that exist in a syngas mixture. The ignition delay time of a syngas mixture with all impurities included was studied by Mathieu *et al.* [104] in a shock tube, where the mixture represented the syngas mixture produced from biomass and therefore consisting of carbon dioxide, methane, and water vapor. The experiments were conducted at high pressures (P = 1.6, 12, and 32 atm) and lean condition (ϕ=0.5). The measured ignition delay time results were compared with the results of simulation as depicted in Fig. 3.19. Around atmospheric pressure (P = 1.6 atm), all of the mechanisms have an almost identical performance, with the average relative error values varying only very slightly from each other (see Supplementary Table A.2). However, at elevated pressure (P = 12 atm), the GRI1999 and Li2007 mechanisms fail to accurately predict the ignition delay time of a real syngas mixture. Only the USC2007, UCSD2014, and NUIG2013 mechanisms are able to accurately predict the ignition delay time of a real syngas mixture at P = 12 atm. For the highest pressure (P = 32 atm) investigated by Mathieu et al. [104], all of the mechanisms failed to accurately predict the ignition delay time of the $H_2/CO/CO_2/CH_4/H_2O$ mixtures (see Fig. 3.19(c)). Since the NUIG2013 mechanism performs remarkably well at predicting the flame speed of syngas/biogas mixtures, it is alarming that this mechanism fails to predict the ignition delay time of a real syngas mixture at P = 32 atm. Therefore, a sensitivity analysis was conducted for $H_2/CO/CO_2/CH_4/H_2O$ mixture to identify which reaction is responsible for the large discrepancy observed in Fig. 3.19(c). The findings of the sensitivity analysis are further discussed in the subsequent section.

$H_2/CO/CH_4$ mixtures

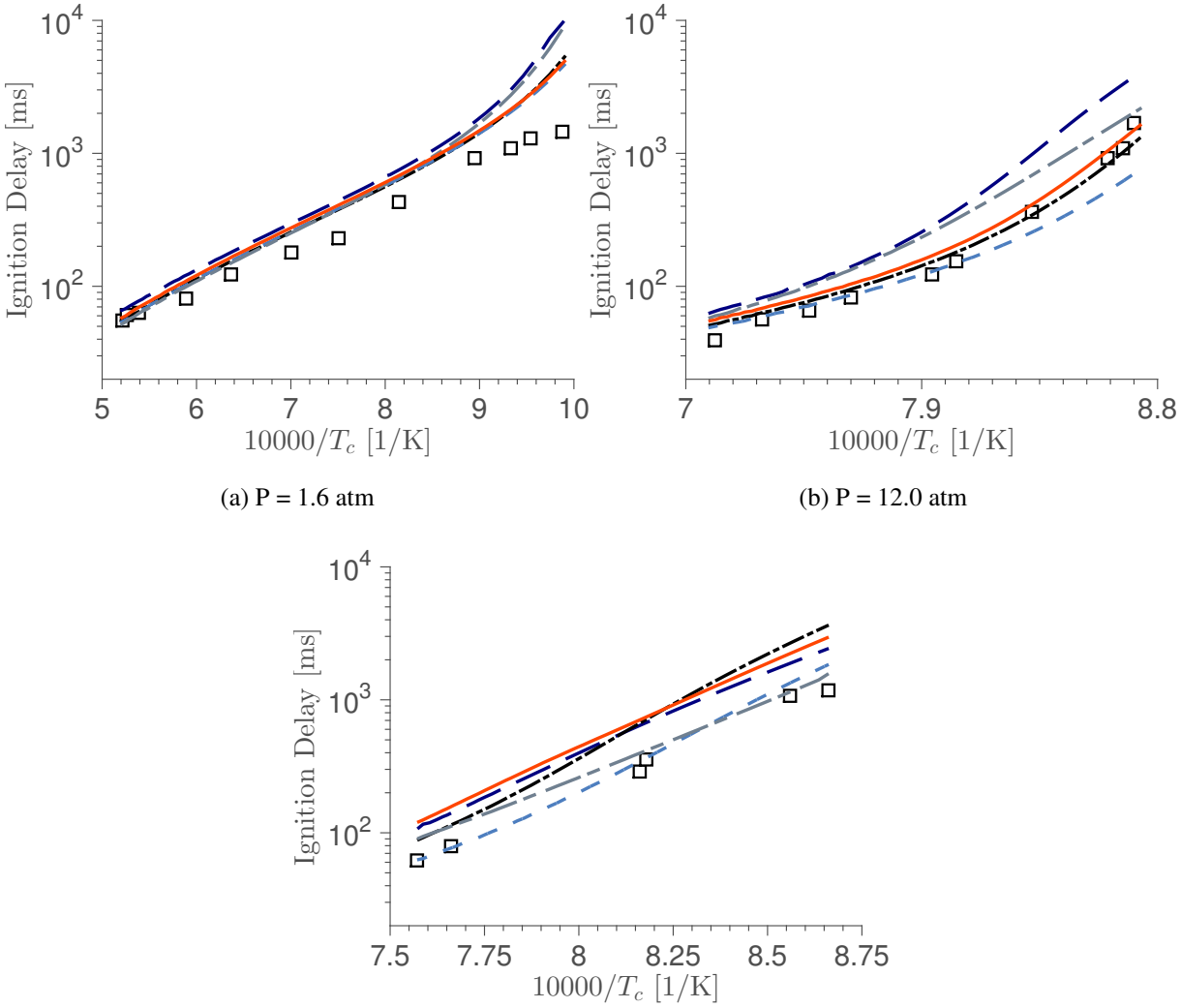

(a) P = 1.6 atm

(b) P = 12.0 atm

(c) P = 32 atm

Figure 3.20: Comparisons of measured and predicted ignition delay time of $H_2/CO/CH_4$ fuel mixture (ϕ=0.5). The experimental data were obtained from [104]. Lines show predictions from the different kinetics models, see Table 3.2 for legend.

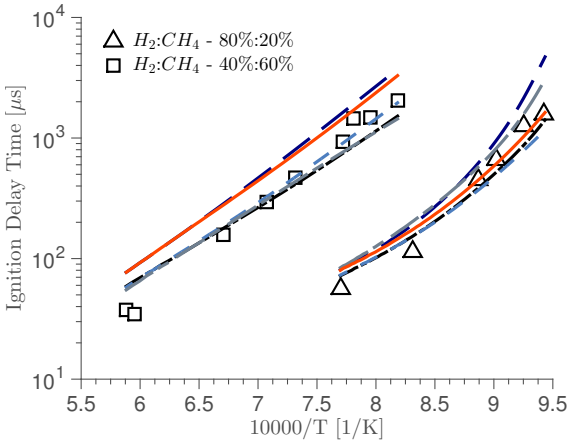

(a) P = 5 atm

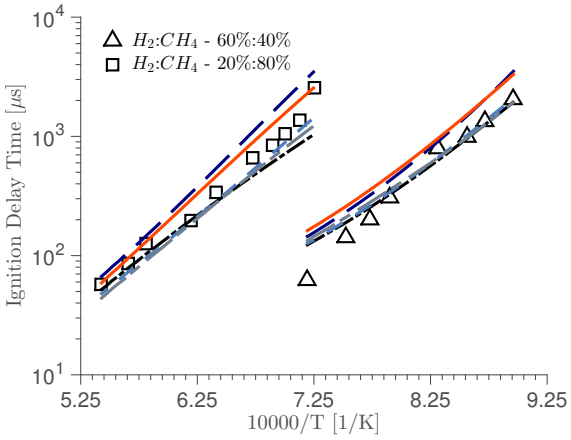

(b) P = 5 atm

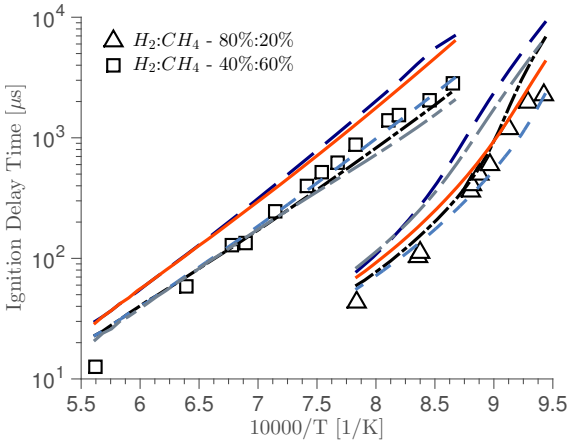

(c) P = 10 atm

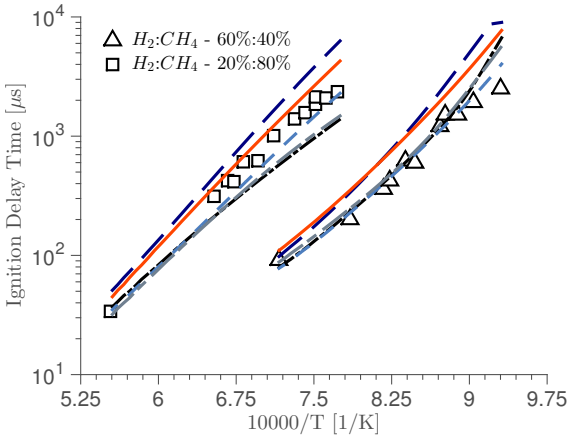

(d) P = 10 atm

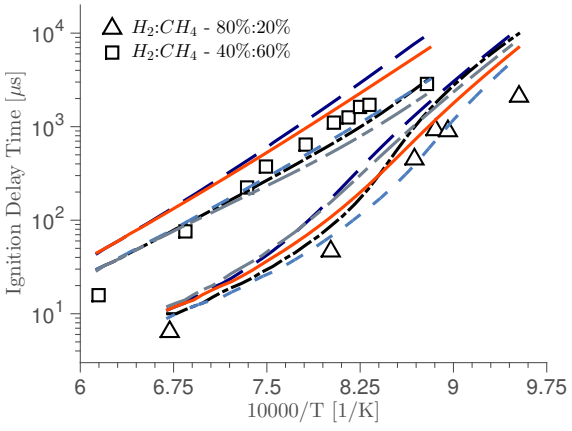

(e) P = 20 atm

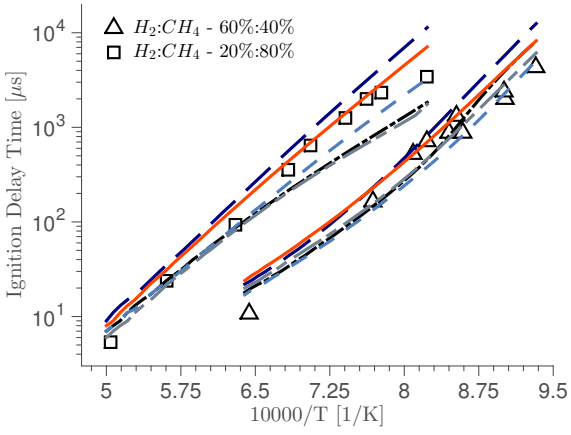

(f) P = 20 atm

Figure 3.21: Comparisons of measured and predicted ignition delay time of H_2/CH_4 fuel mixtures (ϕ = 0.5). The experimental data were obtained from [28]. Lines show predictions from the different kinetics models, see Table 3.2 for legend.

The effect of methane addition to the syngas mixture on the ignition delay time at elevated pressures is shown in Fig. 3.20. In the same way as the results shown in Figs. 3.14(a), 3.15(a), 3.17(a), and 3.19(a), all of the mechanisms produced an identical ignition delay time prediction at high temperatures ($>$ 1100 K). At elevated pressure (P = 12 atm), only the NUIG2013, UCSD2014, and USC2007 mechanisms are able to accurately predict the ignition delay time and they agree very well with the experimental data, with the average relative error values varying between 15% and 27%. At higher pressure condition (P = 32 atm), the USC2007 mechansim is the only one to exhibit good agreement (average relative error = 6.72%; see Supplementary Fig. A.20) with the experimental data (see Fig. 3.20(c)). The NUIG2013 mechanism over-predicts the ignition delay time for the entire temperature range with an average relative error value of 110.17%. Hence, the use of the USC2007 mechanism is highly recommended for studying the ignition delay time of the $H_2/CO/CH_4$ mixture considered by Mathieu et al. [104]. In much the same way as the ignition delay time for the $H_2/CO/CO_2/CH_4/H_2O$ at P = 32 atm, the NUIG2013 mechanism fails to accurately predict the ignition delay time of the $H_2/CO/CH_4$ at P = 32 atm. Hence, sensitivity analysis was also conducted for the $H_2/CO/CH_4$ mixture to identify which reaction is responsible for the discrepancies observed in Figs. 3.19(c) and 3.20(c) at P = 32 atm.

To the best of the authors' knowledge, to date no studies have been made of the ignition delay time for biogas/syngas mixtures. Hence, studies of the ignition delay time for biogas/syngas should be undertaken to further evaluate the efficacy of the current chemical kinetics mechanisms for biogas/syngas applications. Therefore, the measured ignition delay time results for H_2/CH_4 are included in this study and are compared with the predicted ignition delay time, as depicted in Fig. 3.21. The experimental data was obtained at elevated pressures (P = 5 to 20 atm) and temperatures (T = 1050 to 1820 K). Figure 3.21 shows that all of the mechanisms considered in this study are able to provide a reasonable prediction of the ignition delay time trends for H_2/CH_4 under all of the conditions adopted by Zhang et al. [28]. The USC2007 mechanism is the only one capable of accurately predicting the ignition delay time for H_2/CH_4 under all of the pressure conditions and

hydrogen mole fractions investigated by Zhang et al. [28], while yielding the lowest overall mean value of 24.61% (see Supplementary Table A.2).

Similar to the purpose of Fig. 3.13, the overall mean values for the ignition delay time are graphed in Fig. 3.22. Figure 3.22 shows that the USC2007 mechanism offers the best agreement with the experimental results for the $H_2/CO/CH_4$ (Figure-3.20) and H_2/CH_4 (Figure-3.21) mixtures. However, the USC2007 mechanism is not able to predict the ignition delay time for the H_2/H_2O mixture at elevated pressures (Figure-3.16). Furthermore, the performance of the USC2007 mechanism is inferior to that of the NUIG2013 mechanism in predicting both the ignition delay time of the H_2/CO and $H_2/CO/CO_2$ mixtures, and also the flame speed of the $H_2/CO/CH_4/CO_2$ mixtures (see Fig. 3.13). More importantly, the NUIG2013 mechanism has the best performance for predicting the laminar flame speed results of biogas/syngas mixtures. Hence, it appears that if the discrepancies caused by the NUIG2013 mechanism in Figs. 3.18, 3.19, and 3.20 could be resolved, the NUIG2013 mechanism would remain the most suitable mechanism for studying the ignition delay time and also the laminar flame speed of biogas/syngas mixtures. Therefore, the subsequent section addresses the discrepancies caused by the NUIG2013 mechanism, with the aim of yielding the suitable mechanism for biogas/syngas mixtures.

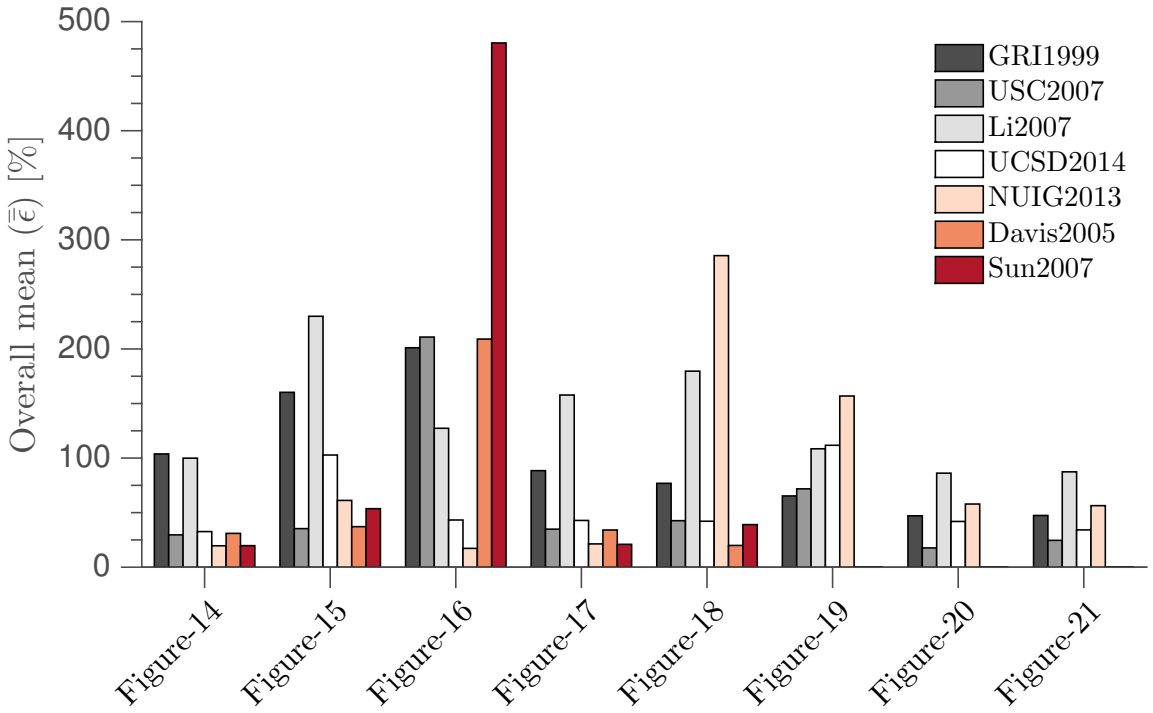

Figure 3.22: Performance of the mechanisms for ignition delay time based on the overall mean value ($\bar{\bar{\epsilon}}$).

3.4 Sensitivity Analysis

A sensitivity analysis was performed for the ignition delay time results shown in Figs. 3.18, 3.19, and 3.20, so as to further elucidate why the NUIG2013 mechanism, which contains the greatest number of reactions, provides unsatisfactory predictions under these specific conditions despite performing remarkably well at predicting the flame speed. In addition, the findings of the sensitivity analysis could aid us in addressing the discrepancies observed. A sensitivity analysis of the ignition delay time results is achieved by multiplying the rate coefficient and dividing both the forward (k^+) and reverse (k^-) rate constant by a factor of two for each reaction in the NUIG2013 mechanism, without affecting the equilibrium. The ignition delay time for each reaction, after being multiplied and divided, are recorded and denoted by τ^+ and τ^-, respectively. The logarithm

sensitivity coefficient (L.S.) for the ignition delay time results is defined as:

$$\text{L.S.} = \frac{\ln(\tau^+/\tau^-)}{\ln(k^+/k^-)} = \frac{\ln(\tau^+/\tau^-)}{\ln(4)}$$

where a positive value of the logarithm sensitivity coefficient indicates that the reaction has an inhibiting effect on the overall reactivity, and vice versa. The logarithm sensitivity coefficient (L.S.) for the laminar flame speed results is defined as:

$$\text{L.S.} = \frac{\ln(\text{S}_\text{u}(k+\Delta k) - S_u(k))}{\ln(1/2)}$$

where the rate of each reaction is multiplied by 1.5 and the flame speed simulation is recomputed to obtain $\text{S}_\text{u}(k+\Delta k)$, and $\text{S}_\text{u}(k)$ represents the laminar flame speed obtained with the original rate constant expression.

3.4.1 $\text{H}_2/\text{CO}/\text{CO}_2$

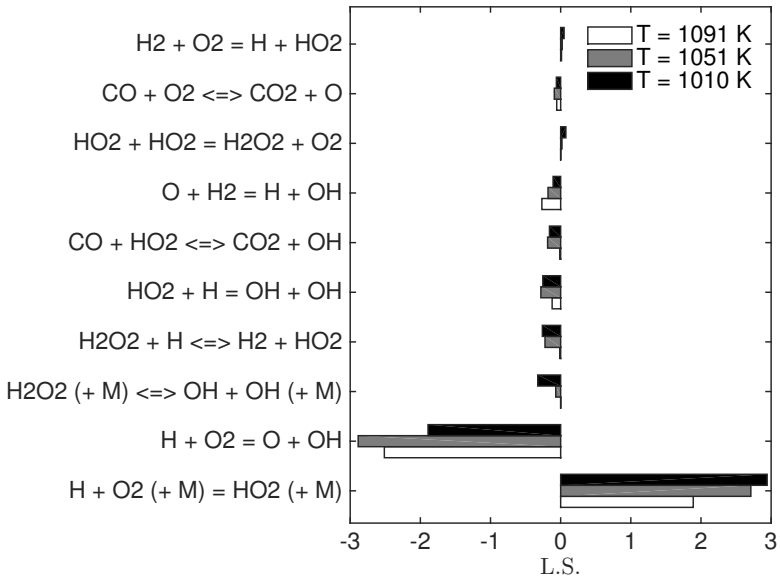

Figure 3.23: Logarithmic sensitivity analysis on the ignition delay time of $\text{H}_2/\text{CO}/\text{CO}_2$ mixture at P = 2.36 atm for NUIG2013 mechanism. Only the ten most sensitive reactions are included, for clarity.

The ignition delay time for stoichiometric $H_2/CO/CO_2/O_2/N_2$ at low pressures (P = 1.24 to 2.36 atm; Fig. 3.18) as predicted by the NUIG2013 mechanism deviates significantly from the experimental data. Interestingly, the Davis2005 mechanism is the only mechanisms that is able to accurately predict the ignition delay time of the H_2/CO mixtures diluted with a large amount of CO_2. However, the NUIG2013 mechanism performs remarkably well when predicting the ignition delay time of $H_2/CO/CO_2/O_2/Ar$ at P = 1.6 to 32 atm, while the Davis2005 mechanism's performances is inferior to that of the NUIG2013 mechanism (see Fig. 3.17). Hence, a sensitivity analysis of the ignition delay time of $H_2/CO/CO_2$ at P = 2.36 atm was conducted as depicted in Fig. 3.23 to further understand which reaction in the NUIG2013 mechanism is responsible for the discrepancy. The result suggests that, at 2.36 atm, the reactivity is mainly controlled by the competition between the chain-branching reaction ($H + O_2 = O + OH$ (R1)) and the chain-terminating reaction ($H + O_2(+M) = HO_2(+M)$ (R2)). Reaction (R1) is not only extremely important in the hydrogen sub-mechanism, but also dominates/controls the oxidation of all fuels undergoing oxidation at high temperatures (T $\geq$ 1000 K, depending on the pressure) [44]. The rate constant (R1) adopted by the NUIG2013 mechanism is identical to several recently published hydrogen mechanisms [118, 119]. In addition, the rate constant has a low uncertainty of less than 10% over a temperature range of 1100 to 3370 K. Therefore, the chain-terminating reaction is further examined. The rate constant (R2) in the NUIG2013 mechanism is adopted from the work of Fernandes et al. [120], which yields excellent results for shock tube measurements (see Fig. 3.17), and when argon is used as the bath gas, as evidenced in Figs. 3.14, 3.15, and 3.17. However, the low-pressure limit rate constant [$k_0(CO_2) = 6.61 \times 10^{19} \times T[K]^{-1.23}(cm^6/mol^2/s)$] employed in the NUIG2013 mechanism for CO_2 as a bath gas reduces the reactivity of $H_2/CO/CO_2$ mixture, resulting in excessively long shock tube ignition delays for a temperature range of 1010 to 1020 K (see Fig. 3.18).

Based on the experimental obtained from a shock tube at temperatures ranging from 900 to 1305 K, Vasu et al. [51] recommended that the low-pressure limiting expression adopted in the GRI1999

mechanism be used for $H + O_2(+CO_2) = HO_2(+CO_2)$ (R2-1). This was because the rate constant provided by the GRI1999 matches the experimental data very well (see Fig. 3.25). However, applying the rate constant [$k_0(CO_2) = 4.20 \times 10^{18} \times T[K]^{-0.86}(cm^6/mol^2/s)$] provided by the GRI1999 for (R2-1) as recommended by Vasu et al. [51] to the NUIG2013 mechanism did not reconcile the discrepancy, as shown in Fig. 3.24. Hence, several rate constants are explored with the NUIG2013 mechanism and finally the rate constant of $k_0(CO_2) = 8.82 \times 10^{19} \times T[K]^{-1.40}(cm^6/mol^2/s)$ (hereafter referred to as NUIG_V1) yields satisfactory results for all the experimental conditions considered by Vasu et al. [51], as depicted in Fig. 3.24. The overall mean value for Fig. 3.18 is significantly reduced from 285.54% (NUIG2013) to 36.45% (NUIG_V1) with a much lower rate constant. Furthermore, the use of the lower rate expression did not significantly affect the excellent prediction produced by the NUIG2013 mechanism in simulating the ignition delay time of other fuel mixtures under other experimental conditions, where almost identical overall mean values are obtained with the NUIG2013 and NUIG_V1 mechanisms, as evidenced in Supplementary Table A.2.

The flame speed results were recomputed using the NUIG_V1 mechanism and it was found that the lower rate expression for (R2-1) improves the predictions of the laminar flame speed for $H_2/CO/CO_2$ under the experimental conditions shown in Figs. 3.4 and 3.6 (see Supplementary Table A.1), but it exacerbates the predictions of the laminar flame speed for $H_2/CO/CO_2$ under the experimental conditions shown in Fig. 3.5 (see Supplementary Table A.1). Interestingly, the lower rate expression for (R2-1) reduces the average relative error value for Fig. 3.9(a), but it increases the average relative error value for Figs. 3.9(c) and 3.9(d). For other fuel combinations or under other experimental conditions, the modification made to the NUIG_V1 mechanism has only a much effect on the flame speed predictions, whereas almost identical overall mean values are obtained with the NUIG_V1 and NUIG2013 mechanisms (see Supplementary Table A.1).

A sensitivity analysis was conducted for the flame speed results shown in Figs. 3.4, 3.5, and 3.6 (see Supplementary Fig. A.24). We found that the (R2-1) reaction exerts the largest influence

on the laminar flame speed of $H_2/CO/CO_2$ at Z_{CO_2} = 0.7 and Z_{H_2} = 0.7. This would explain why, with the lower-rate expression for (R2-1) in the NUIG_V1, the average relative error value decreases from 34.28% to 24.76% for Z_{CO_2} = 0.7 (see Supplementary Table A.1). On the other hand, in comparison with the excellent predictions for the laminar flame speed of $H_2/CO/CO_2$ - 10:40:50 produced by the NUIG2013 mechanism (see Fig. 3.5), those produced with the NUIG_V1 mechanism are inferior, with the average relative error value increasing from 1.47% to 8.34% (see Supplementary Table A.1). This is due to the lower rate expression for (R2) adopted in NUIG_V1 increasing the mixture's reactivity, resulting in a higher flame speed prediction and also a higher average relative error. Therefore, we manipulated the rate expression for other sensitive reactions (see Supplementary Fig. A.24) in the NUIG_V1 mechanism and found that lowering the collision efficiency factor β_{H_2O} for $H + O_2(+M) = HO_2(+M)$ from 12.0 to 8.0 and with multiplying the reaction $HO_2 + H = OH + OH$ by 0.7 (hereafter referred to as NUIG_V2) improved both the predictions of the flame speed results and the grand mean of [A], [B], [C], and [D] (see Table 3.2).

In addition, the modifications made to the NUIG_V2 mechanism did not affect the ability of NUIG_V1 to predict the ignition delay time of all of the fuel mixtures considered in this study, with almost identical grand mean values for [E] and [F] being obtained with the NUIG_V1 and NUIG_V2 mechanisms (see Table 3.2). Although the use of the NUIG_V2 mechanism provides better flame speed results while still producing excellent predictions of the ignition delay time, it was found to exacerbate several flame speed predictions such as those fuel mixtures used in Figs. 3.3a, 3.6b, and 3.9a (see Supplementary Table A.1). Hence, global optimization of the reactions' rate constant is highly recommended so that the accuracy of the NUIG_V1 mechanism can be further improved to predict the flame speed of syngas/biogas fuel mixtures. Nevertheless, the existing NUIG2013 mechanism with the recommended rate constant for (R2-1) offers an adequate level of accuracy in predicting the flame speed of syngas/biogas fuel mixtures and also the ignition delay time of syngas mixtures diluted with CO_2, N_2, and H_2O.

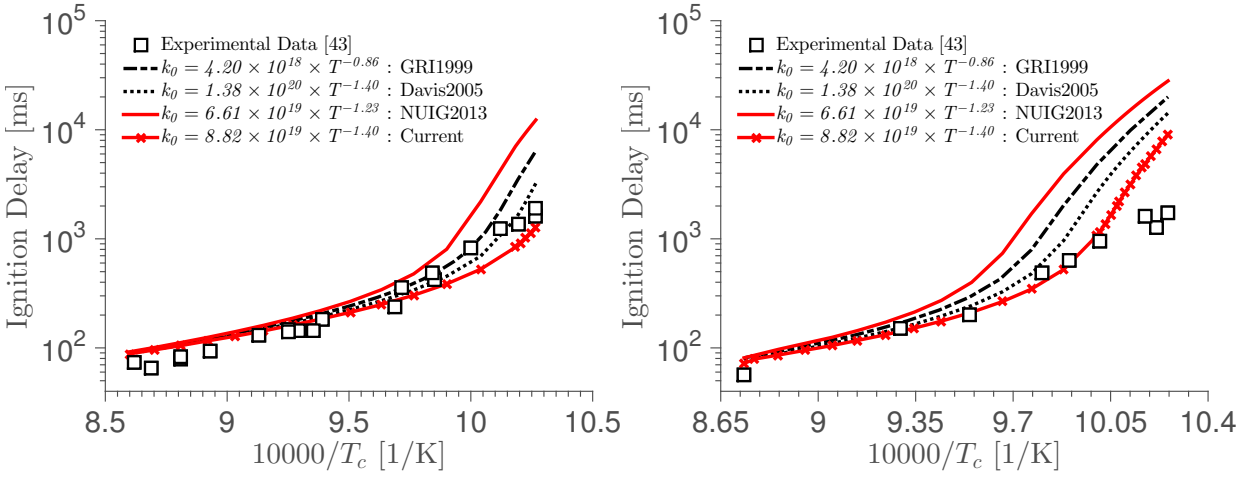

(a) P = 1.21 atm

(b) P = 1.71 atm

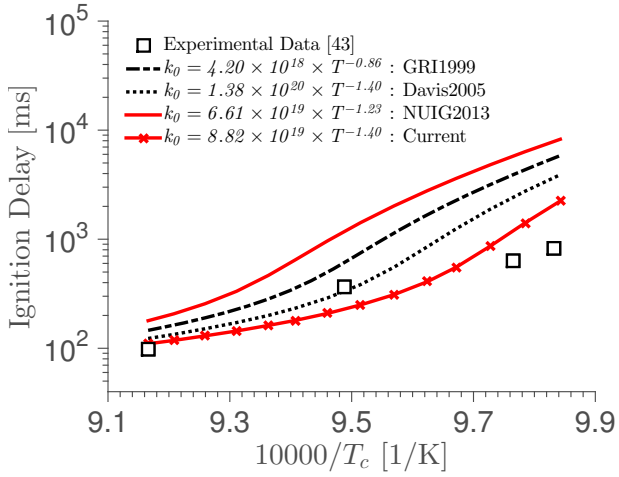

(c) P = 2.36 atm

Figure 3.24: Ignition delay time of $H_2/CO/CO_2$ with various low-pressure limiting expression of $H + O_2 + CO_2 = HO_2 + CO_2$ implemented in the NUIG2013 mechanism.

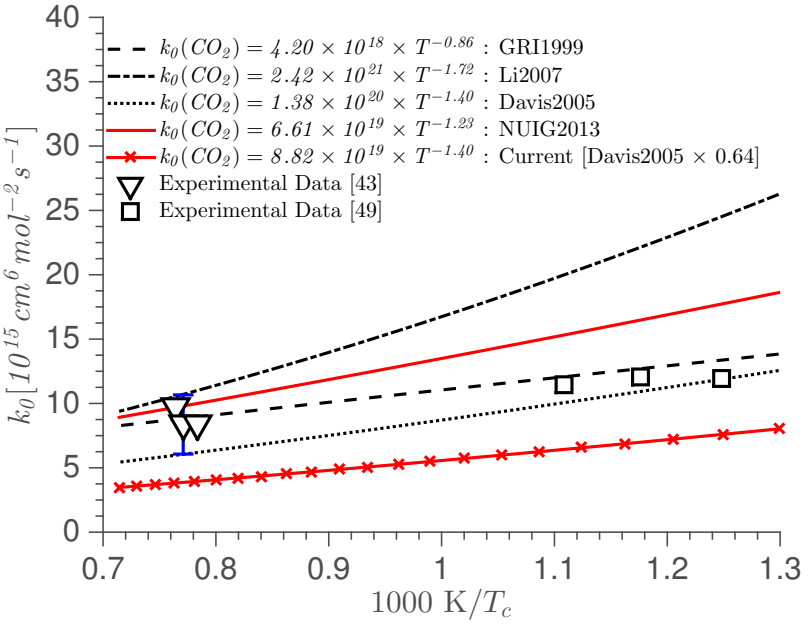

Figure 3.25: Low-pressure limiting expression of $H + O_2 + CO_2 = HO_2 + CO_2$ reaction compared to experimental data. The experimental data were obtained from Vasu et al. [51] and Ashman and Haynes [121].

3.4.2 $H_2/CO/CH_4$

A sensitivity analysis was also performed for the ignition delay time of H_2/CO /CO_2/CH_4/H_2O mixture at P = 32 atm (Fig. 3.17) and for the ignition delay time of $H_2/CO/CH_4$ mixture at P = 32 atm (Fig. 3.20), as large discrepancies between the prediction produced with the NUIG2013 mechanism and the experimental data were observed. The ten most sensitive reactions are plotted in Fig. 3.26(a) for $H_2/CO/CO_2/CH_4/H_2O$ mixture and in Fig. 3.26(b) for $H_2/CO/CH_4$ mixture. As mentioned previously, the rate constants of reaction $H + O_2 = O + OH$ (R1) and $H + O_2(+AR) = HO_2(+AR)$ have received considerable attention such that the uncertainty of (R1) employed in the NUIG2013 mechanism is less than 10% over a temperature range of 1000 to 3370 K [44]. Furthermore, the rate constant employed for reaction (R2) yields excellent results for shock tube measurements when Ar is used as a bath gas, as evidenced in Figs. 3.14, 3.15, and 3.17.

The rate constant for reaction $H_2 + OH = H + H_2O$, incorporated in the NUIG2013 mechanism, was proposed by Lam et al. [122] and is consistent with previous research conducted by Michael and Sutherland [123] and Oldenborg et al. [124], where the uncertainty is less than 17% over a temperature range of 902 to 1518 K. In addition, the discrepancies are observed only for syngas mixtures to which CH_4 has been added. Therefore, we believe that the H_2-CO kinetics are not responsible for the discrepancies observed in Figs. 3.18(c) and Fig. 3.19(c). Nevertheless, readers are referred to [44] for the most up-to-date review of the H_2-CO kinetics. Hence, only the four most sensitive reactions involving C_1 species shown in Fig. 3.26 were further examined to identify which reaction is responsible for the observed disparities:

$$CH_4 + OH = CH_3 + H_2O \tag{R3}$$

$$CH_3 + CH_3(+M) = C_2H_6(+M) \tag{R4}$$

$$CH_3 + HO_2 = CH_3O + OH \tag{R5}$$

$$CH_4 + O = CH_3 + OH \tag{R6}$$

These reactions will be discussed below.

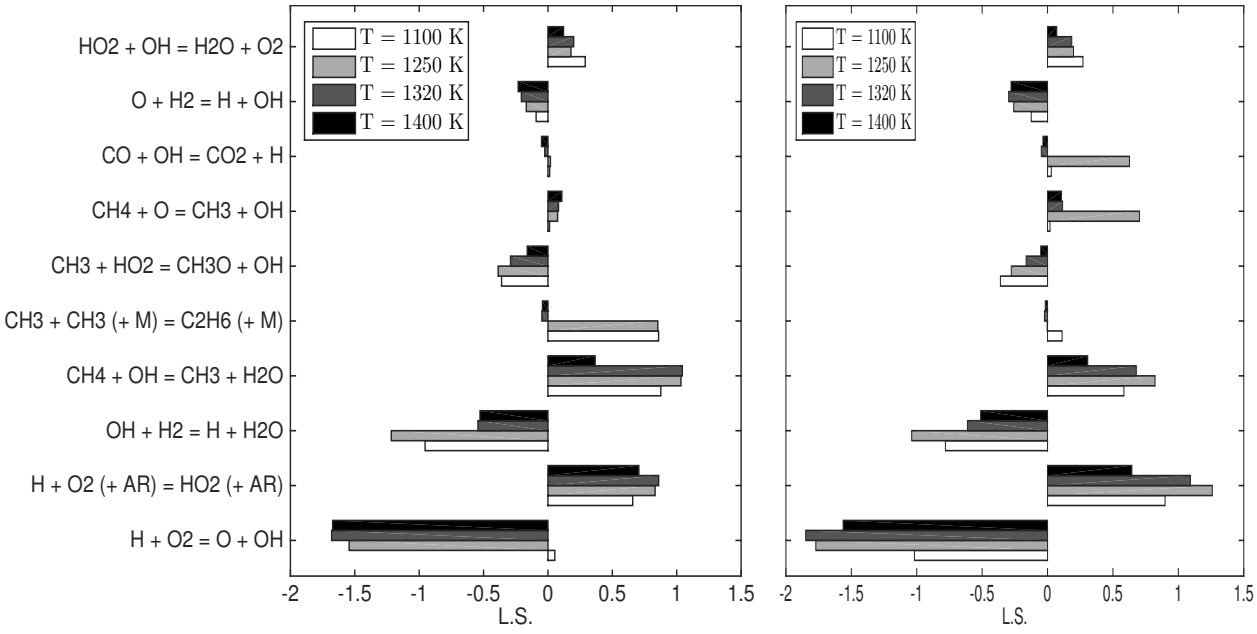

(a) $H_2/CO/CO_2/CH_4/H_2O$ (b) $H_2/CO/CH_4$

Figure 3.26: Logarithmic sensitivity analysis on the ignition delay time of $H_2/CO/CH_4$ and $H_2/CO/CO_2/CH_4/H_2O$ at P = 32 atm for NUIG2013 mechanism. Only the ten most sensitive reactions are included, for clarity.

$CH_4 + OH = CH_3 + H_2O$ (R3)

The reaction abstracting hydrogen from methane by a hydroxyl radical is important reaction to the combustion of syngas with methane added at elevated pressures and temperatures [104], as depicted in Fig. 3.26. The reaction competes with (R1), producing methyl radicals that are less reactive than the hydrogen atoms. Hence, it inhibits the reactivity of the fuel mixtures as indicated by the positive sensitivity coefficient. The rate constant expression of $CH_4 + OH = CH_3 + H_2O$ (R3) employed in the USC2007 mechanism is similar to those incorporated in the GRI1999 mechanism, as provided by Cohen et al. [125]. Although different rate constant expressions are employed in the USC2007 and NUIG2013 mechanisms, they are still close to each other and are in good agreement with the experimentally determined values, as evidenced in supplementary Fig. A.25. In addition, the results of a recent theoretical study by Wang et al. [126] using quantum instanton

calculation to determine the rate constant of (R3), were found to be in excellent agreement with the experimental data. However, further examination of the rate constant expression for (R3) incorporated in all the mechanisms studied in this study at T = 1000 to 2000 K revealed that the rate constant expression incorporated into the NUIG2013 mechanism yields a higher rate constant than the expression adopted by other mechanisms (see Supplementary Fig. A.25). It is worth noting here that reaction (R3) is very sensitive at P = 32 atm and T = 1100 to 1320 K, as evidenced in supplementary Fig. A.27. Hence, we replaced the rate constants of (R3) in the NUIG_V1 mechanism with those expressed in the USC2007, Li2007, and UCSD2014 mechanisms, but none of the rate constants could reconcile the discrepancies. Hence, we fitted a new rate constant expression for (R3) to yield a lower rate constant in the high-temperature region (T = 1000 to 2000 K; see Fig. 3.27), while maintaining excellent agreement with the original rate constant of (R3) used in the NUIG2013 mechanism in the low-temperature region, as evidenced in Supplementary Fig. A.26. Although the newly fitted rate constant predicted a lower rate constant at T = 1000 to 2000 K compared to the rate constant expressed in all of the mechanisms considered in this study (see Supplementary Fig. A.25), the expression still lies within $\pm$ 15% of the experimental data (see Fig. 3.27 and Supplementary Fig. A.26).

The ignition delay time results shown in Figs. 3.19, 3.20, and 3.21 were recomputed with the newly fitted rate constant of (R3) incorporated into the NUIG_V1 mechanism (hereafter referred to as NUIG_V3), and the results are shown in Fig. 3.28 and supplementary Fig. A.28. The newly fitted rate constant expression for (R3) in the NUIG_V3 mechanism reconciled the discrepancies observed in Figs. 3.19(c) and Fig. 3.20(c), as evidenced in Figs. 3.28(a) and 3.28(b). Most importantly, the new rate constant expression of (R3) did not alter the NUIG2013 mechanism's excellent agreement at P = 1.6 and 12.2 atm. Furthermore, the new expression for (R3) improved the NUIG2013 mechanism's predictions of the ignition delay time for H_2/CH_4 at P = 5, 10, and 20 atm (see Supplementary Fig. A.28), and the performance is on par with that of the USC2007 mechanism, where the overall mean values for the USC2007 and NUIG_V3 mechanisms are 24.61% and

24.76%, respectively. The flame speed results are also recomputed using the NUIG_V3 mechanism, producing almost identical results to those output by the NUIG_V1 mechanism, as demonstrated by the almost identical grand mean values for [A] - [D], listed in Table 3.2. To check that the excellent agreement shown in Fig. 3.28 and Supplementary Fig. A.28 was not fortuitous, other sensitive reactions related to the C_1 species were also evaluated and analyzed.

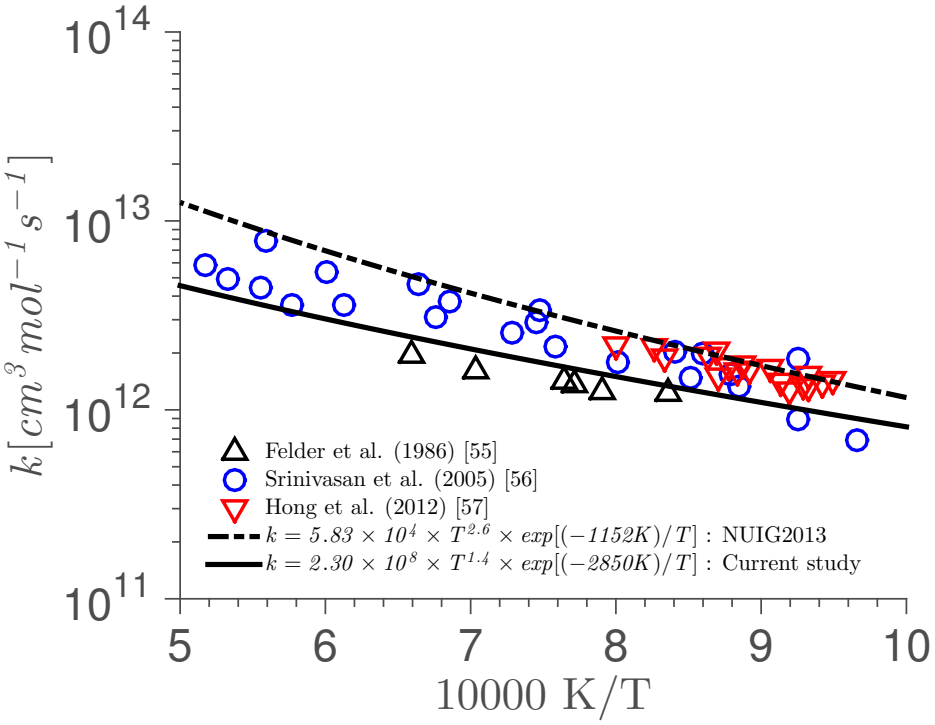

Figure 3.27: Arrhenius plot for $CH_4 + OH = CH_3 + H_2O$. Solid line represents newly fitted rate constant expression and dash-line represents the rate constant expression used in NUIG2013 mechanism. The experimental data were procured from Felder and Madronich [127], Srinivasan et al. [128], and Hong et al. [129].

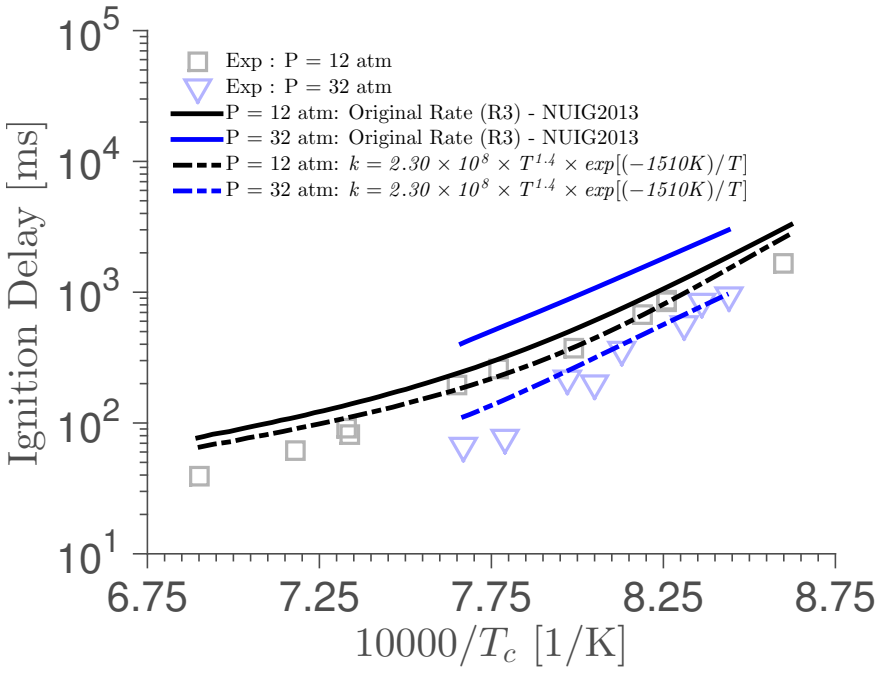

(a) $H_2/CO/CO_2/CH_4/H_2O$

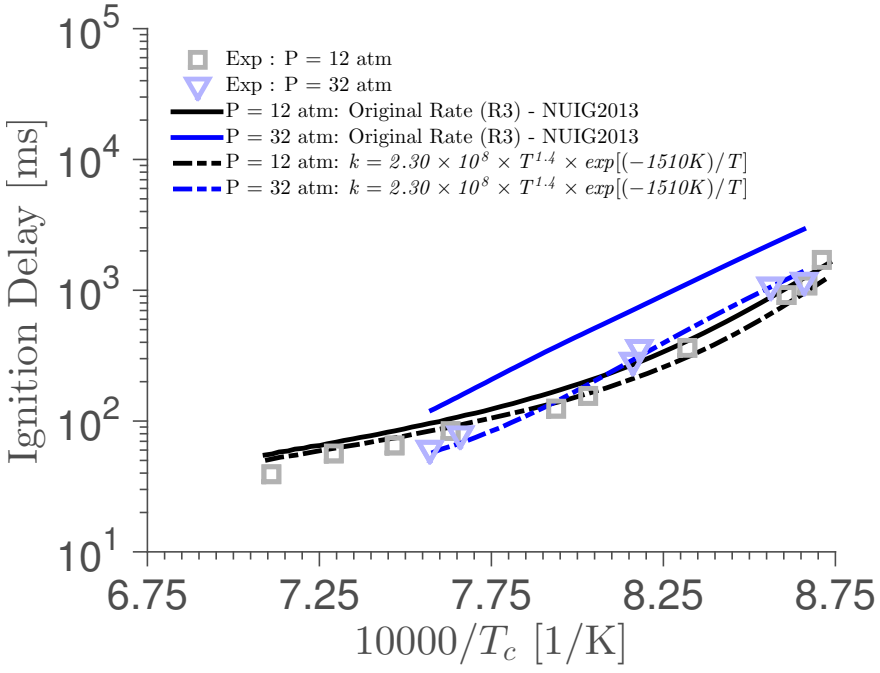

(b) $H_2/CO/CH_4$

Figure 3.28: Comparisons of measured and predicted ignition delay time. Solid-line: NUIG2013 mechanism; dash-line: NUIG_V3 mechanism. The experimental data were procured from [104].

$CH_3 + CH_3(+M) = C_2H_6(+M)$ (R4)

The rate constant for the methyl plus methyl radical recombination, $CH_3 + CH_3(+M) = C_2H_6(+M)$ (R4), has received considerable attention in the past [130, 131, 132, 133]. Therefore, we know that it is not responsible for the discrepancies shown in Figs. 18 and 19. Furthermore, reaction (R4) is only sensitive for the $H_2/CO/CO_2/CH_4/H_2O$ mixture and not sensitive for the $H_2/CO/CH_4$ mixture, as evidenced in supplementary Fig. A.30. Although the rate constant of (R4) employed in the NUIG2013 mechanism differs from those employed in the GRI1999, UCSD2014, and USC2007 mechanisms, they are still within the limits of experimental uncertainty and agree quite well with the experimentally determined values, as shown in supplementary Fig. A.29. More importantly, at P = 32 atm, all of the rate constant expressions predicted an almost identical rate constant, regardless of the temperature (see Supplementary Fig. A.29). Therefore, we can conclude that reaction (R4) does not contribute to the discrepancies that we observed.

$CH_3 + HO2 = CH_3O + OH$ (R5)

This reaction is a major chain-branching reaction and is particularly important during natural gas combustion at intermediate temperatures and high pressures [129]. Similar findings were also observed for syngas mixtures diluted with methane, where reaction (R5) is found to be the most sensitive at T = 1100 K and P = 12 and 32 atm. However, at elevated temperatures (T = 1250, 1320, and 1400 K), reaction (R5) is only sensitive at a high pressure (P = 32 atm), as depicted in Supplementary Fig. A.32. Hence, reaction (R5) could contribute to the discrepancies observed in the previous section. However, the results of a recent experimental study by Hong et al. [129] and a theoretical study by Jasper et al. [134] for reaction (R5) produced results that were in good agreement with each other, as shown in supplementary Fig. A.31. Most importantly, the NUIG2013 mechanism adopts the rate constant proposed by Jasper et al. [134]. Therefore, reaction (R5) can be ruled out as the source of the observed disparities. Nevertheless, it is worth mentioning here that adopting the rate constant for (R5) employed in the GRI1999 mechanism into the NUIG_V1

mechanism would reconcile the discrepancy shown in Figs. 3.19 and Fig. 3.20, but that this rate constant exceeds the rate constant determined through experimental and theoretical studies by a factor of approximately 4.5 (see supplementary Fig. A.31). Hence, the rate constant proposed by Jasper et al. [134] should be retained in the NUIG2013 mechanism. More studies on (R5) at other temperatures are warranted to further substantiate that the rate constant proposed by Jasper et al. [134] is in excellent agreement with the experimental results, as the experimental work conducted by Hong et al. [129] appears to be the first experimental investigation of (R5).

$CH_4 + O = CH_3 + OH$ (R6)

The rate constant of $CH_4 + O = CH_3 + OH$ (R6) incorporated into the NUIG2013, USC2007, UCSD2014, Li2007, and GRI1999 mechanisms are in good agreement with the experimental data, as shown in supplementary Fig. A.33. However, at low temperatures, the NUIG2013, USC2007, and USC2014 mechanisms have almost identical rate constant and they deviate slightly from the rate constant employed in the GRI1999 mechanism. Nevertheless, they are still well within the limits of the experimental uncertainty. Further examination on the reaction (R6) reveals that it is only sensitive to the $H_2/CO/CH_4$ mixture at P = 32 atm and T = 1250 K, and is not very sensitive to the $H_2/CO/CO_2/CH_4/H_2O$ mixture (see Supplementary Fig. A.34). Hence, we believe that the reaction (R6) is not responsible for the discrepancies observed in Figs. 3.19(c) and Fig. 3.20(c).

3.5 Concluding remarks

This Chapter has presented a comprehensive comparison of the most commonly used chemical kinetics mechanisms and published experimental results for mixture compositions that are pertinent to biogas/syngas mixtures. The results that have been compiled and categorized in this study will aid researchers in selecting the best mechanism for simulating a specific fuel combination. The

optimal mechanism for the reproduction of the measured laminar flame speed and the measured ignition delay time of biogas/syngas fuel blends is the NUIG2013 mechanism, which is capable of reproducing the experimental results for most of the mixture compositions considered in this study. In addition, the NUIG2013 mechanism produces the lowest grand mean values for [C] and [D], as tabulated in Table 3.2. Although the NUIG2013 mechanism does not yield the lowest grand mean values for [E] and [F], it is capable of accurately predicting the effect and also the ignition delay time resulting from the addition of H_2O to the H_2 mixture at elevated pressures. The reasons for not identifying the UCSD2014 mechanism as the optimal mechanism for biogas/syngas mixtures include the high grand mean values that it produces for [C] and [D], and its yielding of higher overall mean values compared to the NUIG2013 mechanism for most of the ignition delay time results (see Supplementary Table A.2). However, there are several mixture compositions and conditions for which the NUIG2013 mechanism fails to accurately predict the ignition delay time results. These include the $H_2/CO/CO_2$ mixture at low temperatures ($<$ 1050 K) and low pressures (P = 1.24 - 2.36 atm), the $H_2/CO/CH_4/CO_2/H_2O$ mixture at P = 32 atm, the $H_2/CO/CH_4$ at P = 32 atm, and H_2/CH_4 mixtures at low hydrogen concentrations ($\leq$ 40% H_2). Aside from these conditions, the NUIG2013 mechanism performs remarkably well and produces results that are in excellent agreement with the experimental results. Interestingly, the USC2007 mechanism performs remarkably well for H_2/CH_4 and $H_2/CO/CH_4$ mixtures at standard and elevated pressures, relative to the NUIG2013 mechanism, but still fails to predict the ignition delay time of $H_2/CO/CH_4/CO_2/H_2O$ mixtures at P = 32 atm. Nevertheless, the USC2007 mechanism is able to accurately predict the ignition delay time of $H_2/CO/CH_4$ mixture at elevated pressure (P = 32 atm), while all the other mechanisms over-predict the ignition delay time. Therefore, we have performed a sensitivity analysis on the $H_2/CO/CH_4$ and $H_2/CO/CH_4/CO_2/H_2O$ mixtures using the NUIG2013 mechanism to elucidate why the NUIG2013 mechanism could not accurately predict the ignition delay time results and also why the performance of the NUIG2013 mechanism is below that of the USC2007 mechanism for these particular mixtures and experimental conditions.

Furthermore, we would like to determine why none of the investigated mechanisms are capable of predicting the ignition delay time for $H_2/CO/CH_4/CO_2/H_2O$ mixture diluted with 98% of argon at elevated pressure (P = 32 atm).

It was found that the $CH_4 + OH = CH_3 + H_2O$ (R3) reaction is the reason for the NUIG2013 mechanism to predict longer ignition delay time for $H_2/CO/CH_4$ and $H_2/CO/CH_4/CO_2/H_2O$ mixtures. Therefore, a new rate constant expression for (R3) was fitted so that the NUIG2013 mechanism can predict shorter ignition delay time for these fuel mixtures. The new rate constant expression for (R3) not only allowed the NUIG2013 mechanism to accurately predict the ignition delay time for the $H_2/CO/CH_4$ and $H_2/CO/CH_4/CO_2/H_2O$ mixtures at P = 32 atm, but also improved the performance of the NUIG2013 mechanism in predicting the ignition delay time of H_2/CH_4 at P = 5, 10, and 20 atm, where it was found to be on par with the USC2007 mechanism. Furthermore, the new rate constant expression for (R3) did not affect the excellent performance of the original NUIG2013 mechanism at predicting the laminar flame speed or the ignition delay time for other fuel mixtures and other experimental conditions considered in this study. Most importantly, the newly fitted rate constant expression for (R3) closely matches the experimental data found in literature and agrees particularly well in the low-temperature region. Further examinations on the ignition delay time of the $H_2/CO/CO_2$ mixture reveal that the $H + O_2(+CO_2) = HO_2(+CO_2)$ (R2-1) reaction is responsible for the longer ignition delay time predicted by the NUIG2013 mechanism at P = 1.24 - 2.36 atm and T $<$ 1025 K. To reconcile this discrepancy, the rate constant expression of (R2-1) in the NUIG2013 mechanism should be lowered to $k_0(CO_2) = 8.82 \times 10^{19} \times T[K]^{-1.40} (cm^6/mol^2/s)$. More importantly, the modifications made to (R2-1) and (R3) did not substantially affect the original NUIG2013 mechanism's excellent predictions of the flame speed or ignition delay time results for the other mixture compositions or other experimental conditions considered in this study.

In addition to the modified rate constant of (R2-1), we found that decreasing the collision efficiency factor β = 12.0 for H_2O to β = 8.0 in (R2), and then multiplying the reaction $HO_2 + H = OH + OH$

by 0.7 (NUIG_V2), further improved the overall flame speed calculations, yielding a much lower grand mean value for [A] to [D]. However, these modifications exacerbate the predictions of the laminar flame speed for several fuel mixtures, for which higher overall mean values are obtained. Hence, it is recommended that global optimization be performed to further improve the accuracy of the flame speed and ignition delay time predictions. Nevertheless, the use of the existing NUIG2013 mechanism with the proposed rate constants for (R2-1) and (R3) could provide an adequate level of accuracy when predicting the flame speed and the ignition delay time of syngas/biogas mixtures. Therefore, we highly recommend incorporating the proposed rate constants for (R2-1) and (R3) into the NUIG2013 mechanism to study the combustion characteristics of biogas/syngas fuel mixtures.

Chapter 4

Reduced mechanism for biogas and syngas combustion

Abstract

A genetic algorithm (GA) method was proposed and validated for the optimal extraction of a sub-mechanism for $H_2/CO/CH_4/CO_2$ mixtures from the detailed NUIG2013 chemical kinetics mechanism, which was developed for C_1 - C_5 hydrocarbons and oxygenated fuels. Ninety ignition delay time data involving mixtures containing H_2, CO, CH_4, CO_2, N_2, and H_2O at wide range of experimental conditions were used as optimization targets to guide the GA, so that the final reduced mechanism was able to fully describe the combustion characteristics of syngas and biogas fuel mixtures. The final reduced mechanism for $H_2/CO/CH_4/CO_2$ fuel mixtures comprised of 72 species and 290 reactions, and it was extensively validated against experimental results, including measured ignition delay times and laminar flame speeds, over a wide range of operating conditions. The excellent agreement between the reduced mechanism and NUIG2013 mechanism in predicting the combustion properties of $H_2/CO/CH_4/CO_2$ mixtures with maximum relative error values of only 0.9 % and 2.75 %, respectively for the ignition delay time and laminar flame speed

results, indicates that the proposed reduced mechanism can be used for predicting the combustion characteristics of biogas and syngas fuel mixtures. Furthermore, it was observed that the reduced mechanism shows excellent agreement with the NUIG2013 mechanism in predicting the ignition delay time of mixtures with added ethane and propane. Therefore, the proposed reduced mechanism represents the most up-to-date detailed chemical kinetics mechanism for biogas and syngas fuel mixtures, and it can also be used for predicting the combustion properties of natural gas with impurities such as ethane and propane. The reduced mechanism agreed so well with the NUIG2013 mechanism in predicting the combustion properties of $H_2/CO/CH_4/CO_2$ mixtures, where both mechanisms performed identically in over predicting the ignition delay time for $H_2/CO/CO_2$, CO_2, $H_2/CO/CH_4$, and $H_2/CO/CH_4/CO_2/H_2O$ mixtures at several experimental conditions. These observations were also reported by Lee et al. [135], where they proposed two new rate constants for $H + O_2(+CO_2) = HO_2(+CO_2)$ and $CH_4 + OH = CH_3 + H_2O$ to reconcile the discrepancies observed. These two new rate constants were assessed in this study by incorporating the modified rate constants into the 290Rxn mechanism (referred as 290Rxn-V1), where it was found that the modified rate constants did improve the ignition delay time predictions. However, the two proposed rate constants did not improve the predictions of the laminar flame speed for mixtures with a high CO_2 content at high equivalence ratios ($\phi > 1.2$). Therefore, optimization of the rate constants in the 290Rxn mechanism is highly recommended to further improve its agreement with experimental data for biogas and syngas fuel mixtures.

4.1 Background

Based on the comprehensive comparison of several notable chemical kinetics mechanisms [135] in Chapter 3, including GRI1999 [108], Li2007 [109], Davis2005 [73], USC2007 [110], UCSD2014 [111], Sun2007 [36], and NUIG2013 [1], NUIG2013 mechanism was found to provide the most accurate predictions of the experimental data, while the other mechanisms exhibited varying degrees

of agreement with experimental results. This was not surprising, as the authors of the NUIG2013 paper [1] updated their H/C/O sub-mechanism recently [44], and the NUIG2013 mechanism comprises the most up-to-date rate constants. Syngas mainly comprises CO and H_2 with varying amounts of CO_2, CH_4, and H_2O [136], while biogas consists mainly of CO_2 and CH_4 with varying amounts of N_2 [137]. However, the NUIG2013 mechanism was developed for C_1-C_5 mixtures, and therefore contains many species and reactions that are irrelevant to biogas and syngas combustion. Therefore, the main objective of this chapter is to find a sub-mechanism within the large detailed NUIG2013 chemical kinetics mechanism for application to biogas/syngas combustion. This will lead to a substantially reduced amount of species and reactions in the detailed sub-mechanism for biogas and syngas fuel mixtures, allowing it to be used to conduct large parametric studies on fuel mixtures, or further optimized to improve its prediction capability using significantly less computational time.

There are several systematic methodologies that can reduce a detailed mechanism to a skeleton or reduced mechanism, and comprehensive reviews on these methods are presented in references [138, 139, 140, 141]. The genetic algorithm (GA) method was adopted in this Chapter as it does not require any sensitivity analysis or require any knowledge of the rate constants during the reduction process, but rather it relies on eliminating reactions that are deemed unimportant for biogas and syngas combustion through a fitness function. In addition, methods such as direct path flux analysis [141] and global pathway selection [142] have been tested and used for large detailed mechanism with up to hundreds of species, while studies [143, 144, 145, 146] that employed the GA approach have presented the reduction of a detailed mechanism that consisted of only 338 reactions and 67 species. Therefore, one of the objectives of this study is to test this simple yet robust method for extracting a smaller sub-mechanism for biogas and syngas fuel mixtures from a large detailed mechanism such as the NUIG2013 mechanism. The final mechanism obtained by GA is then compared to the NUIG2013 mechanism and published experimental data to evaluate the performance and assess the limit of the mechanism obtained in this study. Consequently, the

final mechanism presented in this study is the detailed chemical kinetics mechanism that is able to mimic the performance of the NUIG2013 mechanism in predicting the combustion properties of biogas/syngas accurately.

4.2 Methodology

4.2.1 Modeling approach

Numerical simulations were performed using the CANTERA reacting flow software package [106]. Shock tube experiments were simulated by assuming a constant volume and adiabatic conditions. The simulated ignition delay time results were computed as described in the respective publications, i.e., based on the maximum slope of the pressure profile or based on the measurement of the chemiluminescence of OH* or CH*. Laminar flames were simulated using the FreeFlame class included in the CANTERA package, which is identical to the PREMIX code [112] of the CHEMKIN-II package. The jet-wall stagnation flames were simulated using the premixed stagnation flame code of the CANTERA reacting flow software package. The boundary conditions specified in the simulation of the jet-wall stagnation flame were taken directly from the experimental measurements, allowing a direct comparison of the measured and simulated profiles. For more information on the stagnation flames simulation methodology, refer to reference [90]. In all of the laminar flame speed simulations, multicomponent diffusion and Soret effects are included, as these effects have significant impact on the calculated laminar flame speed, especially for H_2/CO mixtures without any dilution at P = 1 atm [135]. The converged solution is obtained for a large number of grid points (approximately 400) by considering a gradient and curvature of 0.1 (see Appendix D.4 in [114]). The standard definition of equivalence ratio (ϕ) is adopted in this work, and it is defined as follows:

$$\phi = \frac{(\mathrm{n_{fuel}}/\mathrm{n_{oxygen}})_{\mathrm{act}}}{(\mathrm{n_{fuel}}/\mathrm{n_{oxygen}})_{\mathrm{st}}}$$

where *n* represents the number of moles, and the suffixes *act* and *st* indicate actual mixture and stoichiometric mixture, respectively.

The agreement between the NUIG2013 and the reduced mechanism obtained from GA was computed using the following objective function:

$$\mathrm{E_{ij}} = \left| \frac{\mathrm{Y_{NUIG2013,ij}} - \mathrm{Y_{reduced,ij}}}{\mathrm{Y_{NUIG2013,ij}}} \right| \times 100\%$$

Here, $\mathrm{E_{ij}}$ is the absolute relative error values for the *i*th case. The *j* represents the *j*th data point in the *i*th case. The values $\mathrm{Y_{NUIG2013,ij}}$ and $\mathrm{Y_{reduced,ij}}$ correspond to the result for the *j*th data point obtained from the NUIG2013 and the reduced mechanism, respectively, in the *i*th case. The parameter used to compare the jet-wall stagnation flames is the reference flame speed, $\mathrm{S_{u,ref}}$. The reference flame speed is defined as the minimum upstream velocity of the flow, prior to the temperature rise. This velocity also represents the local mass-burning rate of the flame at the inlet temperature, composition, and hydrodynamic strain rate. For brevity, only the maximum relative error values in each case ($\mathrm{E_{i,max}}$) and comparison between experimental data and simulated results of selected cases are plotted in this manuscript. Refer to the Supporting Information for full comparison between the experimental data and the simulated results obtained from the NUIG2013 mechanism and the reduced mechanisms.

4.2.2 Genetic algorithm

GA is an adaptive heuristic mathematical techniques based on the ideas of evolutionary natural selection and genetics. GA works particularly well in several fields, especially if the shape of the function to optimize is not known. It finds a near optimal solution to a problem, where the optimal is defined by a criteria function (also called objective or fitness function). This sub-section only

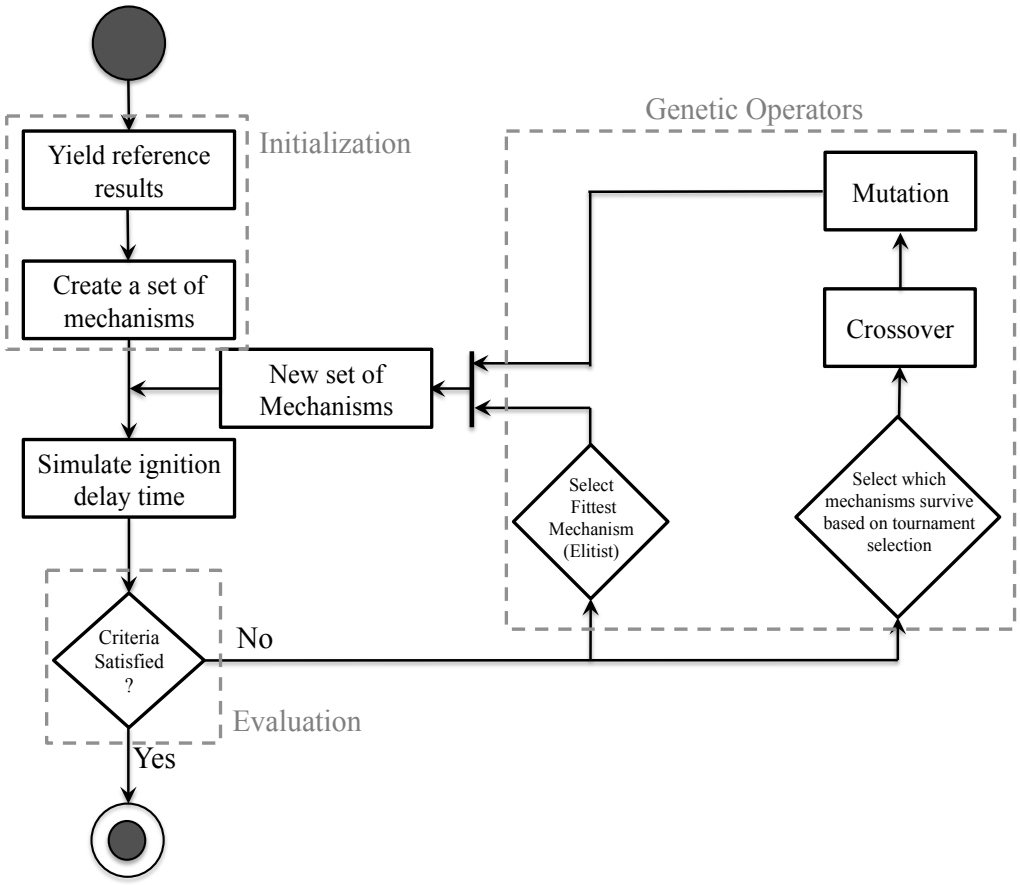

Figure 4.1: Flow chart of the genetic algorithm. [143]

provides a conceptual representative of the algorithm and readers are referred to the work of Sikalo et al. [143] for a more detailed explanation on the algorithm.

Figure 4.1 shows the genetic algorithm procedure adopted for this study and it consists of the following steps:

1. *Initialization*, where a set of initial kinetics mechanisms is generated.
2. *Evaluation*, where the performance of each mechanism is assessed and a corresponding fitness is assigned to each mechanism.
3. Genetic operators consisting of the following three processes:
    (a) *Selection*: The mechanisms are sorted based on their overall fit-

ness, and the fittest kinetics mechanism of the current generation is retained for next generation (Elitist). The remaining new kinetics mechanisms for the next generation are chosen from the current generation based on the tournament selection.

(b) *Crossover*: Two randomly selected mechanisms exchange information to create two new mechanisms for the next generation.

(c) *Mutation*: All mechanisms except for the fittest mechanism go through a mutation with a probability to randomly eliminate reaction(s) from the mechanism in order to increase the diversity of the new set of mechanisms for the next generation.

The new set of mechanisms undergoes evaluation and genetic operators until the termination criteria are satisfied or a given number of generations have passed. The purpose of including elitist selection during the selection process is to ensure that the best solution to the problem, i.e., the best-reduced mechanism is not lost during the crossover and mutation operators. As soon as a better mechanism is found, the newly found mechanism replaces the old elitist mechanism. Table 4.1 shows the 90 data points used as the optimization targets to steer the genetic algorithm in finding a reduced mechanism that is capable of capturing the temperature and pressure dependences of the ignition delay time of biogas/syngas fuel mixtures with minimal difference to the NUIG2013 mechanism.

Table 4.1: Overview of the fuel mixtures and experimental conditions included as optimization targets to guide the genetic algorithm in finding an optimized sub-mechanism for biogas/syngas fuel mixtures.

Case	Fuel Mixture [mol %]								Experimental conditions			Ref.
No.	H_2	CO	O_2	H_2O	CO_2	CH_4	N_2	Ar	T [K]	P [atm]	ϕ	
1	0.500	0.500	1.000	-	-	-	-	98.000	990/1495/2000	1.62	0.50	
2	0.500	0.500	1.000	-	-	-	-	98.000	1095/1240/1385	11.90	0.50	
3	0.500	0.500	1.000	-	-	-	-	98.000	1170/1250/1330	32.20	0.50	
4	0.440	0.440	0.890	0.230	-	-	-	98.000	995/1502/2010	1.750	0.50	
5	0.440	0.440	0.890	0.230	-	-	-	98.000	1085/1243/1400	12.20	0.50	[104]
6	0.440	0.440	0.890	0.230	-	-	-	98.000	1155/1228/1300	32.20	0.50	
7	0.460	0.460	0.930	-	0.150	-	-	98.000	1005/1485/1965	1.72	0.50	
8	0.460	0.460	0.930	-	0.150	-	-	98.000	1105/1233/1360	12.7	0.50	
9	0.460	0.460	0.930	-	0.150	-	-	98.000	1150/1220/1290	31.4	0.50	
10	8.910	11.580	10.250	-	24.44	-	44.830	-	952/1065/1177	1.24	1.00	
11	8.910	11.580	10.250	-	24.44	-	44.830	-	975/1060/1145	1.71	1.00	[51]
12	8.910	11.580	10.250	-	24.44	-	44.830	-	1010/1051/1091	2.36	1.00	
13	0.406	0.406	1.113	-	-	0.075	-	98.000	1010/1465/1920	1.73	0.50	
14	0.406	0.406	1.113	-	-	0.075	-	98.000	1145/1278/1410	12.1	0.50	
15	0.406	0.406	1.113	-	-	0.075	-	98.000	1155/1238/1320	31.1	0.50	
16	0.296	0.296	0.950	0.209	0.157	0.089	-	98.000	1050/1540/2030	1.77	0.50	[104]
17	0.296	0.296	0.950	0.209	0.157	0.089	-	98.000	1160/1305/1450	12.3	0.50	
18	0.296	0.296	0.950	0.209	0.157	0.089	-	98.000	1185/1245/1305	30.7	0.50	
19	1.856	-	3.713	-	-	0.464	-	93.967	1060/1180/1300	5.00	0.50	
20	1.046	-	3.834	-	-	0.697	-	94.423	1116/1258/1400	5.00	0.50	
21	0.558	-	3.907	-	-	0.837	-	94.698	1222/1461/1700	5.00	0.50	
22	0.233	-	3.956	-	-	0.931	-	94.880	1380/1615/1850	5.00	0.50	
23	1.856	-	3.713	-	-	0.464	-	93.967	1060/1168/1275	10.00	0.50	
24	1.046	-	3.834	-	-	0.697	-	94.423	1075/1235/1395	10.00	0.50	
25	0.558	-	3.907	-	-	0.837	-	94.698	1155/1468/1780	10.00	0.50	[28]
26	0.233	-	3.956	-	-	0.931	-	94.880	1295/1548/1800	10.00	0.50	
27	1.856	-	3.713	-	-	0.464	-	93.967	1025/1259/1492	20.00	0.50	
28	1.046	-	3.834	-	-	0.697	-	94.423	1072/1312/1552	20.00	0.50	
29	0.558	-	3.907	-	-	0.837	-	94.698	1140/1383/1625	20.00	0.50	
30	0.233	-	3.956	-	-	0.931	-	94.880	1215/1608/2000	20.00	0.50	

The algorithm was initialized with a total of 24 identical mechanisms to the original mechanism (NUIG2013). We did not deactivate any reactions initially to avoid losing important reactions during the first generation. A fitness function was used to measure the closeness of the reduced mechanism to the original mechanism, where the algorithm searches for the highest fitness value among the set of mechanisms at every generation/iteration. The fitness function is defined as following:

$$\mathrm{F_{overall,i}} = \mathrm{F}_{\tau,\mathrm{i}} + \mathrm{F_{T,i}} + \mathrm{F_{N,i}} \tag{1}$$

where *i* represents the set of mechanisms, and $\mathrm{F}_{\tau,\mathrm{i}}$ and $\mathrm{F_{T,i}}$ are the ignition delay time and the steady state temperature error functions, respectively. They are responsible for computing the deviation of the ignition delay time and the steady state temperature predicted by the NUIG2013 mechanism and the reduced mechanism. Conversely, $\mathrm{F_{N,i}}$ keeps track of the number of reactions remaining in each of the mechanism at every generation. The error functions are given by:

$$\mathrm{F}_{\tau,\mathrm{i}} = \sum_{\mathrm{j=1}}^{\mathrm{k=90}} \ln\left(1 + \sigma_\tau \left| \frac{\tau_{\mathrm{j,reduced}} - \tau_{\mathrm{j,NUIG2013}}}{\tau_{\mathrm{j,NUIG2013}}} \right| \right) \tag{2}$$

$$\mathrm{F_{T,i}} = \sum_{\mathrm{j=1}}^{\mathrm{k=90}} \ln\left(1 + \sigma_\mathrm{T} \left| \frac{\mathrm{T_{j,reduced}} - \mathrm{T_{j,NUIG2013}}}{\mathrm{T_{j,NUIG2013}}} \right| \right) \tag{3}$$

$$\mathrm{F_{T,i}} = \left[1 + \exp\left(\sigma_\mathrm{N} \times \left[1 - \frac{\mathrm{N_{reduced}}}{\lambda \times \mathrm{N_{NUIG2013}}}\right]\right)\right] \tag{4}$$

The k in Eq. 2 and Eq. 3 represents the total of optimization targets in the 30 different fuel mixtures combinations presented in Table 4.1. The datasets tabulated in Table 4.1 are considered on the basis that they are pertinent to biogas and syngas combustion, so that the reduced mechanism can accurately predict the combustion properties of biogas and syngas fuel mixtures. The sharpening factors [σ] in Eq. 2 to 4 were proposed by Sikalo et al. [143] to allow users to put more weight on either the accuracy of the mechanism (leading towards a chemical mechanism that is more accurate in terms of ignition delay time and reaching a steady state temperature) or the size of the mechanism while sacrificing its accuracy. The coefficients of the evaluation functions are presented

Table 4.2: Genetic algorithm parameters and genetic operators used in this study.

Parameters	Value
Number of Generations	3000
Population Size	24
Crossover Rate	0.4
Mutation Rate	0.03
σ_τ	1
σ_T	1
σ_N	3
λ	0.60
Selection	Tournament selection
Crossover	Single point
Mutation	One directional

in Table 4.2, and more weight is put on $\mathrm{F_{N,i}}$ because we would like to obtain a smaller mechanism that is able to describe the combustion properties of biogas/syngas fuel mixtures.

4.3 Results and discussion

4.3.1 Reduced mechanism

The final reduced mechanism was found at the 1349th generation with an overall fitness score of 0.01, as depicted in Fig. 4.2, and consists of 277 reactions and 71 species, which is reduced from the 2067 reactions and 325 species in the NUIG2013 mechanism (hereafter designated as the 277Rxn mechanism). The algorithm continued to search for a smaller mechanism for an additional 1500 generations, but an identical fitness score and number of reactions to that of the 1349th generation was obtained. This indicates that the algorithm has converged and further searching

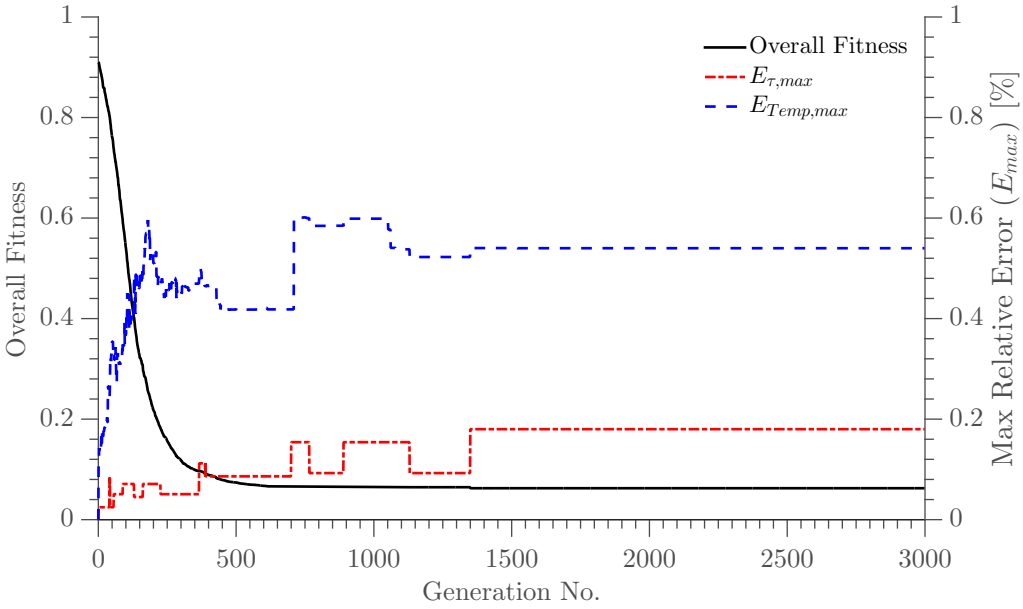

Figure 4.2: Overall fitness and the maximum relative error value among the 90 optimization targets of the reduced mechanism (277Rxn) in 3000 generations.

using the same genetic algorithm parameters will yield an identical result. The highest absolute relative error values (E_{max}) among the 90 data points shown in Table 4.1 are approximately 0.18 % and 0.57 % for ignition delay time and steady state temperature results, respectively (see Fig. 4.2). Upon closer examination of the 277Rxn mechanism, we found that the following reactions were removed during the search process:

$$H + O_2(+HE) = HO_2(+HE) \tag{R1}$$

$$C_2H + O = CO + CH^* \tag{R2}$$

$$C + H + M = CH^* + M \tag{R3}$$

$$C_2H + O_2 = CO_2 + CH^* \tag{R4}$$

$$CH^* + ARCH + AR \tag{R5}$$

$$CH^* + H_2O = CH + H_2O \tag{R6}$$

$$CH^* + CO = CH + CO \tag{R7}$$

$$CH^* + CO_2 = CH + CO_2 \quad \text{(R8)}$$

$$CH^* + O_2 = CH + O_2 \quad \text{(R9)}$$

$$CH^* + H_2 = CH + H_2 \quad \text{(R10)}$$

$$CH^* = CH \quad \text{(R11)}$$

$$CH^* + CH_4 = CH + CH_4 \quad \text{(R12)}$$

$$CH^* + N_2 = CH + N_2 \quad \text{(R13)}$$

This is because HE was not part of the fuel mixtures used to guide the GA, and the CH^* species was not used to determine the ignition delay time in the cases presented in Table 4.1. However, HE is normally used as an inert gas when high-pressure flame speed measurement is involved. Therefore, (R1) with its original parameters from NUIG2013 was added back into the 277Rxn mechanism. The ignition delay time of mixtures comprising mainly CH_4 is normally determined by measuring the time difference between the initiation of the system by the reflected shock wave and the occurrence of the CH^*, as in the studies by Healy et al [147] and Petersen et al. [148]. Therefore, CH^* specie and its related reactions (R2) - (R13) from Aramco 1.3 were added back into the 277Rxn so that an exact comparison of the measured ignition delay time values can be made for fuels with CH_4 addition. Hence, the reduced mechanism has a total of 72 species and 290 reactions, and is referred hereafter as 290Rxn. The 290Rxn mechanism is expected to perform identically to the NUIG2013 mechanism for syngas and hydrogen mixtures because the entire H_2/CO chemistry in the NUIG2013 mechanism is retained with only the formyl radical-radical reaction being removed during the search process:

$$HCO + HCO \rightarrow H_2 + CO + CO \quad \text{(R14)}$$

To further evaluate the performance of 290Rxn mechanism in predicting the ignition delay time of the fuel mixtures shown in Table 4.1 at temperatures that were not optimization targets, the ignition delay time of the 30 cases were recomputed with thirty temperature points between the

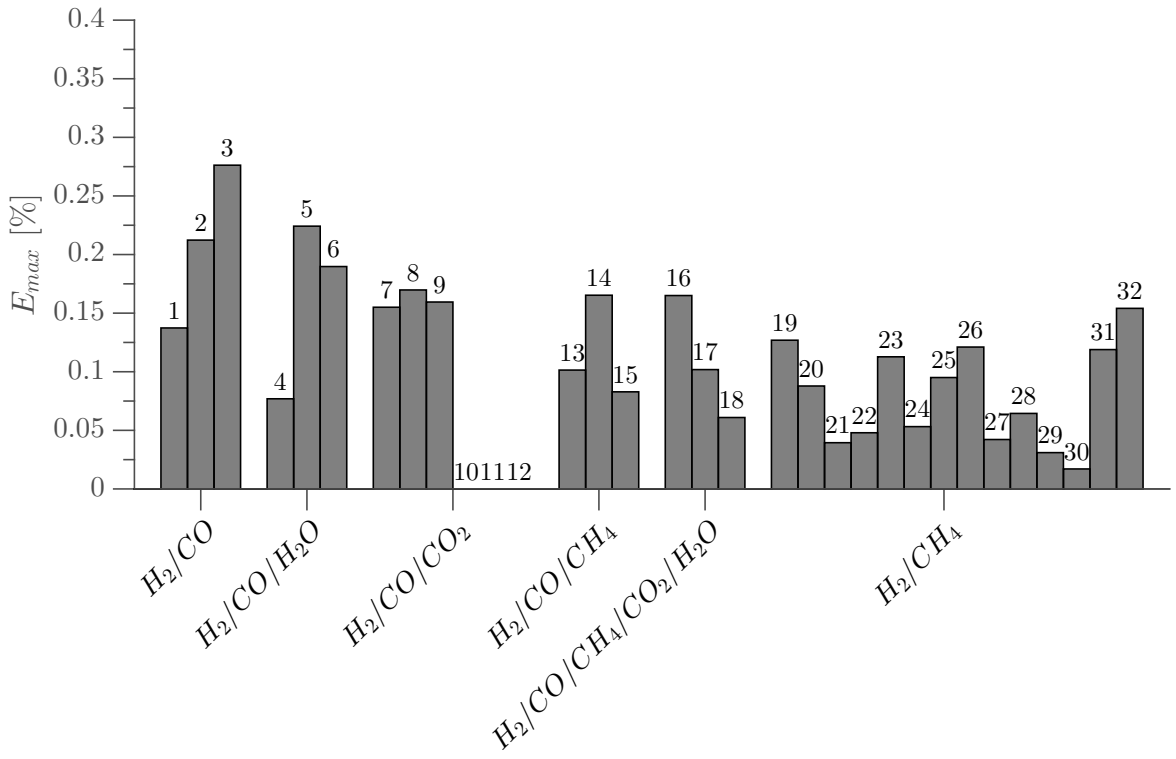

Figure 4.3: The maximum relative error values between the 290Rxn mechanism and the NUIG2013 mechanism for Cases 1 to 32 (Ignition Delay Time). The number above the bar represents the case number and its respective fuel compositions and experimental conditions can be found in Table B or Supplementary Table B.1.

lowest and the highest unburned temperature with the 290Rxn and the NUIG2013 mechanism. The highest relative error values ($\mathrm{E_{max}}$) between the 290Rxn and NUIG2013 mechanism in predicting the ignition delay time of Cases 1 to 30 are plotted in Fig. 4.3, where the $\mathrm{E_{max}}$ values are found to be well below 0.3 %. Further examination of Case 3 at T = 1319 K (which posses the highest $\mathrm{E_{max}}$ value) reveals that the predicted ignition delay time by the 290Rxn and the NUIG2013 are 36.2 μs and 36.1 μs, respectively, i.e., showing no significant difference. For $\mathrm{H_2/CO}$ mixtures with high $\mathrm{CO_2}$ dilution (Cases 10 to 12) and with $\mathrm{CH_4}$ and $\mathrm{CO_2}$ addition (Cases 14 and 15), the 290Rxn and the NUIG2013 mechanisms give identical predictions and they deviate significantly from the experimental data, as shown in Fig. 4.4, 4.5, and 4.6. These findings are consistent with observations reported by Lee et al. [135], wherein they proposed two new rate constants for

$$\mathrm{H + O_2(+CO_2) = HO_2(+CO_2)} \tag{R15}$$

$$\mathrm{CH_4 + OH = CH_3 + H_2O} \tag{R16}$$

to reconcile the discrepancies observed between the measured and simulated ignition delay time in Cases 10 to 30. We developed a variant of 290Rxn to adopt the rate constants proposed by Lee et al. [135], which is referred to hereafter as 290Rxn-V1. The mechanism featuring the two new rate constants for (R15) and (R16) yields satisfactory predictions for Cases 10 to 18, which agree well with the experimental data, as represented in Fig. 4.4, 4.5, and 4.6 by the blue dotted line. In addition, the two new rate constants improve the prediction of the ignition delay time of $\mathrm{H_2/CH_4}$ mixtures, where closer agreement with the experimental data is exhibited by the 290Rxn-V1 mechanism, as shown in Fig. 4.7 for Cases 19 to 30. Interestingly, the proposed rate constants preserved the mechanism's initial excellent predictions for Cases 1 to 9, where 290Rxn, 290Rxn-V1, and NUIG2013 exhibit identical predictions (see Supplementary Fig. B.1 - B.3). The $\mathrm{E_{ij}}$ values were not computed for the 290Rxn-V1 mechanism because the deviations are expected to be quite large, and only direct comparison with experimental data will provide meaningful conclusions.

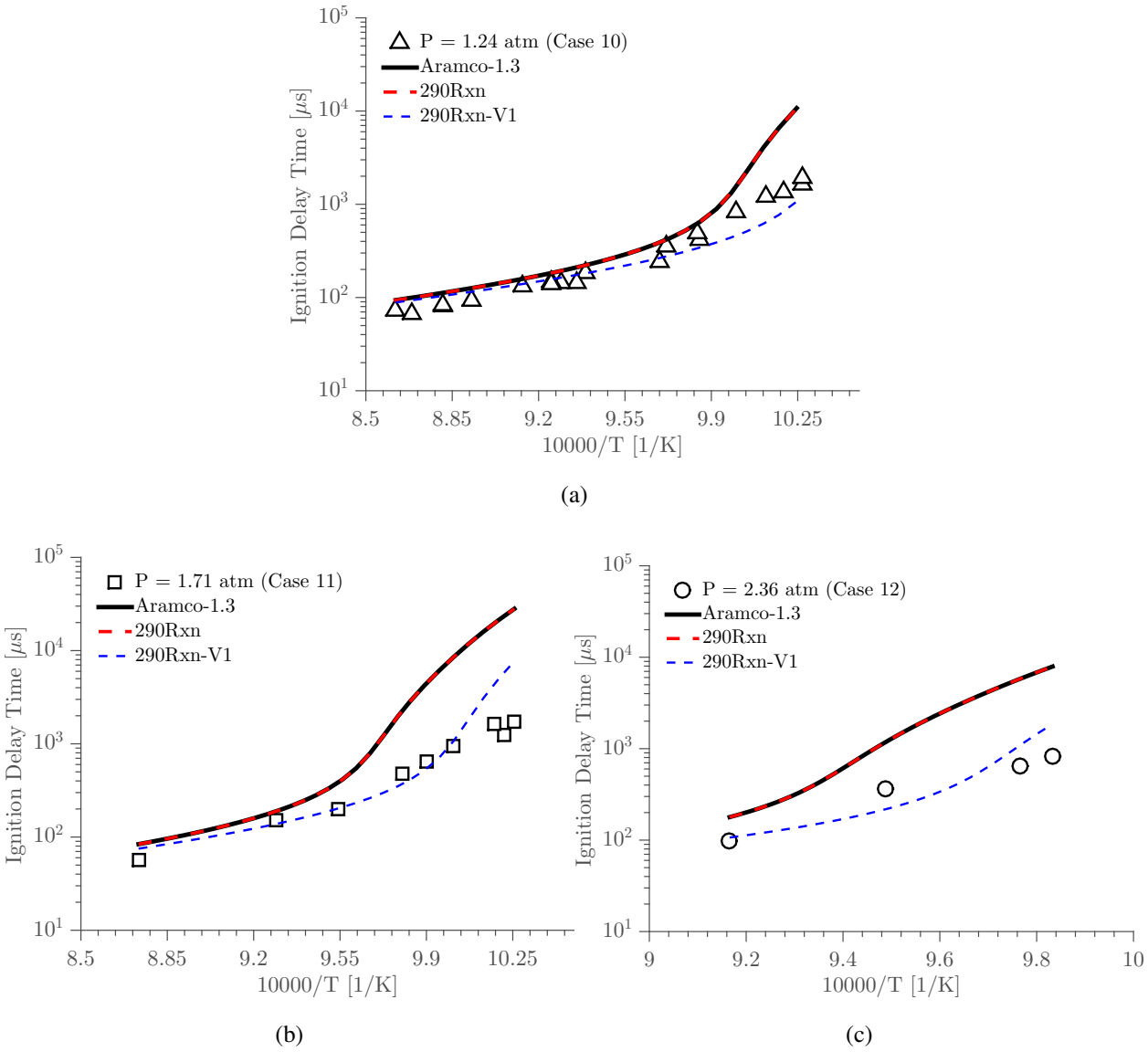

Figure 4.4: Comparisons of measured and predicted ignition delay time of $H_2/CO/CO_2$ fuel mixture (ϕ = 1.0). The experimental data were obtained from ref. [51]. Lines show predictions from the different kinetics models.

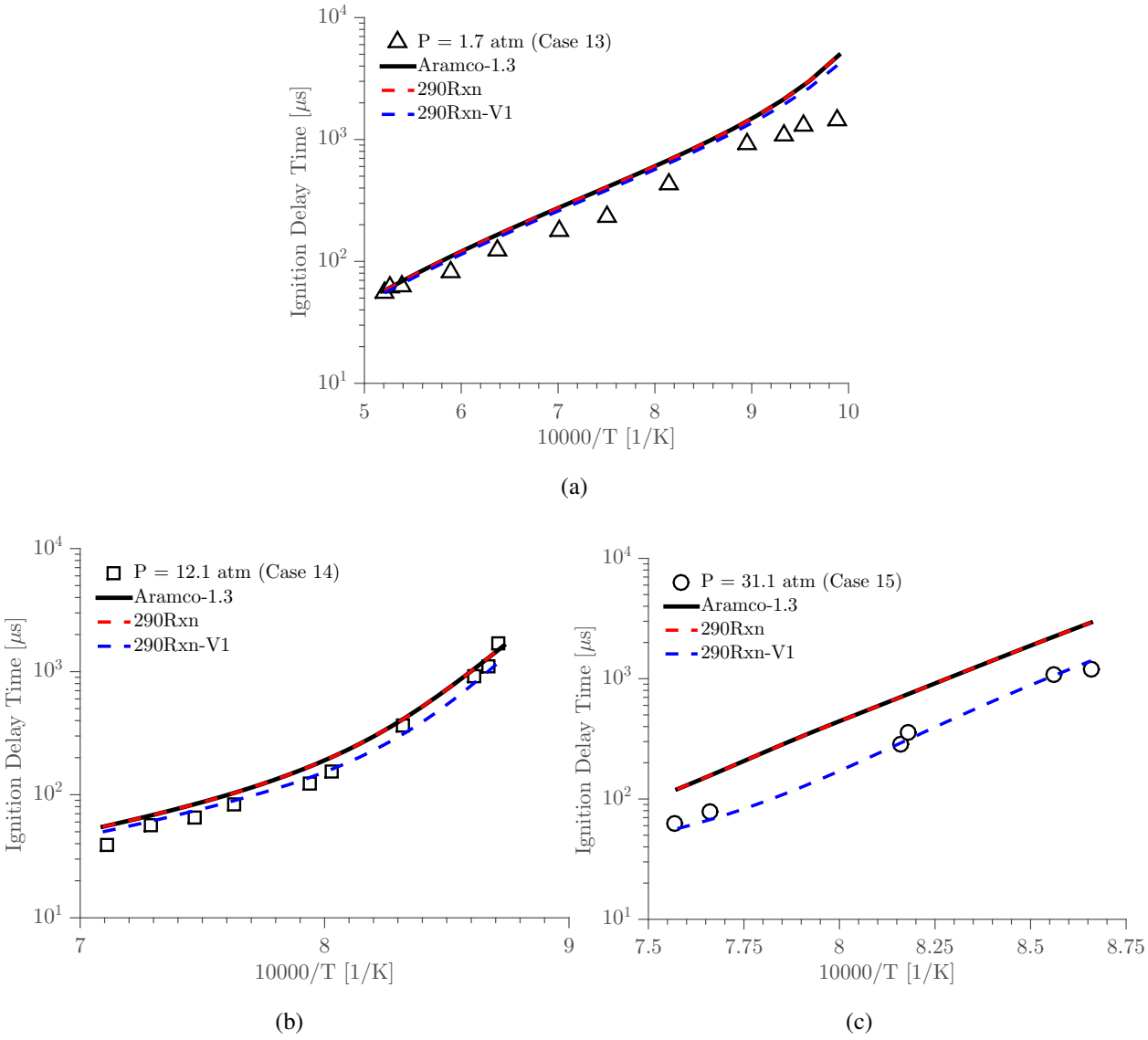

Figure 4.5: Comparisons of measured and predicted ignition delay time of $H_2/CO/CH_4$ fuel mixture (ϕ = 0.5). The experimental data were obtained from ref. [104]. Lines show predictions from the different kinetics models.

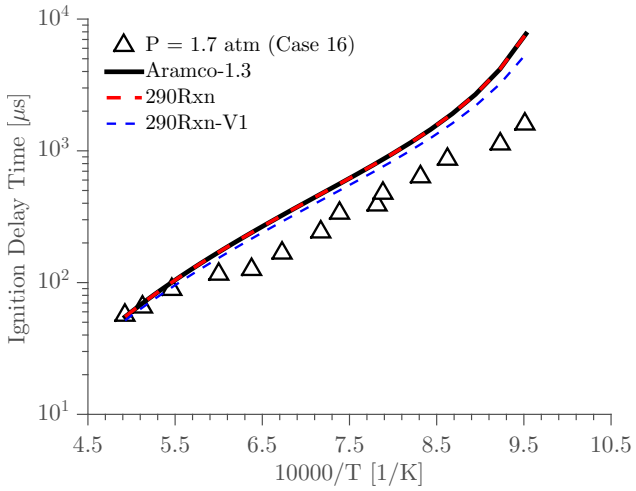

(a)

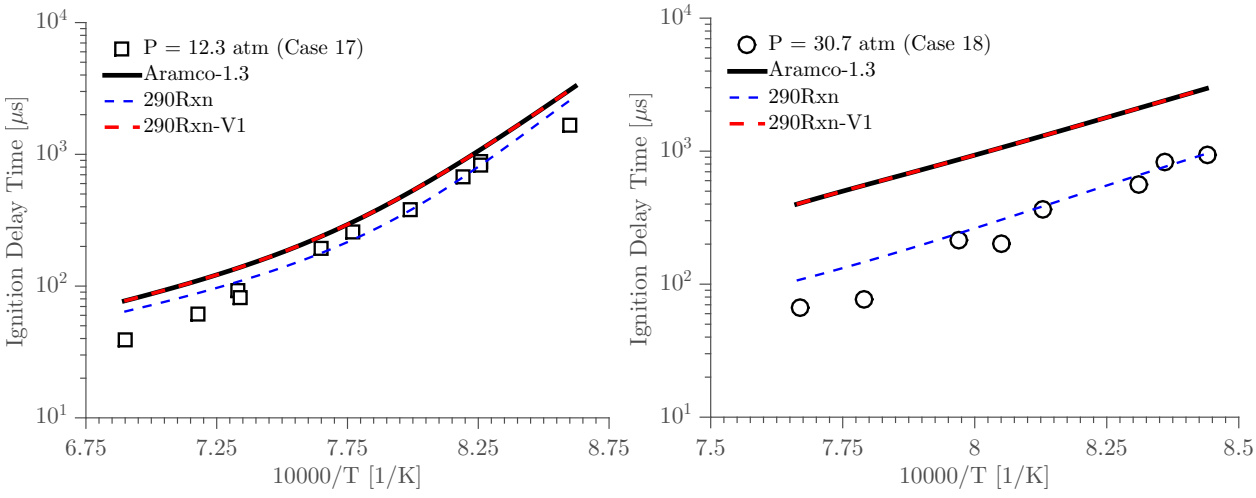

(b) (c)

Figure 4.6: Comparisons of measured and predicted ignition delay time of $H_2/CO/CH_4/CO_2/H_2O$ fuel mixture (ϕ = 0.5). The experimental data were obtained from ref. [104]. Lines show predictions from the different kinetics models.

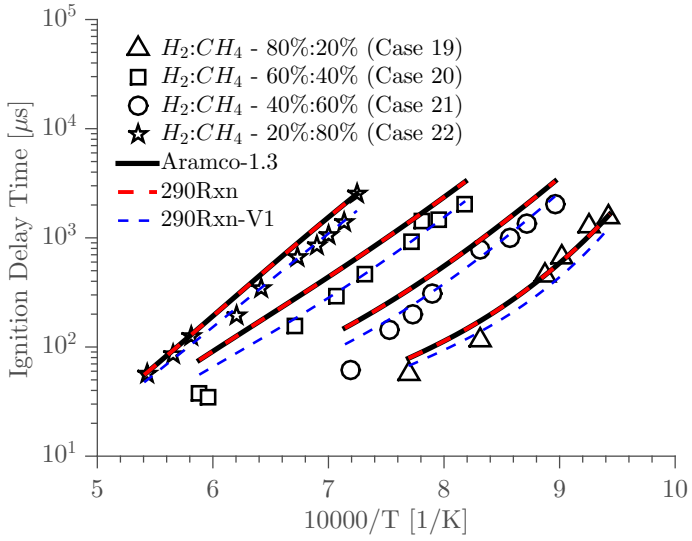

(a) P = 5 atm

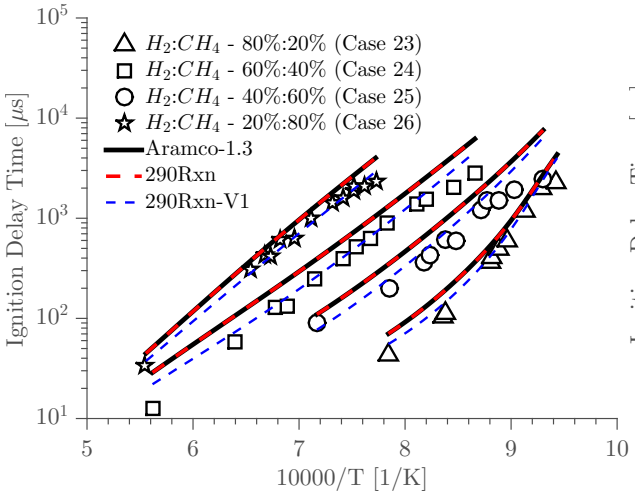

(b) P = 10 atm

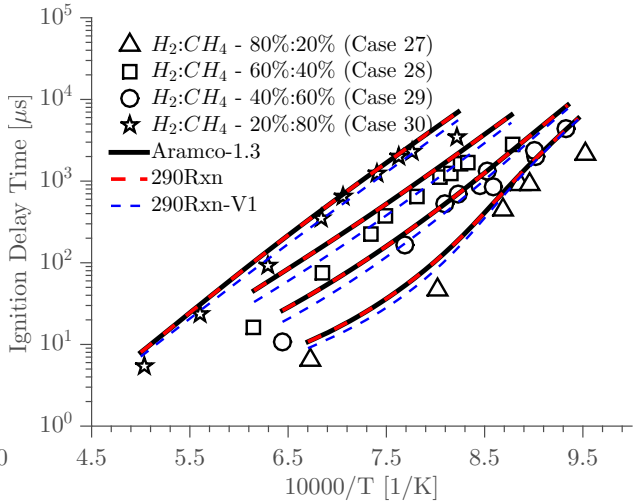

(c) P = 20 atm

Figure 4.7: Comparisons of measured and predicted ignition delay time of H_2/CH_4 fuel mixtures ($\phi = 0.5$) at various pressure conditions. The experimental data were obtained from ref. [28]. Lines show predictions from the different kinetics models.

4.3.2 Validations

Ignition delay time

Table 4.3: Summary of the mixture combinations and the experimental conditions used for mechanism validation. Refer to Supplementary Table B.1 for more detailed information on the fuel compositions and experimental conditions used in each case.

Case No.	Fuel	Experimental conditions			Ref.
		ϕ	P [atm]	T [K]	
		Ignition Delay Time			
1 - 3	H_2/CO	0.5	1.6 - 32.0	990 - 2000	[104]
4-6	$H_2/CO/H_2O$	0.5	1.6 - 32.0	995 - 2010	[104]
7 - 12	$H_2/CO/CO_2$	0.5	1.6 - 32.0	1005 - 1965	[104]
		1.0	1.24 - 2.36	952 - 1091	[51]
13 - 15	$H_2/CO/CH_4$	0.5	1.6 - 32.0	1010 - 1920	[104]
16 - 18	$H_2/CO/CO_2/CH_4/H_2O$	0.5	1.6 - 32.0	1050 - 2030	[104]
19 - 32	H_2/CH_4	0.5	5.0 - 20.0	1050 - 2000	[28, 149]
33 - 39	CH_4	0.5 - 1.0	1.6 - 3.9	1348 - 1881	[150]
40 - 45	CH_4/H_2O	0.5 - 2.0	1.6 - 30.0	1470 - 2128	[151]
46 - 57	$H_2/CH_4/C_2H_6$	0.5 - 1.0	4.0 - 16.0	984 - 1800	[152]
58 - 70	CH_4/C_3H_8	1.0 - 1.5	2.5 - 7.1	1295 - 1682	[148, 153]
71 - 94	$CH_4/C_2H_6/C_3H_8$	0.5 - 2.0	1.0 - 30.0	1021 - 1577	[147]
		Laminar Flame Speed			
95 - 102	H_2/CO	0.5 - 5.0	1	300	[39, 36, 92, 93, 94]
		0.6 - 4.0	5 - 10	300	[43, 35, 36]

Continued on next page

Table 4.3 – *Continued on next page*

Case No.	Fuel	Experimental conditions			Ref.
		ϕ	P [atm]	T [K]	
103 - 116	$H_2/CO/CO_2$	0.7 - 3.5	5 - 40	300	[36, 44]
		0.4 - 1.0	1 - 3	303 - 373	[91]
		0.8 - 2.0	1	303	[95]
		0.4	1 - 2	300	[96]
117 - 122	$H_2/CO/H_2O$	0.4 - 0.9	1	323	[97]
		1.0	1	400	[42]
123 - 126	$H_2/CO/N_2$	0.5 - 1.0	1 - 5	303 - 373	[91]
127 - 130	H_2/CH_4	1.0	1	300	[98, 99, 100]
		0.6 - 2.0	1 - 5	298 - 450	[99, 101, 102, 103, 100]
131 - 143	$H_2/CO/CH_4/CO_2$	0.7 - 1.0	1	300	[90]
144 - 149	CH_4	0.6 - 1.4	1 - 5	300 - 600	[154, 155, 156, 157]

Fuel mixtures and experimental conditions that are not optimization targets, but are pertinent to the biogas and syngas combustions are also included in this study, and are summarized in Table 4.3 (Cases 31 to 149) to assess the accuracy and limits of the 290Rxn and the 290Rxn-V1 mechanisms. The performance of the 290Rxn mechanism is identical to that of the NUIG2013 mechanism in predicting the ignition delay times of CH_4 and CH_4/H_2O mixtures, where the maximum relative error values between the 290Rxn and the NUIG2013 are well below 0.85 % (See Fig. 4.3 and 4.8). Closer examination of Case 37 at T = 1728 K (E = 0.83 %) reveals that the ignition delay time values predicted by 290Rxn and NUIG2013 are 134.2 μs and 133.1 μs, respectively, presenting a difference of only 1.1 μs. Interestingly, the modified rate constant of (R16) does not have a

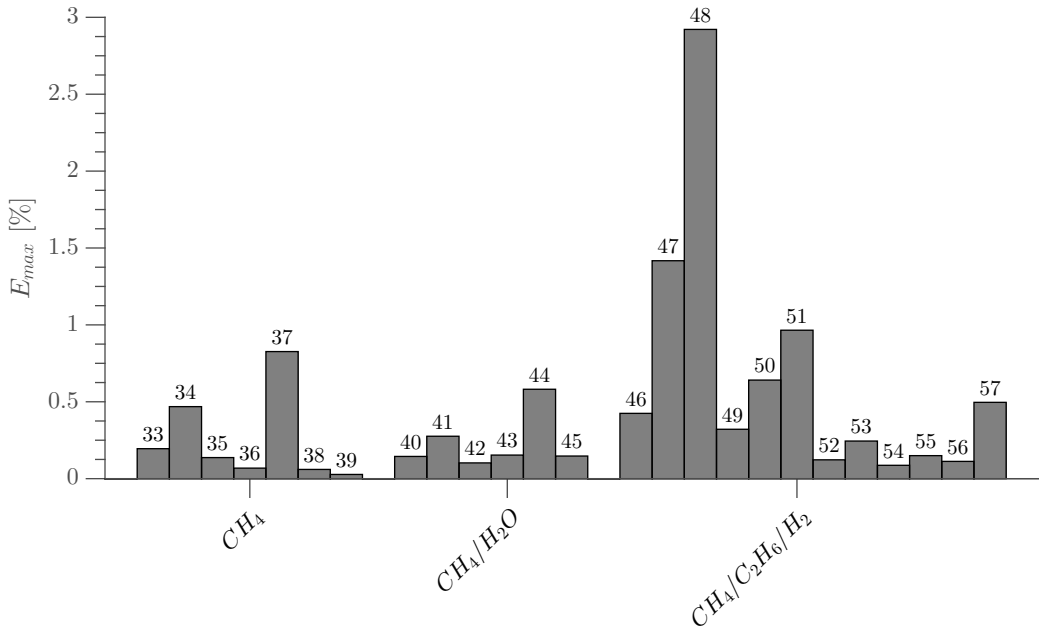

Figure 4.8: The maximum relative error values between the 290Rxn mechanism and the NUIG2013 mechanism for Cases 33 to 57 (Ignition Delay Time). The number above the bar represents the case number and its respective fuel compositions and experimental conditions can be found in Table 4.3 or Supplementary Table B.1.

significant impact on the ignition delay time values for Cases 33 to 45, where 290Rxn-V1 yields almost identical predictions as to those obtained with 290Rxn and NUIG2013, and all the three mechanisms exhibit excellent agreement with the experimental data (see Supplementary Fig. B.7 and B.8).

Since the 290Rxn mechanism consists of C_2H_6 and C_3H_10 species after the search process, CH_4/H_2 mixtures with the addition of C_2H_6 are included in this study to evaluate the performance and limit of the reduced mechanisms. The maximum relative error (E_{max}) values between the 290Rxn and the NUIG2013 range from 0.02 % to 0.16 % for CH_4/H_2 mixtures (see Fig. 4.3), and the E_{max} value increases to 2.92 % in Case 48 when CH_4/H_2 mixtures are diluted with C_2H_6 (see Fig. 4.8). To further examine the impact of the E_{max} of 2.92 % found in Case 48, the predicted and the measured ignition delay time values for Case 48 are plotted in Fig. 4.9. Excellent agreement is

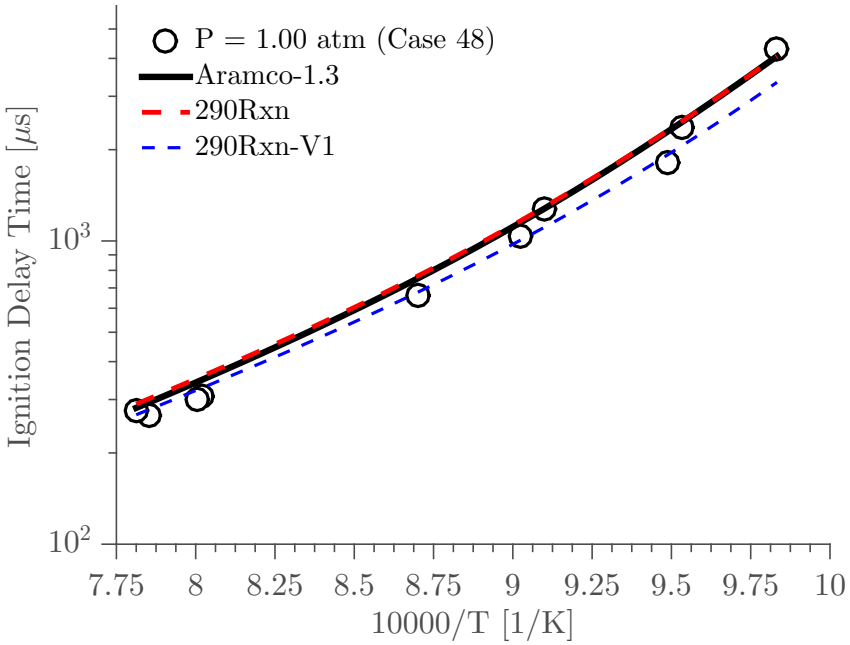

Figure 4.9: Comparisons of measured and predicted ignition delay time of $H_2/CH_4/C_2H_6$ fuel mixtures (ϕ = 0.5). The experimental data were obtained from ref. [152] . Lines show predictions from the different kinetics models.

observed between the 290Rxn mechanism and the NUIG2013 mechanism in the lower temperature range, and the relative error value of 2.92 % occurs at high temperature (T = 1271 K), where the difference between the two mechanisms is insignificant. The modifications performed on (R15) and (R15) increase the reactivity of $CH_4/H_2/C_2H_6$ mixtures, where 290Rxn-V1 mechanism predicted slightly shorter ignition delay time values compared to those obtained with 290Rxn and NUIG2013 (see Supplementary Fig. B.9). Although the modified rate constants do not improve the predictions, the 290Rxn-V1 mechanism still agrees quite well with the experimental data, and is well within the experimental uncertainty for $CH_4/H_2/C_2H_6$ mixtures.

The effect of C_3H_8 addition is also considered in this study, and the maximum relative error values for the ignition delay time of CH_4/C_3H_8 and $CH_4/C_2H_6/C_3H_8$ mixtures are plotted in Fig. 4.10. A maximum relative error value of 11.33 % is found in Case 67 for a CH_4/C_3H_8 mixture at low temperature region, but the 290Rxn mechanism exhibits identical performance to the NUIG2013

mechanism at high temperature region, as depicted in Fig. 4.11(b). Although 11.33 % may seem high, closer examination of Fig. 4.11(b) shows that the 290Rxn exhibits better agreement with the experimental data compared to the NUIG2013 mechanism, and that the difference between the two mechanisms in the low temperature region is not that significant. Similar observations to Case 67 were found for Case 66 and Case 68, where the predictions by the 290Rxn mechanism are closer to the experimental data compared to those of NUIG2013 mechanism (see Fig. 4.11(a) and 4.11(c)), and the difference between the two mechanisms is again almost negligible. The modified rate constants in the 290Rxn-V1 mechanism further improve the predictions of the ignition delay time values for CH_4/C_3H_8 mixtures when compared to the experimental data (see Supplementary Fig. B.10). We would like to stress that although 290Rxn and 290Rxn-V1 show better agreement with the experimental data, the NUIG2013 mechanism's predictions still agree very well with the experimental data and can definitely predict the ignition delay time values of CH_4/C_3H_8 mixtures very well. Case 90 has the highest E_{max} value of 8.45 % among the $CH_4/C_2H_6/C_3H_8$ mixtures at low temperatures but 290Rxn is able to predict the ignition delay time very well and the difference is very small, as shown in Fig. 4.12. Contrary to the observations for $CH_4/H_2/C_2H_6$ mixtures, the 290Rxn-V1 mechanism has better agreement with the experimental data compared to 290Rxn and NUIG2013, as shown in Fig. 12 and Supplementary Fig. B.11(a) - B.11(i). Therefore, the 290Rxn mechanism exhibits identical performance to the NUIG2013 mechanism in predicting the ignition delay time of H_2/CO, H_2/CH_4 and CH_4 mixtures containing a wide range of impurities, such as CO_2, H_2O, N_2, C_2H_6, and C_3H_8, over a wide range of experimental conditions. Surprisingly, the proposed rate constants by Lee et al. [135] improve the ignition delay time predictions for CH_4/C_3H_8, $CH_4/C_3H_8/C_2H_6$, $H_2/CO/CO_2$, $H_2/CO/CO_2/CH_4$ and H_2/CH_4 mixtures while retaining the excellent ignition delay time predictions for H_2/CO mixtures.

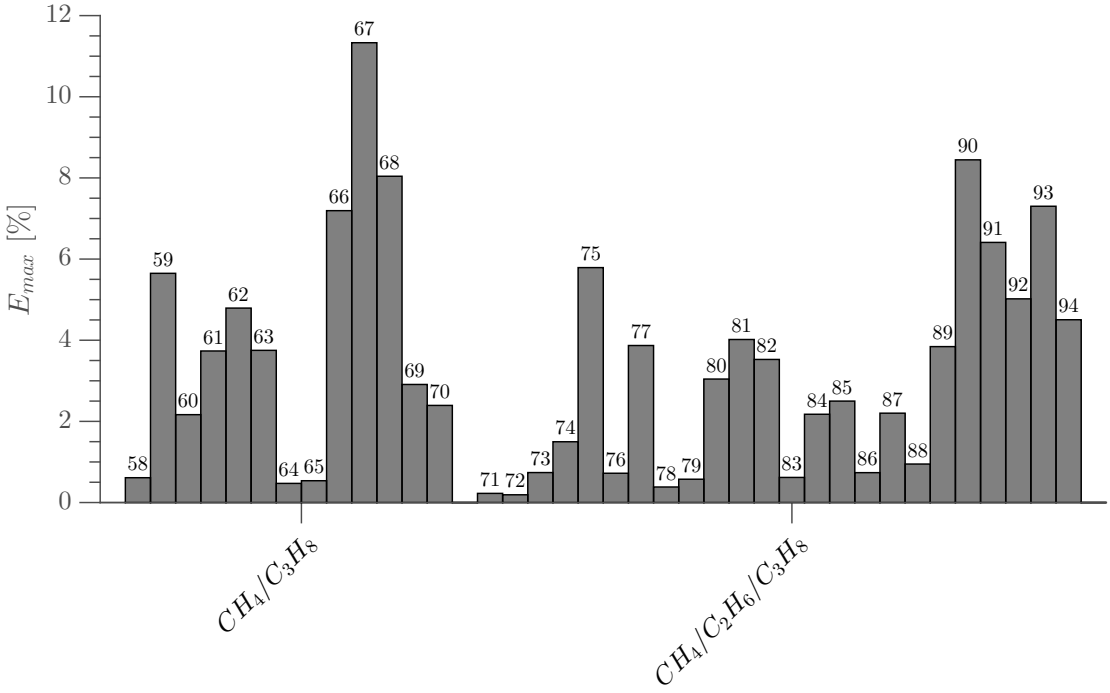

Figure 4.10: The maximum relative error values between the 290Rxn mechanism and the NUIG2013 mechanism for Cases 58 to 94 (Ignition Delay Time). The number above the bar represents the case number and its respective fuel compositions and experimental conditions can be found in Table 4.3 or Supplementary Table B.1.

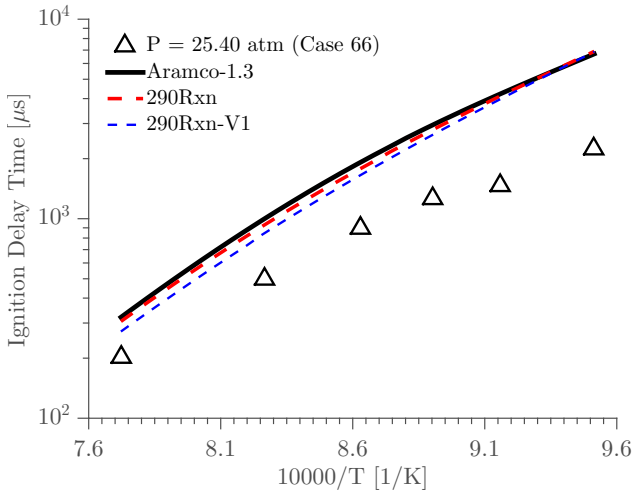

(a) ϕ = 0.5

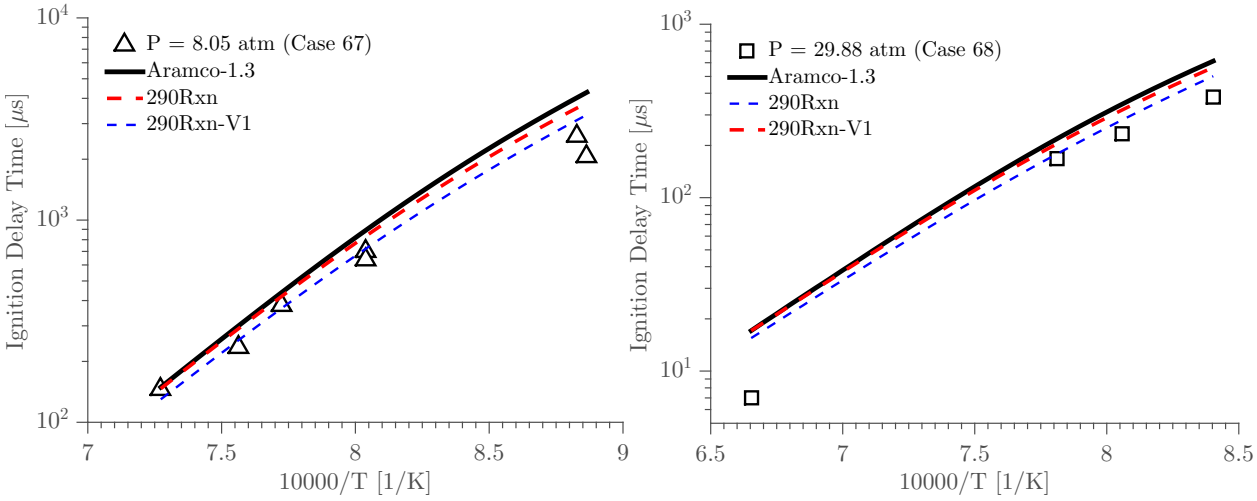

(b) ϕ = 1.0

(c) ϕ = 1.0

Figure 4.11: Comparisons of measured and predicted ignition delay time of CH_4/C_3H_8 fuel mixtures. The experimental data were obtained from ref. [148]. Lines show predictions from the different kinetics models.

Flame speed

Laminar flame speed is considered as an optimization target in this study because computing the flame speed requires more computational time as it involves solving 1-D equations. Therefore, laminar flame speed is an ideal combustion parameter to evaluate the capability of the optimized

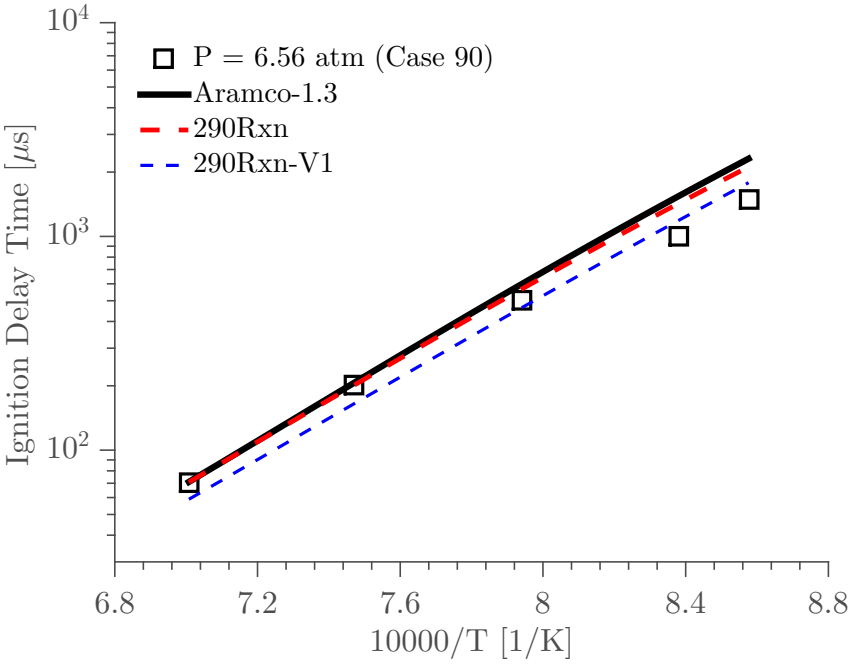

Figure 4.12: Comparisons of measured and predicted ignition delay time of $CH_4/C_2H_6/C_3H_8$ fuel mixtures (ϕ = 0.5). The experimental data were obtained from ref. [147]. Lines show predictions from the different kinetics models.

mechanism to predict combustion properties that are not included in the GA algorithm. A total of 55 different fuel mixtures and experimental conditions that are pertinent to biogas/syngas mixtures were chosen in this study to assess the capability of the 290Rxn and 290Rxn-V1 mechanisms in predicting the laminar flame speeds in biogas/syngas fuel mixtures. The maximum relative error value ($\mathrm{E_{max}}$) between 290Rxn and NUIG2013 for each case is plotted in Fig. 4.13, showing that the highest Emax value of 2.59 % is found for Case 134. The comparisons between the predicted flame speed computed using 290Rxn and NUIG2013 are plotted in Fig. 4.14 along with experimental data obtained from stagnation jet-wall configuration experiments, where the 290Rxn mechanism's prediction affords a lower $\delta \mathrm{S_u}$ value (the relative error between the computed $\mathrm{S_{u,ref}}$ and the measured $\mathrm{S_{u,ref}}$) compared to that of NUIG2013, indicating that 290Rxn more accurately predicts the measured flame speed. Further examination of the second highest $\mathrm{E_{max}}$ value (2.02 %) in Case 129 at ϕ = 1.35 reveals that the relative error value of 2 % can be regarded as negligible (see Fig. 4.15). Therefore, the 290Rxn mechanism mimics the NUIG2013 mechanism in predicting the flame speed of $\mathrm{H_2/CO}$ and $\mathrm{CH_4}$ mixtures containing impurities such as $\mathrm{CO_2}$, $\mathrm{H_2O}$, and $\mathrm{N_2}$.

The modified rate constants in 290Rxn-V1 do not have a significant impact on predictions of the laminar flame speed of $\mathrm{H_2/CO}$ mixtures under atmospheric conditions (see Supplementary Fig. B.12(a) - B.12(d) for Cases 95 to 98). However, the 290Rxn-V1 mechanism predicts slightly higher laminar flame speeds than the 290Rxn mechanism and the NUIG2013 mechanism when the pressure is raised to P = 40 atm (see Supplementary Fig. B.12(e) and B.12(f) for Cases 99 to 102), but the predictions are still well within the experimental uncertainty, as depicted in Supplementary Fig. B.12(e) and B.12(f). For $\mathrm{H_2/CO/CO_2}$ mixtures (Cases 103 to 116), the 290Rxn-V1 mechanism exhibits slightly better agreement with the experimental data when compared to 290Rxn and NUIG2013 mechanisms (see Fig. 4.16(b) and 4.16(c)) with the exception of Cases 106 to 108, where all three mechanisms overestimated the laminar flame speed at rich conditions (see Fig. 4.16(a)). The reason for the discrepancies observed between the simulated and the measured results in Fig. 4.16 is the higher equivalence ratios and higher CO2 compositions used in Cases

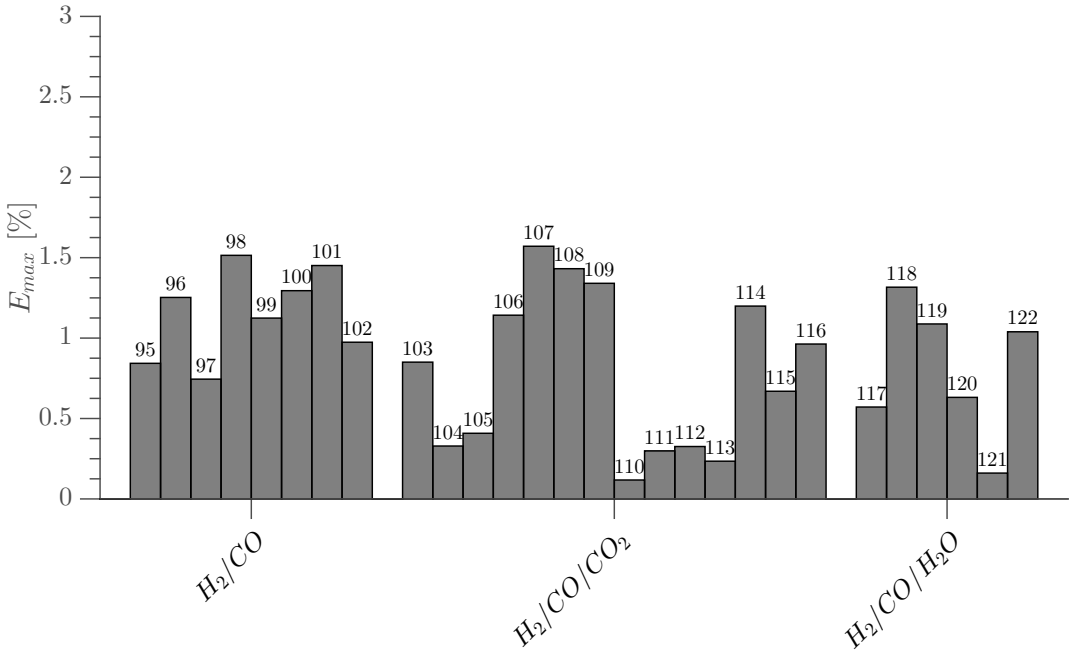

(a) Case 95 - 122

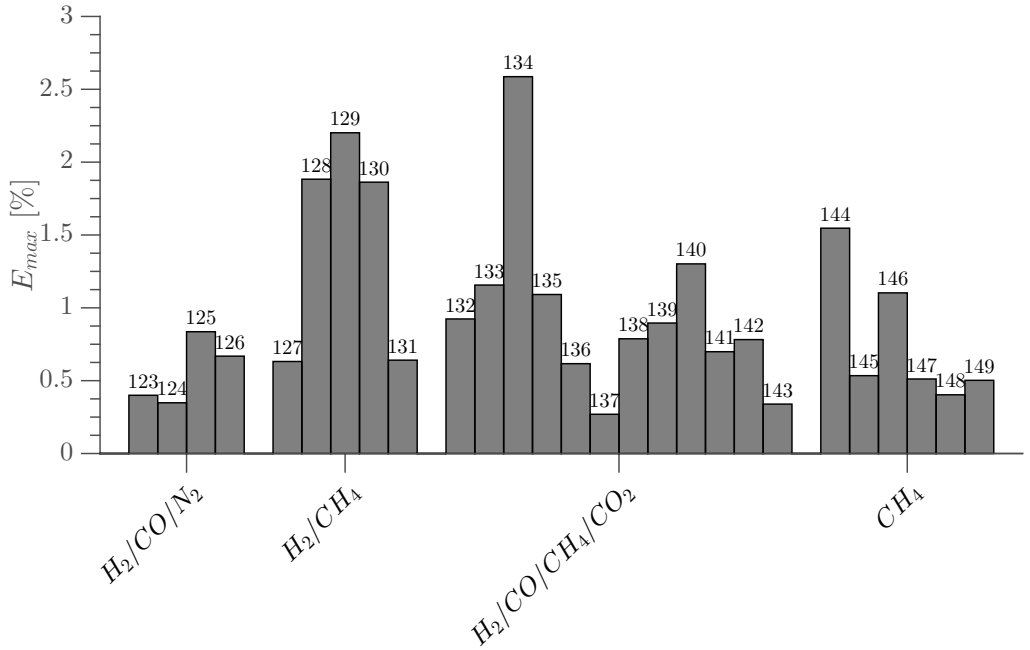

(b) Case 123 - 149

Figure 4.13: The maximum relative error values between the 290Rxn mechanism and the NUIG2013 mechanism for Case 95 to Case 149 (Laminar Flame Speed). The number above the bar represents the case number and its respective fuel compositions and experimental conditions can be found in Table 4.3 or Supplementary Table B.1.

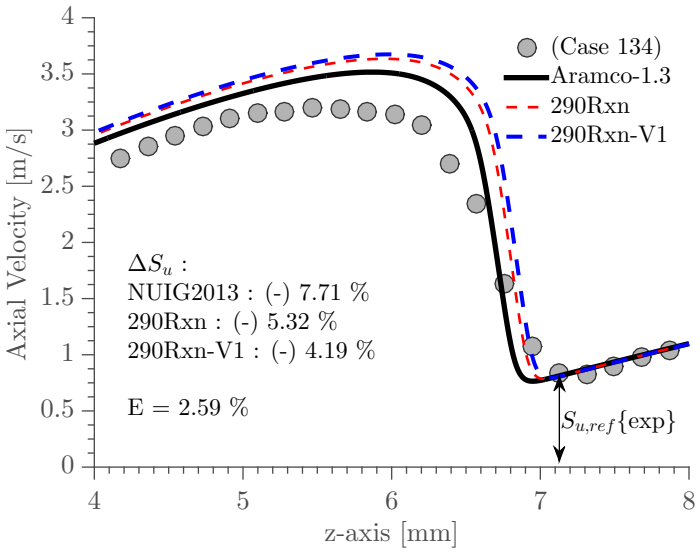

Figure 4.14: Measured and calculated flame speed of $H_2/CO/CH_4/CO_2$ fuel mixture at P = 1 atm and T = 300 K. The experimental data were obtained from ref. [90] and the lines show the predictions from the different kinetics models. The δS_u represents the relative error between the predicted flame speed and the measured flame speed. The E represents the relative error between the 290Rxn mechanism and the NUIG2013 mechanism.

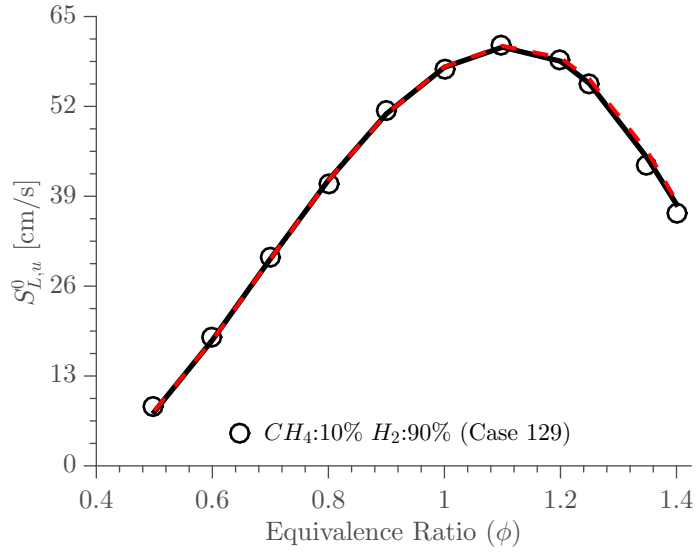

Figure 4.15: Measured and calculated flame speed of CH_4/H_2 at P = 1 atm and T = 300 K. The experimental data were obtained from [100] and the lines show the predictions from the different kinetics models.

106 to 108 compared to the other cases. Nevertheless, the three mechanisms perform very well in capturing the trend upon addition of CO_2. There are no major discrepancies observed between the 290Rxn-V1 mechanism and the NUIG2013 mechanism for other Cases investigated in this study, and the 290Rxn-V1 provides improved predictions for the flame speed values and shows closer agreement to the experimental data (see Supplementary Fig. B.14 - B.19). Consequently,, optimization of the rate constants in the 290Rxn mechanism is highly recommended to further improve the mechanism's predictions for biogas/syngas fuel mixtures, especially for mixtures with CO_2-rich mixtures at $\phi > 1.1$.

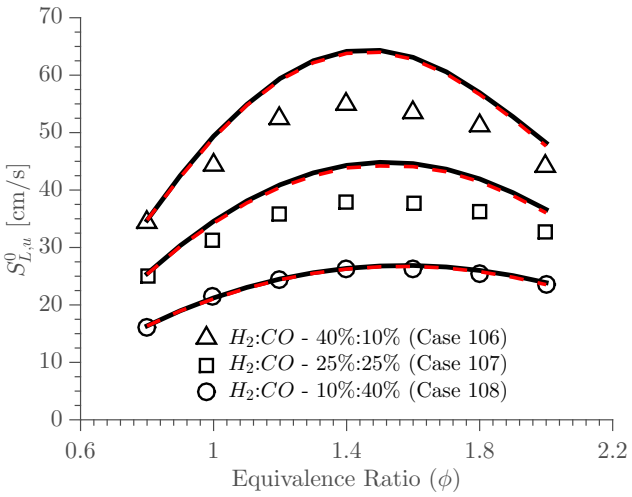

(a) P = 1 atm, T = 300 K

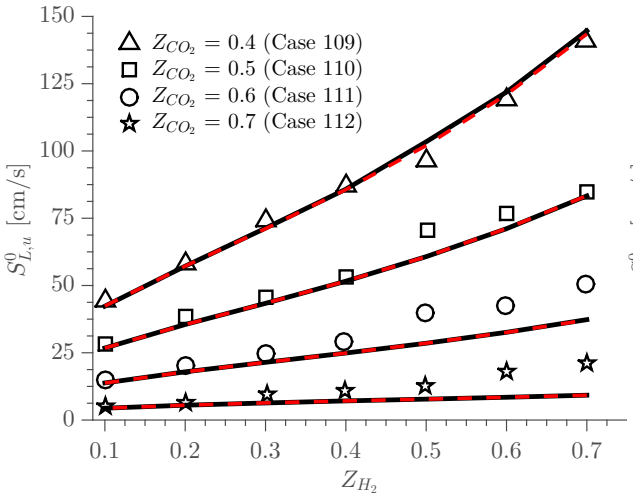

(b) P = 1 atm, T = 300 K, ϕ = 0.4

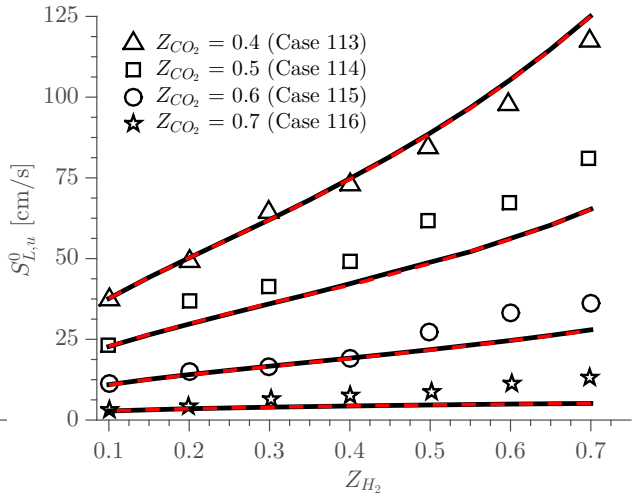

(c) P = 2 atm, T = 300 K, ϕ = 0.4

Figure 4.16: Measured and calculated flame speed of $H_2/CO/CO_2$. The experimental data were obtained from ref. [95, 96] and the lines show the predictions from the different kinetics models.

4.4 Concluding remarks

A detailed chemical kinetics mechanism for biogas/syngas combustion was obtained from a large detailed chemical kinetics (NUIG2013 mechanism: 325 species and 2067 reactions) for $C_1 - C_5$ mixtures by a method based on the GA approach. The final reduced mechanism consisted of 72

species and 290 reactions, and was found to mimic the performance of the large detailed mechanism (325 species and 2067 reactions) with high fidelity, not only for the included ignition delay time results, but also for combustion properties that were not included in the reduction process, such as the laminar flame speed propagation and also ignition delay time, under different fuel mixtures, pressure, and temperature conditions. This shows that GA is not only a viable method, but also a favorable method for reducing large detailed mechanisms, as the sharpening factors in Eq. 2 to Eq. 4 can be easily adjusted without the need for a detailed understanding of the chemistry by the user.

The highest $\mathrm{E_{max}}$ values between the 290Rxn mechanism and the NUIG2013 mechanism were 11.33 % and 2.92 % for the ignition delay time values and the laminar flame speed, respectively. However, further examinations on the $\mathrm{E_{max}}$ values of 11.33 % and 2.92 % show that the 290Rxn mechanism has slightly better agreement with the experimental data than the NUIG2013 mechanism. Therefore, the 290Rxn mechanism can be used to predict the ignition delay time of syngas, biogas, and natural gas combustion with the addition of $\mathrm{H_2O}$, $\mathrm{N_2}$, $\mathrm{C_2H_6}$, and $\mathrm{C_3H_8}$. The mechanism is, however, not suitable for mixtures that have $\mathrm{C_4H_10}$ or $\mathrm{C_5H_12}$ in them as the reactions associated with these species are deemed unimportant by the GA and were removed during the search process.

The proposed rate constants by Lee et al. [135] for (R15) and (R16) were incorporated into 290Rxn and were assessed in this study, where the rate constants were found to improve the predictions of the ignition delay time and the laminar flame speed results in general. However, the rate constants reduced the accuracy of the predictions of the laminar flame speed at high equivalence ratio conditions when high $\mathrm{CO_2}$ levels are present in the fuel mixtures. This is not surprising as the rate constants were obtained through a trial-and-error technique rather than through an optimization method. Therefore, optimization of the rate constants is highly recommended to further improve the predictions of the combustion properties of biogas/syngas fuel mixtures. Since the 290Rxn mechanism was confirmed to be a suitable mechanism for syngas/biogas combustion in this study

and, most importantly, it is significantly smaller than the original detailed mechanism, optimization of the rate constants in the 290Rxn mechanism to further improve its predictions is highly feasible.

Chapter 5

Conclusions

The goal of the present work is the development of an up-to-date chemical kinetics mechanism that is capable of predicting accurately the combustion properties of syngas and biogas fuel mixtures. Based on the comprehensive comparisons of several notable chemical kinetics in Chapter 3, the NUIG2013 mechanism provides the closest agreement with the experimental data. However, the NUIG2013 mechanism is developed for C_1 - C_5 hydrocarbons, consisting of more than 300 over species and 2000 over reactions, which many of the species and reactions are irrelevant for syngas and biogas combustion purpose. Therefore, Genetic Algorithm (GA) approach was adopted in Chapter 4 to optimally search for a smaller sub-mechanism within the large mechanism that will be able to describe accurately the fundamental combustion characteristics of syngas and biogas fuel mixtures. The final reduced mechanism obtained through GA approach yielded 290 reactions and 72 species, reduced from 2067 reactions and 325 species.

The final reduced mechanism is shown, in Chapter 4, to mimic the NUIG2013 mechanism in predicting the ignition delay time and laminar flame speed of a total of 149 cases, where the fuel mixtures and experimental conditions considered in each case are pertinent to syngas and biogas combustion. In addition, the reduced mechanism has almost identical performance with the NUIG2013 mechanism in predicting the ignition delay time of CH_4 mixtures with the addition of C_2H_6 and C_3H_8 mixtures. Therefore, the mechanism (290Rxn) presented in this thesis

represents the most up-to-date detailed chemical kinetics mechanism for syngas and biogas fuel mixtures. The 290Rxn mechanism can also be used for predicting methane fuels with dilutes such as C_2H_6 and C_3H_8. The 290Rxn mechanism mimics the NUIG2013 mechanism so well that both mechanisms predicted longer ignition delay time when compared to experimental results for $H_2/CO/CO_2$ mixture at low temperatures ($<$ 1050 K) and low pressures (P = 1.24 - 2.36 atm), the $H_2/CO/CH_4/CO_2/H_2O$ mixture at P = 32 atm, the $H_2/CO/CH_4$ at P = 32 atm, and H_2/CH_4 mixtures at low hydrogen concentrations ($\leq$ 40% H_2).

Sensitivity analysis at the aforementioned conditions were performed in Chapter 3, where they revealed that $CH_4 + OH = CH_3 + H_2O$ reaction is the reason for the NUIG2013 mechanism to predict longer ignition delay time for $H_2/CO/CH_4$ and $H_2/CO/CH_4/CO_2/H_2O$ mixtures, while $H + O_2(+CO_2) = HO_2(+CO_2)$ reaction is responsible for the longer ignition delay time predicted by the NUIG2013 mechanism at P = 1.24 - 2.36 atm and T $<$ 1025 K for $H_2/CO/CO_2$ mixture. Therefore, two new rate constants were proposed for the reactions to reconcile the observed discrepancies between simulated and measured ignition delay time. The modifications proposed for the two reactions were incorporated into the 290Rxn mechanism (290Rxn-V1), where the proposed rate constants reconciled the discrepancies observed for the $H_2/CO/CH_4/CO_2/H_2O$, $H_2/CO/CH_4$, and H_2/CH_4 mixtures, and most importantly, it retained the NUIG2013 mechanism's excellent predictions of the flame speed or ignition delay time results for the other mixture compositions or other experimental conditions considered in this thesis. Therefore, the 290Rxn-V1 mechanism presented in this thesis is currently the best mechanism in literature for biogas and syngas combustion purpose.

As mentioned in Chapter 4, 290Rxn-V1 and NUIG2013 mechanisms overdetermined the laminar flame speed values for mixtures with high CO_2 levels at $\phi > 1.1$. Therefore, optimization of the rate constants in the 290Rxn mechanism using the GA approach introduced in Chapter 4 is highly recommended to further improve the predictions of the combustion of syngas and biogas. In addition, more data that represents practical syngas and biogas mixtures are needed to further

validate and improve current kinetics models, although lots of progress have been made throughout these years. Nevertheless, the experimental data summarized in Chapter 2 for Syngas mixture and CH_4 fuel mixtures that are tabulated in Table 4.3 can be used as optimization targets for the rate constants and are definitely very beneficial to kineticists, with the goal of developing an optimized chemical kinetics mechanism for syngas and biogas combustion. Furthermore, an up-to-date optimized Nitrogen sub-mechanism can be obtained using the approach introduced in this thesis, where the N sub-mechanism can be merged with the 290Rxn mechanism to study the NO_x formation from biogas and syngas combustion.

Bibliography

[1] Wayne K Metcalfe, Sinéad M Burke, Syed S Ahmed, and Henry J Curran. A hierarchical and comparative kinetic modeling study of C_1 - C_2 hydrocarbon and oxygenated fuels. *International Journal of Chemical Kinetics*, 45(10):638–675, 2013.

[2] A Frassoldati, T Faravelli, and E Ranzi. A wide range modeling study of NO_x formation and nitrogen chemistry in hydrogen combustion. *International Journal of Hydrogen Energy*, 31(15):2310–2328, 2006.

[3] Young Sik Kim, Jong Jun Lee, Tong Seop Kim, and Jeong L Sohn. Effects of syngas type on the operation and performance of a gas turbine in integrated gasification combined cycle. *Energy Convers Manage*, 52(5):2262–2271, 2011.

[4] V Ratna Kishore, M R. Ravi, and Anjan Ray. Adiabatic burning velocity and cellular flame characteristics of H_2–CO–CO_2–air mixtures. *Combustion and Flame*, 158:2149–2164, 2011.

[5] Jay A. Ratafia-Brown, Lynn M. Manfredo, Jeff W. Hoffmann, Massood Ramezan, and Gary J. Stiegel. An environmental assessment of IGCC power systems. In *Nineteenth Annual Pittsburgh Coal Conference*, 2002. 1–16.

[6] Terry F. Wall. Combustion processes for carbon capture. *Proceedings of the Combustion Institute*, 31:31–47, 2007.

[7] Mao Yun He, Bo Xiao, Shi Ming Liu, Zhi Quan Hu, Xian Jun Guo, Si Yi Luo, and Fan Yang. Syngas production from pyrolysis of municipal solid waste (MSW) with dolomite as downstream catalysts. *Journal of Analytical and Applied Pyrolysis*, 87:181–187, 2010.

[8] Q. Xu, P. Lan, B. Zhang, Z. Ren, and Y Yan. Energy Sources, Part A: Recovery,Utilization, and Environmental Effects. *Energy Sources*, 35:848–858, 2013.

[9] Young-Il Son, Sang Jun Yoon, Yong Ku Kim, and Jae-Goo Lee. Gasification and power generation characteristics of woody biomass utilizing a downdraft gasifier. *Biomass Bioenergy*, 35:4215–4220, 2011.

[10] M. Simone, C. Barontini, F.and Nicolella, and L. Tognotti. Experimental characterization of the performance of a downdraft biomass gasifier. In *Proceedings of the European Combustion Meeting*, 2011.

[11] Daniel L. Carpenter, Richard L. Bain, Ryan E. Davis, Abhijit Dutta, Calvin J. Feik, Katherine R. Gaston, Whitney Jablonski, Steven D. Phillips, and Mark R. Nimlos. Pilot-scale gasification of corn stover, switchgrass, wheat straw, and wood: 1. parametric study and comparison with literature. *Industrial & Engineering Chemistry Research*, 49:1859–1871, 2010.

[12] Rudy Michel, Sergio Rapagn, Manuela Di Marcello, Philippe Burg, Muriel Matt, Claire Courson, and Ren? Gruber. Catalytic steam gasification of miscanthus X giganteus in fluidised bed reactor on olivine based catalysts. *Fuel Processing Technology*, 92:1169–1177, 2011.

[13] David Vera, B?rbara de Mena, Francisco Jurado, and Gerhard Schories. Study of a downdraft gasifier and gas engine fueled with olive oil industry wastes. *Applied Thermal Engineering*, 51:119–129, 2013.

[14] Irene Smith. Gas turbine technology for syngas/hydrogen in coal-based igcc. In *IEA Clean*

Coal Center, 2009. PF 09-11.

[15] Jeongjae Hwang, Nicolas Bouvet, Kitae Sohn, and Youngbin Yoon. Stability characteristics of non-premixed turbulent jet flames of hydrogen and syngas blends with coaxial air. *International Journal of Hydrogen Energy*, 38:5139–5149, 2013.

[16] S. Dodo, T. Asai, H. Koizumi, H. Takahashi, S. Yoshida, and H. Inoue. Performance of a multiple-injection dry low NO_x combustor with hydrogen-rich syngas fuels. *Journal of Engineering for Gas Turbines and Power*, 135, 2013.

[17] B. Major and B. Powers. Cost analysis of nox control alternatives for stationary gas turbines. In *Onsite Sycom*, 1999.

[18] K B. Fackler, M F. Karalus, I V. Novosselov, J C. Kramlich, and P C. Malte. Experimental and numerical study of nox formation from the lean premixed combustion of CH_4 mixed with CO_2 and N_2. In *ASME Turbo Expo*, 2011. 1215021-7.

[19] S. Daniele, P. Jansohn, J. Mantzaras, and K. Boulouchos. Turbulent flame speed for syngas at gas turbine relevant conditions. *Proceedings of the Combustion Institute*, 33:2937–2944, 2011.

[20] Arthur Henry Lefebvre, Dilip R Ballal, and Donald W Bahr. *Gas turbine combustion: alternative fuels and emissions*. CRC Press Boca Raton, FL, 3rd edition, 2010.

[21] R. Chacartegui, D. Sánchez, J M. Munoz de Escalona, A. Munoz, and T. Sánchez. Gas and steam combined cycles for low calorific syngas fuels utilization. *Applied Energy*, 101:81–92, 2013.

[22] F. He, Z. Li, P. Liu, L. Ma, and E N. Pistikopoulos. Operation window and part-load performance study of a syngas fired gas turbine. *Applied Energy*, 89:133–141, 2012.

[23] Marissa L. Brower, Olivier Mathieu, Eric L. Petersen, Nicola Donohoe, Alexander Heufer, Wayne K. Metcalfe, Henry J. Curran, Gilles Bourque, Bourque, and Felix Güthe. Ignition

delay time experiments for natural gas/hydrogen blends at elevated pressures. In *ASME Turbo Expo*, 2013. 95151–12.

[24] S Orhan Akansu, Zafer Dulger, Nafiz Kahraman, and T Nejat Veziroğlu. Internal combustion engines fueled by natural gas-hydrogen mixtures. *International Journal of Hydrogen Energy*, 29(14):1527–1539, 2004.

[25] CG Bauer and TW Forest. Effect of hydrogen addition on the performance of methane-fueled vehicles. Part I: effect on SI engine performance. *International Journal of Hydrogen Energy*, 26(1):55–70, 2001.

[26] GA Karim, I Wierzba, and Y Al-Alousi. Methane-hydrogen mixtures as fuels. *International Journal of Hydrogen Energy*, 21(7):625–631, 1996.

[27] T Tahtouh, F Halter, E Samson, and C Mounaïm-Rousselle. Effects of hydrogen addition and nitrogen dilution on the laminar flame characteristics of premixed methane–air flames. *International Journal of Hydrogen Energy*, 34(19):8329–8338, 2009.

[28] Ying Jia Zhang, Zuo Hua Huang, Liang Jie Wei, Jia Xiang Zhang, and Chung K. Law. Experimental and modeling study on ignition delays of lean mixtures of methane, hydrogen, oxygen, and argon at elevated pressures. *Combustion and Flame*, 159:918–931, 2012.

[29] R. Chacartegui, D. Sánchez, J M. Muñoz de Escalona, F. Jimenez-Espadafor, A. Muñoz, and T. Saáchez. Sphera project: Assessing the use of syngas fuels in gas turbines and combined cycles from a global perspective. *Fuel Processing Technology*, 103:134145, 2012.

[30] A Frassoldati, T Faravelli, and E Ranzi. The ignition, combustion and flame structure of carbon monoxide/hydrogen mixtures. Note 1: Detailed kinetic modeling of syngas combustion also in presence of nitrogen compounds. *International Journal of Hydrogen Energy*, 32(15):3471–3485, 2007.

[31] D R. Noble, Q G. Zhang, and T. Lieuwen. Hydrogen effects upon flashback and blowout.

In *Proc. of ICEPAG*, 2006. 24012.

[32] T. Lieuwen. Flashback characteristics of syngas-type fuels under steady and pulsating conditions. In *School of Aerospace Engineering, Georgia Institute of Technology, Atlanta, Georgia*, 2008. DOI: 10.2172/924769.

[33] J. Fu, C. Tang, W. Jin, L D. Thi, Z. Huang, and Y. Zhang. Study on laminar flame speed and flame structure of syngas with varied compositions using oh-plif and spectrograph. *International Journal of Hydrogen Energy*, 38:1636–1643, 2013.

[34] J. Wang, Z. Huang, H. Kobayashi, and Y. Ogami. Laminar burning velocities and flame characteristics of CO–H_2–CO_2–O_2 mixtures. *International Journal of Hydrogen Energy*, 37:19158–19167, 2012.

[35] J Natarajan, T Lieuwen, and J Seitzman. Laminar flame speeds of H_2/CO mixtures: Effect of CO_2, dilution, preheat temperature, and pressure. *Combustion and Flame*, 151(1):104–119, 2007.

[36] Hongyan Sun, SI Yang, G Jomaas, and CK Law. High-pressure laminar flame speeds and kinetic modeling of carbon monoxide/hydrogen combustion. *Proceedings of the Combustion Institute*, 31(1):439–446, 2007.

[37] C Prathap, Anjan Ray, and MR Ravi. Investigation of nitrogen dilution effects on the laminar burning velocity and flame stability of syngas fuel at atmospheric condition. *Combustion and Flame*, 155(1):145–160, 2008.

[38] Chen Dong, Qulan Zhou, Qinxin Zhao, Yaqing Zhang, Tongmo Xu, and Shien Hui. Experimental study on the laminar flame speed of hydrogen/carbon monoxide/air mixtures. *Fuel*, 88(10):1858–1863, 2009.

[39] Nicolas Bouvet, Christian Chauveau, Iskender Gökalp, and Fabien Halter. Experimental studies of the fundamental flame speeds of syngas (H_2/CO/air mixtures). *Proceedings of*

the Combustion Institute, 33(1):913–920, 2011.

[40] Hugo J Burbano, Jhon Pareja, and Andrés A Amell. Laminar burning velocities and flame stability analysis of H_2/CO/air mixtures with dilution of N_2 and CO_2. *International Journal of Hydrogen Energy*, 36(4):3232–3242, 2011.

[41] MC Krejci, AJ Vissotski, S Ravi, WJ Metcalfe, A Keromnes, HJ Curran, and EL Petersen. Laminar flame speed measurements of moist syngas fuel blends at elevated pressures and temperatures. In *Spr Tech Meeting (CSSCI)*, 2012. 1–8.

[42] Deepti Singh, Takayuki Nishiie, Saad Tanvir, and Li Qiao. An experimental and kinetic study of syngas/air combustion at elevated temperatures and the effect of water addition. *Fuel*, 94:448–456, 2012.

[43] Michael C Krejci, Olivier Mathieu, Andrew J Vissotski, Sankaranarayanan Ravi, Travis G Sikes, Eric L Petersen, KÃ Alan, Wayne Metcalfe, Henry J Curran, et al. Laminar flame speed and ignition delay time data for the kinetic modeling of hydrogen and syngas fuel blends. *Journal of Engineering for Gas Turbines and Power*, 135(2):021503, 2013.

[44] Alan Kéromnès, Wayne K Metcalfe, Karl A Heufer, Nicola Donohoe, Apurba K Das, Chih-Jen Sung, Jürgen Herzler, Clemens Naumann, Peter Griebel, Olivier Mathieu, et al. An experimental and detailed chemical kinetic modeling study of hydrogen and syngas mixture oxidation at elevated pressures. *Combustion and Flame*, 160(6):995–1011, 2013.

[45] A K. Das, K. Kumar, and C J. Sung. Laminar flame speeds of moist syngas mixtures. *Combustion and Flame*, 158:345–353, 2011.

[46] E. Hu, J. Fu, L. Pan, X. Jiang, Z H. Huang, and Y. Zhang. Experimental and numerical study on the effect of composition on laminar burning velocities of H_2/CO/N_2/CO_2/air mixtures. *International Journal of Hydrogen Energy*, 37:18509–18519, 2012.

[47] Gaurav Mittal, Chih-Jen Sung, and Richard A Yetter. Autoignition of H_2/CO at elevated

pressures in a rapid compression machine. *International Journal of Chemical Kinetics*, 38(8):516–529, 2006.

[48] Danielle M Kalitan, John D Mertens, Mark W Crofton, and Eric L Petersen. Ignition and oxidation of lean CO/H_2 fuel blends in air. *Journal of Propulsion and Power*, 23(6):1291–1301, 2007.

[49] S. Gersen, H. Darmeveil, and H. Levinsky. The effects of CO addition on the autoignition of H_2, CH_4 and CH_4/H_2 fuels at high pressure in an rcm. *Combustion and Flame*, 159:3472–3475, 2012.

[50] O. Mathieu, M M. Kopp, and E L. Petersen. Shock-tube study of the ignition of multi-component syngas mixtures with and without ammonia impurities. *Proceedings of the combustion institute*, 34:3211–3218, 2013.

[51] S Subith Vasu, F David Davidson, and K Ronald Hanson. Shock tube study of syngas ignition in rich CO_2 mixtures and determination of the rate of $H+O_2+CO_2 \rightarrow HO_2+CO_2$. *Energy & Fuels*, 25(3):990–997, 2011.

[52] S M. Walton, X. He, B T. Zigler, and M S. Wooldridge. An experimental investigation of the ignition properties of hydrogen and carbon monoxide mixtures for syngas turbine applications. *Proceedings of the Combustion Institute*, 31:3147–3154, 2007.

[53] E L. Petersen, D M. Kalitan, A B. Barrett, S C. Reehal, J D. Mertens, D J. Beerer, R L. Hack, and V G. McDonell. New syngas/air ignition data at lower temperature and elevated pressure and comparison to current kinetics models. *Combustion and Flame*, 135149:244–247, 2007.

[54] W T. Peschke and Louis J. Spadaccini. Determination of autoignition and flame speed characteristics of coal gases having medium heating values: Final report: Epri ap-4291. Technical report, Electric Power Research Institute, 1985.

[55] Apurba K Das and Chih-Jen Sung. Ignition delay study of moist syngas/oxidizer and hydrogen/oxidizer mixtures using a rapid compression machine. In *49th AIAA Aero Sci Meeting*, 2011. 1–9.

[56] J. Herzler and C. Naumann. Shock-tube study of the ignition of lean CO/H_2 fuel blends at intermediate temperatures and high pressure. *Combustion Science and Technology*, 180:2015–2028, 2008.

[57] Ian C McLean, David B Smith, and Simon C Taylor. The use of carbon monoxide/hydrogen burning velocities to examine the rate of the $CO + OH$ reaction. In *Symposium (International) on Combustion*, volume 25, pages 749–757. Elsevier, 1994.

[58] MI Hassan, KT Aung, and GM Faeth. Properties of laminar premixed $CO/H/$air flames at various pressures. *Journal of Propulsion and Power*, 13(2):239–245, 1997.

[59] Marcos Chaos and Frederick L Dryer. Syngas combustion kinetics and applications. *Combustion Science and Technology*, 180(6):1053–1096, 2008.

[60] Michael P Burke, Zheng Chen, Yiguang Ju, and Frederick L Dryer. Effect of cylindrical confinement on the determination of laminar flame speeds using outwardly propagating flames. *Combustion and Flame*, 156(4):771–779, 2009.

[61] Chih-Jen Sung and Chung K Law. Fundamental combustion properties of H_2/CO mixtures: ignition and flame propagation at elevated pressures. *Combustion Science and Technology*, 180(6):1097–1116, 2008.

[62] Fujia Wu, Andrew P Kelley, Chenglong Tang, Delin Zhu, and Chung K Law. Measurement and correlation of laminar flame speeds of CO and C_2 hydrocarbons with hydrogen addition at atmospheric and elevated pressures. *International Journal of Hydrogen Energy*, 36(20):13171–13180, 2011.

[63] Chung K. Law. *Combustion physics*. Cambridge University Press, 2006.

[64] CK Law and OC Kwon. Effects of hydrocarbon substitution on atmospheric hydrogen–air flame propagation. *International Journal of Hydrogen Energy*, 29(8):867–879, 2004.

[65] CK Law, G Jomaas, and JK Bechtold. Cellular instabilities of expanding hydrogen/propane spherical flames at elevated pressures: theory and experiment. *Proceedings of the Combustion Institute*, 30(1):159–167, 2005.

[66] Tran Manh Vu, Jeong Park, Oh Boong Kwon, Dae Seok Bae, Jin Han Yun, and Sang In Keel. Effects of diluents on cellular instabilities in outwardly propagating spherical syngas–air premixed flames. *International Journal of Hydrogen Energy*, 35(8):3868–3880, 2010.

[67] Gregory I Sivashinsky. Instabilities, pattern formation, and turbulence in flames. *Annual Review of Fluid Mechanics*, 15(1):179–199, 1983.

[68] Jhon Pareja, Hugo J Burbano, Andrés Amell, and Julián Carvajal. Laminar burning velocities and flame stability analysis of hydrogen/air premixed flames at low pressure. *International Journal of Hydrogen Energy*, 36(10):6317–6324, 2011.

[69] D Bradley, M Lawes, Kexin Liu, Sebastian Verhelst, and R Woolley. Laminar burning velocities of lean hydrogen–air mixtures at pressures up to 1.0 Mpa. *Combustion and Flame*, 149(1):162–172, 2007.

[70] C C. Liu, S S. Shy, C W. Chiu, M W. Peng, and H J. Chung. hydrogen/carbon monoxide syngas burning rates measurements in high-pressure quiescent and turbulent environment. *International Journal of Hydrogen Energy*, 36:8595–8603, 2011.

[71] Santosh K. Paidi, Amrutha Bhavaraju, Mohammad Akram, and Sudarshan Kumar. Effect of N_2/CO_2 dilution on laminar burning velocity of H_2-air mixtures at high temperatures. *International Journal of Hydrogen Energy*, 2013.

[72] SK Alavandi and AK Agrawal. Experimental study of combustion of hydrogen–syngas/methane fuel mixtures in a porous burner. *International Journal of Hydrogen En-*

ergy, 33(4):1407–1415, 2008.

[73] Scott G Davis, Ameya V Joshi, Hai Wang, and Fokion Egolfopoulos. An optimized kinetic model of H_2/CO combustion. *Proceedings of the Combustion Institute*, 30(1):1283–1292, 2005.

[74] J E. EIsworth, W W. Haskell, and I A. Read. Non-uniform ignition processes in rapid-compression machines. *Combustion and Flame*, 13:437–438, 1969.

[75] W W Haskell. Fuel ignition in a rapid compression machine: sensitivity to flame ignition by particles. In *SAE Paper*, 1970. 700059.

[76] A. Mansfield and M S. Wooldridge. An investigation of syngas ignition phenomena. In *Spr Tech Meeting of the Central States Sect of the Combust Inst*, 2012. 1–13.

[77] J W. Meyer and A K. Oppenheim. On the shock induced ignition of explosive gases. *Proc. Combust. Symp.*, 13:1153–1164, 1970.

[78] A K. Oppenheim. Dynamic features of combustion. *Philosophical Transactions of the Royal Society A*, 315:471–508, 1985.

[79] R. Blumenthal, K. Fieweger, K H. Komp, G. Adomeit, and B E. Gelfand. Gas dynamic features of self ignition of non diluted fuel/air mixtures at high pressure. *Combustion Science and Technology*, 113-114:137–166, 1996.

[80] B L. Wang, H. Olivier, and H. Grönig. Ignition of shock-heated H_2-air-steam mixtures. *Combustion and Flame*, 133:93–106, 2003.

[81] DF Davidson, BM Gauthier, and RK Hanson. Shock tube ignition measurements of iso-octane/air and toluene/air at high pressures. *Proceedings of the Combustion Institute*, 30(1):1175–1182, 2005.

[82] GA Pang, DF Davidson, and RK Hanson. Experimental study and modeling of shock tube ignition delay times for hydrogen–oxygen–argon mixtures at low temperatures. *Proceed-*

ings of the Combustion Institute, 32(1):181–188, 2009.

[83] Marcos Chaos and Frederick L Dryer. Chemical-kinetic modeling of ignition delay: Considerations in interpreting shock tube data. *International Journal of Chemical Kinetics*, 42(3):143–150, 2010.

[84] C. Higman and M. Van der Burt. *Gasification*. Gulf Professional Publishing, 2nd edition, 2008.

[85] Kristina Göransson, Ulf Söderlind, Jie He, and Wennan Zhang. Review of syngas production via biomass DFBGs. *Renewable & Sustainable Energy Reviews*, 15(1):482–492, 2011.

[86] R. Chacartegui, M. Torres, D. Sánchez, F. Jiménez, and T. Munoz, A.and Sánchez. Analysis of main gaseous emissions of heavy duty gas turbines burning several syngas fuels. *Fuel Processing Technology*, 92:213–220, 2011.

[87] Wennan Zhang. Automotive fuels from biomass via gasification. *Fuel Processing Technology*, 91(8):866–876, 2010.

[88] Pradeep Chaminda Munasinghe and Samir Kumar Khanal. Biomass-derived syngas fermentation into biofuels: opportunities and challenges. *Bioresource Technology*, 101(13):5013–5022, 2010.

[89] CC Liu, SS Shy, CW Chiu, MW Peng, and HJ Chung. Hydrogen/carbon monoxide syngas burning rates measurements in high-pressure quiescent and turbulent environment. *International Journal of Hydrogen Energy*, 36(14):8595–8603, 2011.

[90] Graeme MG Watson, Jeffrey D Munzar, and Jeffrey M Bergthorson. NO formation in model syngas and biogas blends. *Fuel*, 124:113–124, 2014.

[91] Erjiang Hu, Jin Fu, Lun Pan, Xue Jiang, Zuohua Huang, and Yang Zhang. Experimental and numerical study on the effect of composition on laminar burning velocities of H_2/CO/N_2/CO_2/air mixtures. *International Journal of Hydrogen Energy*, 37(23):18509–

18519, 2012.

[92] MI Hassan, KT Aung, and GM Faeth. Properties of laminar premixed $\mathrm{CO}/\mathrm{H}/\mathrm{air}$ flames at various pressures. *Journal of Propulsion and Power*, 13(2):239–245, 1997.

[93] Ian C McLean, David B Smith, and Simon C Taylor. The use of carbon monoxide/hydrogen burning velocities to examine the rate of the $\mathrm{CO} + \mathrm{OH}$ reaction. In *Symposium (International) on Combustion*, volume 25, pages 749–757. Elsevier, 1994.

[94] C Prathap, Anjan Ray, and MR Ravi. Investigation of nitrogen dilution effects on the laminar burning velocity and flame stability of syngas fuel at atmospheric condition. *Combustion and Flame*, 155(1):145–160, 2008.

[95] V Ratna Kishore, Ringkhang Muchahary, Anjan Ray, and MR Ravi. Adiabatic burning velocity of mixtures diluted with $\mathrm{CO_2}/\mathrm{N_2}/\mathrm{Ar}$. *International Journal of Hydrogen Energy*, 34(19):8378–8388, 2009.

[96] Jinhua Wang, Zuohua Huang, Hideaki Kobayashi, and Yasuhiro Ogami. Laminar burning velocities and flame characteristics of CO–$\mathrm{H_2}$–$\mathrm{CO_2}$–$\mathrm{O_2}$ mixtures. *International Journal of Hydrogen Energy*, 37(24):19158–19167, 2012.

[97] Apurba K Das, Kamal Kumar, and Chih-Jen Sung. Laminar flame speeds of moist syngas mixtures. *Combustion and Flame*, 158(2):345–353, 2011.

[98] CK Law and OC Kwon. Effects of hydrocarbon substitution on atmospheric hydrogen–air flame propagation. *International Journal of Hydrogen Energy*, 29(8):867–879, 2004.

[99] G Yu, CK Law, and CK Wu. Laminar flame speeds of hydrocarbon + air mixtures with hydrogen addition. *Combustion and Flame*, 63(3):339–347, 1986.

[100] Nicola Donohoe, Alexander Heufer, Wayne K Metcalfe, Henry J Curran, Marissa L Davis, Olivier Mathieu, Drew Plichta, Anibal Morones, Eric L Petersen, and Felix Güthe. Ignition delay times, laminar flame speeds, and mechanism validation for natural gas/hydrogen

blends at elevated pressures. *Combustion and Flame*, 161(6):1432–1443, 2014.

[101] F Halter, C Chauveau, N Djebaili-Chaumeix, and I Gökalp. Characterization of the effects of pressure and hydrogen concentration on laminar burning velocities of methane–hydrogen–air mixtures. *Proceedings of the Combustion Institute*, 30(1):201–208, 2005.

[102] Patricia Dirrenberger, Hervé Le Gall, Roda Bounaceur, Olivier Herbinet, Pierre-Alexandre Glaude, Alexander Konnov, and Frédérique Battin-Leclerc. Measurements of laminar flame velocity for components of natural gas. *Energy & Fuels*, 25(9):3875–3884, 2011.

[103] RTE Hermanns, AA Konnov, RJM Bastiaans, LPH De Goey, K Lucka, and H Köhne. Effects of temperature and composition on the laminar burning velocity of CH_4 + H_2 + O_2 + N_2 flames. *Fuel*, 89(1):114–121, 2010.

[104] O Mathieu, MM Kopp, and EL Petersen. Shock-tube study of the ignition of multi-component syngas mixtures with and without ammonia impurities. *Proceedings of the Combustion Institute*, 34(2):3211–3218, 2013.

[105] Apurba K Das, Chih-Jen Sung, Yu Zhang, and Gaurav Mittal. Ignition delay study of moist hydrogen/oxidizer mixtures using a rapid compression machine. *International Journal of Hydrogen Energy*, 37(8):6901–6911, 2012.

[106] Dave Goodwin, Nicholas Malaya, Harry Moffat, and Raymond Speth. Cantera: An object-oriented software toolkit for chemical kinetics, thermodynamics, and transport processes. *Caltech, Pasadena, CA*, 2009.

[107] T Kathrotia, M Fikri, M Bozkurt, M Hartmann, U Riedel, and C Schulz. Study of the H + O + M reaction forming OH: Kinetics of OH chemiluminescence in hydrogen combustion systems. *Combustion and Flame*, 157(7):1261–1273, 2010.

[108] G P. Smith, D M. Golden, M. Frenklach, N W. Moriarty, B. Eiteneer, M. Goldenberg, C T. Bowman, R K. Hanson, S. Song, W J. Gardiner Jr., V V. Lissianski, and Z. Qin. Gri-mech

3.0, 1999.

[109] Juan Li, Zhenwei Zhao, Andrei Kazakov, Marcos Chaos, Frederick L Dryer, and James J Scire. A comprehensive kinetic mechanism for CO, CH_2O, and CH_3OH combustion. *International Journal of Chemical Kinetics*, 39(3):109–136, 2007.

[110] H Wang, X You, AV Joshi, SG Davis, A Laskin, F Egolfopoulos, and CK Law. USC Mech Version II. High-temperature combustion reaction model of $H_2/CO/C_1 - C_4$ compounds, 2007.

[111] Priyank Saxena and Forman A Williams. Testing a small detailed chemical-kinetic mechanism for the combustion of hydrogen and carbon monoxide. *Combustion and Flame*, 145(1):316–323, 2006.

[112] Robert J Kee, Joseph F Grcar, MD Smooke, JA Miller, and E Meeks. PREMIX: a fortran program for modeling steady laminar one-dimensional premixed flames, 1985.

[113] Robert J Kee, James A Miller, Gregory H Evans, and Graham Dixon-Lewis. A computational model of the structure and extinction of strained, opposed flow, premixed methane-air flames. In *Symposium (International) on Combustion*, volume 22, pages 1479–1494. Elsevier, 1989.

[114] Jeffrey Myles Bergthorson. *Experiments and Modeling of Impinging Jets and Premixed Hydrocarbon Stagnation Flames*. PhD thesis, California Institute of Technology, 2005.

[115] Puneet Gupta, Luis G Velazquez-Vargas, and Liang-Shih Fan. Syngas redox (SGR) process to produce hydrogen from coal derived syngas. *Energy & Fuels*, 21(5):2900–2908, 2007.

[116] Sander Gersen, Harry Darmeveil, and Howard Levinsky. The effects of CO addition on the autoignition of H_2, CH_4 and CH_4/H_2 fuels at high pressure in an rcm. *Combustion and Flame*, 159(12):3472–3475, 2012.

[117] HC Lee, LY Jiang, and AA Mohamad. A review on the laminar flame speed and ignition

delay time of syngas mixtures. *International Journal of Hydrogen Energy*, 39(2):1105–1121, 2014.

[118] Zekai Hong, David F Davidson, and Ronald K Hanson. An improved H_2/O_2 mechanism based on recent shock tube/laser absorption measurements. *Combustion and Flame*, 158(4):633–644, 2011.

[119] Michael P Burke, Marcos Chaos, Yiguang Ju, Frederick L Dryer, and Stephen J Klippenstein. Comprehensive H_2/O_2 kinetic model for high-pressure combustion. *International Journal of Chemical Kinetics*, 44(7):444–474, 2012.

[120] RX Fernandes, K Luther, J Troe, and VG Ushakov. Experimental and modelling study of the recombination reaction H + O_2 $(+M) \rightarrow HO_2$ $(+M)$ between 300 and 900 k, 1.5 and 950 bar, and in the bath gases M = He, Ar, and N_2. *Physical Chemistry Chemical Physics*, 10(29):4313–4321, 2008.

[121] PJ Ashman and BS Haynes. Rate coefficient of H + O_2 + M $\rightarrow$ HO_2 + M ($M = H_2O, N_2, Ar, CO_2$). *Proceedings of the Combustion Institute*, 27(1):185–91, 1998.

[122] King-Yiu Lam, David F Davidson, and Ronald K Hanson. A shock tube study of H_2+ OH $\rightarrow$ H_2O + H using OH laser absorption. *International Journal of Chemical Kinetics*, 45(6):363–373, 2013.

[123] JV Michael and JW Sutherland. Rate constant for the reaction of H with H_2O and OH with H_2 by the flash photolysisshock tube technique over the temperature range 12462297 k. *The Journal of Physical Chemistry*, 92(13):3853–3857, 1988.

[124] RC Oldenborg, GW Loge, DM Harradine, and KR Winn. Kinetic study of the hydrogel+ hydrogen reaction from 800 to 1550 k. *The Journal of Physical Chemistry*, 96(21):8426–8430, 1992.

[125] N Cohen. Are reaction rate coefficients additive? revised transition state theory calculations

for $OH+$ alkane reactions. *International Journal of Chemical Kinetics*, 23(5):397–417, 1991.

[126] Wenji Wang and Yi Zhao. Quantum instanton calculation of rate constant for CH_4 + OH $\rightarrow$ CH_3 + H_2O reaction: Torsional anharmonicity and kinetic isotope effect. *The Journal of Chemical Physics*, 137(21):214306, 2012.

[127] W Felder and S Madronich. High temperature photochemistry (HTP): kinetics and mechanism studies of elementary combustion reactions over 300-1700 K. *Combustion Science and Technology*, 50(1-3):135–150, 1986.

[128] NK Srinivasan, M-C Su, JW Sutherland, and JV Michael. Reflected shock tube studies of high-temperature rate constants for OH + CH_4 $\rightarrow$ CH_3 + H_2O and CH_3 + NO_2 $\rightarrow$ CH_3O + NO. *The Journal of Physical Chemistry A*, 109(9):1857–1863, 2005.

[129] Zekai Hong, David Frank Davidson, King-Yiu Lam, and Ronald Kenneth Hanson. A shock tube study of the rate constants of HO_2 and CH_3 reactions. *Combustion and Flame*, 159(10):3007–3013, 2012.

[130] Baoshan Wang, Hua Hou, Laurie M Yoder, James T Muckerman, and Christopher Fockenberg. Experimental and theoretical investigations on the methyl-methyl recombination reaction. *The Journal of Physical Chemistry A*, 107(51):11414–11426, 2003.

[131] JH Kiefer, S Santhanam, NK Srinivasan, RS Tranter, SJ Klippenstein, and MA Oehlschlaeger. Dissociation, relaxation, and incubation in the high-temperature pyrolysis of ethane, and a successful RRKM modeling. *Proceedings of the Combustion Institute*, 30(1):1129–1135, 2005.

[132] Matthew A Oehlschlaeger, David F Davidson, and Ronald K Hanson. High-temperature ethane and propane decomposition. *Proceedings of the Combustion Institute*, 30(1):1119–1127, 2005.

[133] Stephen J Klippenstein, Yuri Georgievskii, and Lawrence B Harding. Predictive theory for the combination kinetics of two alkyl radicals. *Physical Chemistry Chemical Physics*, 8(10):1133–1147, 2006.

[134] Ahren W Jasper, Stephen J Klippenstein, and Lawrence B Harding. Theoretical rate coefficients for the reaction of methyl radical with hydroperoxyl radical and for methylhydroperoxide decomposition. *Proceedings of the Combustion Institute*, 32(1):279–286, 2009.

[135] Hsu Chew Lee, Abdulmajeed A Mohamad, and Lei-Yong Jiang. Comprehensive comparison of chemical kinetics mechanisms for syngas/biogas mixtures. *Energy & Fuels*, 29(9):6126–6145, 2015.

[136] Derek W Griffin and Michael A Schultz. Fuel and chemical products from biomass syngas: a comparison of gas fermentation to thermochemical conversion routes. *Environmental Progress & Sustainable Energy*, 31(2):219–224, 2012.

[137] S Rasi, A Veijanen, and J Rintala. Trace compounds of biogas from different biogas production plants. *Energy*, 32(8):1375–1380, 2007.

[138] CK Law and OC Kwon. Effects of hydrocarbon substitution on atmospheric hydrogenair flame propagation. *International Journal of Hydrogen Energy*, 29(8):867–879, 2004.

[139] Miles S Okino and Michael L Mavrovouniotis. Simplification of mathematical models of chemical reaction systems. *Chemical Reviews*, 98(2):391–408, 1998.

[140] Alison S Tomlin, Tamás Turányi, and Michael J Pilling. Mathematical tools for the construction, investigation and reduction of combustion mechanisms. *Comprehensive Chemical Kinetics*, 35:293–438, 1997.

[141] Wenting Sun, Zheng Chen, Xiaolong Gou, and Yiguang Ju. A path flux analysis method for the reduction of detailed chemical kinetic mechanisms. *Combustion and Flame*, 157(7):1298–1307, 2010.

[142] Xiang Gao, Suo Yang, and Wenting Sun. A global pathway selection algorithm for the reduction of detailed chemical kinetic mechanisms. *Combustion and Flame*, 2016.

[143] N Sikalo, O Hasemann, C Schulz, A Kempf, and I Wlokas. A genetic algorithmbased method for the automatic reduction of reaction mechanisms. *International Journal of Chemical Kinetics*, 46(1):41–59, 2014.

[144] Lionel Elliott, Derek B Ingham, Adrian G Kyne, Nicolae S Mera, Mohamed Pourkashanian, and Sean Whittaker. Reaction mechanism reduction and optimisation for modelling aviation fuel oxidation using standard and hybrid genetic algorithms. *Computers & Chemical Engineering*, 30(5):889–900, 2006.

[145] Lionel Elliott, Derek B Ingham, Adrian G Kyne, Nicolae S Mera, Mohamed Pourkashanian, and Christopher W Wilson. Reaction mechanism reduction and optimization using genetic algorithms. *Industrial & Engineering Chemistry Research*, 44(4):658–667, 2005.

[146] Juan J Hernndez, Rosario Ballesteros, and Josep Sanz-Argent. Reduction of kinetic mechanisms for fuel oxidation through genetic algorithms. *Mathematical and Computer Modelling*, 52(7):1185–1193, 2010.

[147] D Healy, HJ Curran, JM Simmie, DM Kalitan, CM Zinner, AB Barrett, EL Petersen, and G Bourque. Methane/ethane/propane mixture oxidation at high pressures and at high, intermediate and low temperatures. *Combustion and Flame*, 155(3):441–448, 2008.

[148] Eric L Petersen, Danielle M Kalitan, Stefanie Simmons, Gilles Bourque, Henry J Curran, and John M Simmie. Methane/propane oxidation at high pressures: Experimental and detailed chemical kinetic modeling. *Proceedings of the Combustion Institute*, 31(1):447–454, 2007.

[149] Assa Lifshitz, Karl Scheller, Alexander Burcat, and Gordon B Skinner. Shock-tube investigation of ignition in methane-oxygen-argon mixtures. *Combustion and Flame*, 16(3):311–

321, 1971.

[150] Daniel J Seery and Craig T Bowman. An experimental and analytical study of methane oxidation behind shock waves. *Combustion and Flame*, 14(1):37–47, 1970.

[151] Nicola Donohoe, Karl A Heufer, Christopher J Aul, Eric L Petersen, Gilles Bourque, Robert Gordon, and Henry J Curran. Influence of steam dilution on the ignition of hydrogen, syngas and natural gas blends at elevated pressures. *Combustion and Flame*, 162(4):1126–1135, 2015.

[152] J Herzler and C Naumann. Shock-tube study of the ignition of methane/ethane/hydrogen mixtures with hydrogen contents from 0 % to 100 % at different pressures. *Proceedings of the Combustion Institute*, 32(1):213–220, 2009.

[153] Michael Frenklach and David E Bornside. Shock-initiated ignition in methane-propane mixtures. *Combustion and Flame*, 56(1):1–27, 1984.

[154] Christine M Vagelopoulos and Fokion N Egolfopoulos. Direct experimental determination of laminar flame speeds. In *Symposium (International) on Combustion*, volume 27, pages 513–519. Elsevier, 1998.

[155] FN Egolfopoulos, P Cho, and CK Law. Laminar flame speeds of methane-air mixtures under reduced and elevated pressures. *Combustion and Flame*, 76(3):375–391, 1989.

[156] Th. Just. *Personal Communication*, 1994.

[157] A Van Maaren, DS Thung, and L. P. H. de Goey. Measurement of flame temperature and adiabatic burning velocity of methane/air mixtures. *Combustion Science and Technology*, 96(4-6):327–344, 1994.

Appendix A

Supporting Materials for Chapter 3

Table A.1 and A.2 tabulate the average absolute relative error values of each dataset, the overall mean of individual figures, and the grand mean values of six cases, for all the mechanisms investigated in this study. The average absolute relative error ($\bar{\mathrm{E}}$), overall mean ($\bar{\bar{\varepsilon}}$), and grand mean ($\bar{\bar{\psi}}$) are computed as the following: -

$$\bar{\mathrm{E}}_{\mathrm{i}} = \frac{1}{\mathrm{N_i}} \sum_{\mathrm{j}=1}^{\mathrm{N_j}} \left| \frac{\mathrm{Y_{sim,ij}} - \mathrm{Y_{exp,ij}}}{\mathrm{Y_{exp,ij}}} \right| \times 100\%$$

$$\bar{\bar{\varepsilon}} = \frac{1}{\mathrm{N}} \sum_{\mathrm{i}=1}^{\mathrm{M}} \bar{\mathrm{E}}_{\mathrm{i}}$$

$$\bar{\bar{\psi}} = \frac{1}{\mathrm{G}} \sum_{\mathrm{i}=1}^{\mathrm{G}} \bar{\mathrm{E}}_{\mathrm{i}}$$

where $\mathrm{N_i}$ is the number of data points in a dataset, N is the number of datasets in an individual figure, and G is the number of datasets in a considered case.

NUIG_V1, NUIG_V2, and NUIG_V3 are the variants of the NUIG2013 mechanism and the modifications are as the following:

Reaction	NUIG2013 $[cm^6mol^{-2}s^{-1}]$ *or* $[cm^3mol^{-1}s^{-1}]$	NUIG_V1 $[cm^6mol^{-2}s^{-1}]$ *or* $[cm^3mol^{-1}s^{-1}]$	NUIG_V2 $[cm^6mol^{-2}s^{-1}]$ *or* $[cm^3mol^{-1}s^{-1}]$	NUIG_V3 $[cm^6mol^{-2}s^{-1}]$ *or* $[cm^3mol^{-1}s^{-1}]$
$H + O_2(+CO_2)$ $= HO_2(+CO_2)$	$k_\infty = 1.767 \times 10^{13}[T]^{0.44}$ $k_0 = 6.600 \times 10^{19}[T]^{-1.23}$	$k_\infty = 1.116 \times 10^{13}[T]^{0.44}$ $k_0 = 8.820 \times 10^{19}[T]^{-1.40}$	$k_\infty = 1.116 \times 10^{13}[T]^{0.44}$ $k_0 = 8.820 \times 10^{19}[T]^{-1.40}$	$k_\infty = 1.116 \times 10^{13}[T]^{0.44}$ $k_0 = 8.820 \times 10^{19}[T]^{-1.40}$
$H + O_2(+M)$ $= HO_2(+M)$	$k_\infty = 4.650 \times 10^{12}[T]^{0.44}$ $k_0 = 1.737 \times 10^{19}[T]^{-1.23}$ $\beta_{H_2O} = 12.0$	No Changes	$k_\infty = 4.650 \times 10^{12}[T]^{0.44}$ $k_0 = 1.737 \times 10^{19}[T]^{-1.23}$ $\beta_{H_2O} = 8.0$	No Changes
$HO_2 + H$ $= OH + OH$	$k = 7.079 \times 10^{13} e^{-295/T}$	No Changes	$k = 6.079 \times 10^{13} e^{-295/T}$	No Changes
$CH_4 + OH$ $= CH_3 + H_2O$	$k = 5.83 \times 10^{4}[T]^{2.6} e^{-2190/T}$	No Changes	No Changes	$k = 2.3 \times 10^{8}[T]^{1.4} e^{-2850/T}$

Figure A.1 - A.13 show the relative error between the measured and simulated flame speed for each data point. The values listed next to the mechanisms name represent the average absolute relative error of the mechanism for the respective experimental conditions shown in the sub-caption.

Figure A.15 - A.23 show the relative error between the measured and simulated ignition delay time for each data point. The values listed next to the mechanisms name represent the average absolute relative error of the mechanism for the respective experimental conditions shown in the sub-caption.

Figure A.24 shows the sensitivity analysis conducted for the flame speed results shown in Fig. 3.4, 3.5, and 3.6 in the Chapter 3. Only the 10 most sensitive reactions are shown, for clarity. Please refer to the Chapter 3 for an explanation how the logarithm coefficients (L.S.) are computed.

Figure A.25 - A.34 show the comparison between the proposed rate constant expression and the rate constant expressions used in the current mechanisms with the experimentally determined rate constant values procured from literature. In addition, these Figures depict the sensitivity analysis conducted for $H_2/CO/CH_4$ and $H_2/CO/CH_4/CO2/CH_4$ mixtures at various temperatures and pressures, where they are plotted in a 3-D manner for ease of illustration. The ignition delay time results of $H2/CH_4$ mixtures (similar to Fig. 3.21 in manuscript) are recomputed with NUIG_V3

mechanism and they are shown in Fig. A.28.

Table A.1: The average absolute relative error values between the measured and simulated flame speed for all the mechanisms investigated in this study. The grand mean for all the mechanisms sare given for four cases: [A] Flame speed of syngas with all diluents, except He and CH_4; [B] - Flame speed of syngas with all diluents, except CH_4; [C] - Flame speed of syngas with all diluents, except He; [D] - Flame speed of syngas with all diluents. Min value in each category is colored red (modified NUIG mechanisms are not included). Blue colored values indicate the variants of NUIG2013 mechanism; please see Chapter 3 for more information.)

Figure no.		Mixture compositions	Experimental conditions			Average absolute relative error values ($\bar{E}_i$)									
			ϕ	P [atm]	T [K]	GRI 1999	Li 2007	Davis 2005	USC 2007	UCSD 2014	Sun 2007	NUIG 2013	NUIG V1	NUIG V2	NUIG V3
1	(a)	H_2/CO - 5 : 95	0.5 - 5.0	1	300	6.75	9.32	4.31	5.06	15.32	11.06	11.61	12.21	7.18	12.21
	(b)	H_2/CO - 50 : 50				7.72	5.11	5.15	5.13	9.89	5.50	8.46	8.67	5.26	8 .67
Overall mean ($\bar{\varepsilon}$) [%] of **Fig. 1** :						7.24	7.22	4.73	5.10	12.61	8.28	10.04	10.44	6.22	10.44
2	(a)	H_2/CO - 50 : 50	0.8 - 4.0	5	300	-	4.95	4.12	-	8.36	3.57	6.17	5.99	4.61	5.99
	(b)	H_2/CO - 50 : 50	0.8 - 4.0	10		-	10.27	9.29	-	15.10	8.30	10.14	9.56	8.24	9.56
Overall mean ($\bar{\varepsilon}$) [%] of **Fig. 2** :						-	7.61	6.71	-	11.73	5.94	8.16	7.78	6.43	7.78
3	(a)	H_2/CO - 5 : 95	0.7 - 3.5	10	300	-	5.57	5.84	-	7.89	8.36	5.74	6.03	12.58	6.03
			1.2 - 3.0	40		-	23.52	22.34	-	22.03	13.27	19.74	22.71	16.14	22.71
	(b)		0.7 - 3.5	5		-	5.21	5.51	-	10.97	8.58	4.19	4.74	5.55	4.74
			1.0 - 3.5	20		-	22.07	19.28	-	20.39	18.90	18.52	20.80	13.79	20.80
Overall mean ($\bar{\varepsilon}$) [%] of **Fig. 3** :						-	14.09	13.24	-	15.32	12.28	12.05	13.57	12.02	13.57
4	(a)	$H_2/CO/CO_2$ - 35 : 35 : 30	0.4 - 1.0	1	303	24.57	16.24	20.87	19.44	4.49	12.11	13.59	11.83	13.36	11.83
	(b)				373	13.26	6.38	9.90	8.40	9.00	6.75	9.01	8.41	6.99	8.41
	(c)			3	373	21.04	11.99	16.92	13.75	6.80	7.54	10.70	8.56	11.08	8.56
Overall mean ($\bar{\varepsilon}$) [%] of **Fig. 4** :						19.74	11.54	15.90	13.86	6.76	8.80	11.10	9.60	10.48	9.60
5		$H_2/CO/CO_2$ - 40 : 10 : 50	0.8 - 2.0	1	303	7.76	3.81	5.88	5.91	10.80	5.87	11.57	13.51	6.29	13.51
		$H_2/CO/CO_2$ - 25 : 25 : 50				4.75	3.17	5.60	4.59	10.27	6.16	12.74	16.54	9.73	16.54

Continued on next page

Table A.1 – *Continued on next page*

Figure no.		Mixture compositions	Experimental conditions			Average absolute relative error values ($\bar{E}_i$)									
			ϕ	P [atm]	T [K]	GRI 1999	Li 2007	Davis 2005	USC 2007	UCSD 2014	Sun 2007	NUIG 2013	NUIG V1	NUIG V2	NUIG V3
		$H_2/CO/CO_2$ - 10 : 40 : 50				5.74	7.71	9.97	8.64	7.27	5.00	1.47	8.34	2.18	8.34
Overall mean ($\bar{\varepsilon}$) [%] of **Fig. 5** :						6.08	4.90	7.15	6.38	9.45	5.68	8.59	12.80	6.07	12.80
6	(a)	$H_2/CO/CO_2$ - [Z_{H_2} varies from 0.1 to 0.7]	ϕ = 0.4; Z_{CO_2} = 0.4	1	300	5.14	1.77	3.93	3.24	13.12	3.02	3.02	3.02	3.60	2.47
			ϕ = 0.4; Z_{CO_2} = 0.5			10.79	4.73	7.65	6.20	10.90	4.22	5.00	5.00	3.73	3.33
			ϕ = 0.4; Z_{CO_2} = 0.6			10.79	4.73	7.65	6.20	10.90	4.22	5.00	5.00	3.73	3.33
			ϕ = 0.4; Z_{CO_2} = 0.7			10.79	4.73	7.65	6.20	10.90	4.22	5.0	5.00	3.73	3.33
	(b)		ϕ = 0.4; Z_{CO_2} = 0.4	2	300	12.17	4.05	2.18	2.69	16.48	6.73	4.22	4.22	8.15	5.69
			ϕ = 0.4; Z_{CO_2} = 0.4			6.61	12.47	14.83	13.32	5.58	10.46	12.56	12.56	10.52	11.43
			ϕ = 0.4; Z_{CO_2} = 0.4			17.30	11.28	12.83	14.44	18.87	15.00	11.29	11.29	14.63	14.06
			ϕ = 0.4; Z_{CO_2} = 0.4			27.01	32.80	31.91	31.38	24.23	29.36	39.00	39.00	29.93	27.81
Overall mean ($\bar{\varepsilon}$) [%] of **Fig. 6** :						16.81	13.84	14.48	13.96	15.03	13.22	15.70	13.20	12.28	13.20
7	(a)	H_2/CO - 5 : 95 [H_2O % varies 0 - 35 %]	0.9	1	323	2.39	3.10	3.35	2.90	10.83	9.96	3.61	4.48	2.84	4.48
			0.4			30.26	9.70	18.66	15.91	7.12	7.24	11.84	13.59	9.96	13.59
	(b)	H_2/CO - 50 : 50 [H_2O % varies 0 - 35 %]	0.5	1	323	14.81	5.34	7.90	6.25	14.43	6.29	5.60	4.99	6.37	4.99
			0.6			13.97	2.56	9.18	7.51	8.46	2.18	0.99	1.13	1.67	1.13
Overall mean ($\bar{\varepsilon}$) [%] of **Fig. 7** :						15.36	5.18	9.77	8.14	10.21	6.42	5.51	6.05	5.21	6.05
8		H_2/CO - 5 : 95 [H_2O % varies 0 - 40 %]	1.0	1	400	12.42	12.80	9.15	10.32	20.19	20.49	13.50	14.09	12.81	14.09
		H_2/CO - 50 : 50 [H_2O % varies 0 - 20 %]				2.06	2.17	2.26	1.97	11.01	7.32	8.51	8.31	4.42	8.31
Overall mean ($\bar{\varepsilon}$) [%] of **Fig. 8** :						7.24	7.49	5.71	6.15	15.60	13.91	11.00	11.20	8.62	11.20
9	(a)	$H_2/CO/N_2$ - 11 : 31 : 58	0.5-1.0	1	303	21.06	12.44	18.59	16.54	5.67	8.71	13.00	11.60	13.94	11.60
	(b)			1	373	5.54	4.26	3.80	2.47	14.00	8.25	4.56	5.26	2.69	5.26
	(c)			3	373	4.90	19.60	10.84	15.42	35.55	26.00	15.74	18.16	13.84	18.16
	(d)			5	373	3.37	16.90	8.49	14.52	36.09	24.17	11.60	14.71	11.79	14.71
Overall mean ($\bar{\varepsilon}$) [%] of **Fig. 9** :						8.72	13.3	10.43	12.24	22.83	16.78	11.23	12.43	10.57	12.43

Continued on next page

Table A.1 – *Continued on next page*

Figure no.		Mixture compositions	Experimental conditions			Average absolute relative error values ($\bar{E}_i$)									
			ϕ	P [atm]	T [K]	GRI 1999	Li 2007	Davis 2005	USC 2007	UCSD 2014	Sun 2007	NUIG 2013	NUIG V1	NUIG V2	NUIG V3
10		H_2/CH_4 [CH_4 % varies 0 - 100 %]	1.0	1	300	15.56	20.43	-	20.11	19.37	-	17.51	17.95	17.36	17.15
			Overall mean ($\bar{\varepsilon}$) [%] of **Fig. 10** :			15.56	20.43	-	20.11	19.37	-	17.51	17.95	17.36	17.15
11	(a)	H_2/CH_4 - 20 : 80	0.6 - 1.55	1	298	14.89	19.20	-	17.39	18.95	-	11.97	11.17	11.16	10.32
	(b)	H_2/CH_4 - 50 : 50	0.5 - 1.4	1	300	3.97	11.68	-	6.37	7.49	-	3.98	4.26	3.71	4.71
	(c)	H_2/CH_4 - 70 : 30	0.6 - 1.6	5	450	-	4.89	-	-	6.64	-	1.70	1.56	3.14	4.10
	(d)	H_2/CH_4 - 90 : 10	0.6 - 2.0	1	450	5.94	3.98	-	4.87	6.77	-	5.25	3.95	3.30	3.72
			Overall mean ($\bar{\varepsilon}$) [%] of **Fig. 11** :			8.27	9.94	-	9.54	9.96	-	5.73	5.24	5.33	5.71
12	(a)	$H_2/CO/CH_4/CO_2$ - 37.5 : 37.5 : 5.0 : 20.0	0.7	1	300	6.63	2.13	-	2.00	8.61	-	0.10	0.54	0.08	0.78
	(b)	$H_2/CO/CH_4/CO_2$ - 18.8 : 18.8 : 52.50 : 10.0				12.07	1.44	-	12.46	14.69	-	8.56	7.37	10.15	8.55
	(b)	$H_2/CO/CH_4/CO_2$ - 28.1 : 28.1 : 28.80 : 15.0				2.72	7.11	-	0.71	3.48	-	3.60	6.24	4.42	5.41
	(c)	$H_2/CO/CH_4/CO_2$ - 37.5 : 37.5 : 5.0 : 20.0	0.8	1	300	10.26	5.22	-	11.27	2.25	-	4.79	4.05	4.97	3.79
	(d)	$H_2/CO/CH_4/CO_2$ - 18.8 : 18.8 : 52.50 : 10.0				5.67	1.88	-	7.91	9.06	-	3.04	1.86	3.87	3.34
	(e)	$H_2/CO/CH_4/CO_2$ - 28.1 : 28.1 : 28.80 : 15.0				4.45	8.72	-	5.20	1.75	-	5.27	5.60	4.51	4.67
	(f)	$H_2/CO/CH_4/CO_2$ - 37.5 : 37.5 : 5.0 : 20.0	0.9	1	300	9.87	8.79	-	12.43	3.17	-	6.10	5.90	7.32	5.67
	(g)	$H_2/CO/CH_4/CO_2$ - 18.8 : 18.8 : 52.50 : 10.0				1.72	4.52	-	1.65	0.07	-	4.17	4.78	4.63	4.16
	(h)	$H_2/CO/CH_4/CO_2$ - 28.1 : 28.1 : 28.80 : 15.0				3.76	8.72	-	7.34	3.84	-	5.72	5.99	5.35	5.67
	(i)	$H_2/CO/CH_4/CO_2$ - 37.5 : 37.5 : 5.0 : 20.0	1.0	1	300	10.21	11.34	-	11.83	5.83	-	5.37	6.93	8.25	6.55
	(j)	$H_2/CO/CH_4/CO_2$ - 18.8 : 18.8 : 52.50 : 10.0				5.80	7.42	-	8.69	7.16	-	7.73	9.48	8.87	7.72
	(k)	$H_2/CO/CH_4/CO_2$ - 28.1 : 28.1 : 28.80 : 15.0				5.84	11.33	-	11.24	7.63	-	7.43	7.97	7.26	6.98
			Overall mean ($\bar{\varepsilon}$) [%] of **Fig. 12** :			6.58	6.55	-	7.73	5.63	-	5.1	5.56	5.81	5.27
Grand mean ($\bar{\psi}$) [%]		Flame speed of syngas, all diluents except He and CH_4 [A]				12.96	10.13	11.02	10.63	13.75	11.01	11.30	11.92	9.54	11.92
		Flame speed of syngas, all diluents except CH_4 [B]				-	10.47	11.03	-	13.82	10.85	11.20	11.87	9.65	11.87

Continued on next page

Table A.1 – *Continued on next page*

Figure no.	Mixture compositions	Experimental conditions			Average absolute relative error values ($\bar{E}_i$)									
		ϕ	P [atm]	T [K]	GRI 1999	Li 2007	Davis 2005	USC 2007	UCSD 2014	Sun 2007	NUIG 2013	NUIG V1	NUIG V2	NUIG V3
Grand mean ($\bar{\bar{\psi}}$) [%]	Flame speed of syngas, all diluents except He [C]				10.87	9.46	-	9.95	11.37	-	9.39	9.86	8.41	9.74
	Flame speed of syngas, all diluents [D]				-	9.67	-	-	11.61	-	9.40	9.91	8.52	9.86

Table A.2: The average relative error values between the measured and simulated ignition delay time for all the mechanisms investigated in this study. The grand mean for all the mechanisms are given for two cases: [E] Ignition delay time of syngas with all diluents, except CH_4; [F] - Ignition delay time of syngas with all diluents. NUIG_V1, NUIG_V2, and NUIG_V3 are the variants of NUIG2013 mechanism with one or more rate constants being replaced; see manuscript for more information. Min value in each category is colored red (modified NUIG mechanisms are not included).

Figure no.		Mixture compositions	Experimental conditions			Average absolute relative error values ($\bar{E}_i$)									
			ϕ	P [atm]	T [K]	GRI 1999	Li 2007	Davis 2005	USC 2007	UCSD 2014	Sun 2007	NUIG 2013	NUIG V1	NUIG V2	NUIG V3
14	(a)	$H_2/CO/O_2/Ar$	0.5	1.60	990 - 2000	35.83	33.92	33.82	33.95	32.60	35.89	38.47	38.78	39.41	38.78
	(b)	–0.5 : 0.5 : 1.0 : 98.0		12.0	1095 - 1385	102.25	159.07	11.89	11.21	22.43	7.60	8.07	8.54	13.98	8.54
	(c)			32.0	1170 - 1330	173.39	106.82	47.30	43.77	42.85	15.75	12.39	12.46	12.30	12.46
Overall mean ($\bar{\varepsilon}$) [%] of **Fig. 14** :						103.82	99.94	31.00	29.64	32.63	19.75	19.64	19.93	21.90	19.93
15	(a)	$H_2/CO/H_2O/O_2/Ar$	0.5	1.60	995 - 2010	75.96	73.75	65.66	65.50	66.74	73.47	73.66	73.51	75.35	73.51
	(b)	–0.444 : 0.444 : 0.223		12.0	1085 - 1400	247.95	350.63	31.41	30.20	119.52	50.92	61.81	65.60	62.43	65.60
	(c)	0.889 : 98		32.0	1155 - 1300	156.85	265.48	14.38	10.38	122.17	36.49	48.15	50.48	53.57	50.49
Overall mean ($\bar{\varepsilon}$) [%] of **Fig. 15** :						160.25	229.95	37.15	35.36	102.81	53.63	61.21	63.20	63.78	63.20
16	(a)	$H_2/H_2O/N_2/O_2$	1.0	10.0	996 - 1048	122.66	74.73	106.83	108.33	75.13	243.44	26.24	33.55	16.89	33.55
	(b)	–12.5 : 10 : 6.25 : 71.25		70.0	907 - 1000	174.36	122.12	193.095	193.25	38.16	453.7	11.05	10.94	11.08	10.94
	(c)	$H_2/H_2O/N_2/O_2$ –12.5 : 40 : 6.25 : 41.25		70.0	924 - 977	306.28	185.09	327.31	331.17	16.49	744.17	14.48	14.20	15.26	14.20
Overall mean ($\bar{\varepsilon}$) [%] of **Fig. 16** :						201.10	127.31	209.08	210.91	43.26	480.44	17.26	19.56	14.41	19.56
17	(a)	$H_2/CO/CO_2/O_2/Ar$	0.5	1.60	1005 - 1965	35.68	34.86	32.83	32.58	31.97	33.38	37.43	37.36	38.04	37.36
	(b)	–0.46 : 0.46 : 0.15 : 0.93 : 98		12.0	1105 - 1360	176.90	305.37	25.99	21.27	58.18	10.39	10.24	10.37	17.02	10.12
	(c)			32.0	1150 - 1290	52.85	133.18	54.51	50.74	38.40	19.12	16.39	16.80	16.30	16.78
Overall mean ($\bar{\varepsilon}$) [%] of **Fig. 17** :						88.48	157.80	34.11	34.86	42.85	20.96	21.35	21.42	23.79	21.42

Continued on next page

Table A.2 – *Continued on next page*

Figure no.		Mixture compositions	Experimental conditions			Average absolute relative error values ($\bar{E}_i$)									
			ϕ	P [atm]	T [K]	GRI 1999	Li 2007	Davis 2005	USC 2007	UCSD 2014	Sun 2007	NUIG 2013	NUIG V1	NUIG V2	NUIG V3
18	(a)	$H_2/CO/CO_2/O_2/N_2$	1.0	1.24	952 - 982	30.52	29.31	19.14	17.18	15.84	22.24	37.09	29.54	34.94	29.54
	(b)	–8.91 : 11.58 : 24.44 : 10.25 : 44.83		1.71	975 - 1000	84.62	194.15	15.03	18.83	28.24	18.06	322.94	19.69	24.70	19.69
	(c)			2.36	1010 - 1091	115.46	315.51	25.64	91.92	82.29	76.85	496.60	60.13	60.81	60.13
Overall mean ($\bar{\varepsilon}$) [%] of **Fig. 18** :						76.87	179.66	19.94	42.64	42.12	39.05	285.54	36.45	40.15	36.45
19	(a)	$H_2/CO/CO_2/CH_4/H_2O/O_2/Ar$	0.5	1.60	1050 - 2030	60.8	83.43	-	57.96	54.54	-	68.21	68.10	71.14	51.01
	(b)	–0.297 : 0.297 : 0.157 :		12.0	1160 - 1450	63.31	95.94	-	30.34	24.79	-	49.00	48.26	52.02	20.58
	(c)	0.089 : 0.21 : 0.95 : 98		32.0	1185 - 1305	71.86	146.21	-	127.14	255.87	-	353.43	345.49	345.91	31.35
Overall mean ($\bar{\varepsilon}$) [%] of **Fig. 19** :						65.32	108.52	-	71.81	111.73	-	156.88	153.95	156.36	34.31
20	(a)	$H_2/CO/CH_4/O_2/Ar$	0.5	1.60	1010 - 1920	32.51	55.98	-	30.07	29.51	-	36.68	36.64	37.73	29.78
	(b)	–0.406 : 0.406 : 0.075 :		12.0	1145 - 1410	71.32	110.55	-	16.23	17.07	-	26.84	26.87	31.69	13.66
	(c)	1.113 : 98		32.0	1155 - 1320	37.51	92.02	-	6.72	79.20	-	110.17	110.95	118.23	9.50
Overall mean ($\bar{\varepsilon}$) [%] of **Fig. 20** :						47.11	86.18	-	17.67	41.93	-	57.90	58.15	62.55	17.65
21	(a)	H_2/CH_4 - 80 : 20	0.5	5.00	1060 - 1300	45.08	47.73	-	26.74	24.49	-	25.61	24.96	26.12	24.65
		H_2/CH_4 - 40 : 60			1222 - 1700	45.08	47.73	-	26.74	24.49	-	25.61	24.96	26.12	24.65
	(b)	H_2/CH_4 - 60 : 40	0.5	5.00	1116 - 1390	39.26	59.78	-	33.69	30.99	-	74.40	73.46	85.91	26.27
		H_2/CH_4 - 20 : 80			1380 - 1842	19.98	50.07	-	15.01	15.77	-	27.79	26.67	27.59	9.30
	(c)	H_2/CH_4 - 80 : 20	0.5	10.00	1060 - 1276	131.76	179.62	-	20.13	29.09	-	51.19	51.80	55.71	18.28
		H_2/CH_4 - 40 : 60			1154 - 1780	25.22	78.18	-	19.40	24.99	-	67.32	66.17	67.78	15.11
	(d)	H_2/CH_4 - 60 : 40	0.5	10.00	1074 - 1396	13.62	68.64	-	11.26	12.12	-	67.67	67.37	67.11	27.19
		H_2/CH_4 - 20 : 80			1290 - 1800	29.58	56.77	-	21.57	30.73	-	26.11	25.20	25.88	9.65
	(e)	H_2/CH_4 - 80 : 20	0.5	20.00	1050 - 1492	133.34	171.95	-	27.20	110.02	-	75.43	76.81	75.51	53.52
		H_2/CH_4 - 40 : 60			1135 - 1630	40.61	106.79	-	33.38	36.28	-	91.81	90.77	47.90	37.78
	(f)	H_2/CH_4 - 60 : 40	0.5	20.00	1072 - 1564	34.48	71.63	-	35.5	36.11	-	48.51	48.28	90.60	29.61
		H_2/CH_4 - 20 : 80			1215 - 2000	27.7	64.20	-	22.16	27.77	-	35.69	34.77	36.19	20.50

Continued on next page

Table A.2 – *Continued on next page*

Figure no.	Mixture compositions	Experimental conditions			Average absolute relative error values ($\bar{E}_i$)									
		ϕ	P [atm]	T [K]	GRI 1999	Li 2007	Davis 2005	USC 2007	UCSD 2014	Sun 2007	NUIG 2013	NUIG V1	NUIG V2	NUIG V3
Overall mean ($\bar{\epsilon}$) [%] of **Fig. 21** :					47.41	87.39	-	24.61	34.18	-	56.41	55.84	56.85	24.76
Grand mean ($\bar{\bar{\psi}}$) [%]	Ignition delay time, all diluents except CH_4 [E]				126.10	158.93	66.99	70.69	52.73	122.76	81.00	32.13	32.81	32.11
	Ignition delay time, all diluents [F]				84.78	121.72	-	49.21	50.37	-	76.86	54.19	55.48	28.32

A.1 Relative error values - Laminar flame speed

A.1.1 Mixture Combination: H_2/CO

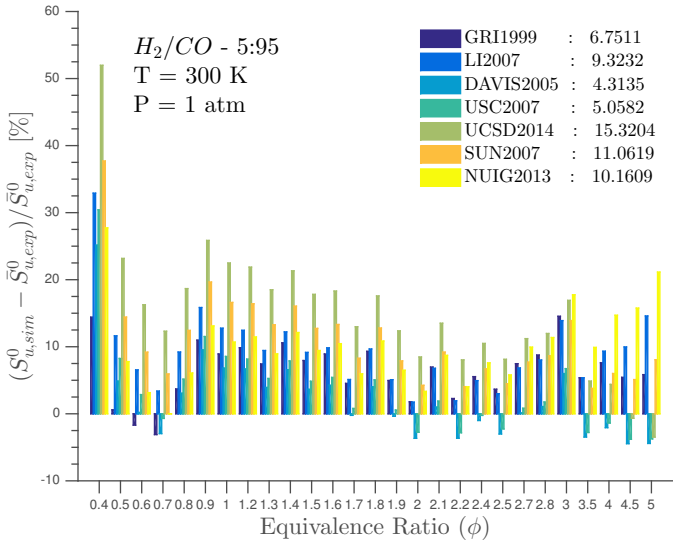

(a) H_2/CO - 5:95, T = 300 K, P = 1 atm

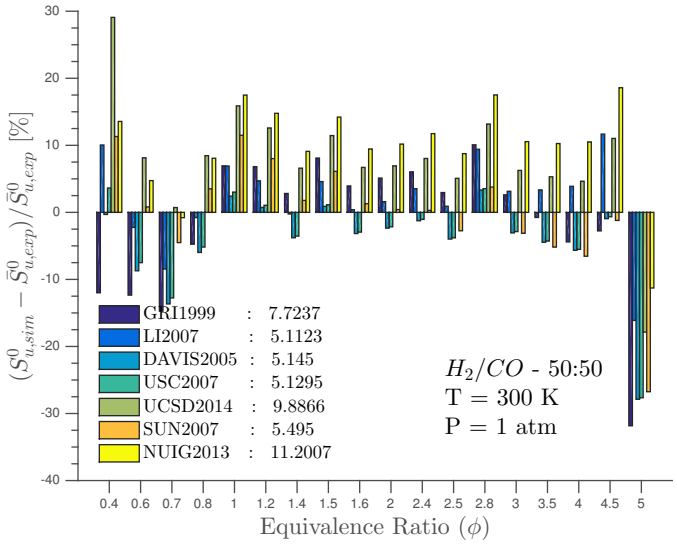

(b) H_2/CO - 50:50, T = 300 K, P = 1 atm

Figure A.1: The relative error between the simulated and measured laminar flame speed for H_2/CO mixtures, as shown in Fig. 3.1. The values next to the mechanism name represent the average relative error for the experimental condition shown in the sub-caption.

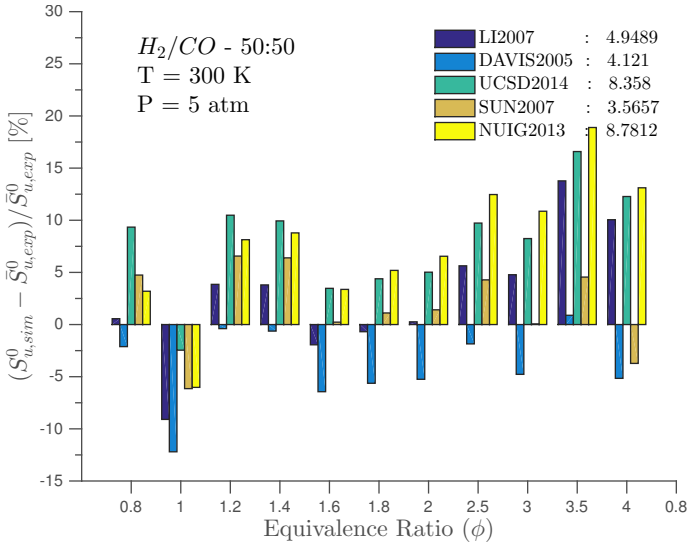

(a) H_2/CO - 50:50, T = 300 K, P = 5 atm

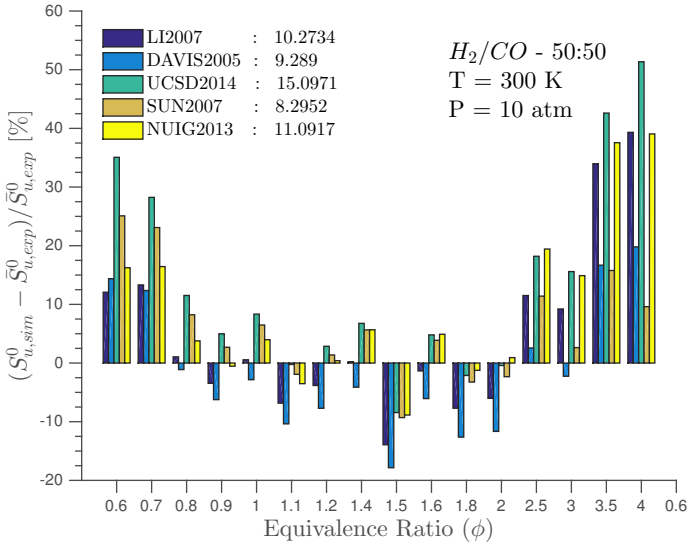

(b) H_2/CO - 50:50, T = 300 K, P = 10 atm

Figure A.2: The relative error between the simulated and measured laminar flame speed for H_2/CO mixtures, as shown in Fig. 3.2. The values next to the mechanism name represent the average relative error for the experimental condition shown in the sub-caption.

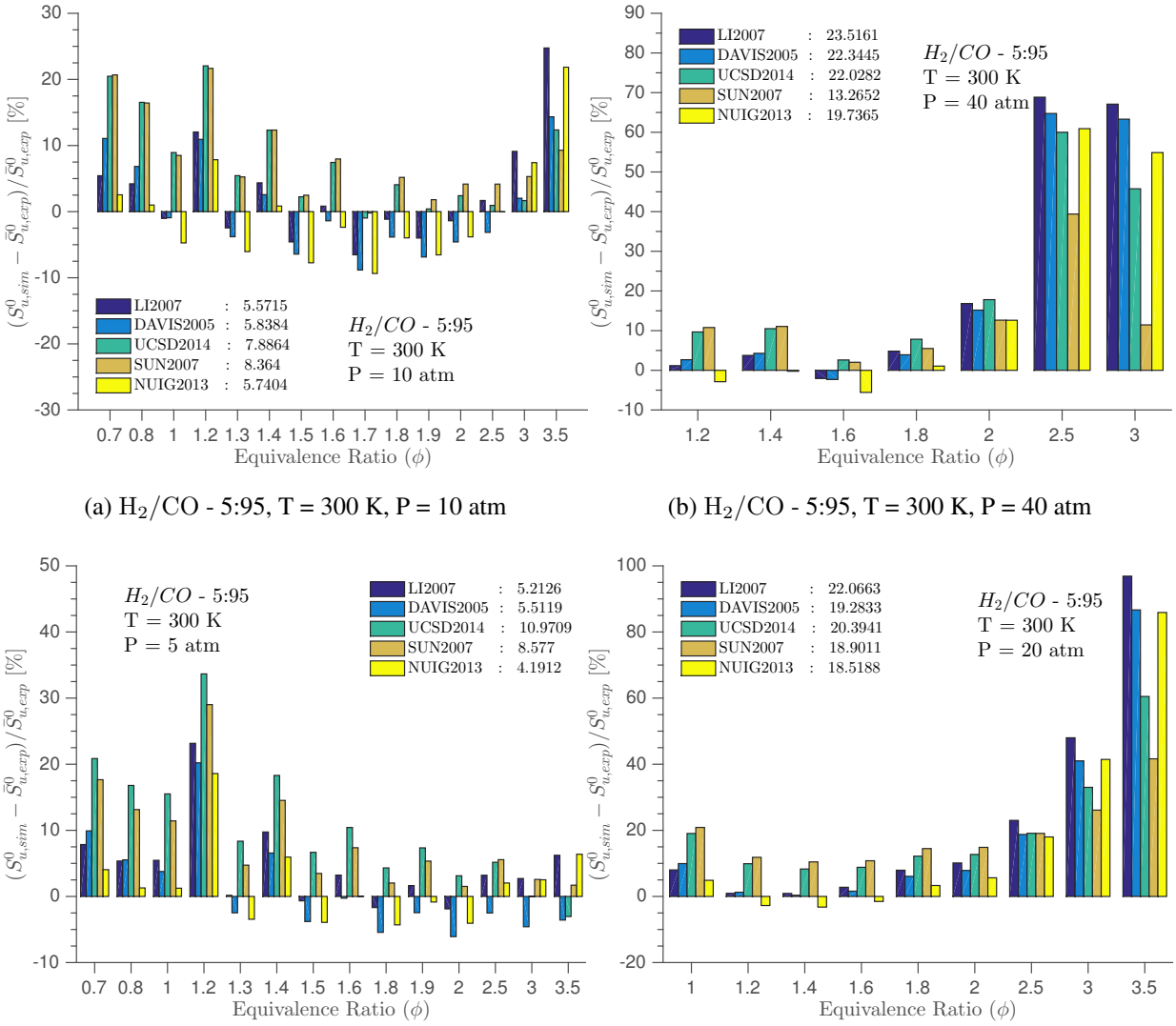

(a) H_2/CO - 5:95, T = 300 K, P = 10 atm

(b) H_2/CO - 5:95, T = 300 K, P = 40 atm

(c) H_2/CO - 5:95, T = 300 K, P = 5 atm

(d) H_2/CO - 5:95, T = 300 K, P = 20 atm

Figure A.3: The relative error between the simulated and measured laminar flame speed for H_2/CO mixtures, as shown in Fig. 3.3. The values next to the mechanism name represent the average relative error for the experimental condition shown in the sub-caption.

A.1.2 Mixture Combination: $H_2/CO/CO_2$

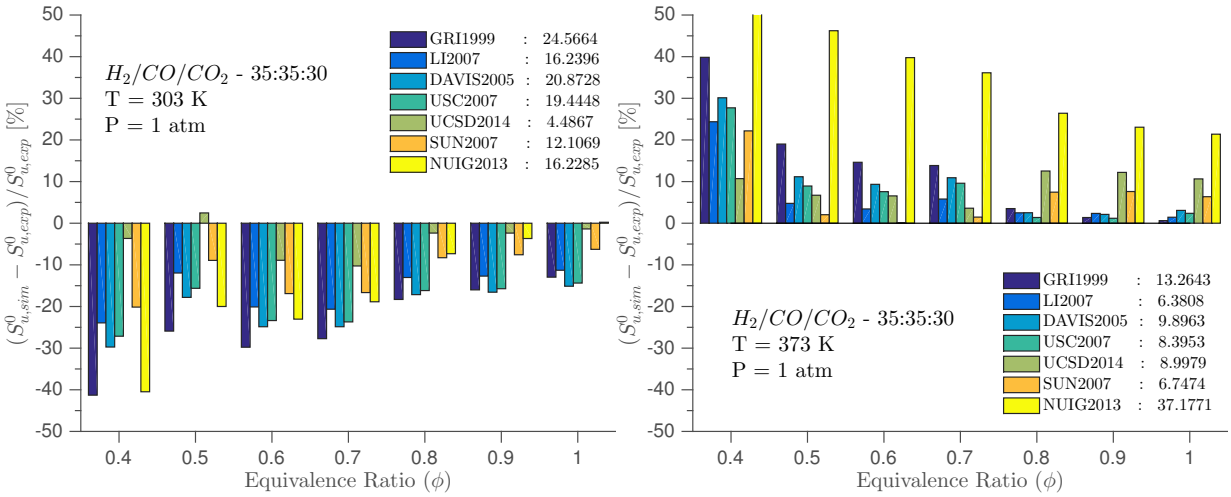

(a) $H_2/CO/CO_2$ - 35:35:30, T = 303 K, P = 1 atm

(b) $H_2/CO/CO_2$ - 35:35:30, T = 373 K, P = 1 atm

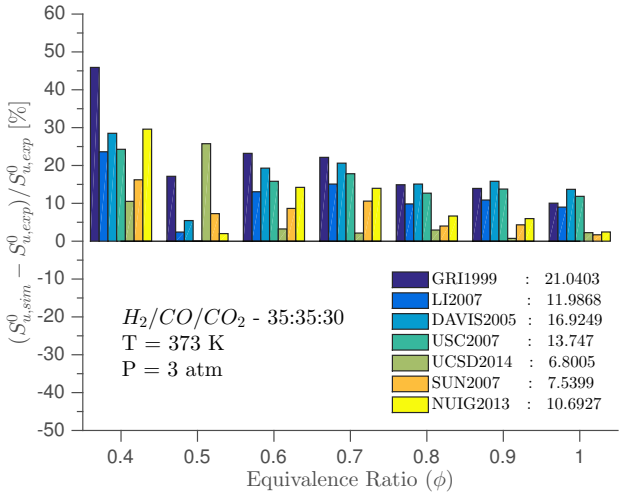

(c) $H_2/CO/CO_2$ - 35:35:30, T = 373 K, P = 3 atm

Figure A.4: The relative error between the simulated and measured laminar flame speed for $H_2/CO/CO_2$ mixtures, as shown in Fig. 3.4. The values next to the mechanism name represent the average relative error for the experimental condition shown in the sub-caption.

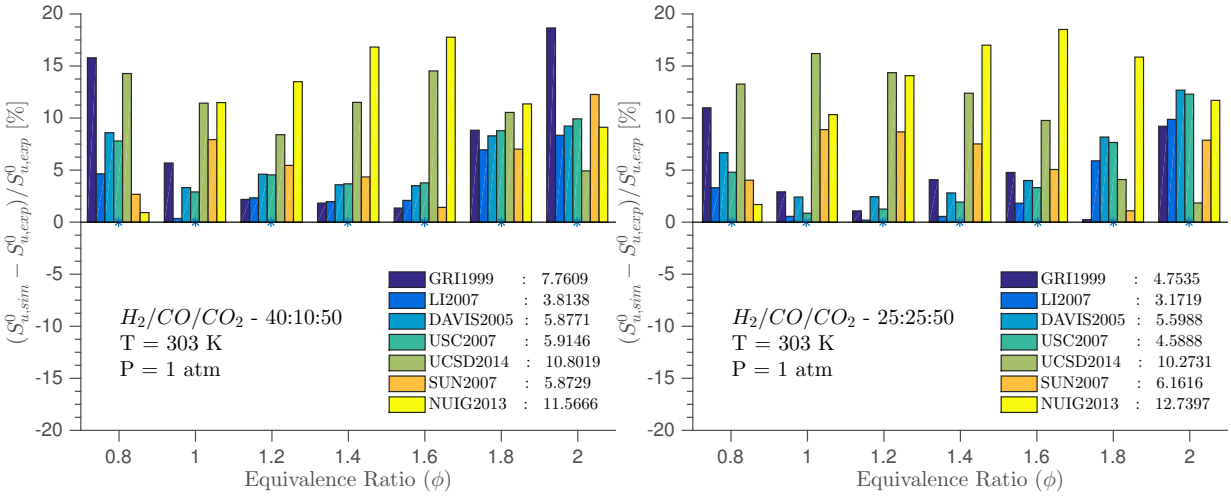

(a) $H_2/CO/CO_2$ - 40:10:50, T = 303 K, P = 1 atm

(b) $H_2/CO/CO_2$ - 25:25:50, T = 303 K, P = 1 atm

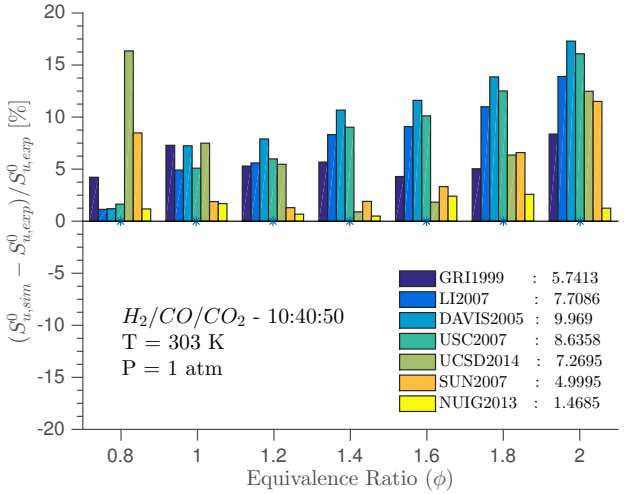

(c) $H_2/CO/CO_2$ - 10:40:50, T = 303 K, P = 1 atm

Figure A.5: The relative error between the simulated and measured laminar flame speed for $H_2/CO/CO_2$ mixtures, as shown in Fig. 3.5. The values next to the mechanism name represent the average relative error for the experimental condition shown in the sub-caption.

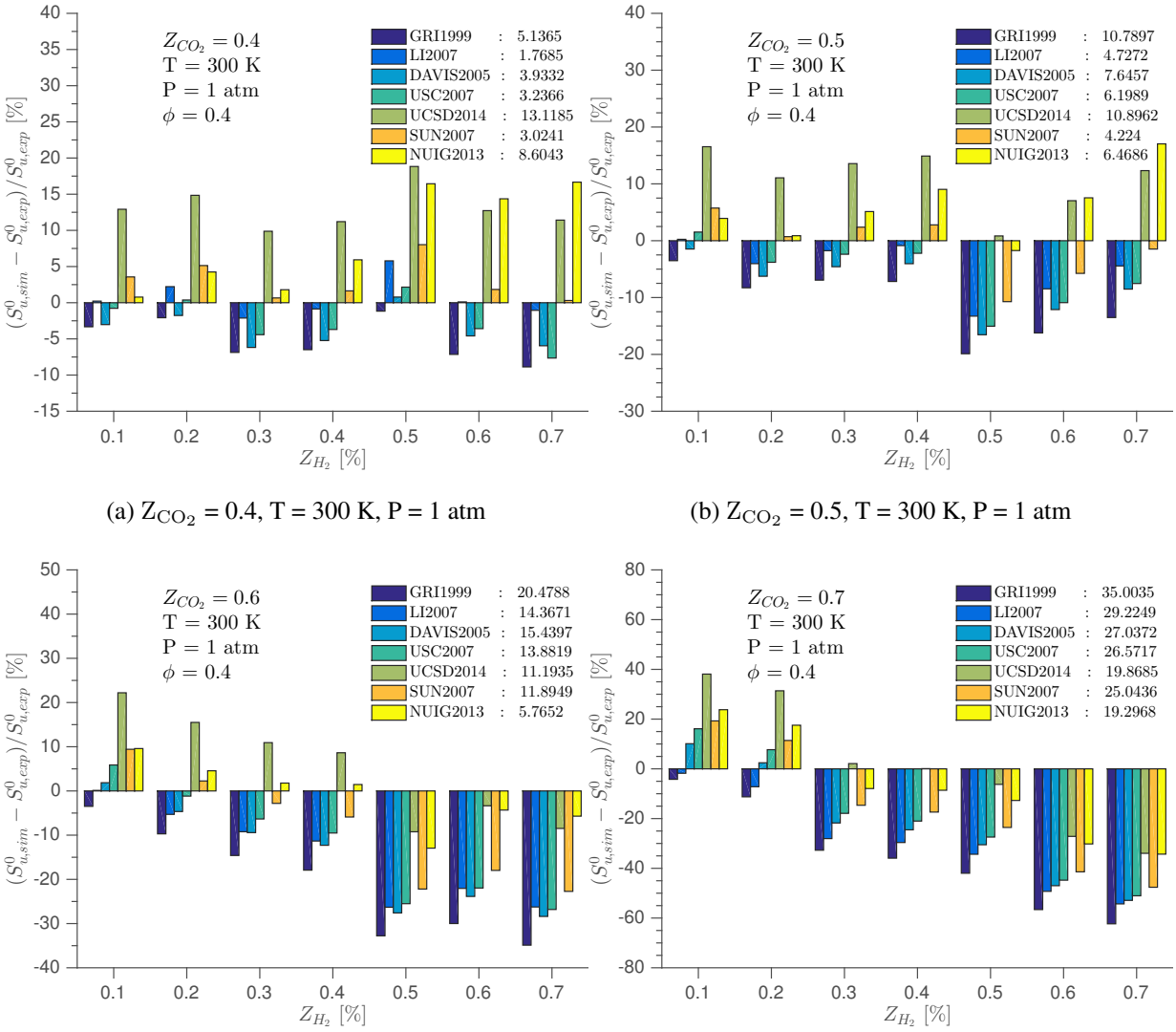

(a) Z_{CO_2} = 0.4, T = 300 K, P = 1 atm

(b) Z_{CO_2} = 0.5, T = 300 K, P = 1 atm

(c) Z_{CO_2} = 0.6, T = 300 K, P = 1 atm

(d) Z_{CO_2} = 0.7, T = 300 K, P = 1 atm

Figure A.6: The relative error between the simulated and measured laminar flame speed for $H_2/CO/CO_2$ mixtures, as shown in Fig. 3.6(a). The values next to the mechanism name represent the average relative error for the experimental condition shown in the sub-caption.

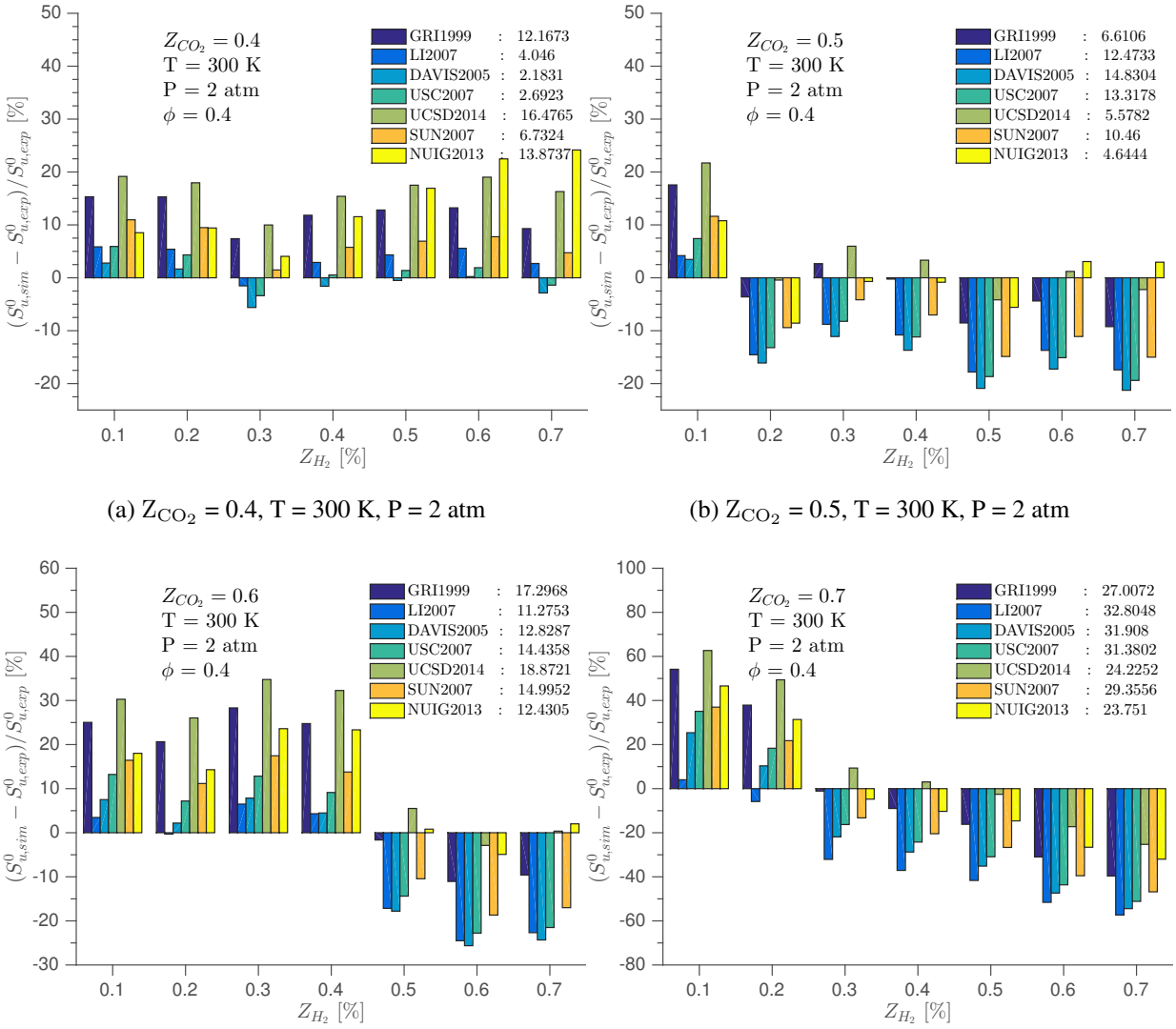

(a) Z_{CO_2} = 0.4, T = 300 K, P = 2 atm

(b) Z_{CO_2} = 0.5, T = 300 K, P = 2 atm

(c) Z_{CO_2} = 0.6, T = 300 K, P = 2 atm

(d) Z_{CO_2} = 0.7, T = 300 K, P = 2 atm

Figure A.7: The relative error between the simulated and measured laminar flame speed for $H_2/CO/CO_2$ mixtures, as shown in Fig. 3.6(b). The values next to the mechanism name represent the average relative error for the experimental condition shown in the sub-caption.

A.1.3 Mixture Combination: $H_2/CO/H_2O$

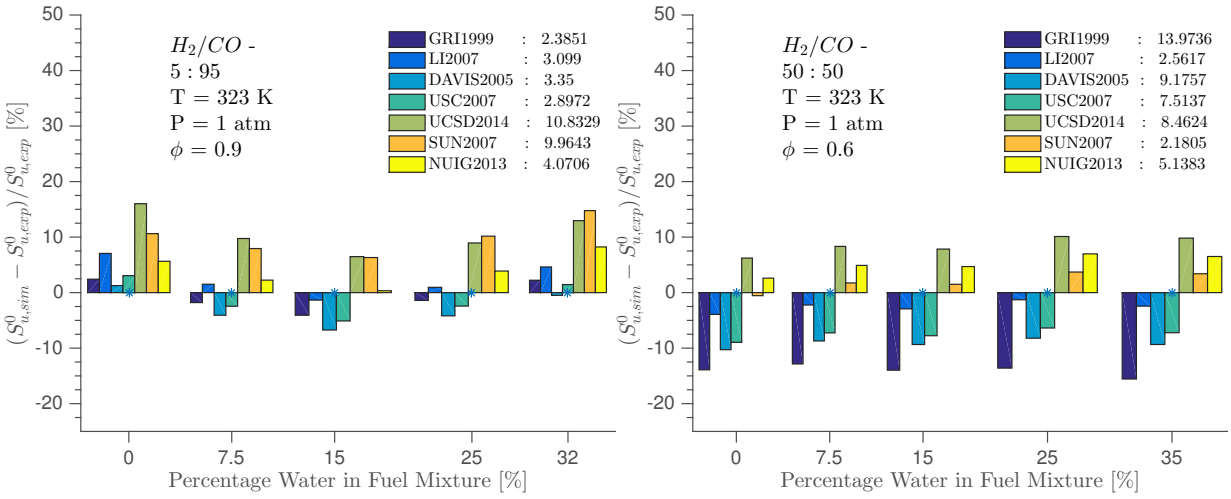

(a) H_2/CO = 5:95, T = 323 K, P = 1 atm, ϕ = 0.9

(b) H_2/CO = 50:50, T = 323 K, P = 1 atm, ϕ = 0.6

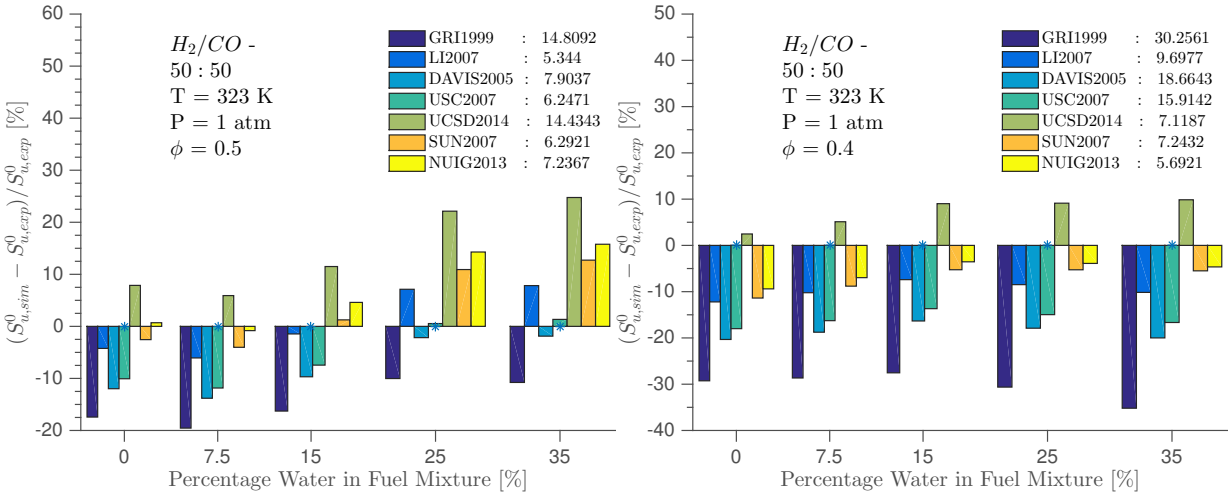

(c) H_2/CO = 50:50, T = 323 K, P = 1 atm, ϕ = 0.5

(d) H_2/CO = 50:50, T = 323 K, P = 1 atm, ϕ = 0.4

Figure A.8: The relative error between the simulated and measured laminar flame speed for $H_2/CO/H_2O$ mixtures, as shown in Fig. 3.7. The values next to the mechanism name represent the average relative error for the experimental condition shown in the sub-caption.

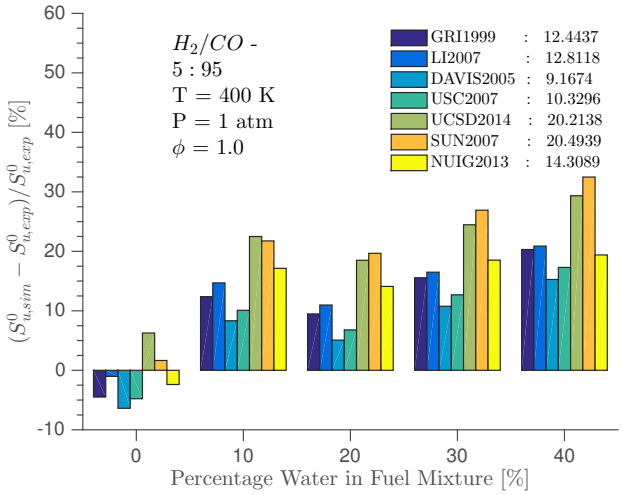

(a) H_2/CO - 5:95, T = 400 K, P = 1 atm, ϕ = 1.0

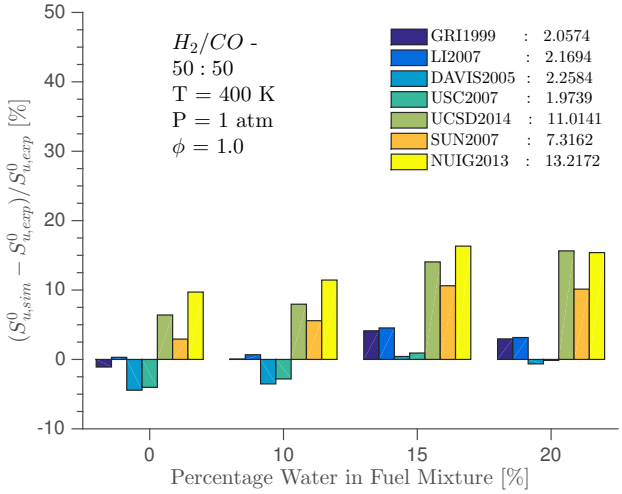

(b) H_2/CO - 50:50, T = 400 K, P = 1 atm, ϕ = 1.0

Figure A.9: The relative error between the simulated and measured laminar flame speed for $H_2/CO/H_2O$ mixtures, as shown in Fig. 3.8. The values next to the mechanism name represent the average relative error for the experimental condition shown in the sub-caption.

A.1.4 Mixture Combination: $H_2/CO/N_2$

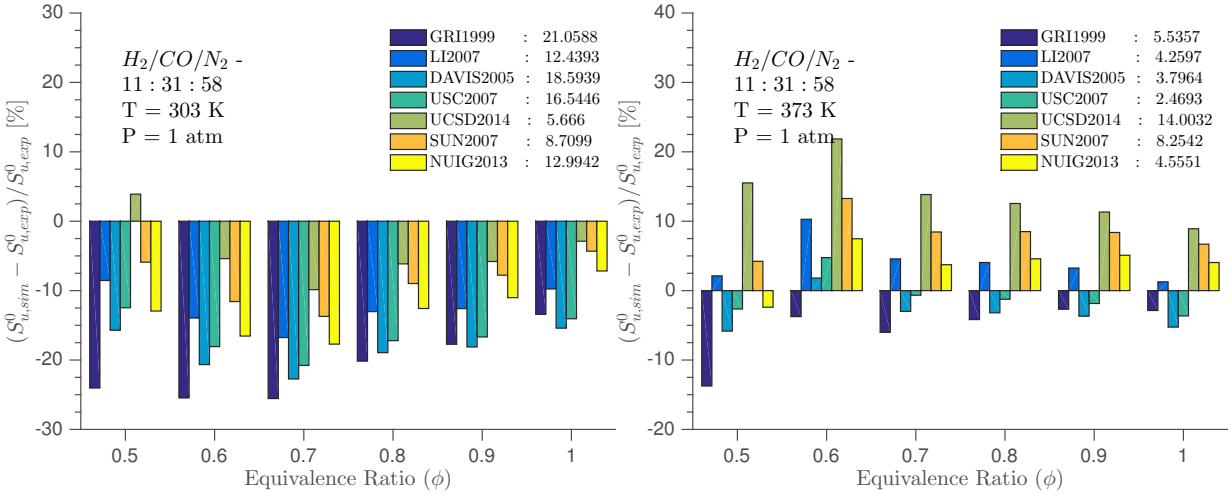

(a) $H_2/CO/N_2$ = 11:31:58, T = 303 K, P = 1 atm

(b) $H_2/CO/N_2$ = 11:31:58, T = 303 K, P = 1 atm

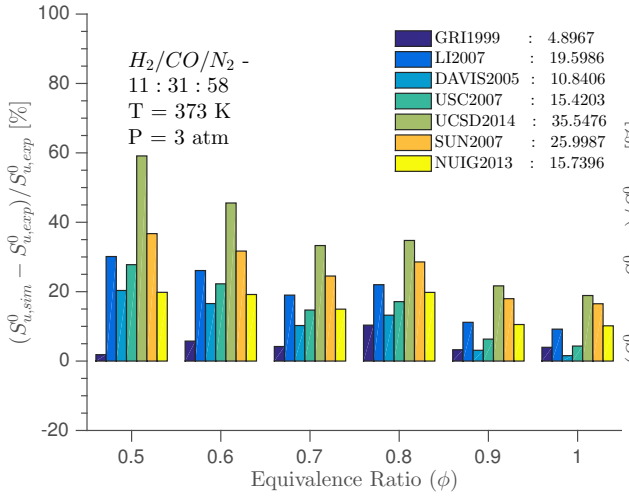

(c) $H_2/CO/N_2$ = 11:31:58, T = 373 K, P = 3 atm

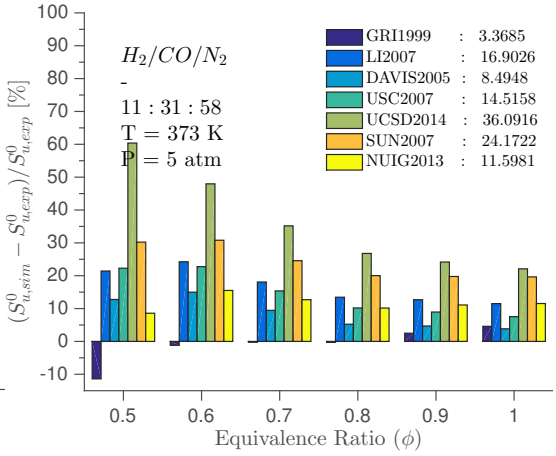

(d) $H_2/CO/N_2$ = 11:31:58, T = 373 K, P = 5 atm

Figure A.10: The relative error between the simulated and measured laminar flame speed for $H_2/CO/N_2$ mixtures, as shown in Fig. 3.9. The values next to the mechanism name represent the average relative error for the experimental condition shown in the sub-caption.

A.1.5 Mixture Combination: $H_2/CO/CH_4$

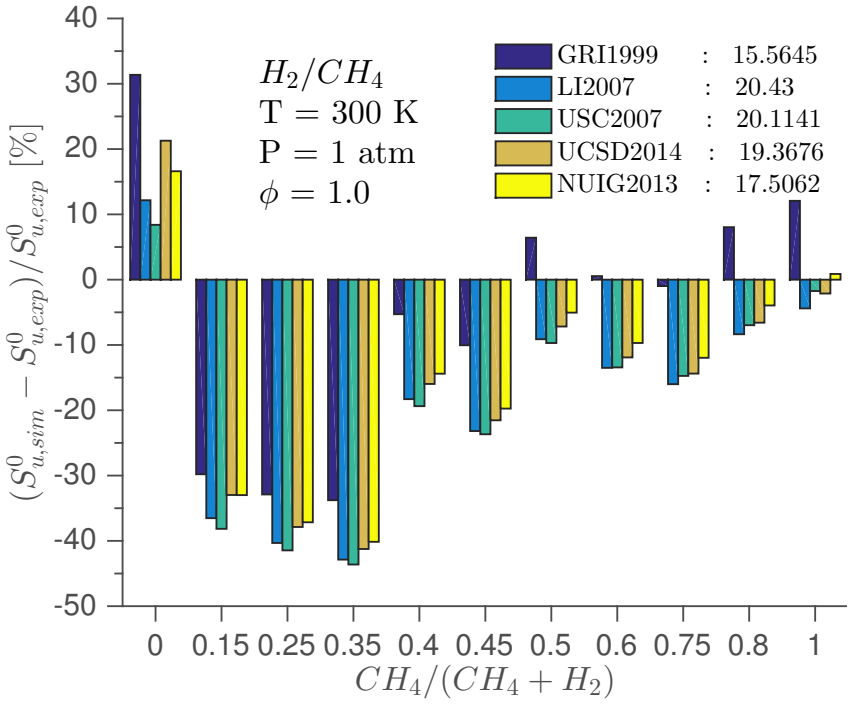

(a) H_2/CH_4, T = 300 K, P = 1 atm, ϕ = 1.0

Figure A.11: The relative error between the simulated and measured laminar flame speed for H_2/CH_4 mixtures, as shown in Fig. 3.10. The values next to the mechanism name represent the average relative error for the experimental condition shown in the sub-caption.

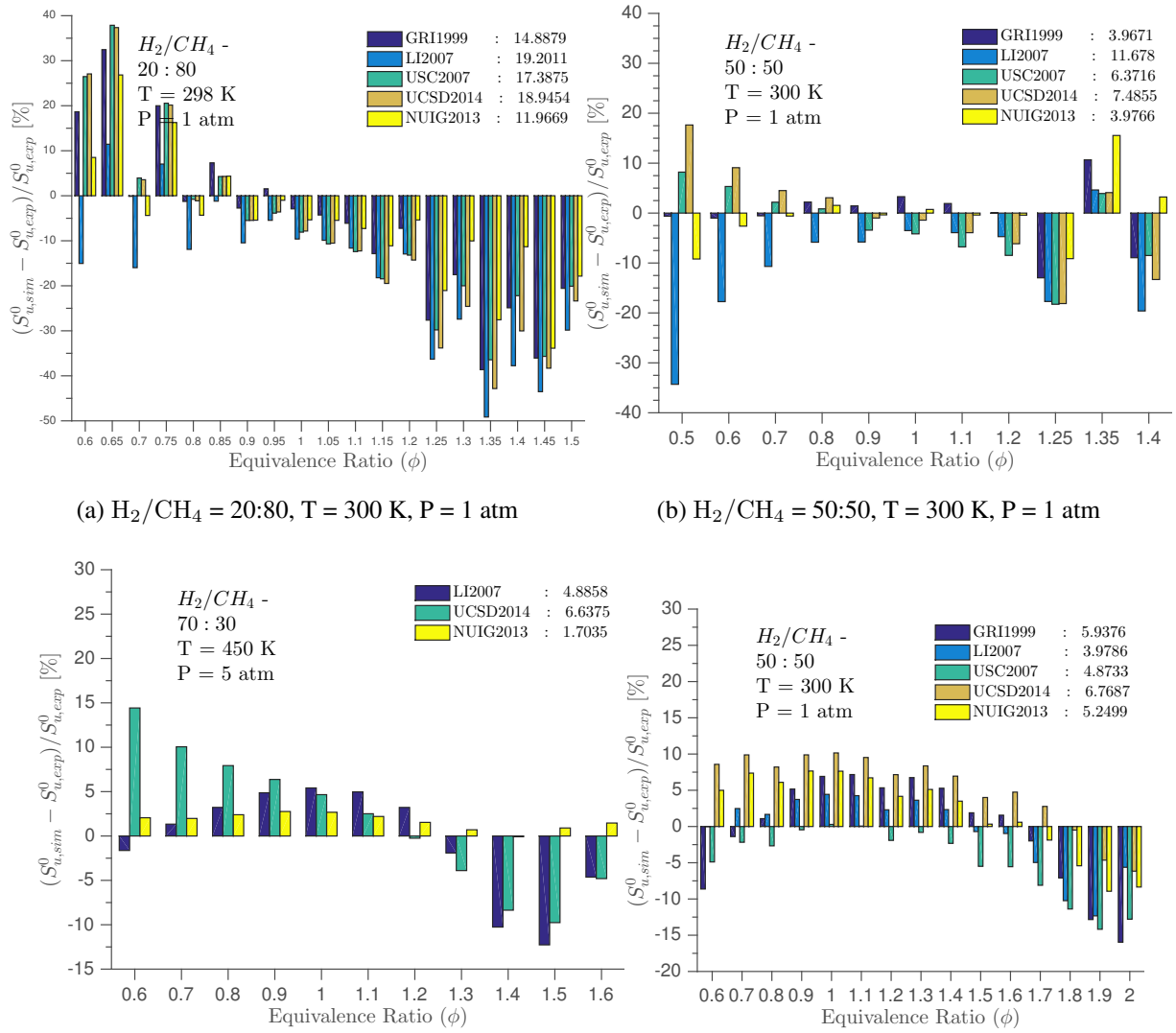

(a) H_2/CH_4 = 20:80, T = 300 K, P = 1 atm

(b) H_2/CH_4 = 50:50, T = 300 K, P = 1 atm

(c) H_2/CH_4 = 70:30, T = 450 K, P = 5 atm

(d) H_2/CH_4 = 90:10, T = 450 K, P = 1 atm

Figure A.12: The relative error between the simulated and measured laminar flame speed for H_2/CH_4 mixtures, as shown in Fig. 3.11. The values next to the mechanism name represent the average relative error for the experimental condition shown in the sub-caption.

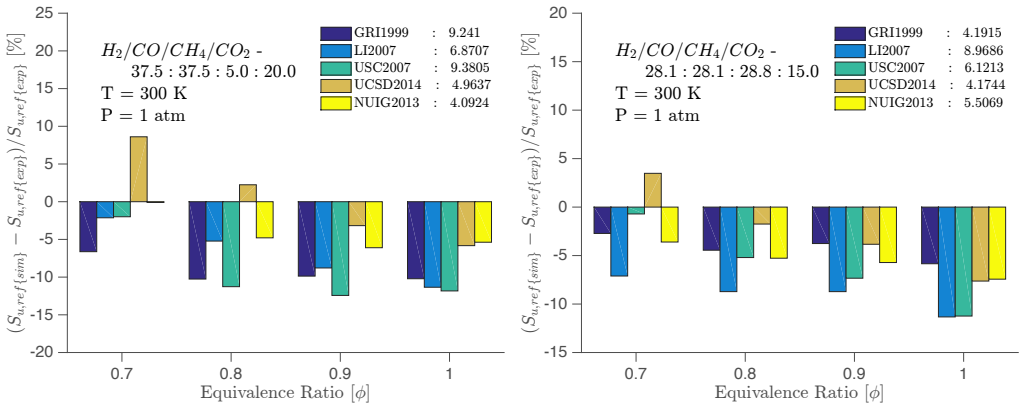

(a) $H_2/CO/CH_4/CO_2$ = 37.5:37.5:5:20 (b) $H_2/CO/CH_4/CO_2$ = 28.1:28.1:28.8:15

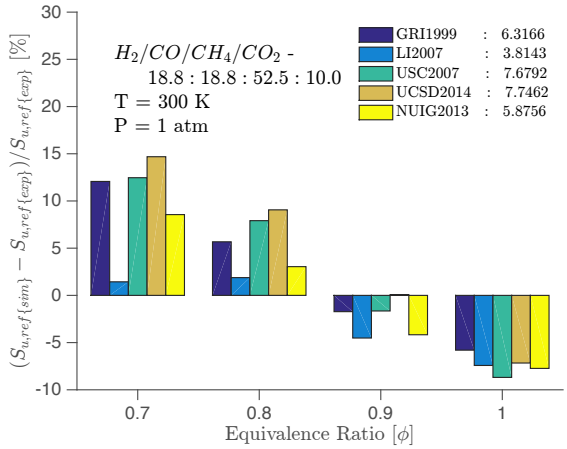

(c) $H_2/CO/CH_4/CO_2$ = 18.8:18.8:52.5:10

Figure A.13: The relative error between the simulated and measured reference flame speed ($S_{u,ref}$) for $H_2/CO/CH_4/CO_2$ mixtures with air, as shown in Fig. 3.12. The values next to the mechanism name represent the average relative error for the experimental condition shown in the sub-caption.

A.2 Relative error values – Ignition delay time

A.2.1 Mixture Combination: H_2/CO

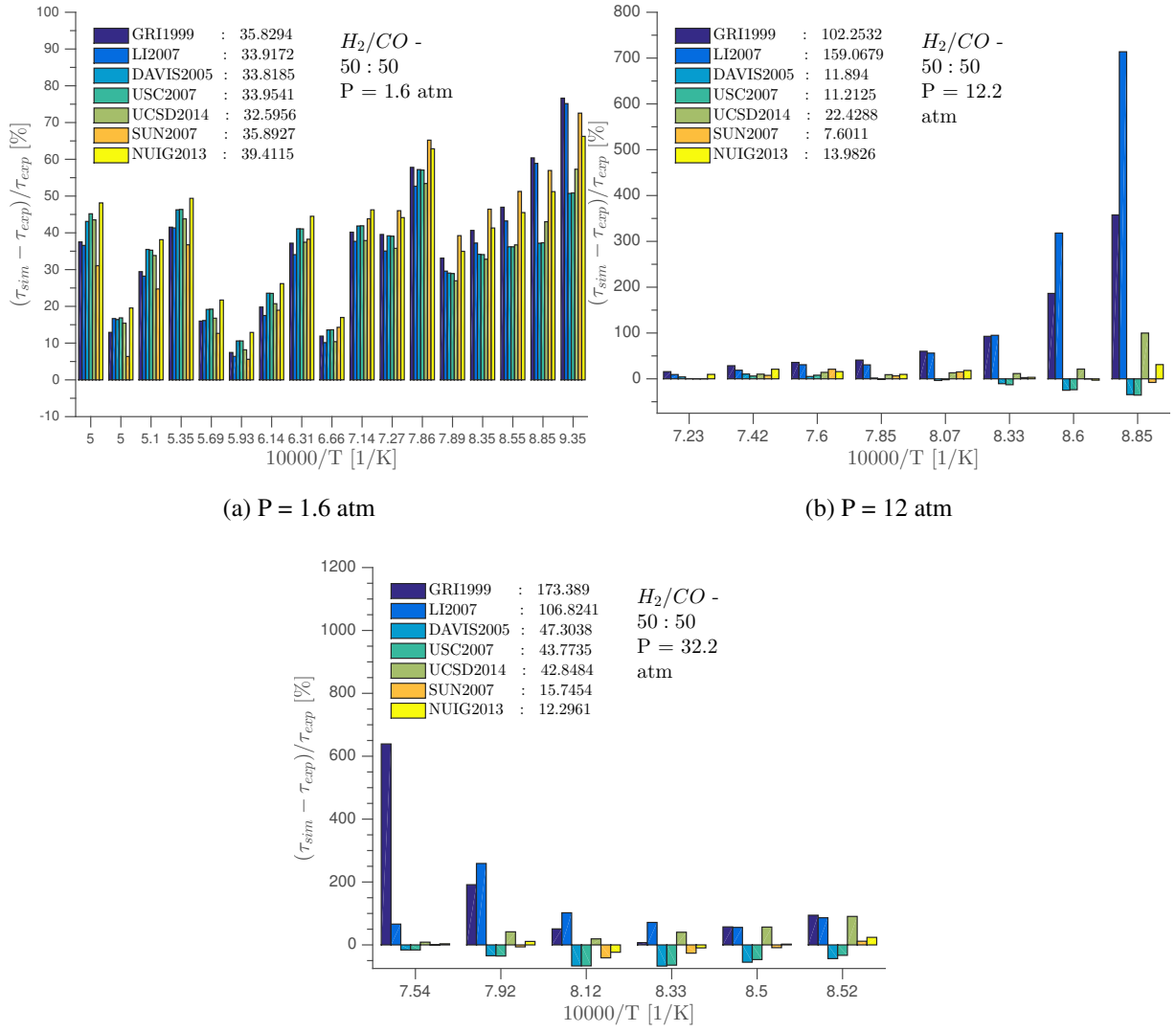

(a) P = 1.6 atm

(b) P = 12 atm

(c) P = 32 atm

Figure A.14: The relative error between the simulated and measured ignition delay time for H_2/CO - 50:50 mixture, as shown in Fig. 3.14. The values next to the mechanism name represent the average relative error for the experimental condition shown in the sub-caption.

A.2.2 Mixture Combination: $H_2/CO/H_2O$

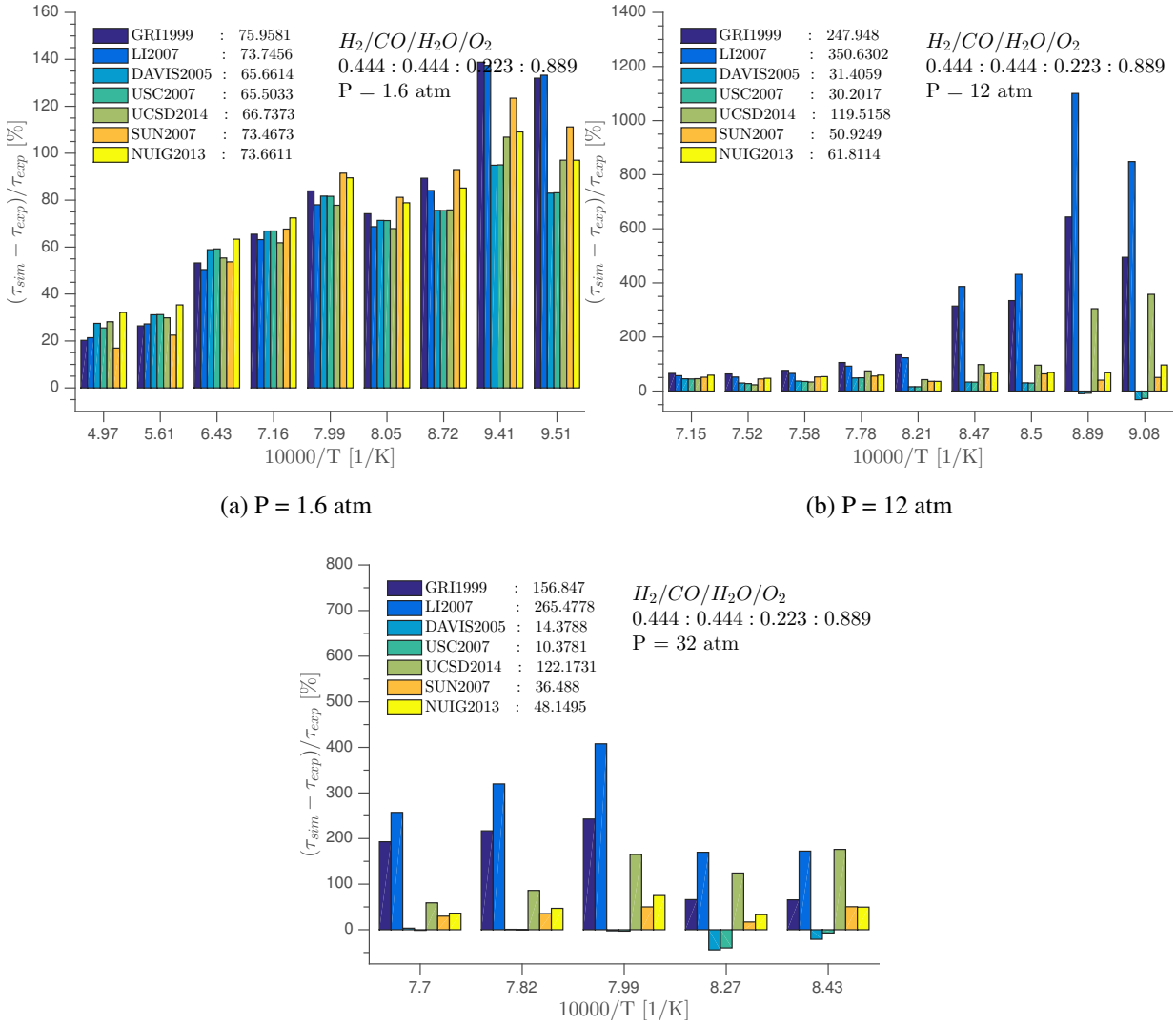

(a) P = 1.6 atm

(b) P = 12 atm

(c) P = 32 atm

Figure A.15: The relative error between the simulated and measured ignition delay time for $H_2/CO/H_2O/O_2$ - 0.444:0.444:0.223:0.889 mixture, as shown in Fig. 3.15. The values next to the mechanism name represent the average relative error for the experimental condition shown in the sub-caption.

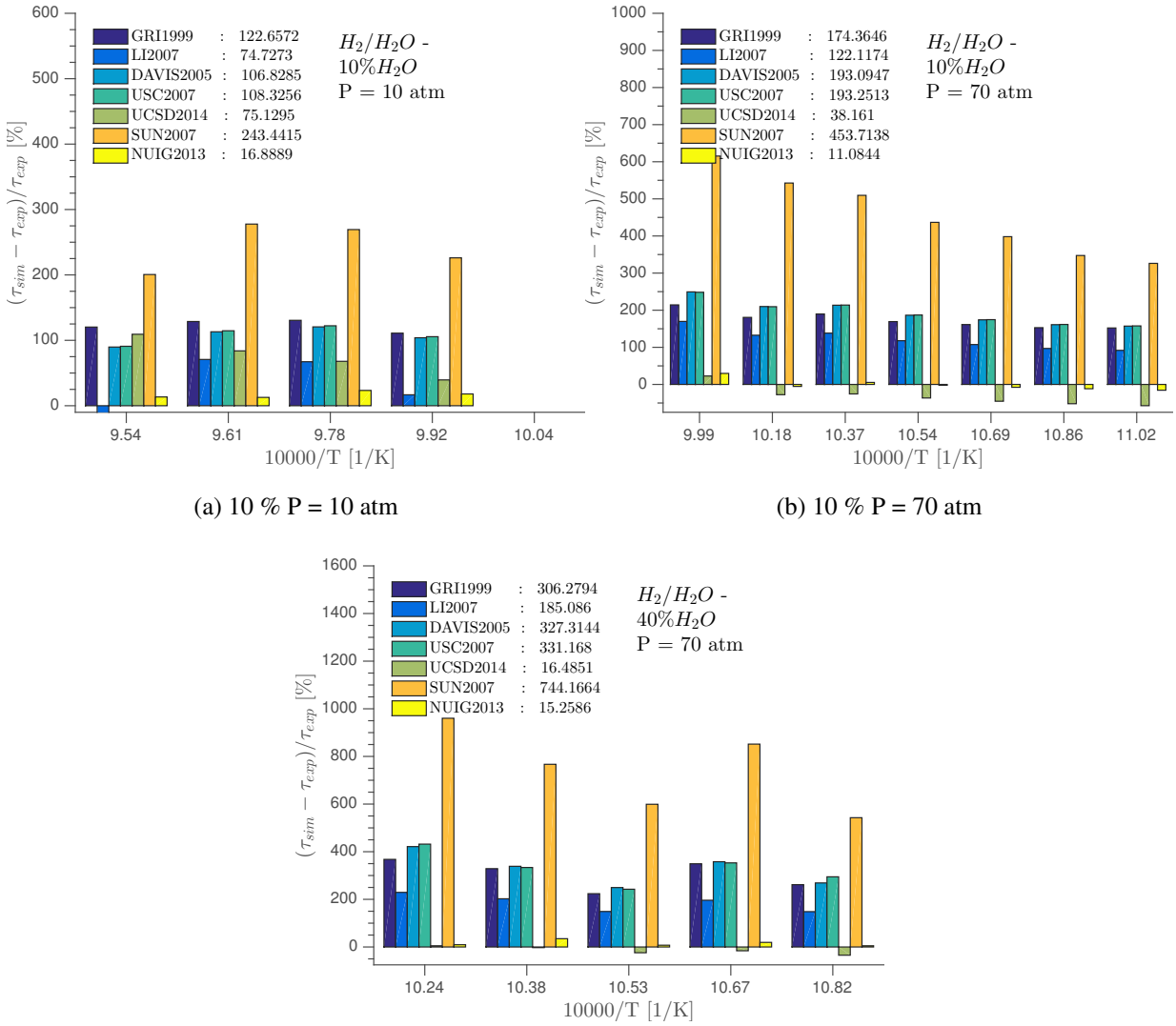

(a) 10 % P = 10 atm

(b) 10 % P = 70 atm

(c) 40 % P = 10 atm

Figure A.16: The relative error between the simulated and measured ignition delay time for H_2/H_2O mixture, as shown in Fig. 3.16. The values next to the mechanism name represent the average relative error for the experimental condition shown in the sub-caption.

A.2.3 Mixture Combination: $H_2/CO/CO_2$

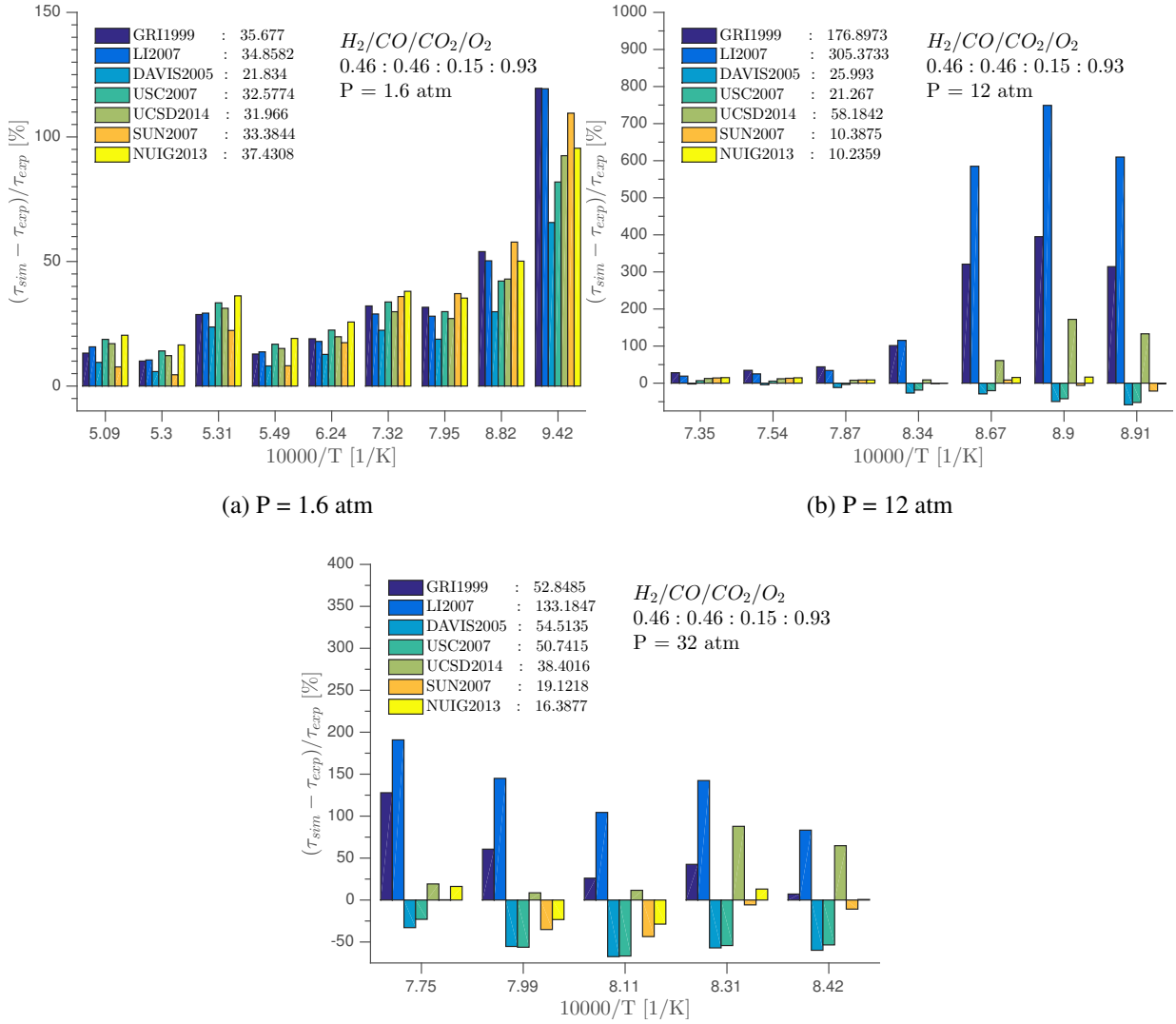

(a) P = 1.6 atm

(b) P = 12 atm

(c) P = 32 atm

Figure A.17: The relative error between the simulated and measured ignition delay time for $H_2/CO/CO_2/O_2$ - 0.46:0.46:0.15:0.93 mixture, as shown in Fig. 3.17. The values next to the mechanism name represent the average relative error for the experimental condition shown in the sub-caption.

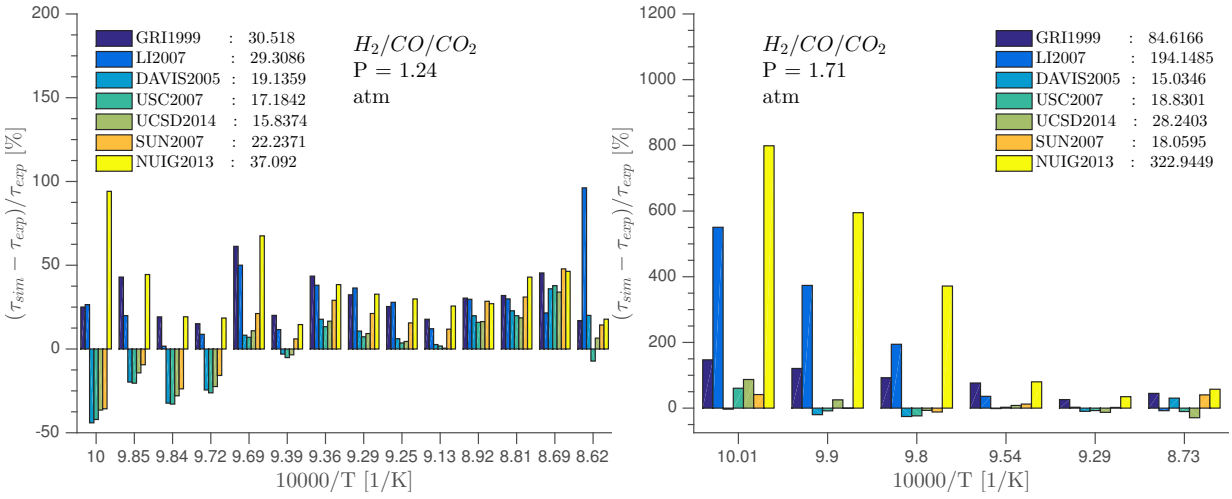

(a) P = 1.24 atm

(b) P = 1.71 atm

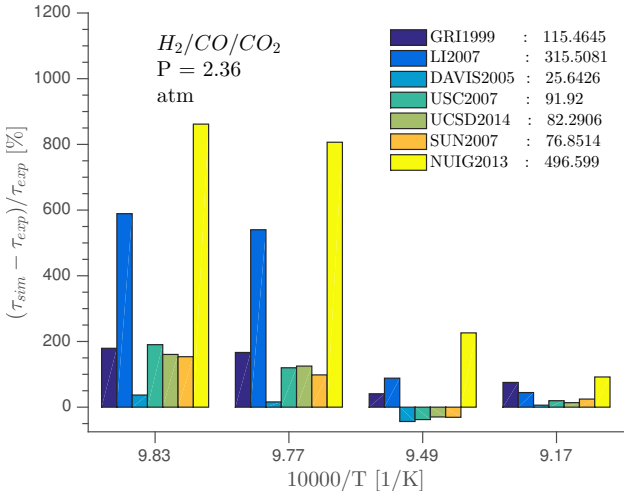

(c) P = 2.36 atm

Figure A.18: The relative error between the simulated and measured ignition delay time for $H_2/CO/CO_2$ mixture, as shown in Fig. 3.18. The values next to the mechanism name represent the average relative error for the experimental condition shown in the sub-caption.

A.2.4 Mixture Combination: $H_2/CO/CH_4$

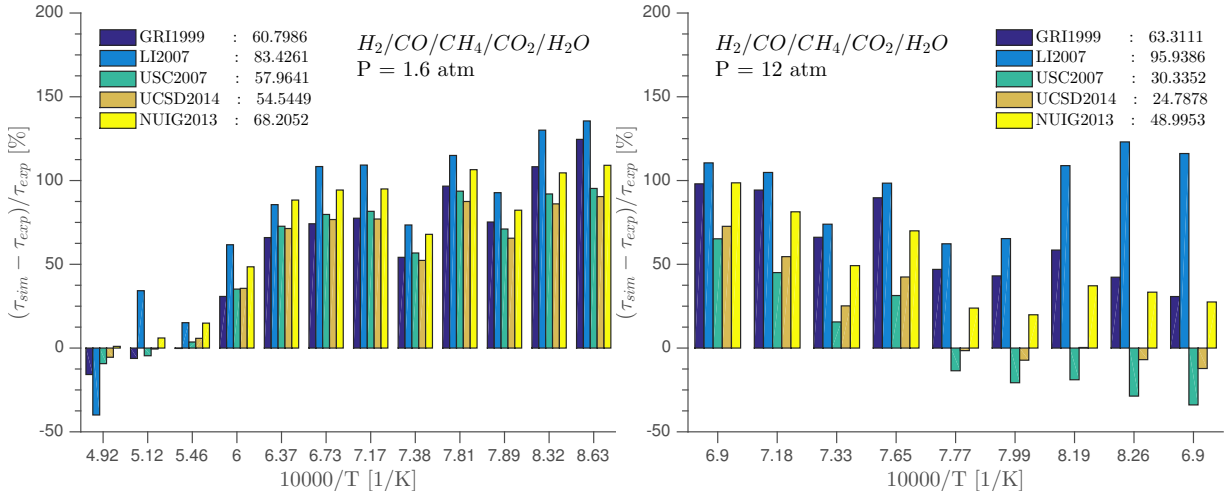

(a) P = 1.6 atm

(b) P = 12 atm

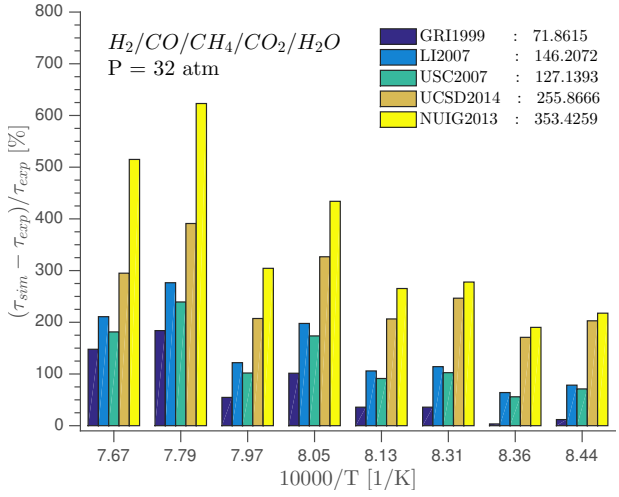

(c) P = 32 atm

Figure A.19: The relative error between the simulated and measured ignition delay time for $H_2/CO/CO_2/CH_4/H_2O$ mixture, as shown in Fig. 3.19. The values next to the mechanism name represent the average relative error for the experimental condition shown in the sub-caption.

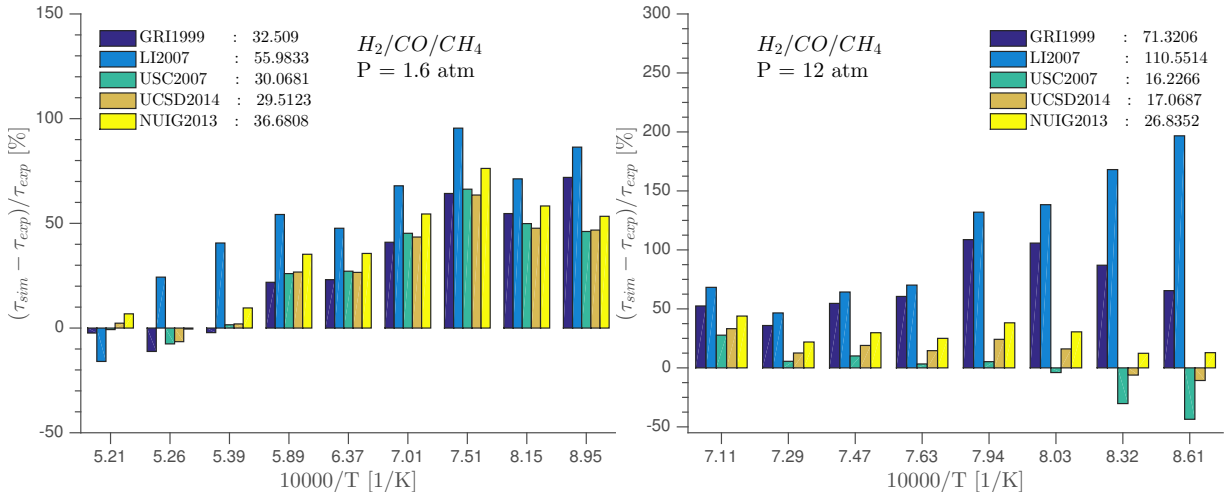

(a) P = 1.6 atm

(b) P = 12 atm

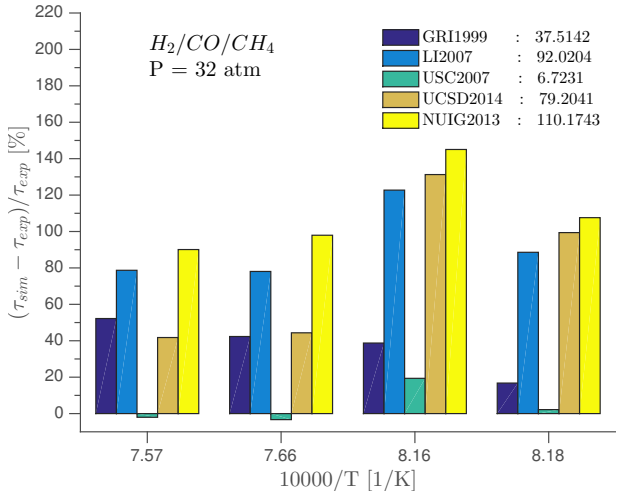

(c) P = 32 atm

Figure A.20: The relative error between the simulated and measured ignition delay time for $H_2/CO/CH_4$ mixture, as shown in Fig. 3.20. The values next to the mechanism name represent the average relative error for the experimental condition shown in the sub-caption.

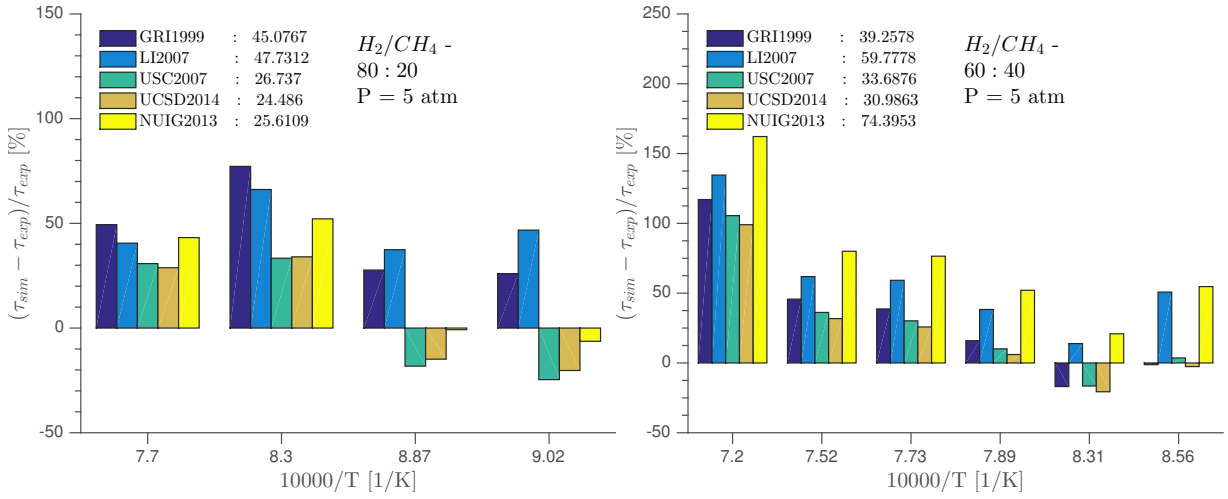

(a) H_2/CH_4 = 80:20, P = 5 atm

(b) H_2/CH_4 = 60:40, P = 5 atm

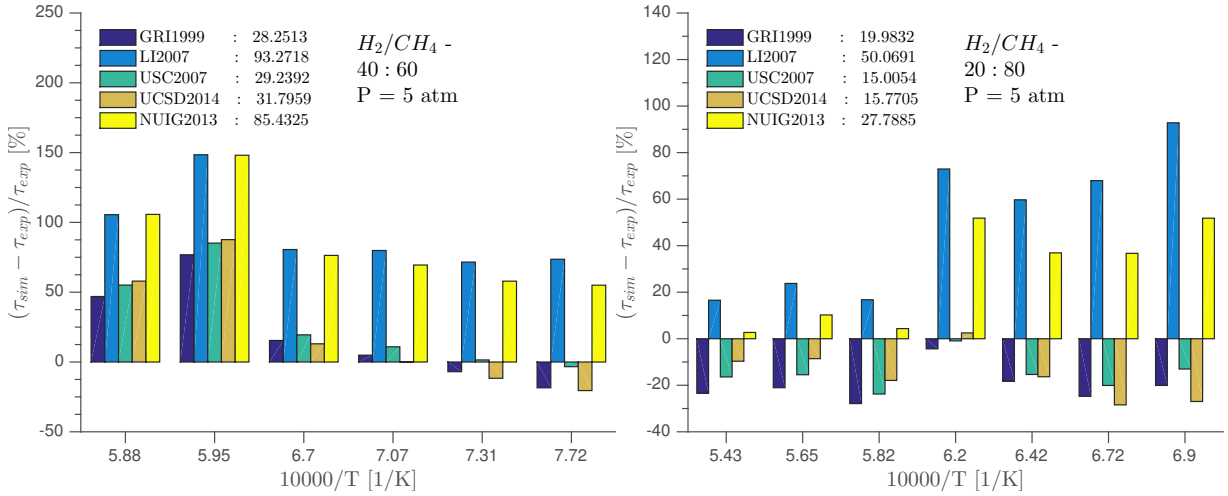

(c) H_2/CH_4 = 40:60, P = 5 atm

(d) H_2/CH_4 = 20:80, P = 5 atm

Figure A.21: The relative error between the simulated and measured ignition delay time for H_2/CH_4 mixtures, as shown in Fig. 3.21(a) and 3.21(b). The values next to the mechanism name represent the average relative error for the experimental condition shown in the sub-caption.

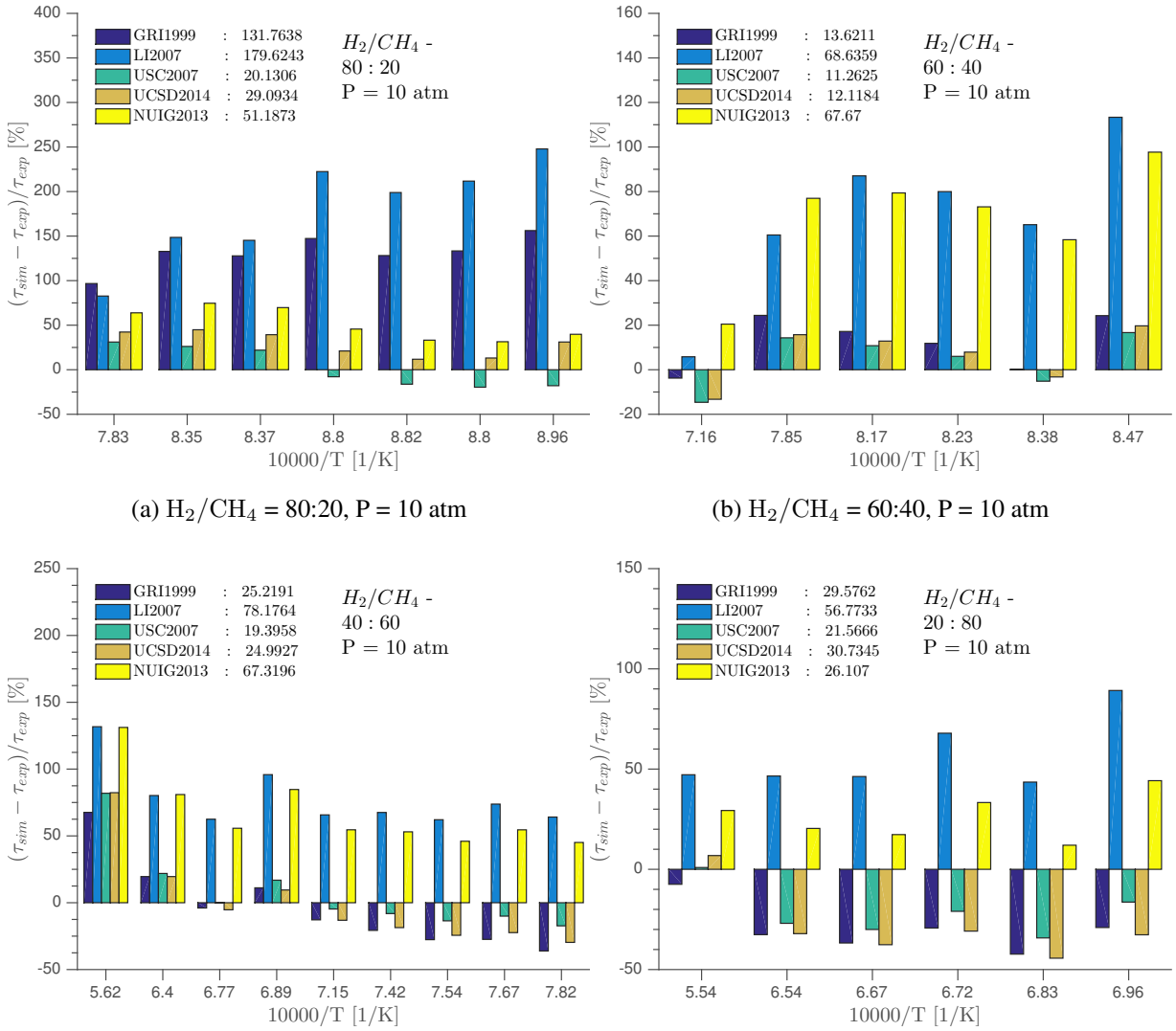

(a) H_2/CH_4 = 80:20, P = 10 atm

(b) H_2/CH_4 = 60:40, P = 10 atm

(c) H_2/CH_4 = 40:60, P = 10 atm

(d) H_2/CH_4 = 20:80, P = 10 atm

Figure A.22: The relative error between the simulated and measured ignition delay time for H_2/CH_4 mixtures, as shown in Fig. 3.21(c) and 3.21(d). The values next to the mechanism name represent the average relative error for the experimental condition shown in the sub-caption.

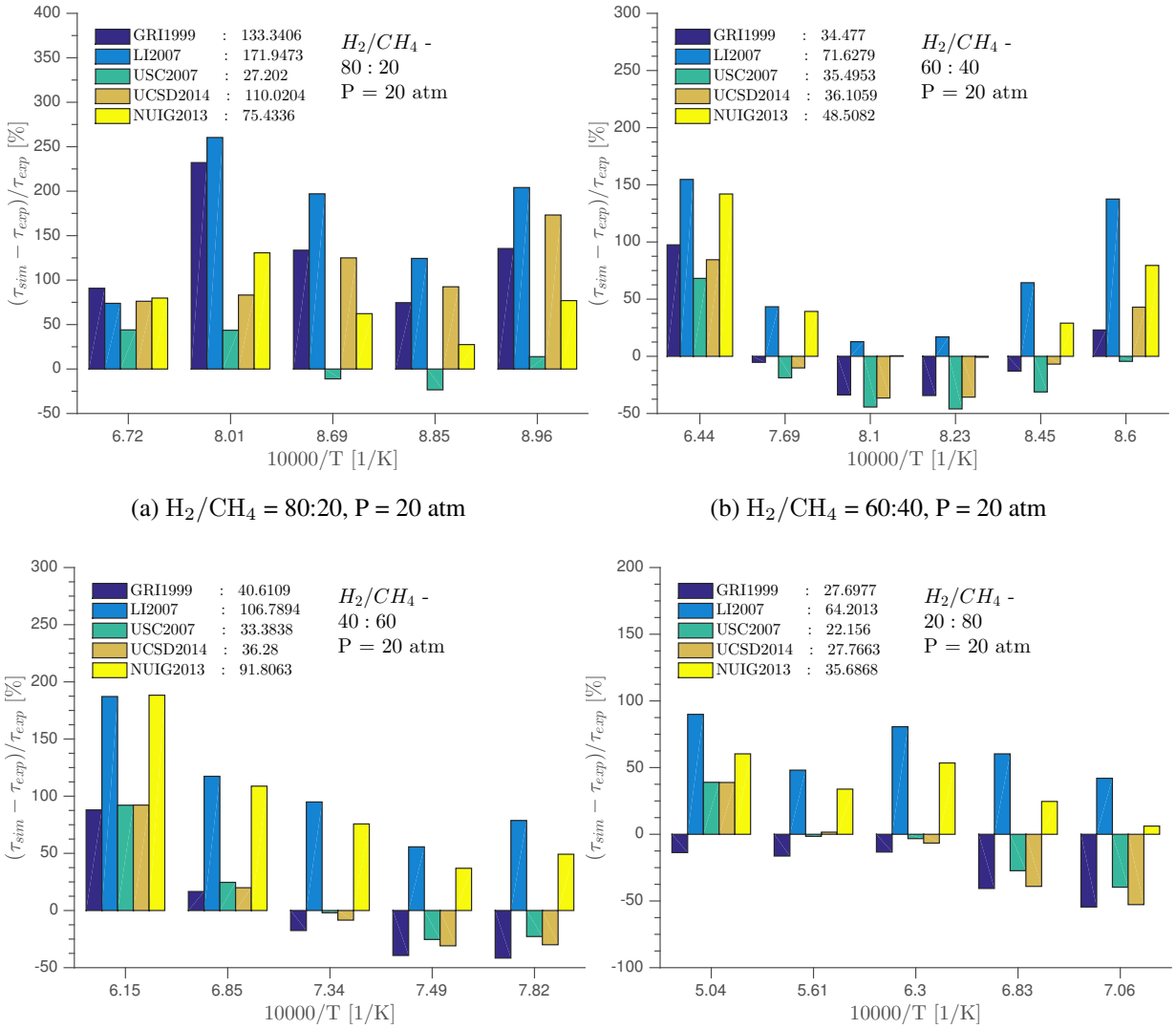

(a) H_2/CH_4 = 80:20, P = 20 atm

(b) H_2/CH_4 = 60:40, P = 20 atm

(c) H_2/CH_4 = 40:60, P = 20 atm

(d) H_2/CH_4 = 20:80, P = 20 atm

Figure A.23: The relative error between the simulated and measured ignition delay time for H_2/CH_4 mixtures, as shown in Fig. 3.21(e) and 3.21(f). The values next to the mechanism name represent the average relative error for the experimental condition shown in the sub-caption.

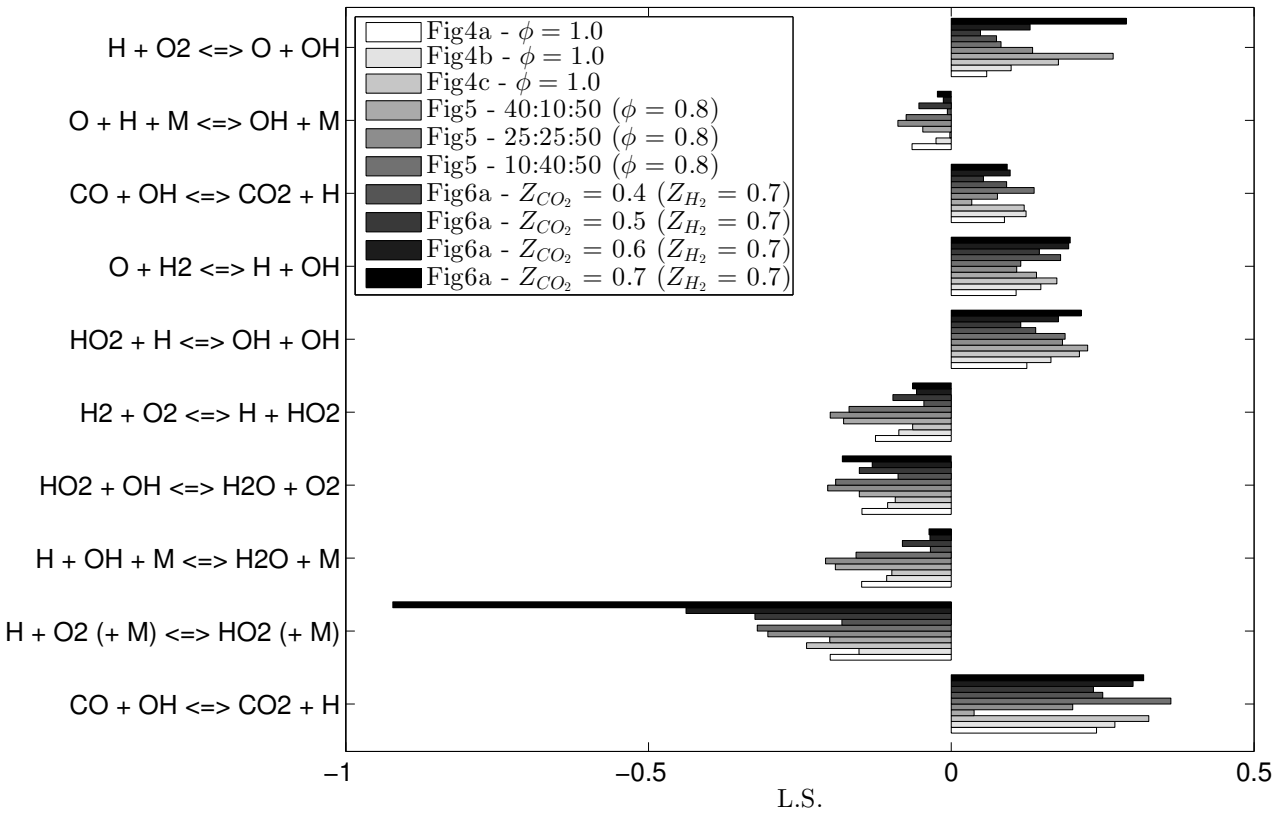

Figure A.24: Logarithmic sensitivity analysis on the laminar flame speed of syngas mixtures diluted with CO_2 at experimental conditions shown in Fig. 3.4, 3.5, and 3.6 for NUIG2013 mechanism. Only the ten most sensitive reactions are included, for clarity.

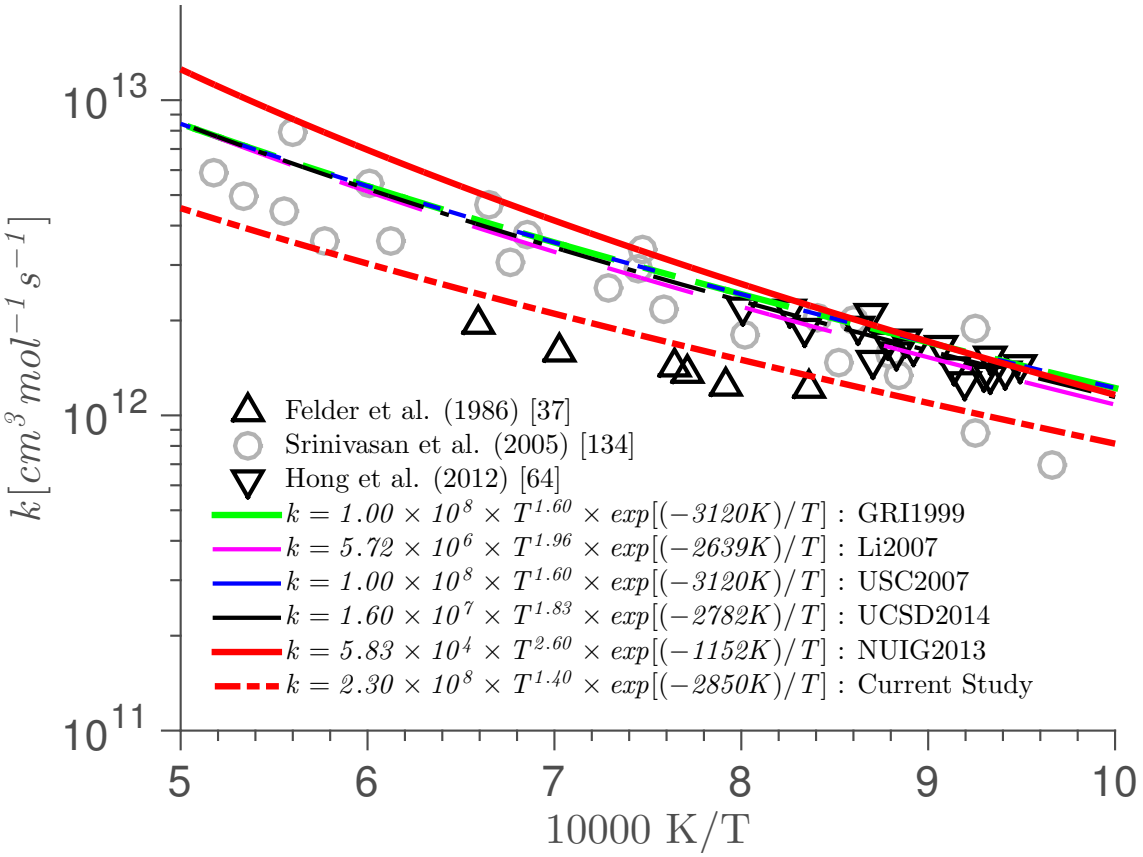

Figure A.25: The rate constants of reaction $CH_4 + OH = CH_3 + H_2O$ at T = 1000 2000 K. Lines show the rate constant of $CH_4 + OH = CH_3 + H_2O$ incorporated in the kinetics mechanisms investigated in this study and the red dotted line represents the newly fitted rate constant expression. Symbols represent data taken from [1, 2, 3]

A.3 Sensitivity Analysis

A.4 Rate constant expressions and sensitivity analysis

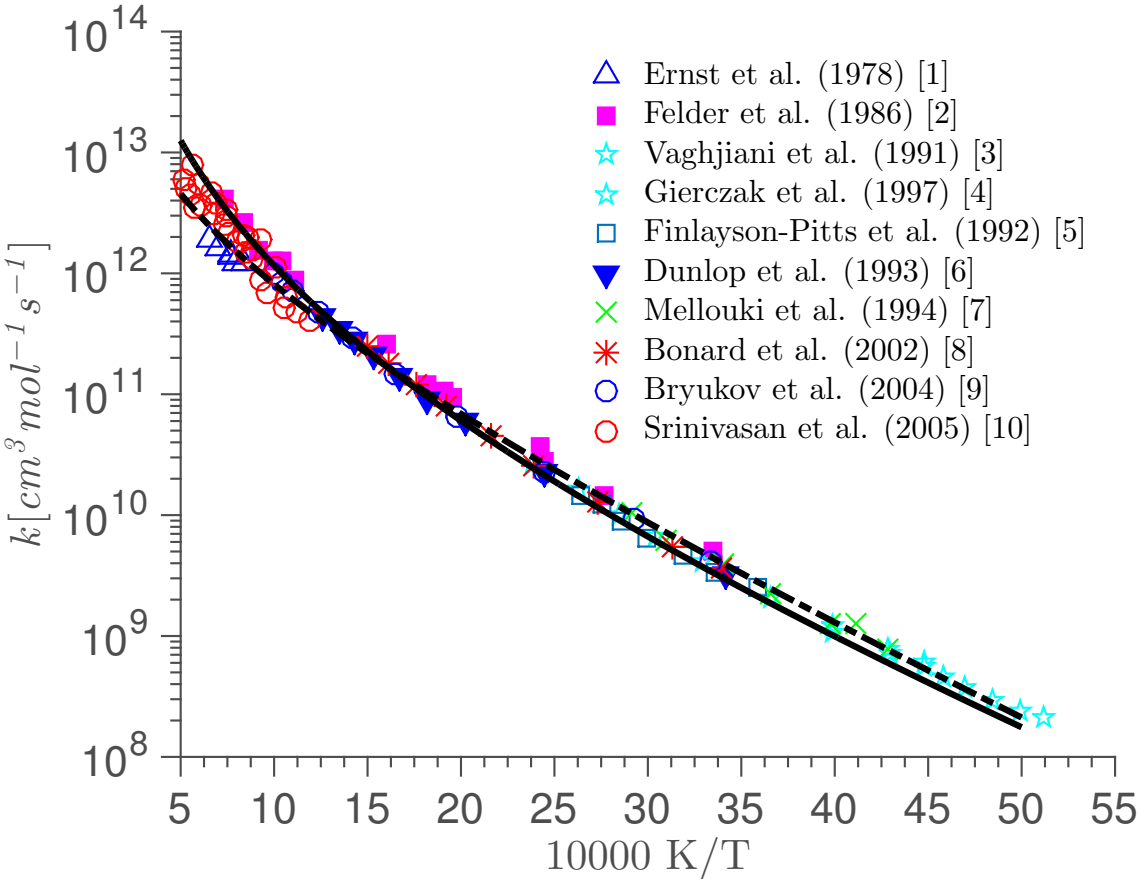

Figure A.26: The rate constants of reaction $CH_4 + OH = CH_3 + H_2O$ at T = 200 2000 K. Solid line represents $k = 5.83 \times 10^4 \times T^{2.60} \times exp[(-1152K)/T]$ from NUIG2013; dashed line represents $k = 2.30 \times 10^8 \times T^{1.40} \times exp[(-2850K)/T]$ from Current Study. Symbols represent data taken from [4, 1, 5, 6, 7, 8, 9, 10, 11, 2]

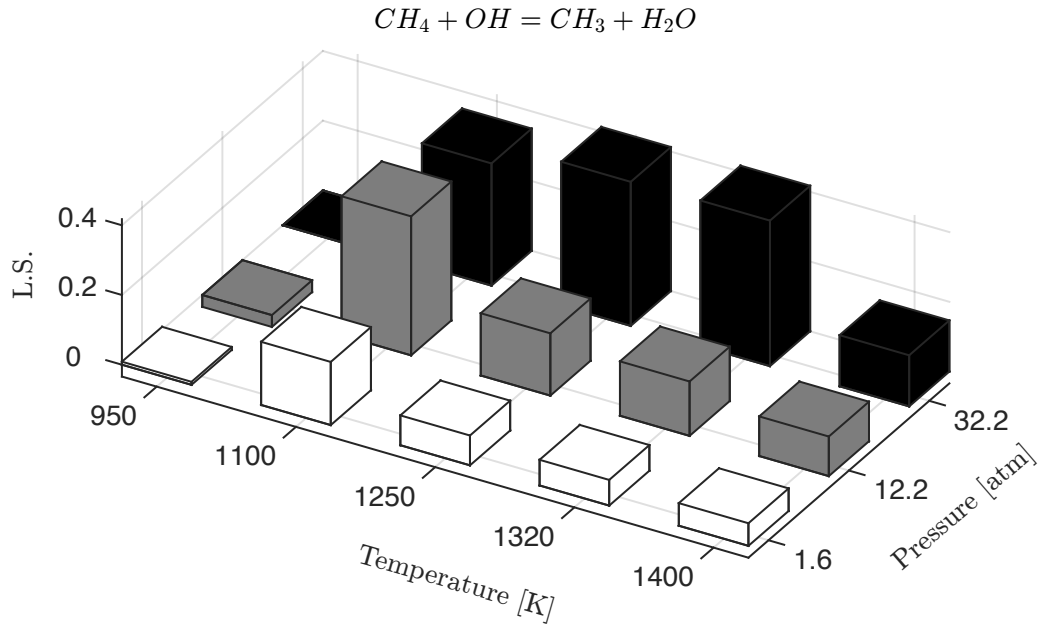

(a) Mixture: $H_2/CO/CO_2/CH_4/H_2O/O_2/Ar$

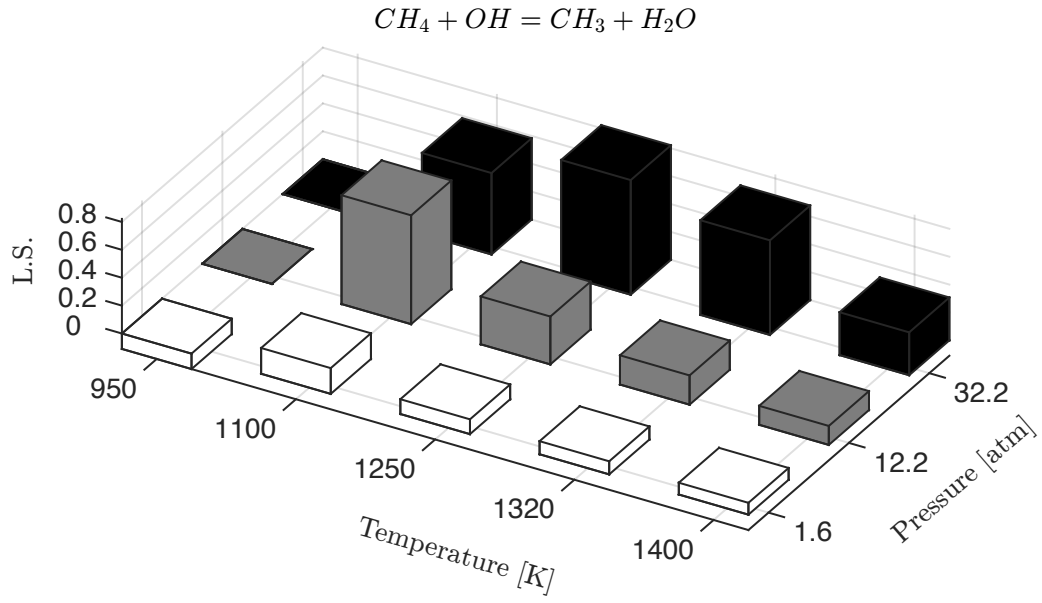

(b) Mixture: $H_2/CO/CH_4$

Figure A.27: Sensitivity analysis for $CH_4 + OH = CH_3 + H_2O$ reaction at several different pressures and temperatures.

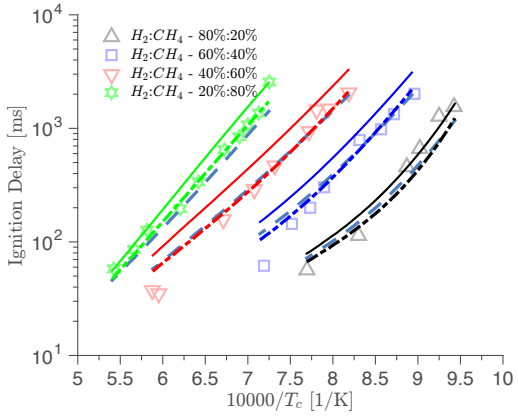

(a) P = 5 atm

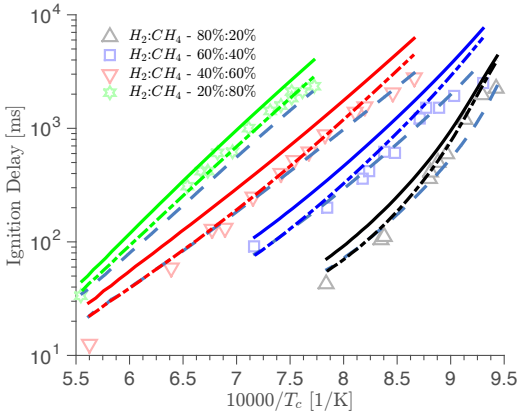

(b) P = 10 atm

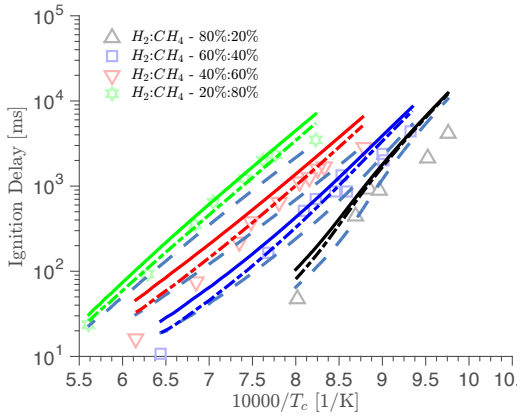

(c) P = 20 atm

Figure A.28: Comparisons of measured and predicted ignition delay time of H_2/CH_4 mixtures computed using NUIG_V3 mechanism. Symbols represent experimental data; please refer to Fig. 3.21 in manuscript for more information. Solid-line: NUIG2013 mechanism; dash-line: USC2007; dash-dot-line: NUIG_V3.

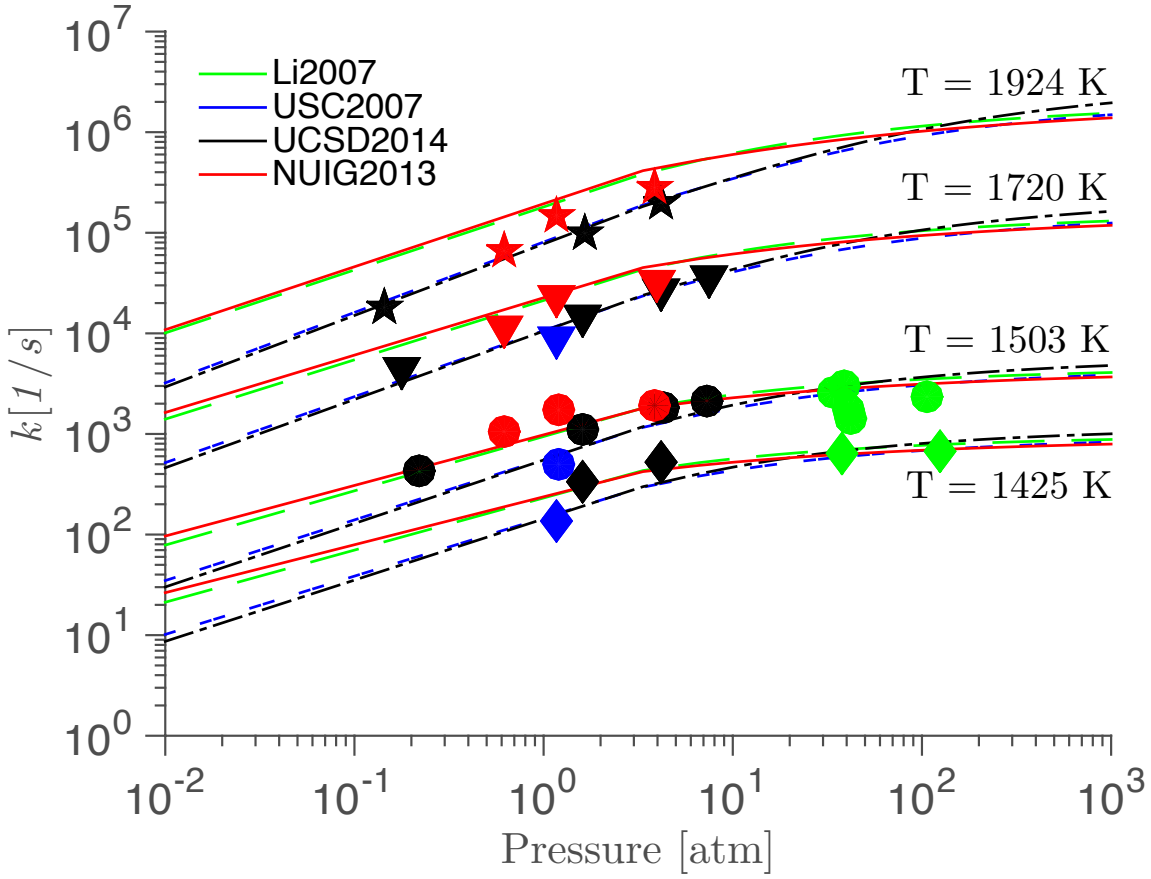

Figure A.29: The rate constants of reaction $C_2H_6 = CH_3 + CH_3$. Symbol patterns represent the temperatures and colors of the symbol represent where the experimental data were obtained. Blue colored symbols, Du et al. [12]; green colored symbols, Hwang et al. [13]; red colored symbols, Davison et al. [14]; black colored symbols, Oehlschlaeger et al. [15]. (◊) : T = 1425 K; (O): T = 1503; (▽): T = 1720 K; (★): T = 1924 K. The lines denote the rate constant of $C_2H_6 = CH_3 + CH_3$ incorporated in the kinetics mechanisms investigated in this study.

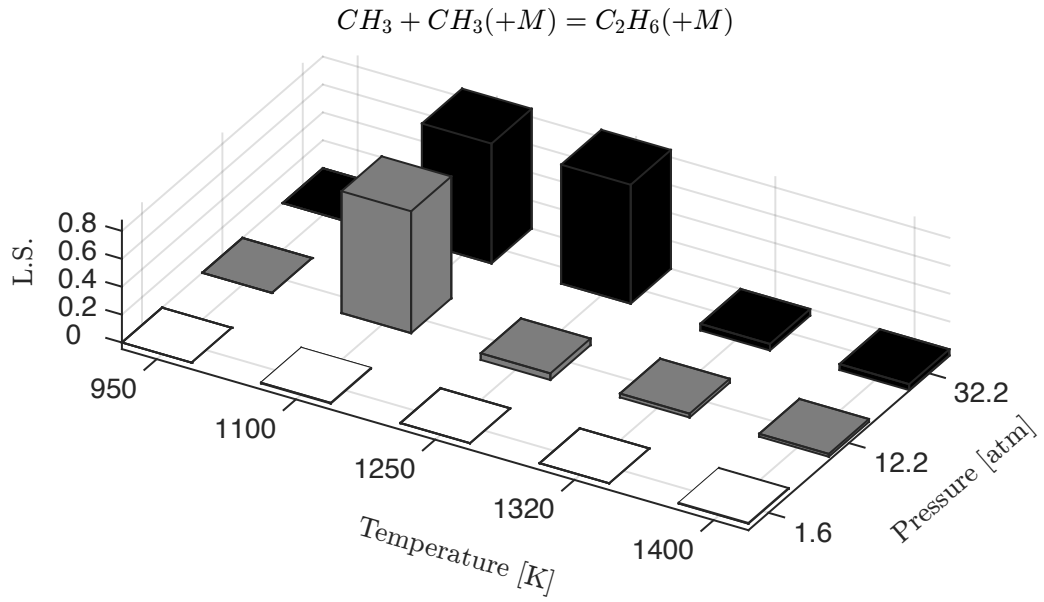

(a) Mixture: $H_2/CO/CO_2/CH_4/H_2O/O_2/Ar$

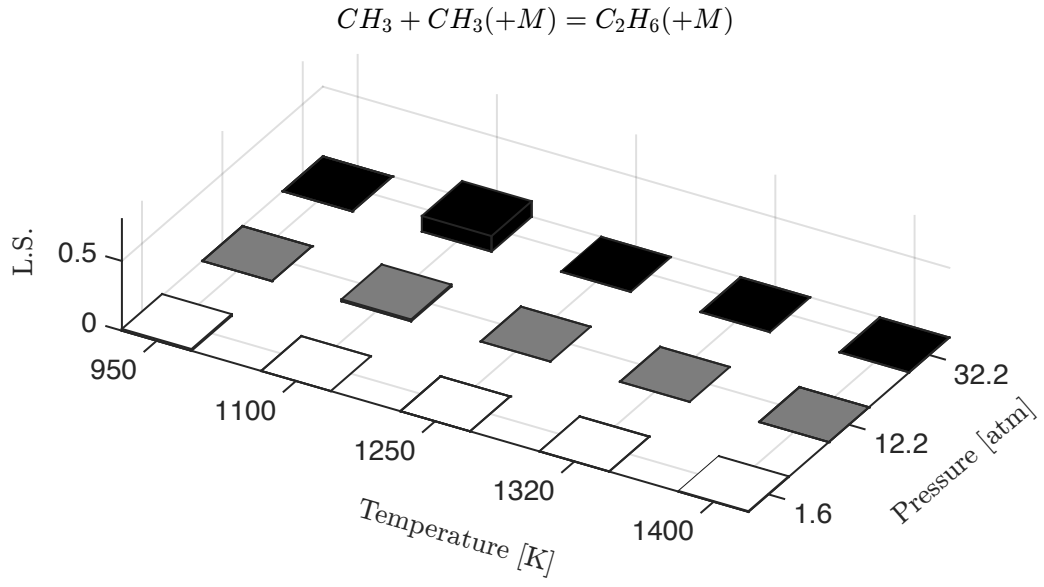

(b) Mixture: $H_2/CO/CH_4$

Figure A.30: Sensitivity analysis for $CH_3 + CH_3(+M) = C_2H_6(+M)$ reaction at several different pressures and temperatures.

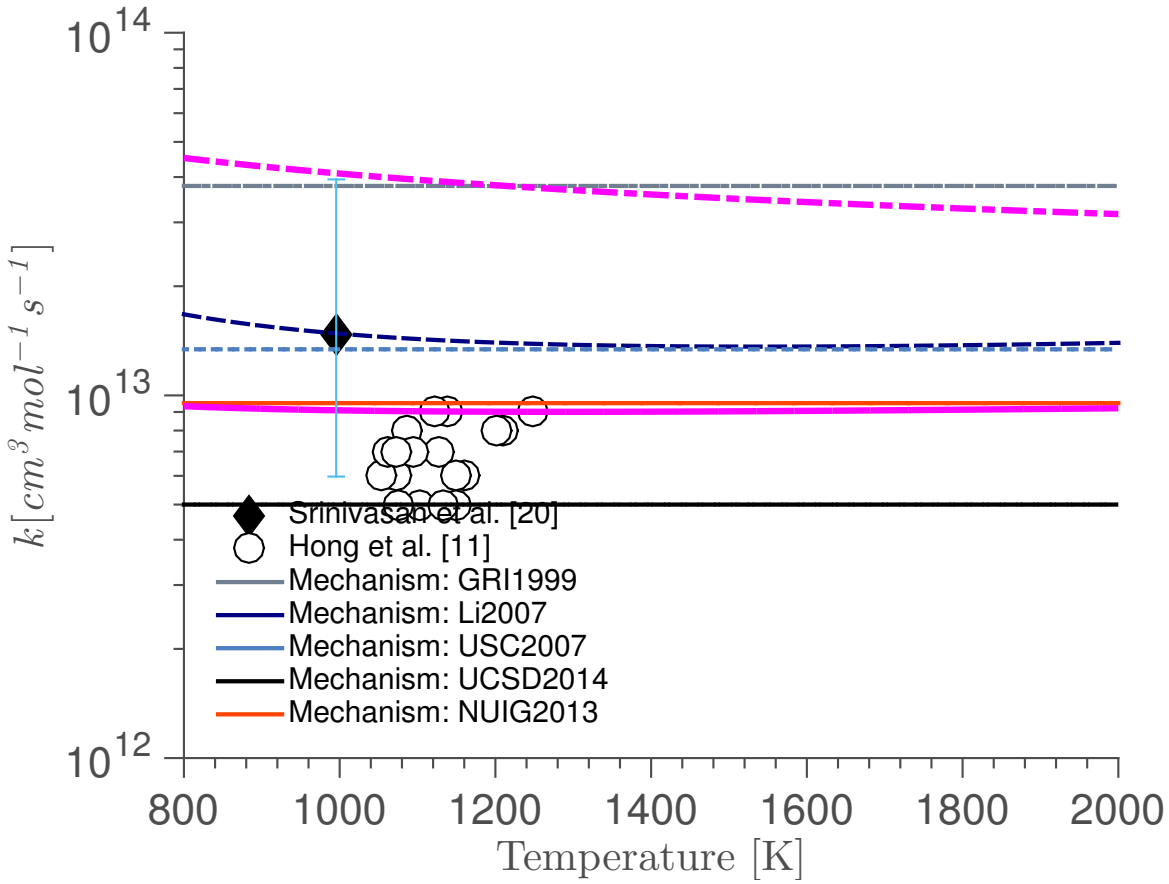

Figure A.31: The rate constants of reaction $CH_3 + HO_2 = CH_3O + OH$. The pink lines denote the rate constant determined from theoretical studies. Solid pink line, Jasper et al. [16]; dash pink line, Lin and Zhu [17]. The rate constant of $CH_3 + HO_2 = CH_3O + OH$ employed in NUIG2013 is identical to the rate constant proposed by Jasper et al. [16], which explains why the line is masked by the solid pink line.

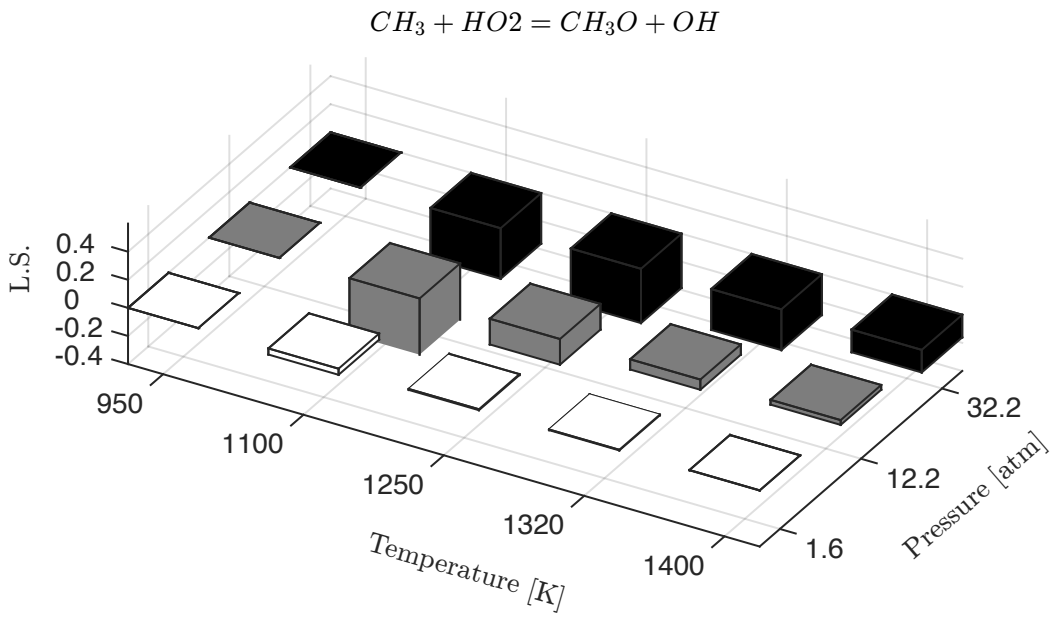

(a) Mixture: $H_2/CO/CO_2/CH_4/H_2O/O_2/Ar$

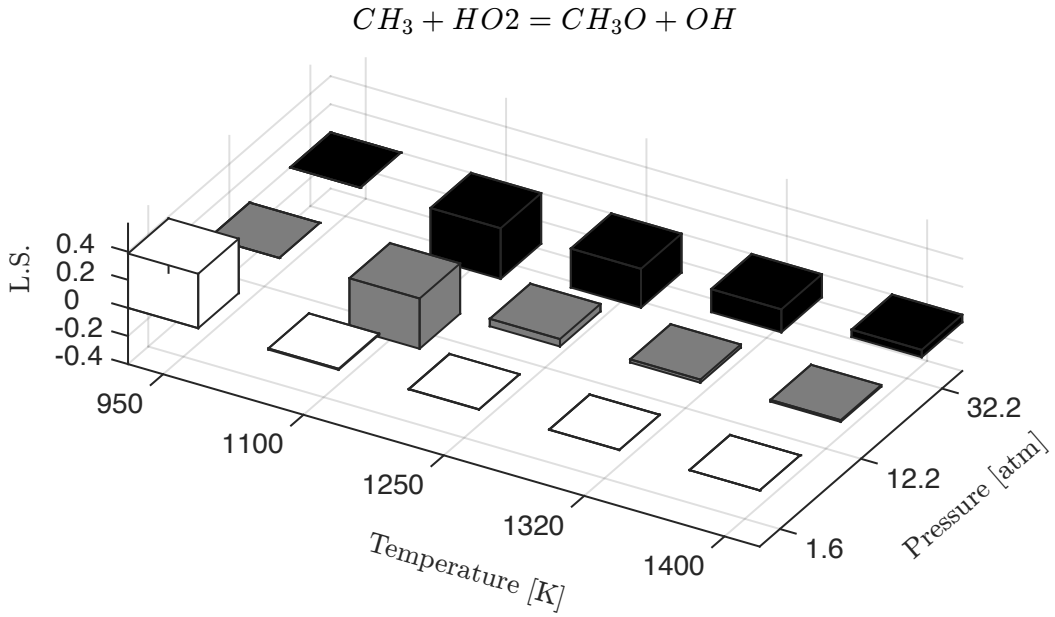

(b) Mixture: $H_2/CO/CH_4$

Figure A.32: Sensitivity analysis for $CH_3 + HO_2 = CH_3O + OH$ reaction at several different pressures and temperatures.

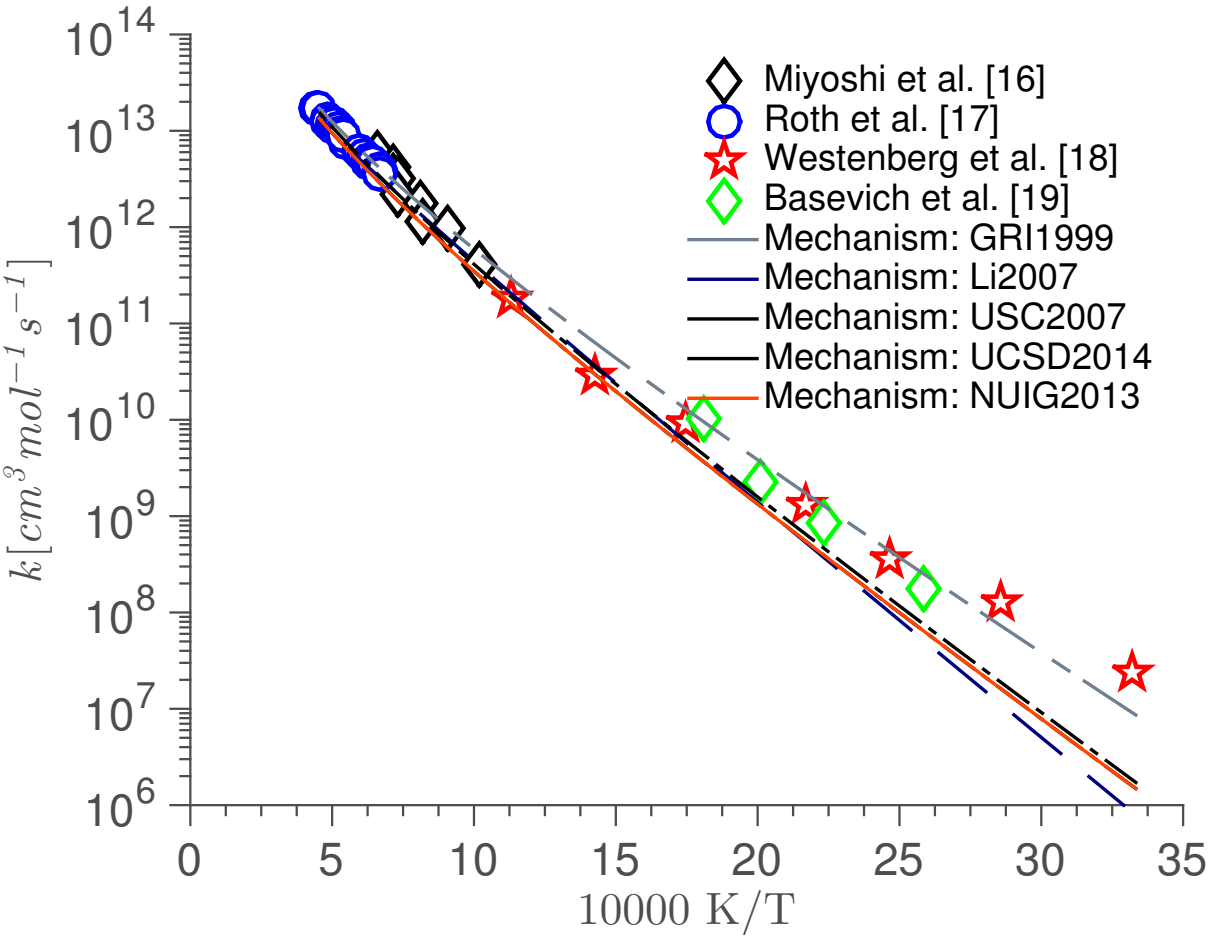

Figure A.33: The rate constants of reaction $CH_4 + O = CH_3 + OH$. The lines denote the rate constant of $CH_4 + O = CH_3 + OH$ incorporated in the kinetics mechanisms investigated in this study.

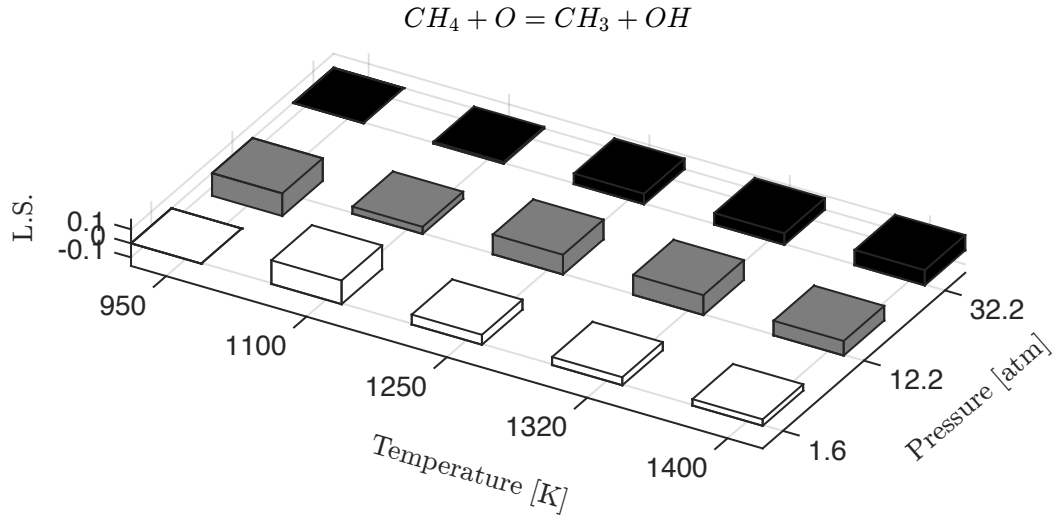

(a) Mixture: $H_2/CO/CO_2/CH_4/H_2O/O_2/Ar$

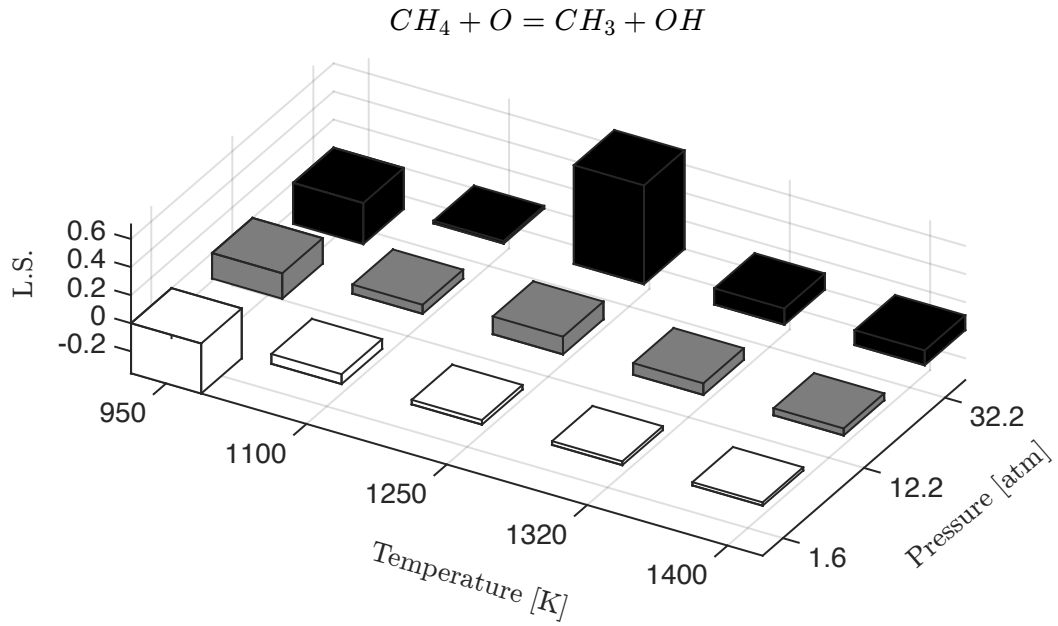

(b) Mixture: $H_2/CO/CH_4$

Figure A.34: Sensitivity analysis for $CH_4 + O = CH_3 + OH$ reaction at several different pressures and temperatures.

Appendix B

Supporting Materials for Chapter 4

Table B.1 tabulates the fuel mixtures and the experimental conditions used in this study and they are systematically organized with case number. Case numbers ranging from 1 to 30 are included in the search space to search for the reduced mechanism for biogas/syngas mixtures, and Case numbers ranging from 31 to 149 are used to validate the reduced mechanism. The relative error in each case is computed as the following: -

$$\bar{\mathrm{E}_{\mathrm{i}}} = \left| \frac{\mathrm{Y_{sim,ij}} - \mathrm{Y_{exp,ij}}}{\mathrm{Y_{exp,ij}}} \right| \times 100\%$$

where *i* represents the case number and *j* represents the data point in *i*th case. The maximum relative error $\mathrm{E_{i,max}}$ of each case is tabulated in Table B.1.

Figure B.1 - B.11 show the predicted ignition delay time of the 94 cases (Case 1 94) tabulated in Table 1 plotted against experimental data. The ignition delay time values were predicted by the reduced mechanism and the Aramco-1.3 mechanism. The fuel compositions and the experimental conditions can be found in Table A by looking up the case number.

Figure B.12 - B.19 show the predicted flame speed of the 55 cases (Case 95 149) tabulated in Table 1 plotted against experimental data. The flame speed values were predicted by the reduced mecha-

nism and the Aramco-1.3 mechanism. The fuel compositions and the experimental conditions can be found in Table A by looking up the case number.

Table B.1: Fuel matrix and experimental conditions used in this study for the validation of the reduced mechanism. The highest relative error (E_{max}) in each case is computed and tabulated.

Case	Fuel Mixture [mol %]											Experimental Conditions			E_{max}	Ref.
No.	H_2	CO	O_2	H_2O	CO_2	CH_4	C_2H_6	C_3H_8	N_2	Ar	He	T[K]	P [atm]	ϕ	[%]	
Ignition Delay Time																
1	0.500	0.500	1.000	-	-	-	-	-	-	98.000	-	990-2000	1.62	0.50	0.137	
2	0.500	0.500	1.000	-	-	-	-	-	-	98.000	-	1095-1385	11.90	0.50	0.212	
3	0.500	0.500	1.000	-	-	-	-	-	-	98.000	-	1170-1330	32.20	0.50	0.276	
4	0.440	0.440	0.890	0.230	-	-	-	-	-	98.000	-	995-2010	1.750	0.50	0.077	
5	0.440	0.440	0.890	0.230	-	-	-	-	-	98.000	-	1085-1400	12.20	0.50	0.224	[18]
6	0.440	0.440	0.890	0.230	-	-	-	-	-	98.000	-	1155-1300	32.20	0.50	0.189	
7	0.460	0.460	0.930	-	0.150	-	-	-	-	98.000	-	1005-1965	1.72	0.50	0.155	
8	0.460	0.460	0.930	-	0.150	-	-	-	-	98.000	-	1105-1360	12.7	0.50	0.169	
9	0.460	0.460	0.930	-	0.150	-	-	-	-	98.000	-	1150-1290	31.4	0.50	0.159	
10	8.910	11.580	10.250	-	24.44	-	-	-	44.830	-	-	952-1177	1.24	1.00	0	
11	8.910	11.580	10.250	-	24.44	-	-	-	44.830	-	-	975-1145	1.71	1.00	0	[19]
12	8.910	11.580	10.250	-	24.44	-	-	-	44.830	-	-	1010-1091	2.36	1.00	0	
13	0.406	0.406	1.113	-	-	0.075	-	-	-	98.000	-	1010-1920	1.73	0.50	0.101	
14	0.406	0.406	1.113	-	-	0.075	-	-	-	98.000	-	1145-1410	12.1	0.50	0.165	
15	0.406	0.406	1.113	-	-	0.075	-	-	-	98.000	-	1155-1320	31.1	0.50	0.082	
16	0.296	0.296	0.950	0.209	0.157	0.089	-	-	-	98.000	-	1050-2030	1.77	0.50	0.165	[18]
17	0.296	0.296	0.950	0.209	0.157	0.089	-	-	-	98.000	-	1160-1450	12.3	0.50	0.101	
18	0.296	0.296	0.950	0.209	0.157	0.089	-	-	-	98.000	-	1185-1305	30.7	0.50	0.060	
19	1.856	-	3.713	-	-	0.464	-	-	-	93.967	-	1060-1300	5.00	0.50	0.126	
20	1.046	-	3.834	-	-	0.697	-	-	-	94.423	-	1116-1400	5.00	0.50	0.087	
21	0.558	-	3.907	-	-	0.837	-	-	-	94.698	-	1222-1700	5.00	0.50	0.039	

Continued on next page

[20]

Table B.1 – *Continued on next page*

Case	Fuel Mixture [mol %]											Experimental Conditions			E_{max}	Ref.
no.	H_2	CO	O_2	H_2O	CO_2	CH_4	C_2H_6	C_3H_8	N_2	Ar	He	T[K]	P [atm]	ϕ	[%]	
22	0.233	-	3.956	-	-	0.931	-	-	-	94.880	-	1380-1850	5.00	0.50	0.047	
23	1.856	-	3.713	-	-	0.464	-	-	-	93.967	-	1060-1275	10.00	0.50	0.112	
24	1.046	-	3.834	-	-	0.697	-	-	-	94.423	-	1075-1395	10.00	0.50	0.053	
25	0.558	-	3.907	-	-	0.837	-	-	-	94.698	-	1155-1780	10.00	0.50	0.095	
26	0.233	-	3.956	-	-	0.931	-	-	-	94.880	-	1295-1800	10.00	0.50	0.121	
27	1.856	-	3.713	-	-	0.464	-	-	-	93.967	-	1025-1492	20.00	0.50	0.042	
28	1.046	-	3.834	-	-	0.697	-	-	-	94.423	-	1072-1552	20.00	0.50	0.064	
29	0.558	-	3.907	-	-	0.837	-	-	-	94.698	-	1140-1625	20.00	0.50	0.030	
30	0.233	-	3.956	-	-	0.931	-	-	-	94.880	-	1215-2000	20.00	0.50	0.017	
31	0.073	-	7.00	-	-	3.50	-	-	-	89.427	-	1630-1760	10.39	1.00	0.118	[21]
32	0.52	-	7.00	-	-	3.50	-	-	-	88.98	-	1645-1732	10.35	1.00	0.154	
33	-	-	1.6	-	-	0.4	-	-	-	98.00	-	1667-2083	1.6	0.5	0.195	
34	-	-	1.0	-	-	1.0	-	-	-	98.00	-	1612-1923	11	2.0	0.468	
35	-	-	1.33	-	-	0.67	-	-	-	98.00	-	1492-1818	30	1.0	0.137	
36	-	-	18.2	-	-	9.1	-	-	-	72.70	-	1430-1770	1.80	1.0	0.068	[22, 23]
37	-	-	13.3	-	-	33.3	-	-	-	53.40	-	1510-1735	3.80	5.0	0.826	
38	-	-	19.10	-	-	4.8	-	-	-	76.10	-	1464-1881	1.97	0.5	0.060	
39	-	-	19.10	-	-	4.8	-	-	-	76.10	-	1348-1594	3.90	0.5	0.027	
40	-	-	1.44	0.2	-	0.36	-	-	-	98.00	-	1492-1818	11	0.5	0.145	
41	-	-	0.9	0.2	-	0.90	-	-	-	98.00	-	1538-1818	30	2.0	0.276	
42	-	-	1.2	0.2	-	0.6	-	-	-	98.00	-	1694-2041	1.6	1.0	0.103	[23]
43	-	-	1.12	0.6	-	0.28	-	-	-	98.00	-	1470-1755	30	0.5	0.153	
44	-	-	0.7	0.6	-	0.70	-	-	-	98.00	-	1754-2128	1.6	1.0	0.581	
45	-	-	0.9332	0.6	-	0.47	-	-	-	98.00	-	1515-1887	11	2.0	0.147	

Continued on next page

Table B.1 – *Continued on next page*

Case	Fuel Mixture [mol %]											Experimental Conditions			E_{max}	Ref.
no.	H_2	CO	O_2	H_2O	CO_2	CH_4	C_2H_6	C_3H_8	N_2	Ar	He	T[K]	P [atm]	ϕ	[%]	
46	1.82	-	3.74	-	-	0.42	0.0356	-	-	94.00	-	1045-1249	16.15	0.5	0.425	[24]
47	1.82	-	3.74	-	-	0.42	0.0356	-	-	94.00	-	984-1212	4.13	0.5	1.417	
48	1.82	-	3.74	-	-	0.42	0.0356	-	-	94.00	-	1017-1280	1.00	0.5	2.921	
49	3.29	-	3.38	-	-	0.77	0.0651	-	-	92.48	-	1035-1242	15.88	1.0	0.321	
50	3.29	-	3.38	-	-	0.77	0.0651	-	-	92.48	-	1028-1306	3.99	1.0	0.641	
51	3.29	-	3.38	-	-	0.77	0.0651	-	-	92.48	-	1098-1409	1.02	1.0	0.965	
52	0.51	-	3.90	-	-	0.73	0.0645	-	-	94.80	-	1129-1401	15.91	0.5	0.122	
53	0.51	-	3.90	-	-	0.73	0.0645	-	-	94.80	-	1131-1398	4.13	0.5	0.245	
54	0.51	-	3.90	-	-	0.73	0.0645	-	-	94.80	-	1198-1537	1.01	0.5	0.087	
55	0.96	-	3.60	-	-	1.35	0.1175	-	-	93.96	-	1102-1472	15.55	1.0	0.150	
56	0.96	-	3.60	-	-	1.35	0.1175	-	-	93.96	-	1186-1560	3.94	1.0	0.112	
57	0.96	-	3.60	-	-	1.35	0.1175	-	-	93.96	-	1274-1800	1.03	1.0	0.496	
58	-	-	19.00	-	-	9.50	-	1.90	-	69.60	-	1295-1433	2.5	1.5	0.612	[25]
59	-	-	20.54	-	-	2.01	-	0.22	77.23	-	-	1202-1476	9.0	0.5	5.649	[26]
60	-	-	20.54	-	-	2.01	-	0.22	77.23	-	-	1252-1369	30.3	0.5	2.166	
61	-	-	20.10	-	-	3.93	-	0.437	75.54	-	-	1201-1465	8.07	1.0	3.735	
62	-	-	20.10	-	-	3.93	-	0.437	75.54	-	-	1142-1271	16.65	1.0	4.792	
63	-	-	20.10	-	-	3.93	-	0.437	75.54	-	-	1117-1193	23.47	1.0	3.750	
64	-	-	19.25	-	-	7.53	-	0.837	72.38	-	-	1222-1337	7.2	2.0	0.472	
65	-	-	19.25	-	-	7.53	-	0.837	72.38	-	-	1150-1426	25.4	2.0	0.534	
66	-	-	20.59	-	-	1.58	-	0.396	77.43	-	-	1051-1295	25.54	0.5	7.193	
67	-	-	20.27	-	-	2.45	-	1.05	76.23	-	-	1128-1375	8.05	1.0	11.33	
68	-	-	20.27	-	-	2.45	-	1.05	76.23	-	-	1190-1503	29.88	1.0	8.041	
69	-	-	19.59	-	-	4.73	-	2.03	73.66	-	-	1159-1585	7.55	2.0	2.909	
70	-	-	19.59	-	-	4.73	-	2.03	73.66	-	-	1142-1298	27.1	2.0	2.393	

Continued on next page

Table B.1 – *Continued on next page*

Case	Fuel Mixture [mol %]											Experimental Conditions			E_{max}	Ref.
no.	H_2	CO	O_2	H_2O	CO_2	CH_4	C_2H_6	C_3H_8	N_2	Ar	He	T[K]	P [atm]	ϕ	[%]	
71	-	-	17.63	-	-	14.43	1.07	1.09	66.33	-	-	1322-1577	1.2	2.0	0.226	
72	-	-	17.63	-	-	14.43	1.07	1.09	66.33	-	-	1253-1526	5.49	2.0	0.191	
73	-	-	17.63	-	-	14.43	1.07	1.09	66.33	-	-	1156-1405	15.41	2.0	0.739	
74	-	-	18.15	-	-	9.5	2.04	0.075	68.28	-	-	1279-1490	1.1	2.0	1.498	
75	-	-	18.15	-	-	9.5	2.04	0.075	68.28	-	-	1021-1379	17.8	2.0	5.790	
76	-	-	18.08	-	-	9.74	2.78	1.39	68.01	-	-	1370-1542	1.0	2.0	0.722	
77	-	-	18.08	-	-	9.74	2.78	1.39	68.01	-	-	1039-1393	17.67	2.0	3.870	
78	-	-	19.17	-	-	7.84	0.58	0.29	72.11	-	-	1301-1487	1.20	1.0	0.383	
79	-	-	19.17	-	-	7.84	0.58	0.29	72.11	-	-	1208-1447	28.45	1.0	0.575	
80	-	-	19.47	-	-	5.1	1.09	1.09	73.25	-	-	1225-1467	1.30	1.0	3.043	
81	-	-	19.47	-	-	5.1	1.09	1.09	73.25	-	-	1093-1383	6.96	1.0	4.018	
82	-	-	19.47	-	-	5.1	1.09	1.09	73.25	-	-	1167-1286	29.83	1.0	3.526	[27]
83	-	-	19.43	-	-	5.23	1.49	0.75	73.10	-	-	1336-1564	1.20	1.0	0.619	
84	-	-	19.43	-	-	5.23	1.49	0.75	73.10	-	-	1032-1132	19.75	1.0	2.176	
85	-	-	19.43	-	-	5.23	1.49	0.75	73.10	-	-	1329-1486	45.46	1.0	2.500	
86	-	-	20.04	-	-	4.1	0.31	0.15	75.40	-	-	1297-1528	1.23	1.0	0.737	
87	-	-	20.04	-	-	4.1	0.31	0.15	75.40	-	-	1182-1456	5.73	1.0	2.202	
88	-	-	20.04	-	-	4.1	0.31	0.15	75.40	-	-	1297-1528	29.98	0.5	0.945	
89	-	-	20.21	-	-	2.64	0.57	0.57	76.02	-	-	1182-1456	1.27	0.5	3.842	
90	-	-	20.21	-	-	2.64	0.57	0.57	76.02	-	-	1169-1278	6.56	0.5	8.445	
91	-	-	20.21	-	-	2.64	0.57	0.57	76.02	-	-	1060-1253	19.32	0.5	6.410	
92	-	-	20.18	-	-	2.72	0.78	0.39	75.93	-	-	1194-1390	1.46	0.5	5.019	
93	-	-	20.18	-	-	2.72	0.78	0.39	75.93	-	-	1113-1384	7.03	0.5	7.301	
94	-	-	20.18	-	-	2.72	0.78	0.39	75.93	-	-	1063-1251	19.32	0.5	4.504	

Laminar Flame Speed

Continued on next page

Table B.1 – *Continued on next page*

Case	Fuel Mixture [mol %]											Experimental Conditions			E_{max}	Ref.
no.	H_2	CO	O_2	H_2O	CO_2	CH_4	C_2H_6	C_3H_8	N_2	Ar	He	T[K]	P [atm]	ϕ	[%]	
95	0.05	0.95	1/(2ϕ)	-	-	-	-	-	3.76/(2ϕ)	-	-	300	1.00	0.4 - 5.5	0.8431	[28, 29, 30, 31, 32]
96	0.50	0.50	1/(2ϕ)	-	-	-	-	-	3.76/(2ϕ)	-	-	300	1.00	0.4 - 5.5	1.2527	
97	0.50	0.50	1/(2ϕ)	-	-	-	-	-	-	-	7.00/(2ϕ)	300	5.00	0.5 - 4.1	0.7447	[28, 33, 34, 35]
98	0.50	0.50	1/(2ϕ)	-	-	-	-	-	-	-	7.00/(2ϕ)	300	10.00	0.5 - 4.1	1.5144	
99	0.05	0.95	1/(2ϕ)	-	-	-	-	-	-	-	7.00/(2ϕ)	300	10.00	0.5 - 3.6	1.1243	
100	0.05	0.95	1/(2ϕ)	-	-	-	-	-	-	-	7.00/(2ϕ)	300	40.00	0.5 - 3.6	1.2947	
101	0.05	0.95	1/(2ϕ)	-	-	-	-	-	-	-	7.00/(2ϕ)	300	5.00	0.5 - 4.1	1.4510	
102	0.05	0.95	1/(2ϕ)	-	-	-	-	-	-	-	7.00/(2ϕ)	300	20.00	0.5 - 3.6	0.9743	
103	0.35	0.35	0.35/ϕ	-	0.3	-	-	-	1.32/ϕ	-	-	303	1.00	0.4 - 1.2	0.8504	[36, 37]
104	0.35	0.35	0.35/ϕ	-	0.3	-	-	-	1.32/ϕ	-	-	373	1.00	0.4 - 1.2	0.3289	
105	0.35	0.35	0.35/ϕ	-	0.3	-	-	-	1.32/ϕ	-	-	373	3.00	0.4 - 1.2	0.4082	
106	0.25	0.25	1/(2ϕ)	-	0.5	-	-	-	3.76/(2ϕ)	-	-	303	1.00	0.8 - 2.1	1.1423	
107	0.40	0.10	1/(2ϕ)	-	0.5	-	-	-	3.76/(2ϕ)	-	-	303	1.00	0.8 - 2.1	1.5709	
108	0.10	0.40	1/(2ϕ)	-	0.5	-	-	-	3.76/(2ϕ)	-	-	303	1.00	0.8 - 2.1	1.4314	
109	0.1-0.7	0.3-0.9	1/(2ϕ)	-	0.67/(2ϕ)	-	-	-	-	-	-	300	1.00	0.4	1.3405	[38]
110	0.1-0.7	0.3-0.9	1/(2ϕ)	-	1/(2ϕ)	-	-	-	-	-	-	300	1.00	0.4	0.1177	
111	0.1-0.7	0.3-0.9	1/(2ϕ)	-	1.5/(2ϕ)	-	-	-	-	-	-	300	1.00	0.4	0.2984	
112	0.1-0.7	0.3-0.9	1/(2ϕ)	-	2.3/(2ϕ)	-	-	-	-	-	-	300	1.00	0.4	0.3258	
113	0.1-0.7	0.3-0.9	1/(2ϕ)	-	0.67/(2ϕ)	-	-	-	-	-	-	300	2.00	0.4	0.2347	
114	0.1-0.7	0.3-0.9	1/(2ϕ)	-	1/(2ϕ)	-	-	-	-	-	-	300	2.00	0.4	1.1989	
115	0.1-0.7	0.3-0.9	1/(2ϕ)	-	1.5/(2ϕ)	-	-	-	-	-	-	300	2.00	0.4	0.6695	
116	0.1-0.7	0.3-0.9	1/(2ϕ)	-	2.3/(2ϕ)	-	-	-	-	-	-	300	2.00	0.4	0.9630	
117	0.038-0.05	0.73-0.95	1/(2ϕ)	0-0.32	-	-	-	-	3.76/(2ϕ)	-	-	323	1.00	0.9	0.5713	[39]
118	0.325-0.5	0.325-0.5	1/(2ϕ)	0-0.35	-	-	-	-	3.76/(2ϕ)	-	-	323	1.00	0.4	1.3164	

Continued on next page

Table B.1 – *Continued on next page*

Case	Fuel Mixture [mol %]											Experimental Conditions			E_{max}	Ref.
no.	H_2	CO	O_2	H_2O	CO_2	CH_4	C_2H_6	C_3H_8	N_2	Ar	He	T[K]	P [atm]	ϕ	[%]	
119	0.325-0.5	0.325-0.5	1/(2ϕ)	0-0.35	-	-	-	-	3.76/(2ϕ)	-	-	323	1.00	0.5	1.0878	
120	0.325-0.5	0.325-0.5	1/(2ϕ)	0 - 0.35	-	-	-	-	3.76/(2ϕ)	-	-	323	1.00	0.6	0.6314	
121	0.0362-0.05	0.6884-0.95	1/(2ϕ)	0 - 0.4	-	-	-	-	3.76/(2ϕ)	-	-	400	1.00	1.0	0.1607	[40]
122	0.4 -0.5	0.4 - 0.5	1/(2ϕ)	0 - 0.2	-	-	-	-	3.76/(2ϕ)	-	-	400	1.00	1.0	1.0390	
123	0.11	0.31	0.21/ϕ	-	-	-	-	-	(0.79/ϕ)+0.58	-	-	303	1.00	0.5 - 1.1	0.3997	
124	0.11	0.31	0.21/ϕ	-	-	-	-	-	(0.79/ϕ)+0.58	-	-	373	1.00	0.5 - 1.1	0.3482	[36]
125	0.11	0.31	0.21/ϕ	-	-	-	-	-	(0.79/ϕ)+0.58	-	-	373	3.00	0.5 - 1.1	0.8360	
126	0.11	0.31	0.21/ϕ	-	-	-	-	-	(0.79/ϕ)+0.58	-	-	373	5.00	0.5 - 1.1	0.6683	
127	0-1.0	-	1.0-2.0	-	-	0 - 1.0	-	-	3.76-7.52	-	-	300	1.00	1.0	0.6317	[41, 42, 43]
128	0.2	-	1.7/ϕ	-	-	0.8	-	-	6.39/ϕ	-	-	300	1.00	0.5 - 1.5	1.8827	
129	0.5	-	1.25/ϕ	-	-	0.5	-	-	4.7/ϕ	-	-	300	1.00	0.5 - 1.4	2.2015	[42, 41, 44, 45, 46]
130	0.7	-	0.95/ϕ	-	-	0.3	-	-	3.572/ϕ	-	-	450	5.00	0.6 - 1.6	1.8624	
131	0.9	-	0.65/ϕ	-	-	0.1	-	-	2.44/ϕ	-	-	450	1.00	0.5 - 2.0	0.6408	
132	0.375	0.375	0.658	-	0.20	0.05	-	-	2.474	-	-	300	1.00	0.722	0.0436	
133	0.375	0.375	0.574	-	0.20	0.05	-	-	2.160	-	-	300	1.00	0.827	0.5122	
134	0.375	0.375	0.510	-	0.20	0.05	-	-	1.918	-	-	300	1.00	0.931	0.3623	
135	0.375	0.375	0.460	-	0.20	0.05	-	-	1.727	-	-	300	1.00	1.034	0.9497	
136	0.188	0.188	1.727	-	0.10	0.525	-	-	6.492	-	-	300	1.00	0.717	1.5834	
137	0.188	0.188	1.517	-	0.10	0.525	-	-	5.705	-	-	300	1.00	0.816	2.0105	
138	0.188	0.188	1.349	-	0.10	0.525	-	-	5.071	-	-	300	1.00	0.918	2.1214	[47]
139	0.188	0.188	1.211	-	0.10	0.525	-	-	4.555	-	-	300	1.00	1.022	3.8089	
140	0.281	0.281	1.290	-	0.15	0.288	-	-	4.853	-	-	300	1.00	0.664	0.2150	
141	0.281	0.281	1.119	-	0.15	0.288	-	-	4.21	-	-	300	1.00	0.766	0.7324	
142	0.281	0.281	0.986	-	0.15	0.288	-	-	3.708	-	-	300	1.00	0.869	0.5492	
143	0.281	0.281	0.8835	-	0.15	0.288	-	-	3.322	-	-	300	1.00	0.970	2.2399	

Continued on next page

Table B.1 – *Continued on next page*

Case	Fuel Mixture [mol %]											Experimental Conditions			E_{max}	Ref.
no.	H_2	CO	O_2	H_2O	CO_2	CH_4	C_2H_6	C_3H_8	N_2	Ar	He	T[K]	P [atm]	ϕ	[%]	
144	-	-	2/ϕ	-	-	1.0	-	-	7.52/ϕ	-	-	300	1.00	0.6 - 1.6	1.5466	[48, 49, 50, 51]
145	-	-	2/ϕ	-	-	1.0	-	-	7.52/ϕ	-	-	300	2.00	0.6 - 1.6	0.5343	
146	-	-	2/ϕ	-	-	1.0	-	-	7.52/ϕ	-	-	300	3.00	0.6 - 1.6	1.1027	
147	-	-	2/ϕ	-	-	1.0	-	-	7.52/ϕ	-	-	400	5.00	0.6 - 1.6	0.5115	
148	-	-	2/ϕ	-	-	1.0	-	-	7.52/ϕ	-	-	500	5.00	0.6 - 1.6	0.4030	
149	-	-	2/ϕ	-	-	1.0	-	-	7.52/ϕ	-	-	600	5.00	0.6 - 1.6	0.5023	

B.1 Comparison with experimental data - Ignition delay time

B.1.1 Mixture combination: H_2/CO

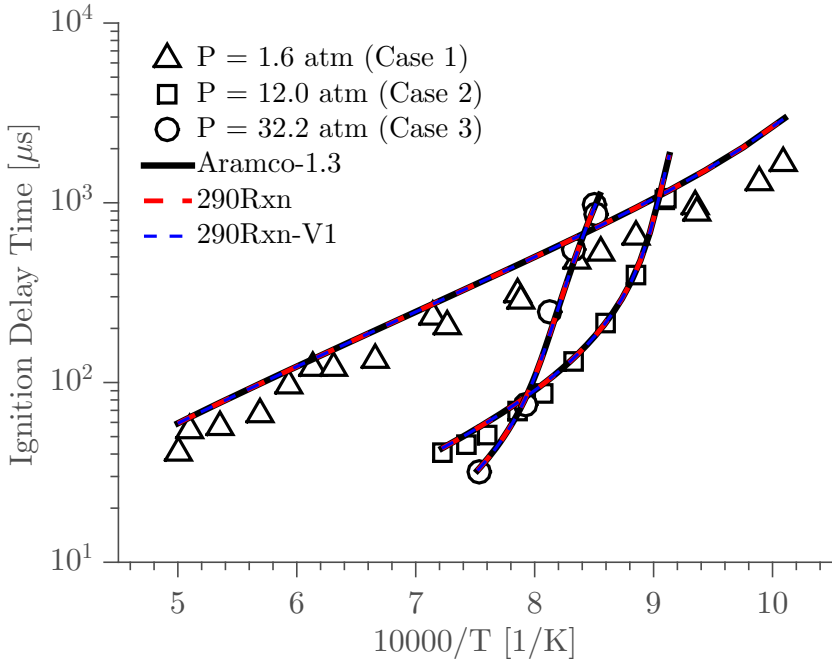

Figure B.1: Comparisons of measured and predicted ignition delay time of H_2/CO mixtures computed using Aramco-1.3, 290Rxn, and 290Rxn-V1 mechanisms. Symbols represent experimental data; please refer to Table B.1 for references and more information on the fuel compositions and the experimental conditions.

B.1.2 Mixture combination: $H_2/CO/H_2O$

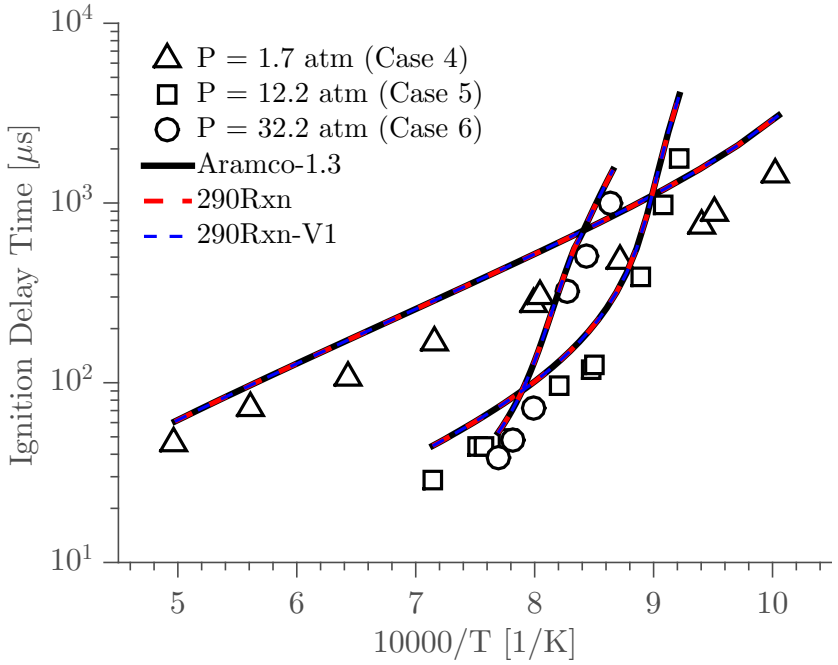

Figure B.2: Comparisons of measured and predicted ignition delay time of $H_2/CO/H_2O$ mixtures computed using Aramco-1.3, 290Rxn, and 290Rxn-V1 mechanisms. Symbols represent experimental data; please refer to Table B.1 for references and more information on the fuel compositions and the experimental conditions.

B.1.3 Mixture combination: $H_2/CO/CO_2$

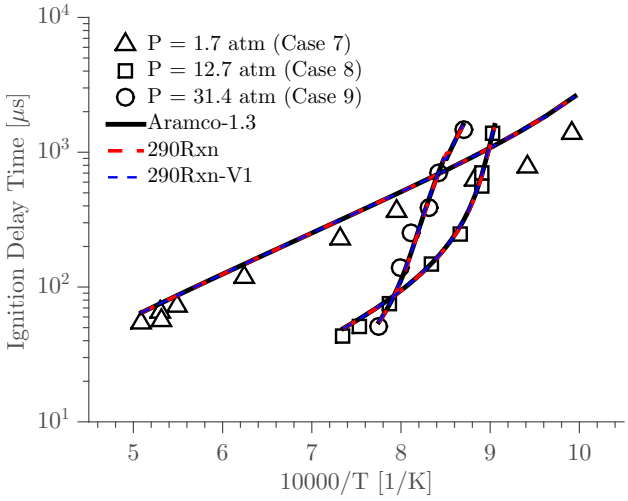

(a)

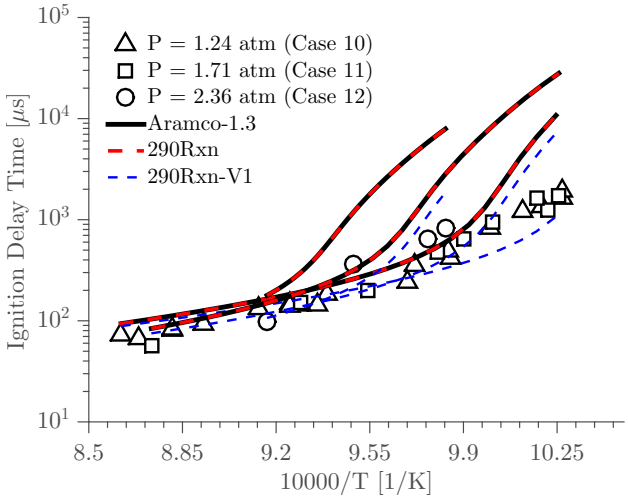

(b)

Figure B.3: Comparisons of measured and predicted ignition delay time of $H_2/CO/CO_2$ mixtures computed using Aramco-1.3, 290Rxn, and 290Rxn-V1 mechanisms. Symbols represent experimental data; please refer to Table B.1 for references and more information on the fuel compositions and the experimental conditions.

B.1.4 Mixture combination: $H_2/CO/CH_4$

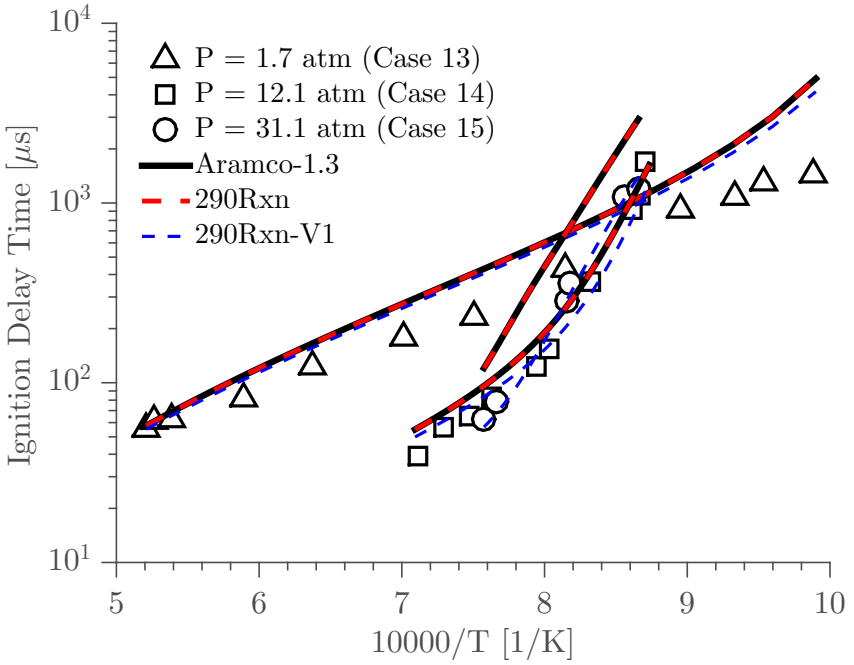

Figure B.4: Comparisons of measured and predicted ignition delay time of $H_2/CO/CH_4$ mixtures computed using Aramco-1.3, 290Rxn, and 290Rxn-V1 mechanisms. Symbols represent experimental data; please refer to Table B.1 for references and more information on the fuel compositions and the experimental conditions.

B.1.5 Mixture combination: $H_2/CO/CO_2/H_2O/CH_4$

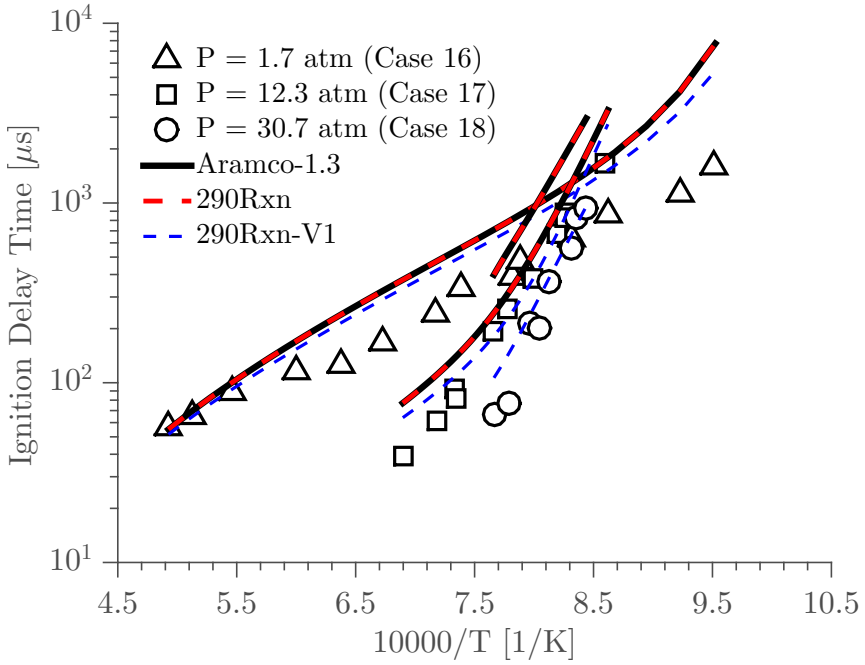

Figure B.5: Comparisons of measured and predicted ignition delay time of $H_2/CO/CO_2/H_2O/CH_4$ mixtures computed using Aramco-1.3, 290Rxn, and 290Rxn-V1 mechanisms. Symbols represent experimental data; please refer to Table B.1 for references and more information on the fuel compositions and the experimental conditions.

B.1.6 Mixture combination: H_2/CH_4

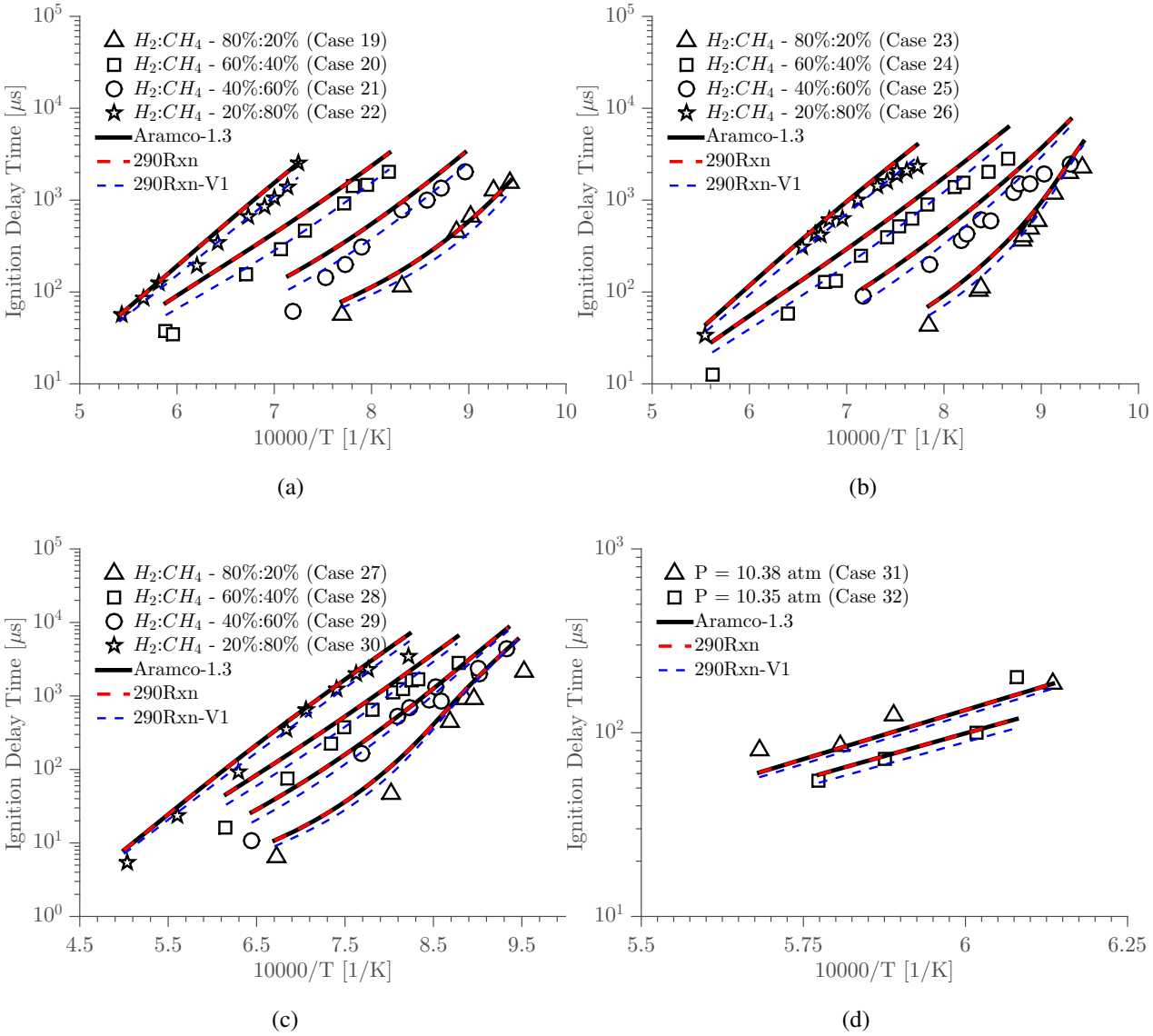

Figure B.6: Comparisons of measured and predicted ignition delay time of H_2/CH_4 mixtures computed using Aramco-1.3, 290Rxn, and 290Rxn-V1 mechanisms. Symbols represent experimental data; please refer to Table B.1 for references and more information on the fuel compositions and the experimental conditions.

B.1.7 Mixture combination: CH_4

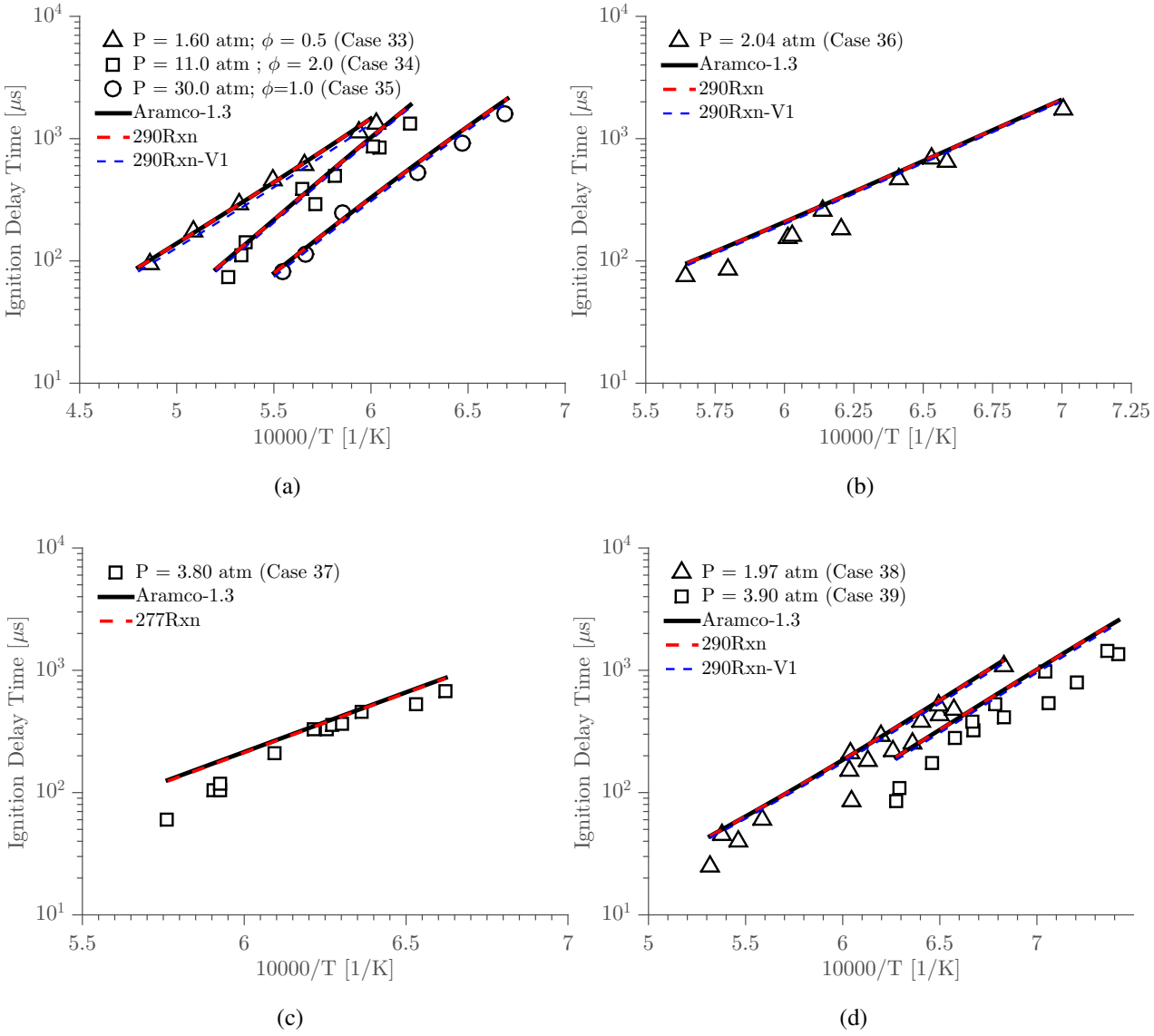

Figure B.7: Comparisons of measured and predicted ignition delay time of CH_4 mixtures computed using Aramco-1.3, 290Rxn, and 290Rxn-V1 mechanisms. Symbols represent experimental data; please refer to Table B.1 for references and more information on the fuel compositions and the experimental conditions.

B.1.8 Mixture combination: CH_4/H_2O

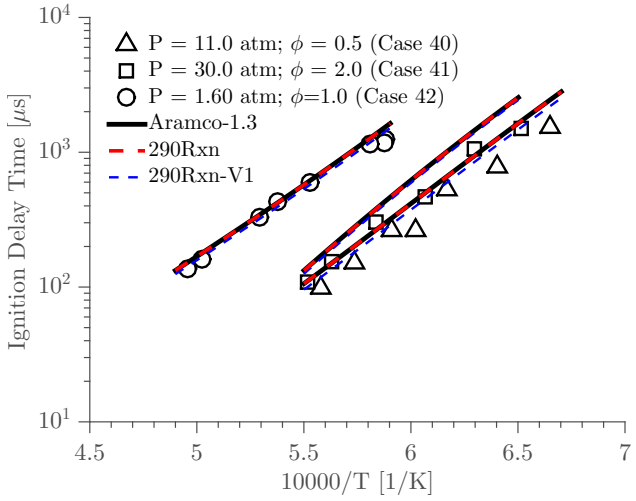

(a)

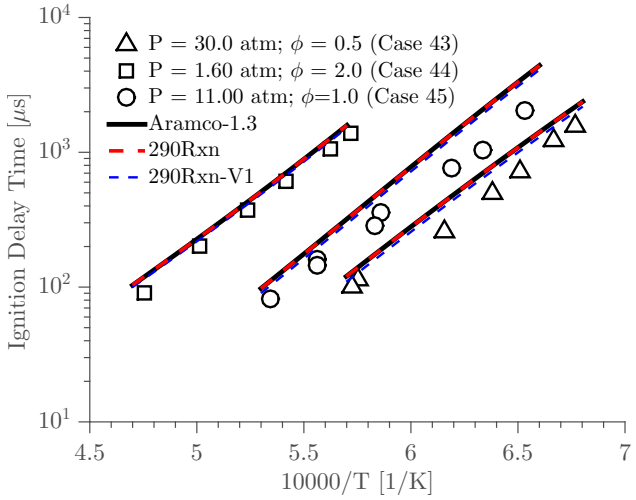

(b)

Figure B.8: Comparisons of measured and predicted ignition delay time of CH_4/H_2O mixtures computed using Aramco-1.3, 290Rxn, and 290Rxn-V1 mechanisms. Symbols represent experimental data; please refer to Table B.1 for references and more information on the fuel compositions and the experimental conditions.

B.1.9 Mixture combination: $CH_4/C_2H_6/H_2$

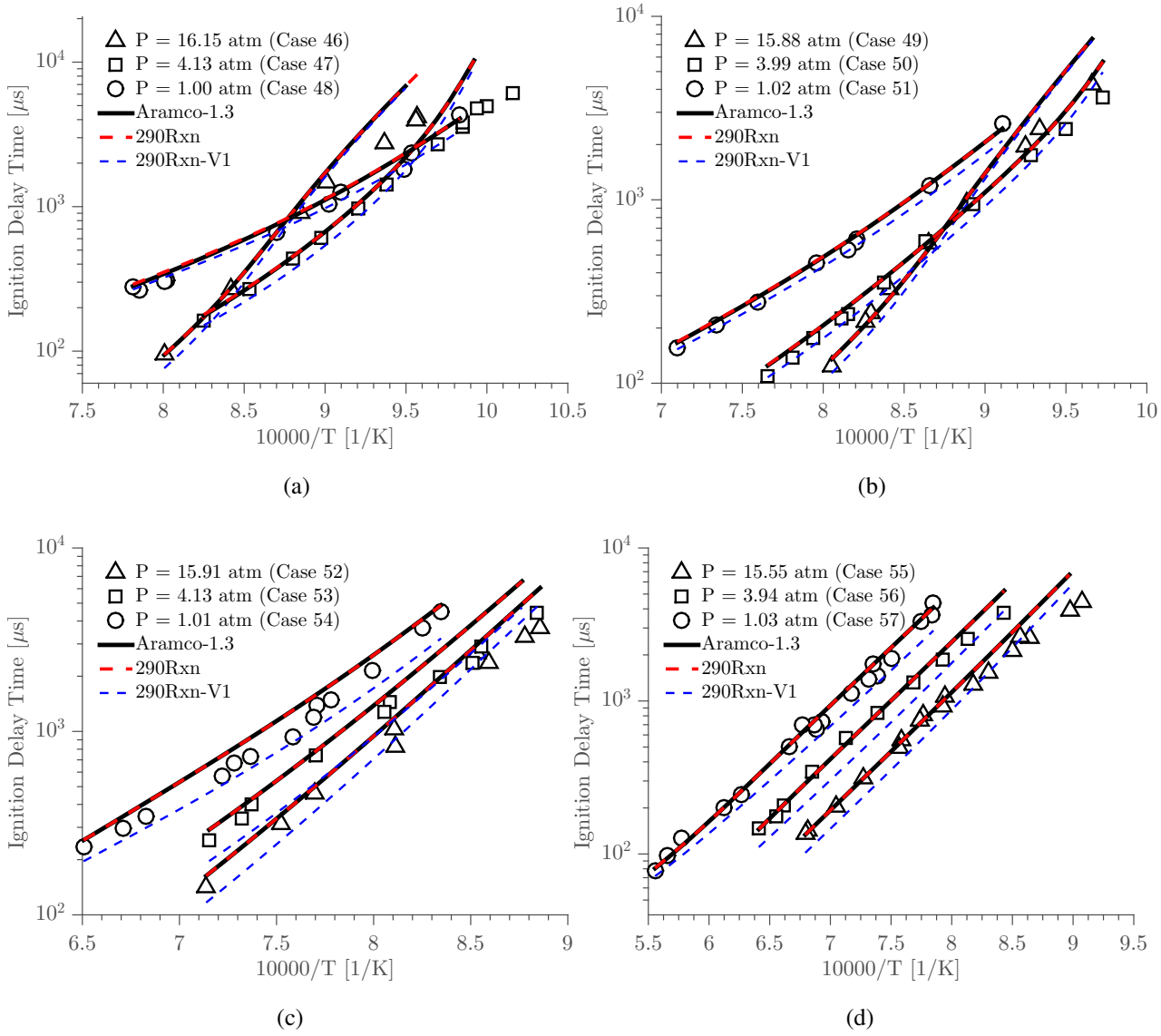

Figure B.9: Comparisons of measured and predicted ignition delay time of $CH_4/C_2H_6/H_2$ mixtures computed using Aramco-1.3, 290Rxn, and 290Rxn-V1 mechanisms. Symbols represent experimental data; please refer to Table B.1 for references and more information on the fuel compositions and the experimental conditions.

B.1.10 Mixture combination: CH_4/C_3H_8

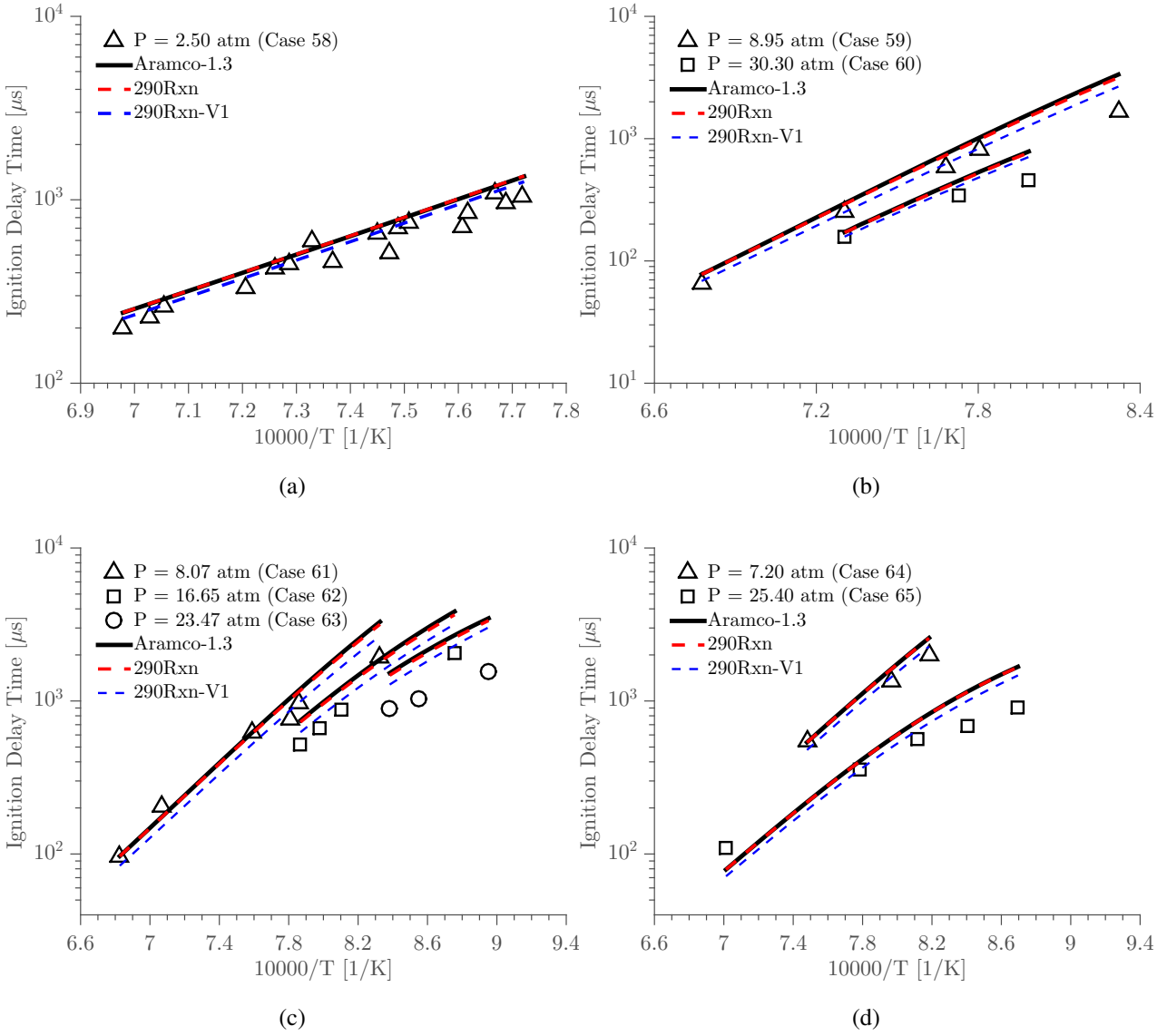

Figure B.10: Comparisons of measured and predicted ignition delay time of CH_4/C_3H_8 mixtures computed using Aramco-1.3, 290Rxn, and 290Rxn-V1 mechanisms. Symbols represent experimental data; please refer to Table B.1 for references and more information on the fuel compositions and the experimental conditions.

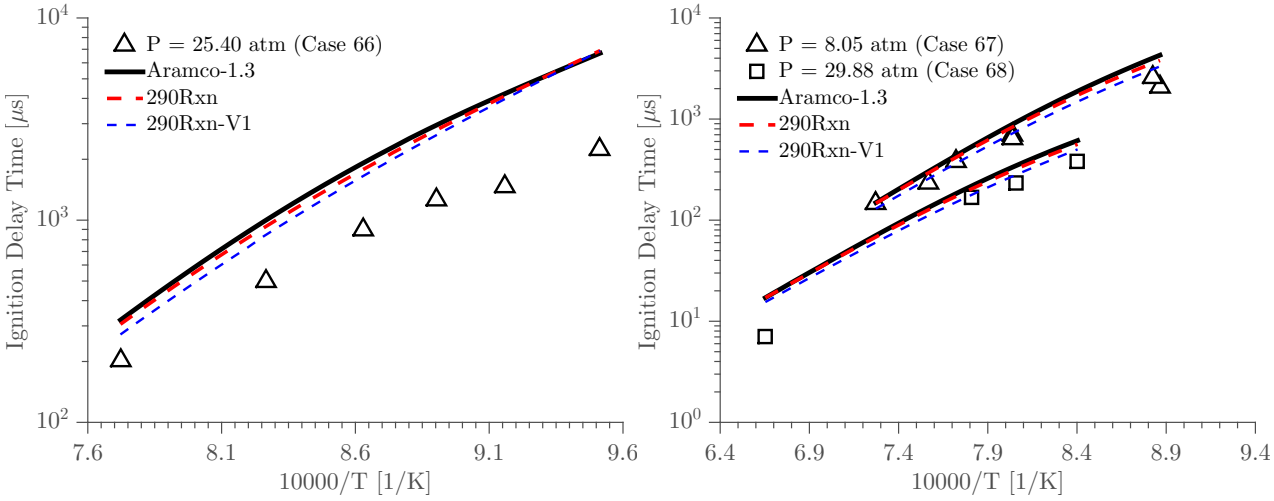

(e) (f)

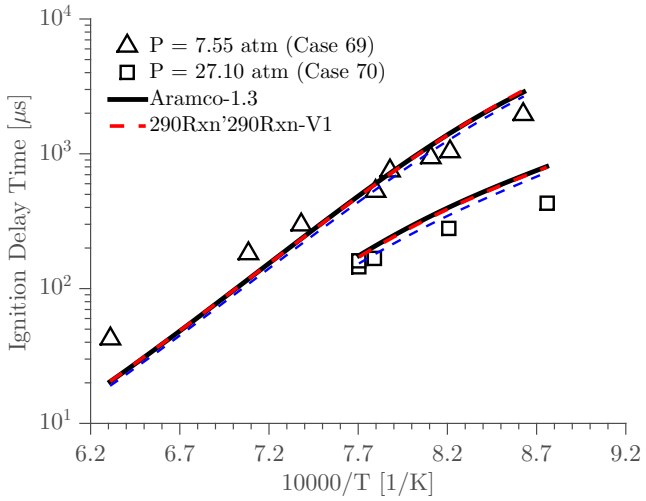

(g)

Figure B.10: Comparisons of measured and predicted ignition delay time of CH_4/C_3H_8 mixtures computed using Aramco-1.3, 290Rxn, and 290Rxn-V1 mechanisms. Symbols represent experimental data; please refer to Table B.1 for references and more information on the fuel compositions and the experimental conditions (continued).

B.1.11 Mixture combination: $CH_4/C_2H_6/C_3H_8$

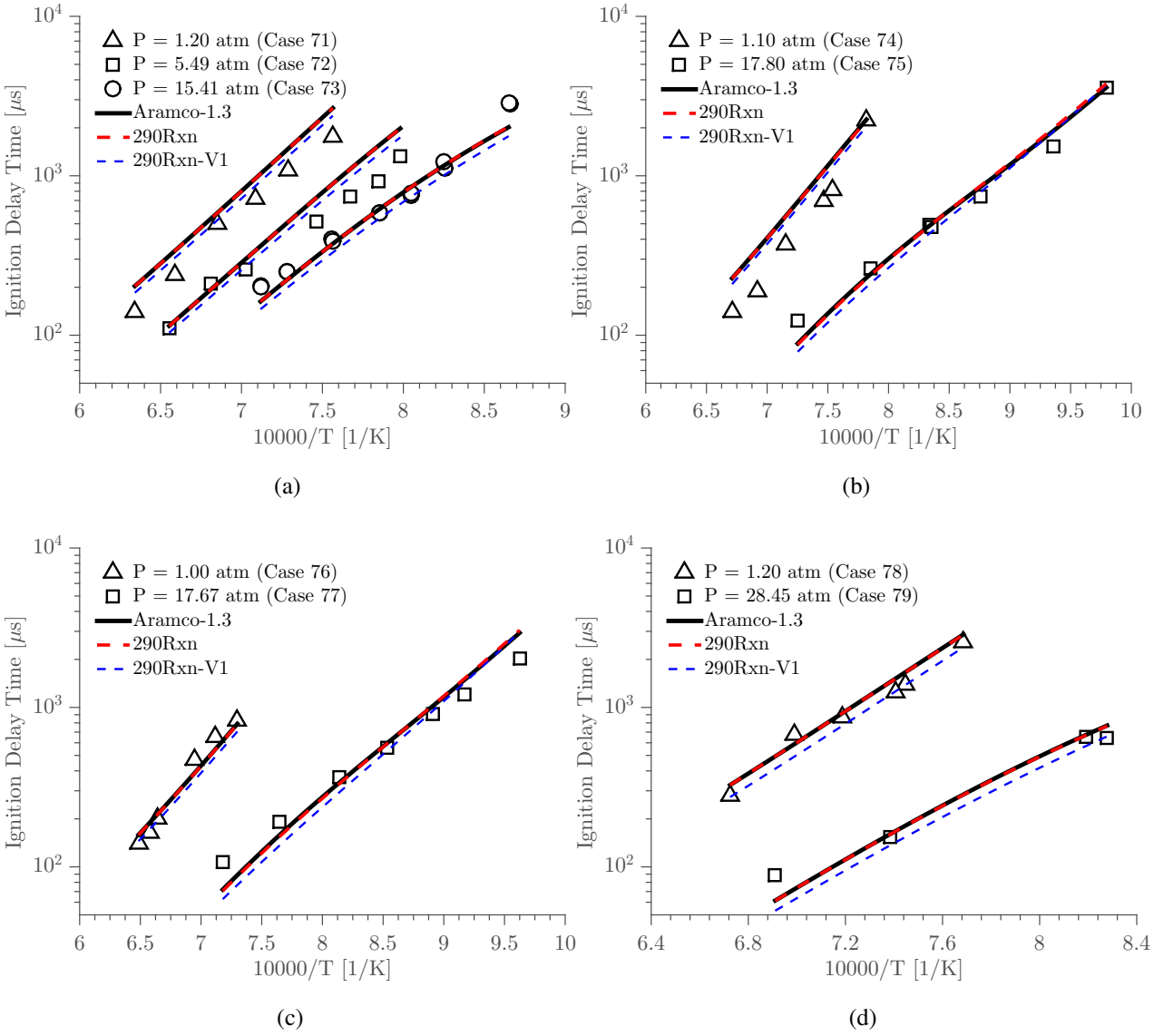

Figure B.11: Comparisons of measured and predicted ignition delay time of $CH_4/C_2H_6/C_3H_8$ mixtures computed using Aramco-1.3, 290Rxn, and 290Rxn-V1 mechanisms. Symbols represent experimental data; please refer to Table B.1 for references and more information on the fuel compositions and the experimental conditions.

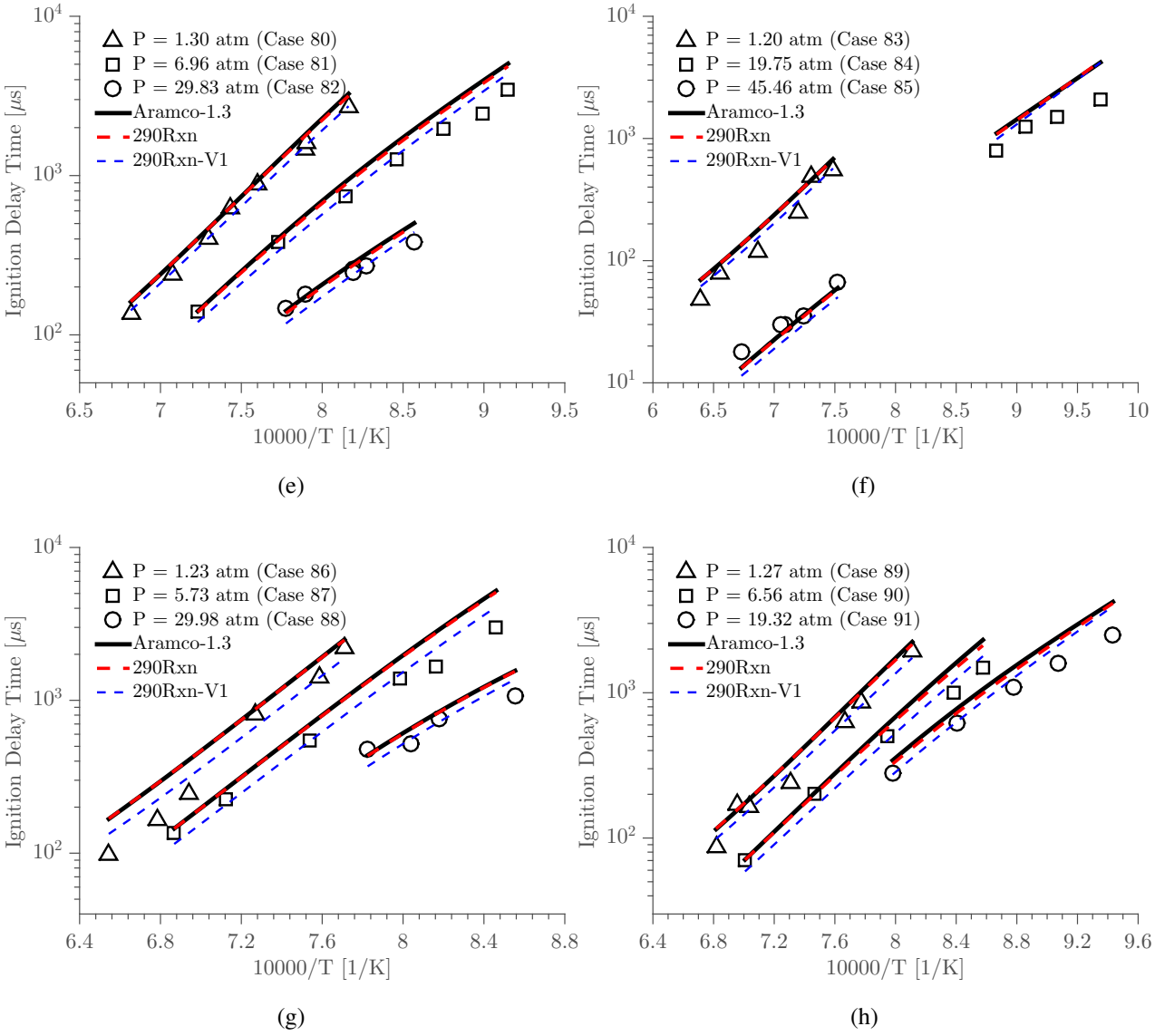

Figure B.11: Comparisons of measured and predicted ignition delay time of $CH_4/C_2H_6/C_3H_8$ mixtures computed using Aramco-1.3, 290Rxn, and 290Rxn-V1 mechanisms. Symbols represent experimental data; please refer to Table B.1 for references and more information on the fuel compositions and the experimental conditions (continued).

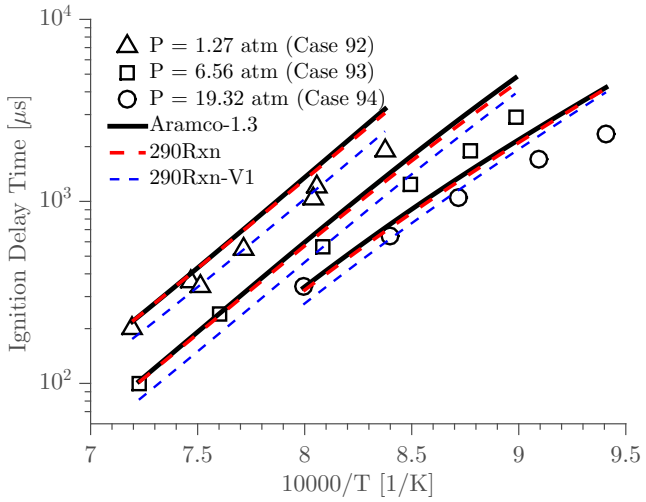

(i)

Figure B.11: Comparisons of measured and predicted ignition delay time of $CH_4/C_2H_6/C_3H_8$ mixtures computed using Aramco-1.3, 290Rxn, and 290Rxn-V1 mechanisms. Symbols represent experimental data; please refer to Table B.1 for references and more information on the fuel compositions and the experimental conditions (continued).

B.2 Comparison with experimental data - Flame speed

B.2.1 Mixture combination: H_2/CO

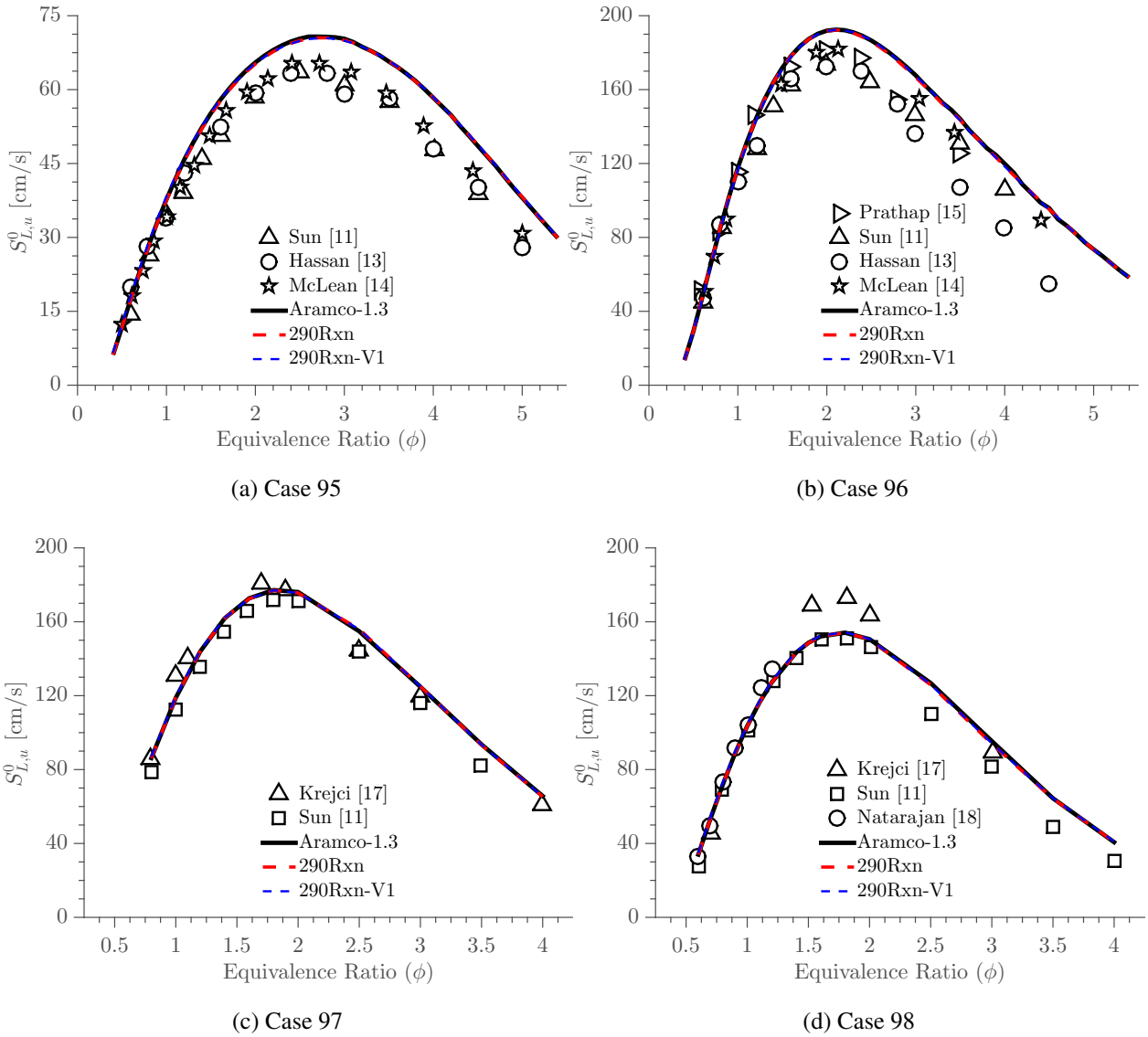

(a) Case 95

(b) Case 96

(c) Case 97

(d) Case 98

Figure B.12: Comparisons of measured and predicted laminar flame speed of H_2/CO mixtures computed using Aramco-1.3, 290Rxn, and 290Rxn-V1 mechanisms. Symbols represent experimental data; please refer to Table B.1 for references and more information on the fuel compositions and the experimental conditions.

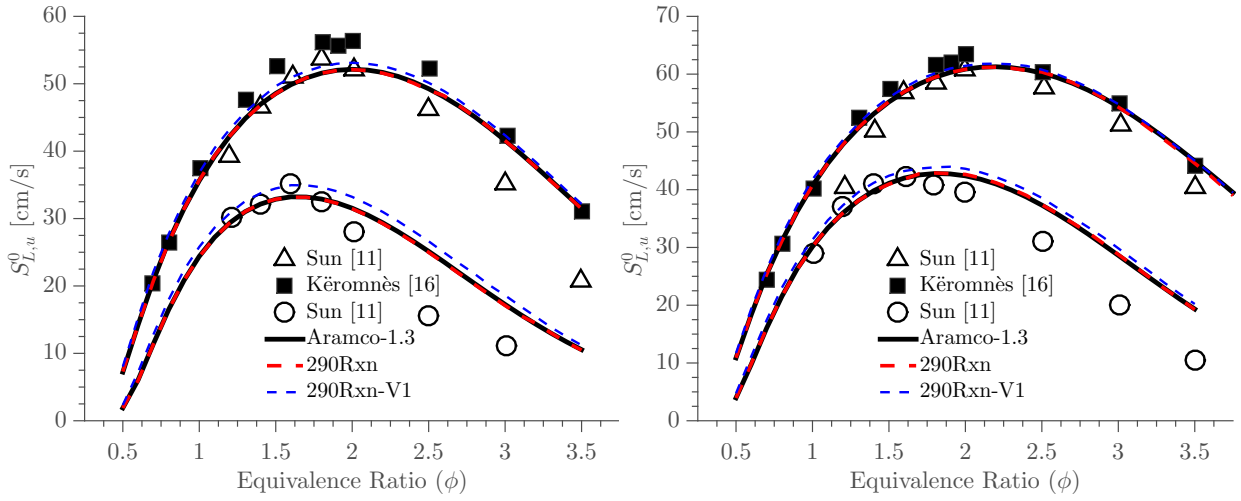

(e) Case 99 and Case 100

(f) Case 101 and Case 102

Figure B.12: Comparisons of measured and predicted laminar flame speed of H_2/CO mixtures computed using Aramco-1.3, 290Rxn, and 290Rxn-V1 mechanisms. Symbols represent experimental data; please refer to Table B.1 for references and more information on the fuel compositions and the experimental conditions (continued).

B.2.2 Mixture combination: $H_2/CO/CO_2$

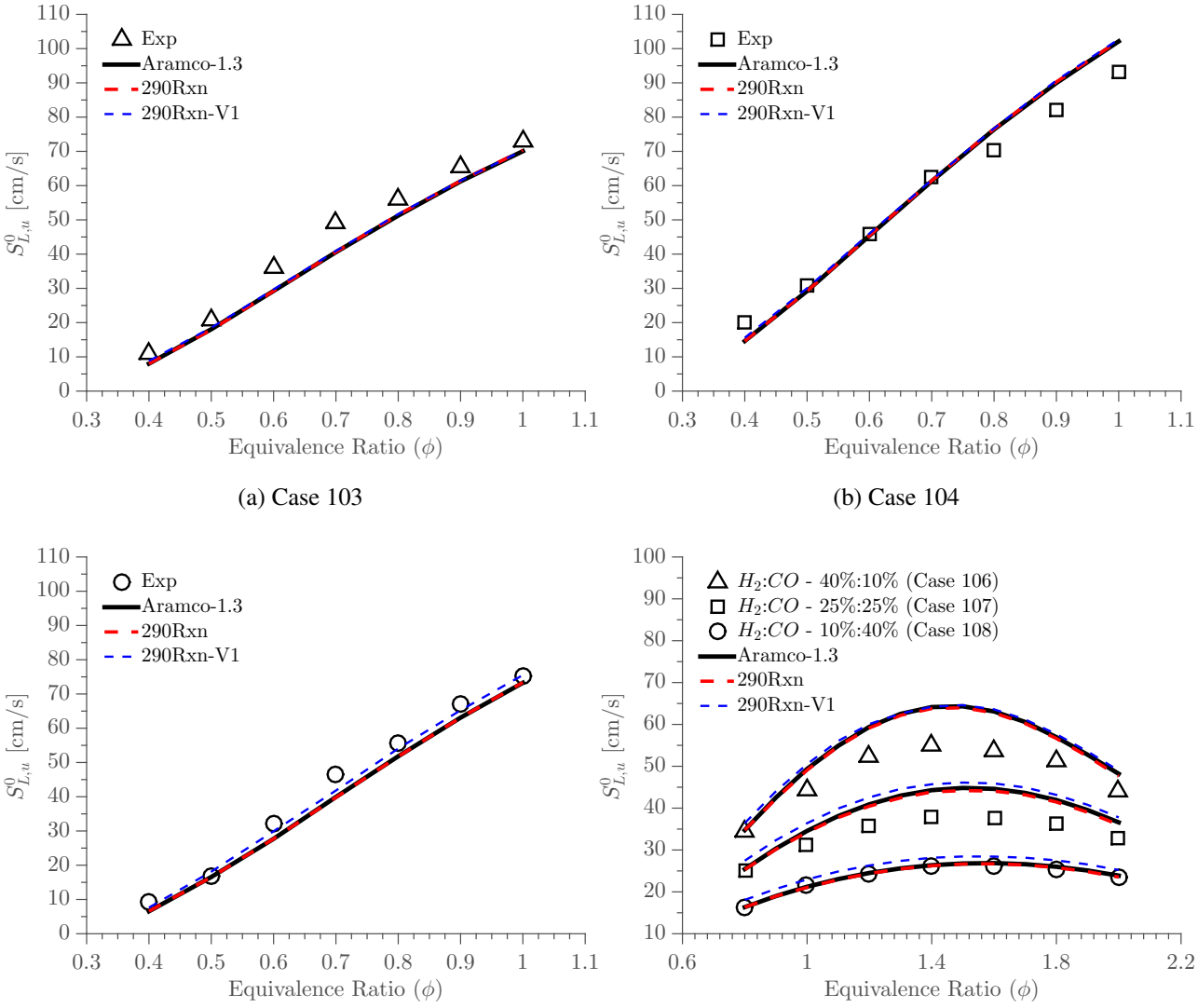

(a) Case 103

(b) Case 104

(c) Case 105

(d) Case 106 - Case 108

Figure B.13: Comparisons of measured and predicted laminar flame speed of $H_2/CO/CO_2$ mixtures computed using Aramco-1.3, 290Rxn, and 290Rxn-V1 mechanisms. Symbols represent experimental data; please refer to Table B.1 for references and more information on the fuel compositions and the experimental conditions.

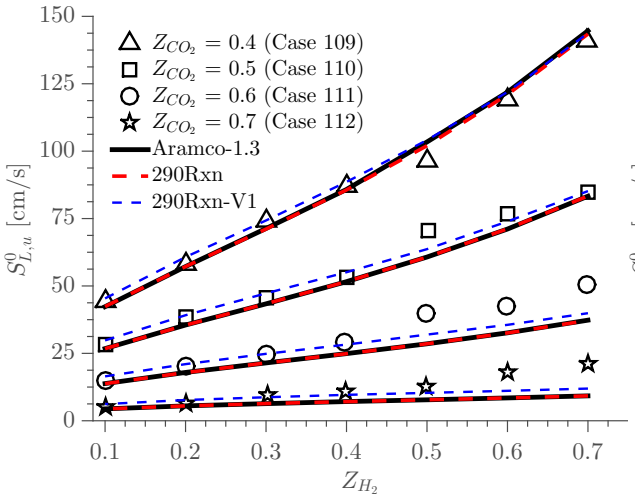

(e) Case 109 - Case 112

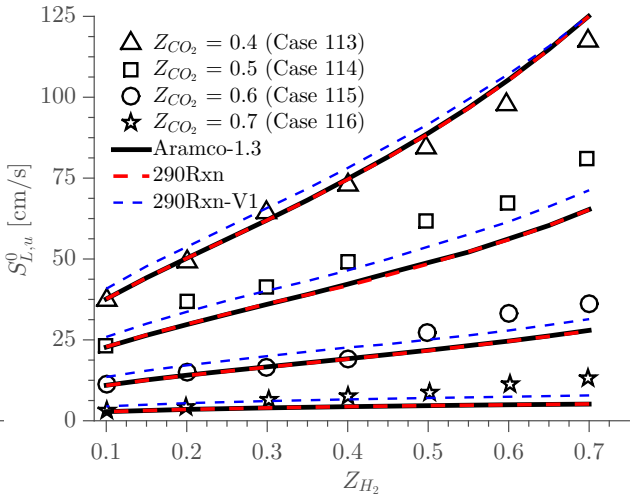

(f) Case 113 - Case 116

Figure B.13: Comparisons of measured and predicted laminar flame speed of $H_2/CO/CO_2$ mixtures computed using Aramco-1.3, 290Rxn, and 290Rxn-V1 mechanisms. Symbols represent experimental data; please refer to Table B.1 for references and more information on the fuel compositions and the experimental conditions (continued).

B.2.3 Mixture combination: $H_2/CO/H_2O$

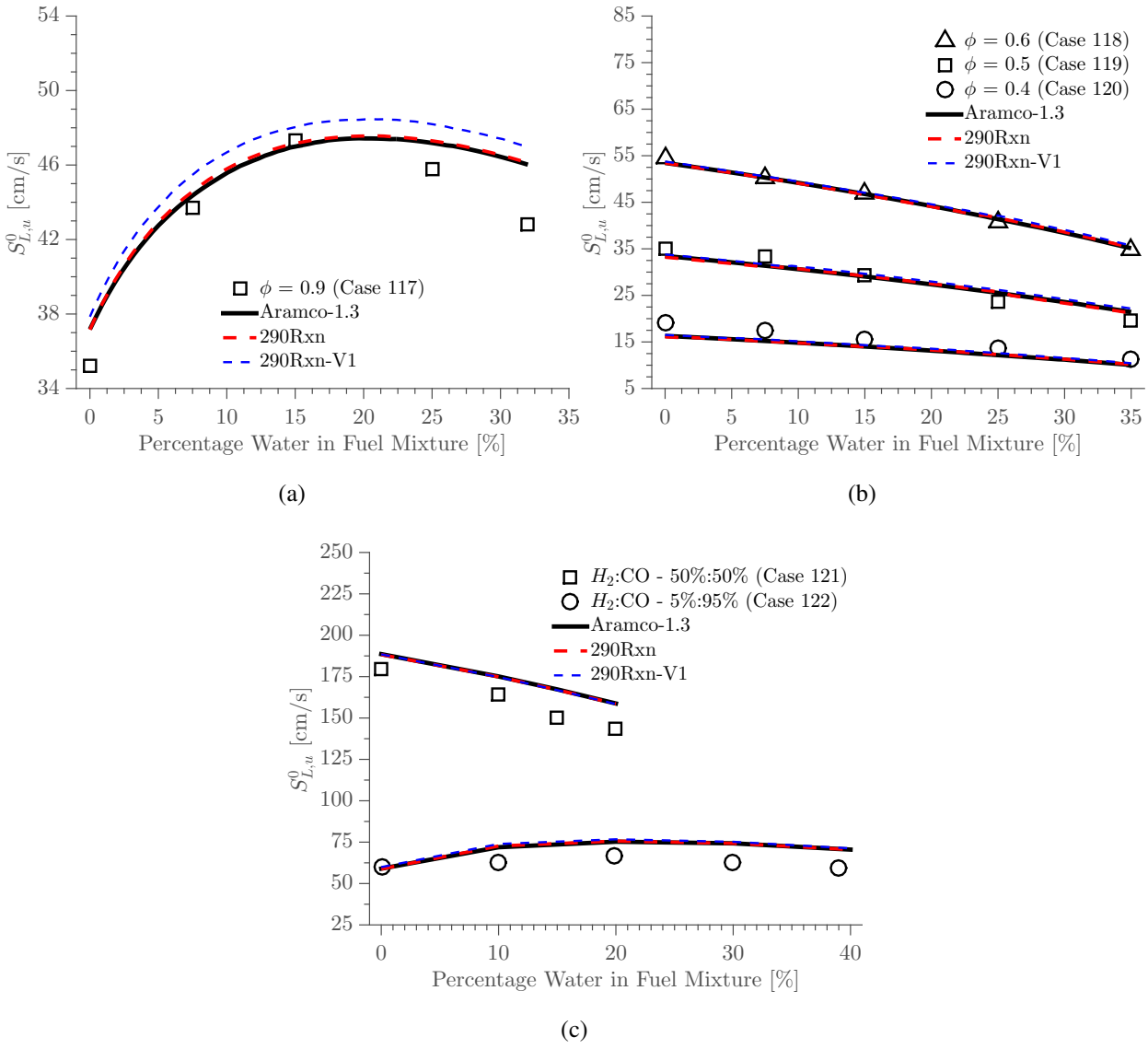

Figure B.14: Comparisons of measured and predicted laminar flame speed of $H_2/CO/H_2O$ mixtures computed using Aramco-1.3, 290Rxn, and 290Rxn-V1 mechanisms. Symbols represent experimental data; please refer to Table B.1 for references and more information on the fuel compositions and the experimental conditions.

B.2.4 Mixture combination: $H_2/CO/N_2$

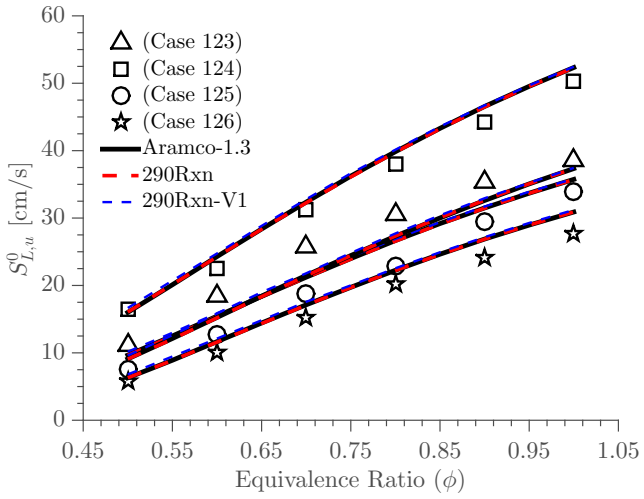

(a)

Figure B.15: Comparisons of measured and predicted laminar flame speed of $H_2/CO/N_2$ mixtures computed using Aramco-1.3, 290Rxn, and 290Rxn-V1 mechanisms. Symbols represent experimental data; please refer to Table B.1 for references and more information on the fuel compositions and the experimental conditions.

B.2.5 Mixture combination: H_2/CH_4

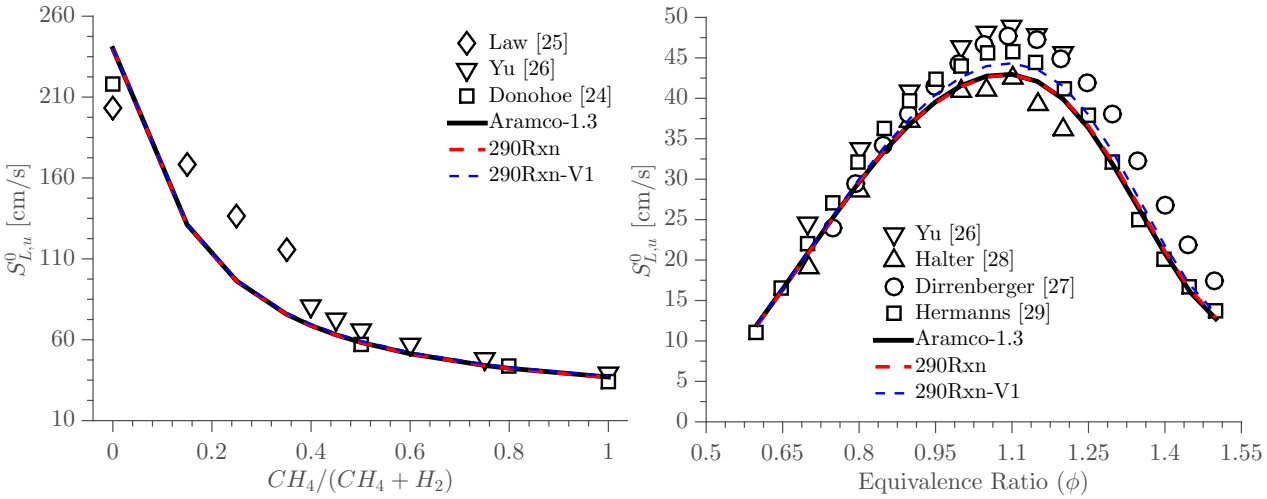

(a) Case 127

(b) Case 128

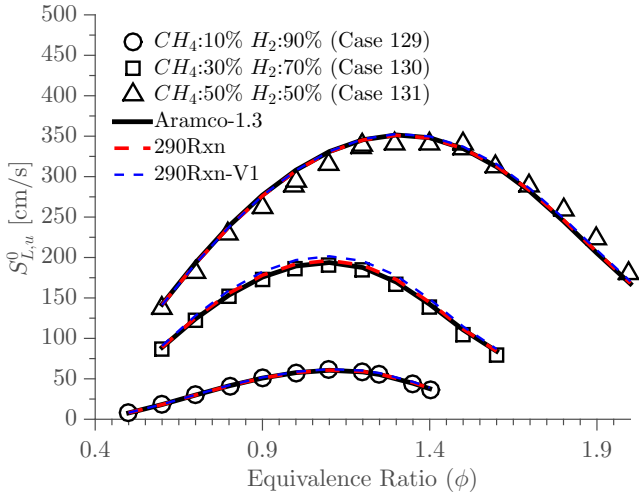

(c) Case 129 - Case 131

Figure B.16: Comparisons of measured and predicted laminar flame speed of H_2/CH_4 mixtures computed using Aramco-1.3, 290Rxn, and 290Rxn-V1 mechanisms. Symbols represent experimental data; please refer to Table B.1 for references and more information on the fuel compositions and the experimental conditions.

B.2.6 Mixture combination: $H_2/CO/CH_4/CO_2$

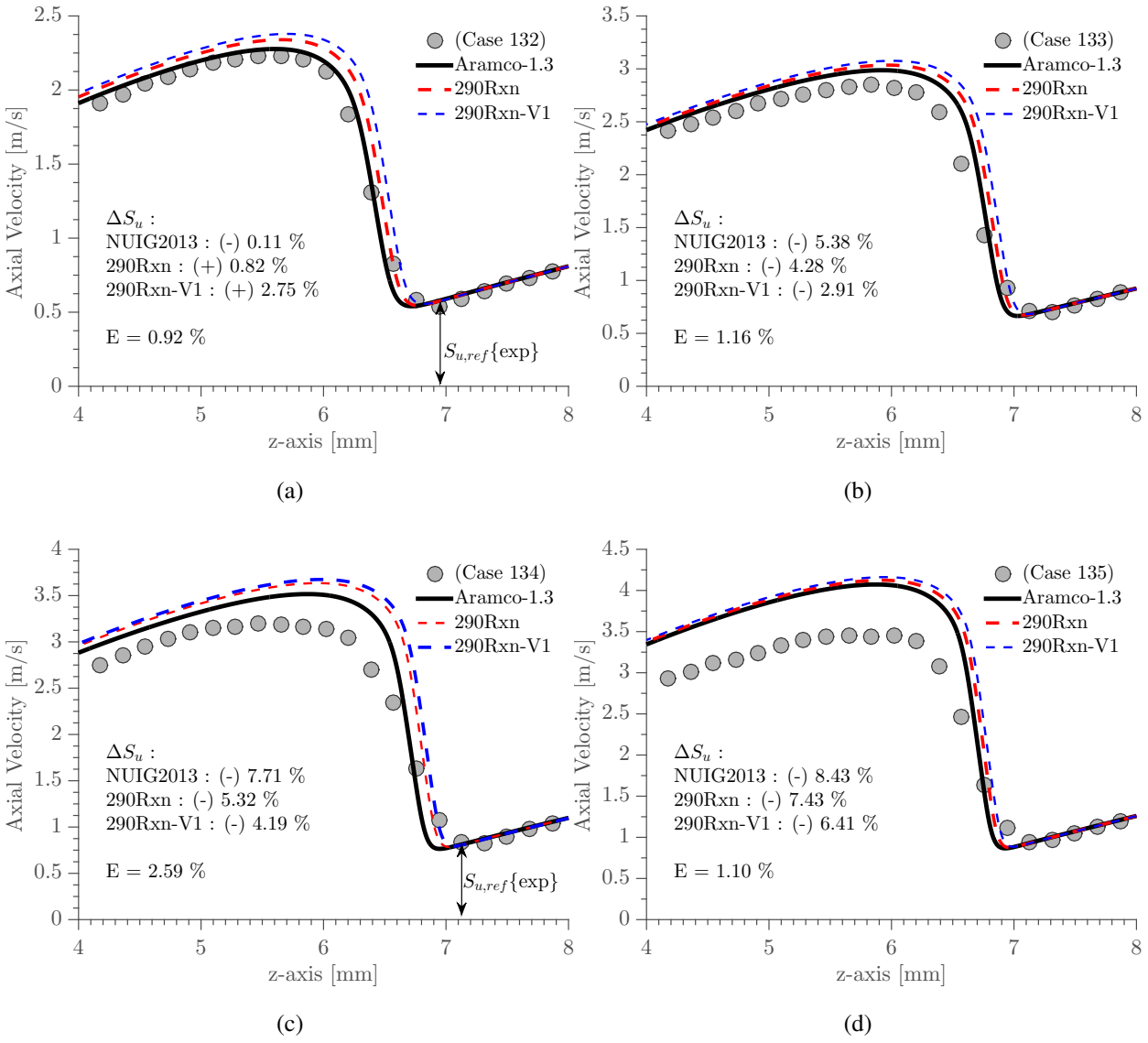

Figure B.17: Comparisons of measured and predicted laminar flame speed of $H_2/CO/CH_4/CO_2$ mixtures computed using Aramco-1.3, 290Rxn, and 290Rxn-V1 mechanisms. Symbols represent experimental data; please refer to Table B.1 for references and more information on the fuel compositions and the experimental conditions.

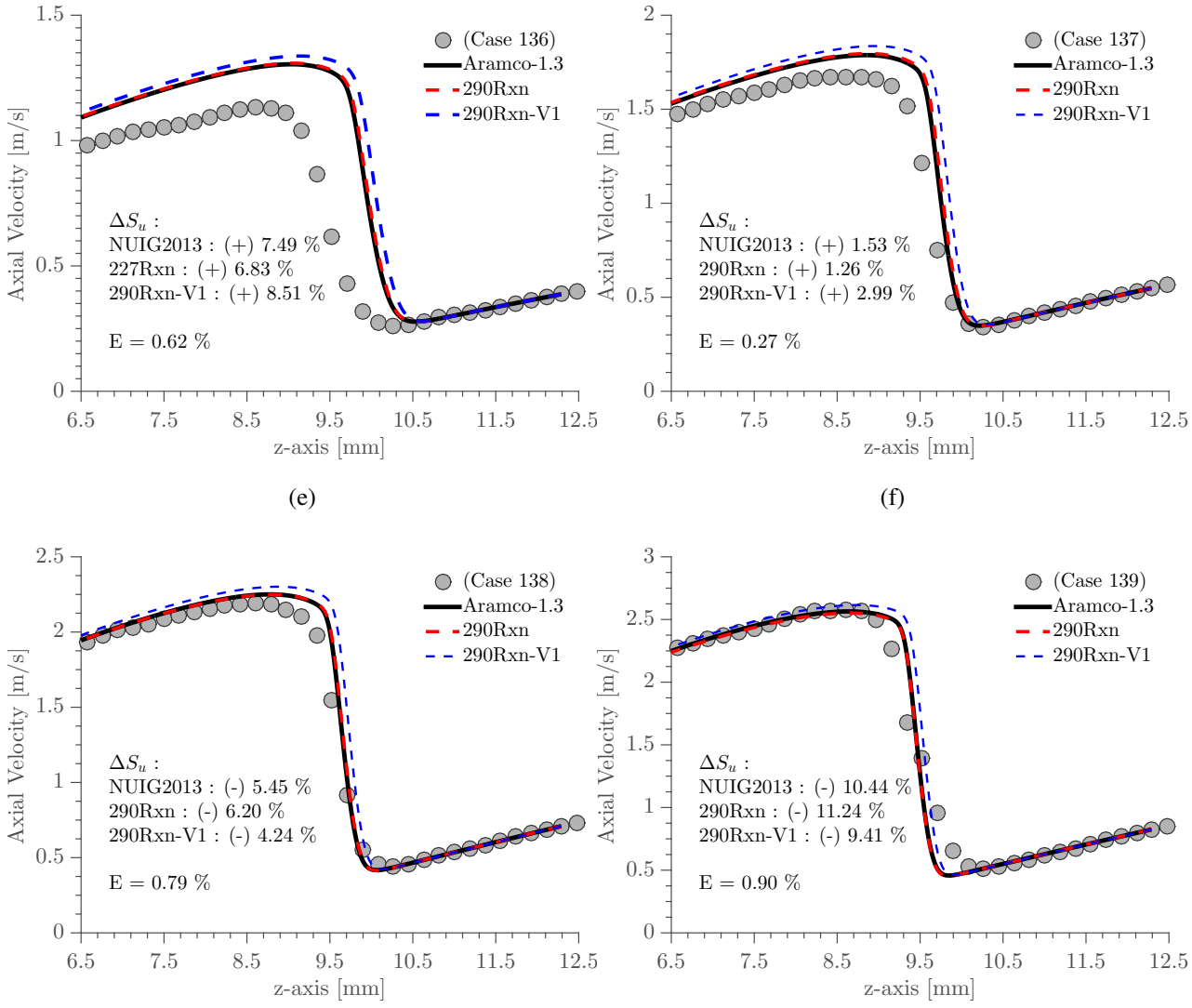

Figure B.17: Comparisons of measured and predicted laminar flame speed of $H_2/CO/CH_4/CO_2$ mixtures computed using Aramco-1.3, 290Rxn, and 290Rxn-V1 mechanisms. Symbols represent experimental data; please refer to Table B.1 for references and more information on the fuel compositions and the experimental conditions (continued).

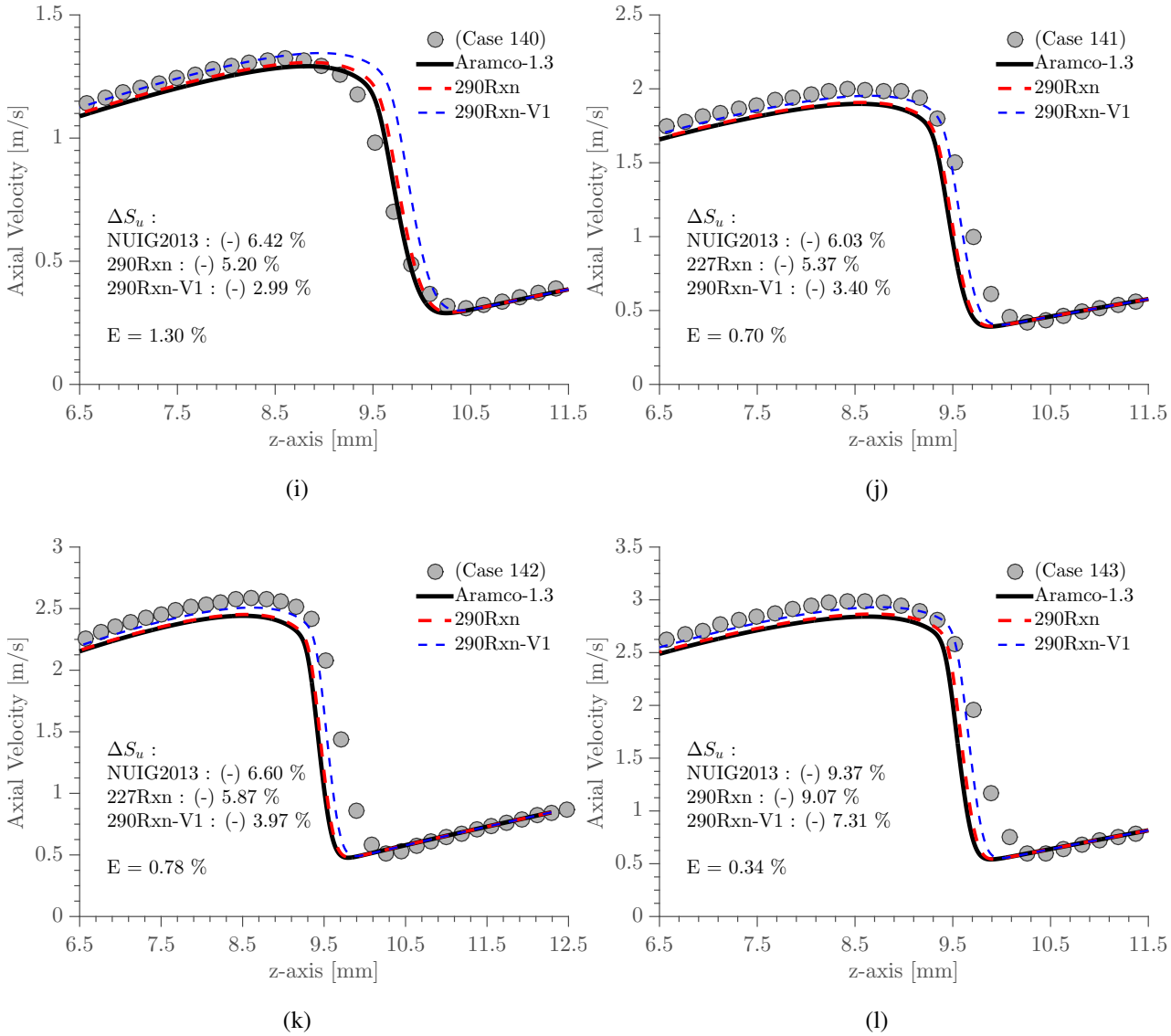

Figure B.18: Comparisons of measured and predicted laminar flame speed of $H_2/CO/CH_4/CO_2$ mixtures computed using Aramco-1.3, 290Rxn, and 290Rxn-V1 mechanisms. Symbols represent experimental data; please refer to Table B.1 for references and more information on the fuel compositions and the experimental conditions (continued).

B.2.7 Mixture combination: CH_4

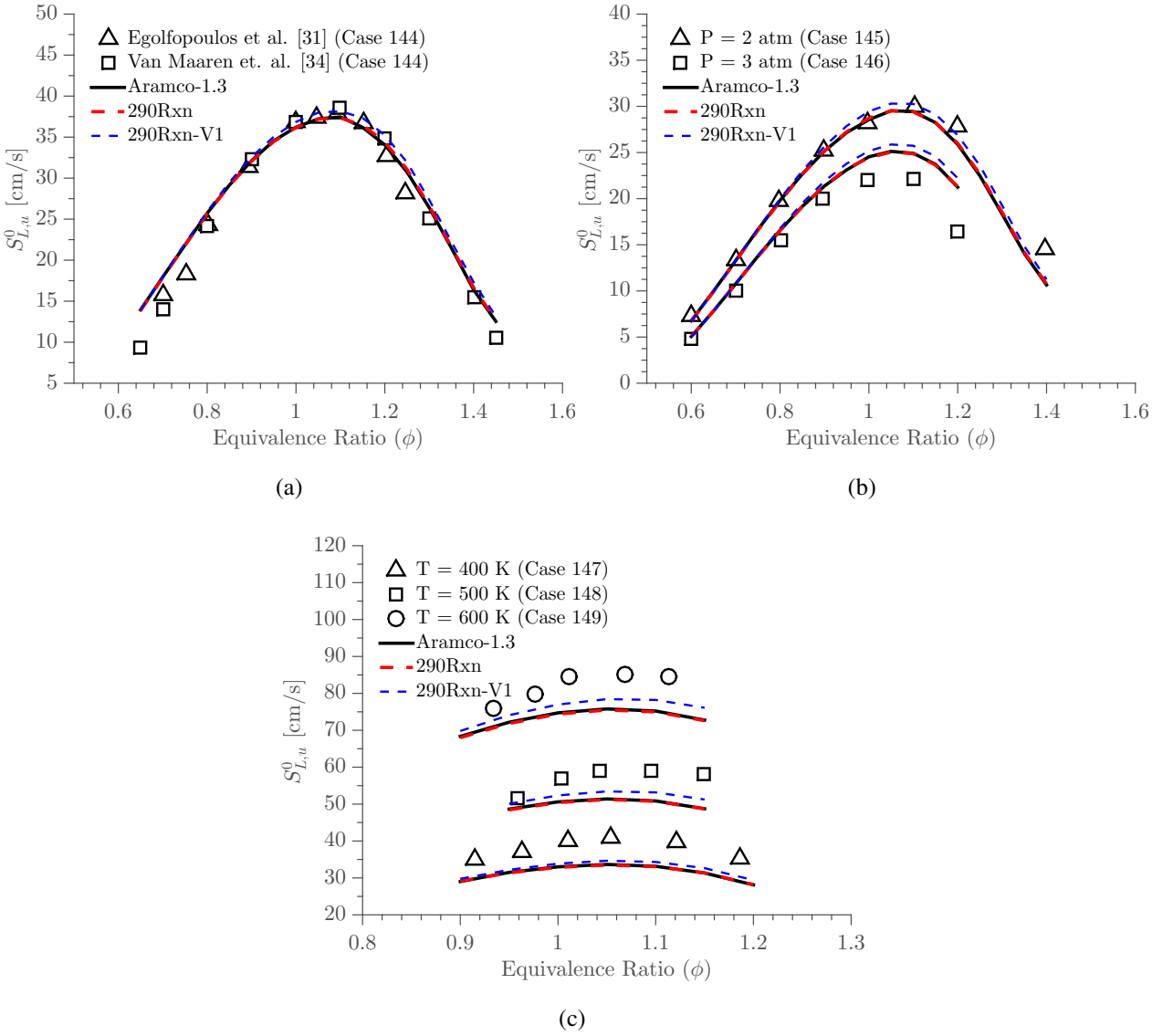

Figure B.19: Comparisons of measured and predicted laminar flame speed of CH_4 mixtures computed using Aramco-1.3, 290Rxn, and 290Rxn-V1 mechanisms. Symbols represent experimental data; please refer to Table B.1 for references and more information on the fuel compositions and the experimental conditions.

Appendix C

Code Snippets

The first script provided here shows how the logarithmic-sensitivty coefficients were calculated for the ignition delay time using Message Passing Interface (MPI). Parallelization of the code is crucial for large mechanism such as Aramco-1.3 because it contains over two thousands reactions, allowing us to conduct more analysis on different experimental conditions. The logarithm sensitivity coefficient (L.S.) for the ignition delay time results is defined as:

$$\text{L.S.} = \frac{\ln(\tau^+/\tau^-)}{\ln(k^+/k^-)} = \frac{\ln(\tau^+/\tau^-)}{\ln(4)}$$

where a positive value of the logarithm sensitivity coefficient indicates that the reaction has an inhibiting effect on the overall reactivity, and vice versa.

C.1 Sensitivity Analysis for Ignition Delay Time - Parallelized Version

```
1 from __future__ import print_function
2 from mpi4py import MPI
3 import cantera as ct
4 import os
5 import numpy as np
6 import sys
7 import inspect
8 import glob
9 filename=os.path.splitext(inspect.getfile(inspect.currentframe()))[0]
10 Mechanism=os.path.splitext(glob.glob('*.xml')[0])[0]
```

```
f1=open('./'+filename+'_Sensitivity_'+Mechanism+'.txt', 'w+')
comm = MPI.COMM_WORLD
nprocs = comm.Get_size()
myrank = comm.Get_rank()

Ign_Case= [1094, # Temperature
              16.13, # Pressure
              'CH4:0.968867071,C3H8:0.645911381;O2:20.66916419,N2:77.71605736',
    # Fuel Mixtures
              1.0e-6, # Delta-t
              6e-3, # Final Time
              3, # Type of measurements. "1": Pressure Gradient; "2": OH*
    Gradient; "3": CH* Gradient
              Mechanism]

gas = ct.Solution(Ign_Case[6]+'.xml')
gas.transport_model = 'Mix'
Num_Reac=(gas.n_reactions)

IgnTT=np.zeros((Num_Reac,6))
IgnTT_Receive=np.zeros((Num_Reac,6))

if (myrank<nprocs-1):
   istart=((Num_Reac-(Num_Reac%(nprocs-1)))/(nprocs-1))*myrank
   iend=istart+((((Num_Reac-(Num_Reac%(nprocs-1)))))/(nprocs-1))-1
else:
   istart=(Num_Reac-(Num_Reac%(nprocs-1)))
   iend=Num_Reac-1

for m in range(istart,iend+1):
   for i in range(0,2):
      gas.set_multiplier(1.0) # reset all multipliers
      if (i==0):
         gas.set_multiplier(0.5, m) # perturb reaction m
      else:
         gas.set_multiplier(2.0, m) # perturb reaction m

      tout =[]
      Tout =[]
      Pout =[]
      DTout=[]
      gas.TPX = Ign_Case[0],Ign_Case[1]*ct.one_atm,Ign_Case[2]
      r = ct.IdealGasReactor(gas)
      sim = ct.ReactorNet([r])
      time = 0.0

      sim.rtol = 1.0e-6
      sim.atol = 1.0e-15
      sim.rtol_sensitivity = 1.0e-6
      sim.atol_sensitivity = 1.0e-6

```

```
60        while time <= Ign_Case[4]:
61           if Ign_Case[5]==1:
62              Pold=r.thermo.P
63              time += Ign_Case[3]
64              sim.advance(time)
65              dt=(r.thermo.P-Pold)/Ign_Case[5]
66              tout.append(sim.time)
67              Tout.append(r.T)
68              Pout.append(r.thermo.P)
69              DTout.append(dt)
70           if Ign_Case[5]==2:
71              Yold=gas['OH*'].Y
72              time += Ign_Case[3]
73              sim.advance(time)
74              dY=(gas['OH*'].Y-Yold)
75              tout.append(time)
76              Tout.append(r.T)
77              Pout.append(r.thermo.P)
78              DTout.append(dY)
79              if Ign_Case[5]==3:
80              Yold=gas['CH*'].Y
81              time += Ign_Case[3]
82              sim.advance(time)
83              dY=(gas['CH*'].Y-Yold)
84              tout.append(time)
85              Tout.append(r.T)
86              Pout.append(r.thermo.P)
87              DTout.append(dY)
88              DTout_max = max(DTout)
89        for j in range(len(DTout)):
90           if DTout[j]==DTout_max:
91              if (i==0):
92                 IgnTT[m][0]=m
93                 IgnTT[m][1]=Ign_Case[0]
94                 IgnTT[m][2]=Tout[j]
95                 IgnTT[m][3]=tout[j]
96              else:
97                 IgnTT[m][4]=tout[j]
98
99  IgnTT=np.asarray(IgnTT)
100 IgnTT_Receive=np.asarray(IgnTT_Receive)
101
102 comm.Reduce(IgnTT,IgnTT_Receive,op=MPI.SUM)
103
104 if (myrank==0):
105    for m in range(Num_Reac):
106
       IgnTT_Receive[m][5]=(np.log(IgnTT_Receive[m][4]/IgnTT_Receive[m][3]))/(np.log(4))
107    f1.write('{: 5d}   {: 10.5e} {: 10.5e} {: 10.5e}  {}\n'.format(m,
       IgnTT_Receive[m][3], IgnTT_Receive[m][4], IgnTT_Receive[m][5],
       gas.reaction_equation(m)))
```

```
108     print('{: 5d}   {: 10.5e} {: 10.5e} {: 10.5e}  {}\n'.format(m,
        IgnTT_Receive[m][3],IgnTT_Receive[m][4], IgnTT_Receive[m][5],
        gas.reaction_equation(m)))
```

C.2 Genetic Algorithm - Parallelized Version

The second script provided shows how the reduced mechanism is obtained in Chapter 4 through Genetic Algorithm.

```
1  from mpi4py import MPI
2  import os
3  import numpy as np
4  import sys
5  import random
6  import time
7  import copy
8  import operator
9
10 # This depends on how you install cantera in the HPC cluster
11 os.chdir(os.getenv('PBS_O_WORKDIR','/home/hsulee/Project/P2_Genetic/ReduceNUIG'))
12 sys.path.append('/home/hsulee/software/cantera/lib/python2.7/site-packages')
13
14 import cantera as ct
15 import ctml_writer
16 import gc
17
18 def chunks(l, n):
19     if n < 1:
20         n = 1
21     return [l[i:i + n] for i in range(0, len(l), n)]
22
23
24 def createPop(Num_Population,Num_Reac,choice,Num_off):
25    if choice==1:
26       Pop= [[1 for x in range(Num_Reac)] for x in xrange(Num_Population)]
27    if choice==2:
28       Pop= [[1 for x in range(Num_Reac)] for x in xrange(Num_Population)]
29       for y in range(Num_Population):
30          for k in range(Num_off):
31             x=random.randint(0,Num_Reac-1)
32             Pop[y][x]=0
33    return Pop
34 def Chrom2Reac(Num_Population,Num_Reac,Pop,Pop0):
35    Population= [["" for x in range(Num_Reac)] for x in xrange(Num_Population)]
36    for i in range(Num_Population):
37       for j in range(Num_Reac):
```

```
38
39          if Pop[i][j]==1:
40             Population[i][j]=Pop0[j]
41          else:
42             Population[i][j]=""
43    return Population
44
45 def WritePop(Num_Population,Start_Reac,data,Population):
46    for iii in range(0,Num_Population):
47       NewData=data[0:Start_Reac]+Population[iii][:]
48       Pop0=open('Population_%d' % iii +'.cti','w')
49       for i in range(0, len(NewData)):
50          Pop0.write(NewData[i])
51          Pop0.write("\n")
52       Pop0.close()
53
54 def compute_Ign(Temp,Pressure,Species,deltat,tend,selection,mech):
55    gri3 = ct.Solution(mech)
56    IgnTT=np.zeros(3)
57
58    tout =[]
59    Tout =[]
60    Pout =[]
61    DTout=[]
62
63    gri3.TPX = Temp,Pressure*ct.one_atm,Species
64    r = ct.IdealGasReactor(gri3)
65    sim = ct.ReactorNet([r])
66    time = 0.0
67
68    while time <= tend:
69
70       if selection==1:
71          Pold=r.thermo.P
72          time += deltat
73          sim.advance(time)
74          dt=(r.thermo.P-Pold)/deltat
75          tout.append(sim.time)
76          Tout.append(r.T)
77          Pout.append(r.thermo.P)
78          DTout.append(dt)
79       if selection==2:
80          Yold=gri3['OH*'].Y
81          time += deltat
82          sim.advance(time)
83          dY=(gri3['OH*'].Y-Yold)
84          tout.append(time)
85          Tout.append(r.T)
86          Pout.append(r.thermo.P)
87          DTout.append(dY)
88    m = max(DTout)
```

```
89    for j in range(len(DTout)):
90       if DTout[j]==m:
91          IgnTT[0]=Tout[j]
92          IgnTT[1]=tout[j]
93          IgnTT[2]=Temp
94
95    del gri3
96    del r
97    del sim
98    gc.collect()
99
100   return IgnTT
101
102 def TournamentSelection(Total_Ign,tournamentSize=2):
103   popSize = len(Total_Ign)
104   individuals= []
105
106   indices = range(popSize)
107   random.shuffle(indices)
108   for i in range(tournamentSize):
109      individuals.append(Total_Ign[indices[i]])
110
111   individuals=sorted(individuals,key=operator.itemgetter(1),reverse=False)
112   print
      indices[0],Total_Ign[indices[0]][1],indices[1],Total_Ign[indices[1]][1],individuals[0]
113   return individuals[0]
114
115 def Crossover(cx,Population,Cross_Rate):
116   NewPop=[[0 for x in range(len(Population[1]))] for x in
      xrange(len(Population))]
117   if cx==1:
118      for i in range(len(Population)-1,-1,-1):
119         cxpoint=random.randint(0,len(Population[0]))
120         if i==0:
121            NewPop[i][:]=Population[i][:]
122         else:
123            if (random.random() <= Cross_Rate):
124               NewPop[i][:]=Population[0][:cxpoint]+Population[i][cxpoint:]
125            else:
126               NewPop[i][:]=Population[i][:]
127   return NewPop
128
129 def Mutation(cM,mutation_rate,Population):
130   if cM==1:
131      for i in range(0,len(Population)):
132         for j in range(0,len(Population[i])):
133            x=random.random()
134            if (x <= mutation_rate):
135               Population[i][j]=0
136   return Population
137 #=========================================================================#
```

```
138 #                              User Input
        #
139 #================================================================================#
140 Mechanism='AramcoMech_1.3_C5chem.cti'
141 Ori_Mech='AramcoMech_1.3_C5chem.xml'
142 npoints=3
143 sigma_ign=1.0
144 sigma_reac=3.0
145 lamda_reac=0.60
146 Mutation_Rate=0.03
147 Cross_Rate = 0.4
148 Generations=3000
149 Num_Population=24
150 StartFrom=0
151 mpi_x=6# Processors for Num of Populations
152 mpi_y=30 # Processors for Num of Cases
153 mpi_z=3 # Processors for Num of Points in each Cases
154 f2=open('Population_Generated.txt','w+')
155 f3=open('Population_Ign.txt','w+')
156 f4=open('FullData_Iteration.txt','w+')
157
158
159 Ign_Case=[  [2000,990
    ,npoints,1.62,'H2:0.5,CO:0.5,O2:1.0,AR:98.00',1.e-6,6e-3,2],
160
    [1385,1095,npoints,11.9,'H2:0.5,CO:0.5,O2:1.0,AR:98.00',1e-6,2e-3,2],
161             [1330,1170,npoints,32.2,'H2:0.5,CO:0.5,O2:1.0,AR:98.00',1e-6,2e-3,2],
162             [2010,995
    ,npoints,1.75,'H2:0.444,CO:0.444,O2:0.889,H2O:0.223,AR:98.00',
163                 1e-6,7e-3,2],
164
    [1400,1085,npoints,12.2,'H2:0.444,CO:0.444,O2:0.889,H2O:0.223,AR:98.00',
165                 1e-6,5e-3,2],
166
    [1300,1155,npoints,32.2,'H2:0.444,CO:0.444,O2:0.889,H2O:0.223,AR:98.00',
167                 1e-6,2e-3,2],
168             [1965,1005,npoints,1.72,'H2:0.46,CO:0.46,O2:0.93,CO2:0.15,AR:98.00',
169                 1e-6,7e-3,2],
170             [1360,1105,npoints,12.7,'H2:0.46,CO:0.46,O2:0.93,CO2:0.15,AR:98.00',
171                 1e-6,2e-3,2],
172             [1290,1150,npoints,31.4,'H2:0.46,CO:0.46,O2:0.93,CO2:0.15,AR:98.00',
173                 1e-6,4e-3,2],
174             [1177,952
    ,npoints,1.24,'H2:8.91,CO:11.58,O2:10.25,CO2:24.44,N2:44.83',
175                 1e-6,3e-2,2],
176             [1145,975
    ,npoints,1.71,'H2:8.91,CO:11.58,O2:10.25,CO2:24.44,N2:44.83',
177                 1e-6,3e-2,2],
178
    [1091,1010,npoints,2.36,'H2:8.91,CO:11.58,O2:10.25,CO2:24.44,N2:44.83',
179                 1e-6,7e-3,2],
```

```
180
    [2030,1050,npoints,1.77,'H2:0.29659,CO:0.29659,O2:0.95013,CH4:0.08924,
181                  CO2:0.15748,H2O:0.20997,AR:98.00',1e-6,10e-3,2],
182
    [1450,1160,npoints,12.3,'H2:0.29659,CO:0.29659,O2:0.95013,CH4:0.08924,
183                  CO2:0.15748,H2O:0.20997,AR:98.00',1e-6,10e-3,2],
184
    [1305,1185,npoints,30.7,'H2:0.29659,CO:0.29659,O2:0.95013,CH4:0.08924,
185                  CO2:0.15748,H2O:0.20997,AR:98.00',1e-6,10e-3,2],
186
    [1920,1010,npoints,1.73,'H2:0.406,CO:0.406,O2:1.113,CH4:0.075,AR:98.00',
187                  1e-6,10e-3,2],
188
    [1410,1145,npoints,12.1,'H2:0.406,CO:0.406,O2:1.113,CH4:0.075,AR:98.00',
189                  1e-6,10e-3,2],
190
    [1320,1155,npoints,31.1,'H2:0.406,CO:0.406,O2:1.113,CH4:0.075,AR:98.00',
191                  1e-6,10e-3,2],
192
    [1300,1060,npoints,5,'H2:1.856,O2:3.713,CH4:0.464,AR:93.967',1e-6,6e-3,2],
193
    [1400,1116,npoints,5,'H2:1.046,O2:3.834,CH4:0.697,AR:94.423',1e-6,10e-3,2],
194
    [1700,1222,npoints,5,'H2:0.558,O2:3.907,CH4:0.837,AR:94.698',1e-6,10e-3,2],
195
    [1850,1380,npoints,5,'H2:0.233,O2:3.956,CH4:0.931,AR:94.88',1e-6,10e-3,2],
196
    [1275,1060,npoints,10,'H2:1.856,O2:3.713,CH4:0.464,AR:93.967',1e-6,10e-3,2],
197
    [1395,1075,npoints,10,'H2:1.046,O2:3.834,CH4:0.697,AR:94.423',1e-6,30e-3,2],
198
    [1780,1155,npoints,10,'H2:0.558,O2:3.907,CH4:0.837,AR:94.698',1e-6,0.01,2],
199
    [1800,1295,npoints,10,'H2:0.233,O2:3.956,CH4:0.931,AR:94.88',1e-6,7e-3,2],
200
    [1492,1025,npoints,20,'H2:1.856,O2:3.713,CH4:0.464,AR:93.967',1e-6,0.015,2],
201
    [1552,1072,npoints,20,'H2:1.046,O2:3.834,CH4:0.697,AR:94.423',1e-6,0.015,2],
202
    [1625,1140,npoints,20,'H2:0.558,O2:3.907,CH4:0.837,AR:94.698',1e-6,0.015,2],
203
    [2000,1215,npoints,20,'H2:0.233,O2:3.956,CH4:0.931,AR:94.88',1e-6,0.015,2]]
204
205
206 #=========================================================================#
207 #                    End of User Input
208 #=========================================================================#
209
210 Temp=np.zeros((len(Ign_Case),Ign_Case[0][2]))
211 Pressure=np.zeros((len(Ign_Case),Ign_Case[0][2]))
212 Species=[["" for x in range(Ign_Case[0][2])] for x in xrange(len(Ign_Case))]
```

```
deltat=np.zeros((len(Ign_Case),Ign_Case[0][2]))
Tend=np.zeros((len(Ign_Case),Ign_Case[0][2]))
Sel=np.zeros((len(Ign_Case),Ign_Case[0][2]))
Mecha=[[["" for x in range(Ign_Case[0][2])] for x in xrange(len(Ign_Case))] for
    x in xrange(Num_Population)]
Temp1=np.zeros((Num_Population,len(Ign_Case),Ign_Case[0][2]))
Pressure1=np.zeros((Num_Population,len(Ign_Case),Ign_Case[0][2]))
Species1=[[["" for x in range(Ign_Case[0][2])] for x in xrange(len(Ign_Case))]
    for x in xrange(Num_Population)]
deltat1=np.zeros((Num_Population,len(Ign_Case),Ign_Case[0][2]))
Tend1=np.zeros((Num_Population,len(Ign_Case),Ign_Case[0][2]))
Sel1=np.zeros((Num_Population,len(Ign_Case),Ign_Case[0][2]))
for k in range(Num_Population):
   for i in range(len(Ign_Case)):
      for j in range(Ign_Case[0][2]):

    Temp[i][j]=Ign_Case[i][0]-(Ign_Case[i][0]-Ign_Case[i][1])*j/(Ign_Case[0][2]-1)
         Pressure[i][j]=Ign_Case[i][3]
         Species[i][j]=Ign_Case[i][4]
         deltat[i][j]=Ign_Case[i][5]
         Tend[i][j]=Ign_Case[i][6]
         Sel[i][j]=Ign_Case[i][7]


    Temp1[k][i][j]=Ign_Case[i][0]-(Ign_Case[i][0]-Ign_Case[i][1])*j/(Ign_Case[0][2]-1)
         Pressure1[k][i][j]=Ign_Case[i][3]
         Species1[k][i][j]=Ign_Case[i][4]
         deltat1[k][i][j]=Ign_Case[i][5]
         Tend1[k][i][j]=Ign_Case[i][6]
         Sel1[k][i][j]=Ign_Case[i][7]
         Mecha[k][i][j]='Population_%d' % k +'.xml'
#==============================================================================#
#                                 MPI Communication World                      #
#==============================================================================#
comm = MPI.COMM_WORLD
nprocs = comm.Get_size()
myrank = comm.Get_rank()
ccomm = comm.Create_cart( (mpi_x, mpi_y,mpi_z), periods=(True, True,True),
    reorder=True)
my_x, my_y,my_z = ccomm.Get_coords( ccomm.rank )
Chunk=chunks(range(0,Num_Population),mpi_x)
#==============================================================================#
#                                 End of the MPI Communication World           #
#==============================================================================#
results=compute_Ign(Temp[my_y][my_z],
                        Pressure[my_y][my_z],
                        Species[my_y][my_z],
                        deltat[my_y][my_z],
                        Tend[my_y][my_z],
                        Sel[my_y][my_z],Ori_Mech)
comm.Barrier()
```

```
Ori_Ign=copy.deepcopy(comm.gather(results,root=0))
if myrank ==0:
   X_Ori=np.zeros((len(Ign_Case),5,3))
   P_Ign=np.zeros((Generations,Num_Population,len(Ign_Case),5,3))
   counter=0
   for j in range (mpi_y):
      for k in range (mpi_z):
         X_Ori[j][k][0]=Ori_Ign[counter][0]
         X_Ori[j][k][1]=Ori_Ign[counter][1]
         X_Ori[j][k][2]=Ori_Ign[counter][2]
         counter=counter+1

#=============================================================================#
#           End: Computing Original Mechanism's Ignition Delay Time
#                    [No Manipulation of Mech]
#=============================================================================#
if myrank==0:
   gas = ct.Solution(Ori_Mech)
   Num_Reac=gas.n_reactions
   del gas
   data=[line.rstrip() for line in open(Mechanism)]
   #Find the Starting Point of Reactions in *cti File
   for i in range(0, len(data)):
      if 'Reaction data' in data[i]:
            Start_Reac=i+2
   # Find the Find Reactions Array in *cti File
   Reac=(np.array([]))
   for j in range(Start_Reac, len(data)):
      if 'Reaction' in data[j]:
         Reac=np.append(Reac,j)
         Reac=Reac.astype(np.int64)
   # Convert reactions to single string for randomization
   k=0
   Pop0= ["" for x in range(Num_Reac)]
   for ii in range(0,Num_Reac):
      if ii==Num_Reac-1:
         for jj in range(Reac[-1]+1,len(data)):
            Pop0[Num_Reac-1]=Pop0[Num_Reac-1]+data[jj]
      else:
         for jj in range(Reac[ii]+1,Reac[ii+1]):
            Pop0[k]=Pop0[k]+data[jj]
      k=k+1
   ReactionArray=copy.deepcopy(Pop0)
else:
   pass
#=============================================================================#
#            End: Organizing Reactions into Arrays
#=============================================================================#

if myrank==0:
   # Randomizing the Reactions to create Initial Populations.
```

```
310    # No reactions are "turned off" during the 1st Generation.
311    Population= [["" for x in range(Num_Reac)] for x in xrange(Num_Population)]
312    OffSpring=[[2 for x in range(Num_Reac)] for x in xrange(Num_Population)]
313    PopArray=createPop(Num_Population,Num_Reac,1,0)
314    Population=Chrom2Reac(Num_Population,Num_Reac,PopArray,ReactionArray)
315    WritePop(Num_Population,Start_Reac,data,Population)
316
317    for i in range(0,Num_Population):
318       ctml_writer.convert('Population_%d' % i +'.cti')
319       reload(ctml_writer)
320    oldPopulation=copy.deepcopy(Population)
321    oldPopArray=copy.deepcopy(PopArray)
322 else:
323    pass
324
325 comm.Barrier()
326 #=============================================================================#
327 #            End of Initialization
328 #=============================================================================#
329 if myrank==0:
330    Fit_Ign=np.zeros((Generations,Num_Population,len(Ign_Case),Ign_Case[0][2],2))
331    Fit_NumReac=np.zeros((Generations,Num_Population,1))
332    RReac=np.ones((Generations,len(Population)))*Num_Reac
333    Total_Ign=np.zeros((Generations,Num_Population,3))
334    OverallFittest=[]
335    icount=0
336 #=============================================================================#
337 #            Starting of Genetic Algorithm
338 #=============================================================================#
339 comm.Barrier()
340 start=time.time()
341 for num_gen in range(0,Generations):
342    if myrank==0:
343       print
    '#=============================================================================#'
344       print '                Start of Generation: %d' % num_gen
345       print '                Min (# of Reaction): %d' % np.min(RReac[num_gen-1])
346
347
348        #Store Population Generated from Each Generation
349       gen_write=num_gen+StartFrom
350       f2.write('Generation: %d \n'% gen_write)
351       f2.write('\n')
352       for i in range(len(PopArray)):
353          a=''
354          for j in range(len(PopArray[0])):
355             a=a+str(PopArray[i][j])+','
356          f2.write('Pop #%d:\t' %(i))
357          f2.write(a)
358          f2.write('\n')
359       for i in range(Num_Population):
```

```
360                RReac[num_gen][i]=PopArray[i].count(1.0)
361    else:
362       pass
363    comm.Barrier()
364    for i in range(len(Chunk)):
365       da=my_x+(mpi_x*i)
366       Presults=compute_Ign(Temp1[da][my_y][my_z],\
367                            Pressure1[da][my_y][my_z],\
368                             Species1[da][my_y][my_z],\
369                              deltat1[da][my_y][my_z],\
370                                Tend1[da][my_y][my_z],\
371                                 Sel1[da][my_y][my_z],\
372                                Mecha[da][my_y][my_z])
373       gc.collect()
374       comm.Barrier()
375       Pop_Ign=comm.gather(Presults,root=0)
376
377       if myrank ==0:
378
379          counter=0
380          for ix in range(mpi_x):
381             for jx in range (mpi_y):
382                for kx in range (mpi_z):
383                   da0=Chunk[i][ix]
384                   P_Ign[num_gen][da0][jx][kx][0]=Pop_Ign[counter][0]
385                   P_Ign[num_gen][da0][jx][kx][1]=Pop_Ign[counter][1]
386                   P_Ign[num_gen][da0][jx][kx][2]=Pop_Ign[counter][2]
387                   counter=counter+1
388                   f3.write('%d\t%d\t%d\t%d\t%f\t%f\t%f'% (num_gen+StartFrom,
389                               da0,
390                               jx,
391                               kx,
392                               P_Ign[num_gen][da0][jx][kx][0],
393                               P_Ign[num_gen][da0][jx][kx][1],
394                               P_Ign[num_gen][da0][jx][kx][2]))
395                   f3.write('\n')
396    if myrank==0:
397       Tout_Ign=[]
398       Tout_Ign1=[]
399       for iv in range(0,Num_Population):
400          for jv in range(0,mpi_y):
401             for kv in range(0,mpi_z):
402                Fit_Ign[num_gen][iv][jv][kv][0]=np.log(1+sigma_ign*
403
    abs((P_Ign[num_gen][iv][jv][kv][0]-X_Ori[jv][kv][0])
404                                        /(X_Ori[jv][kv][0]-X_Ori[jv][kv][2])))
405                Fit_Ign[num_gen][iv][jv][kv][1]=np.log(1+sigma_ign
406                                        *abs(
    (P_Ign[num_gen][iv][jv][kv][1]-X_Ori[jv][kv][1])
407                                        /(X_Ori[jv][kv][1]) ) )
408          Fit_NumReac[num_gen][iv][0]=1/(1+np.exp(sigma_reac
```

```
                                        *(1-(RReac[num_gen][iv]/
                                        (lamda_reac*Num_Reac)))))
      for iw in range(0,Num_Population):
         sum1=[0.0,0.0]
         for jw in range(0,mpi_y):
            sum1=sum1+sum(Fit_Ign[num_gen][iw][jw])
            Total_Ign[num_gen][iw][0]=sum1[0]
            Total_Ign[num_gen][iw][1]=sum1[1]
         Total_Ign[num_gen][iw][2]=Total_Ign[num_gen][iw][0]+
                                          Total_Ign[num_gen][iw][1]+
                                          Fit_NumReac[num_gen][iw][0]
         Tout_Ign.append([iw,Total_Ign[num_gen][iw][2]])
      for ie in range(Num_Population):
         ax=TournamentSelection(Tout_Ign)
         Tout_Ign1.append(Tout_Ign[ax[0]])
      Tout_Ign1=sorted(Tout_Ign1,key=operator.itemgetter(1),reverse=False)
      OverallFittest.append([num_gen,Tout_Ign1[0][0],Tout_Ign1[0][1]])
      for ir in range(Num_Population):
         OffSpring[ir]=PopArray[Tout_Ign1[ir][0]]
      OffSpring=Crossover(1,OffSpring,Cross_Rate)
      OffSpring=Mutation(1,Mutation_Rate,OffSpring)
      PopArray=OffSpring
      Population=Chrom2Reac(Num_Population,Num_Reac,PopArray,ReactionArray)
      WritePop(Num_Population,Start_Reac,data,Population)
      for iz in range(0,Num_Population):
         ctml_writer.convert('Population_%d' % iz +'.cti')
         reload(ctml_writer)
      print '                End of Generation  : %d' % num_gen
      print '                Min (# of Reaction): %d' % np.min(RReac[num_gen])
      print
    '#=============================================================================#'
      icount=icount+1
      gc.collect()
   else:
      gc.collect()
      pass
end=time.time()-start
comm.Barrier()
f5=open('FinalFullData.txt','w+')
f6=open('FinalFullData_Display.txt','w+')
f7=open('OverallFittest_Generated.txt','w+')
#=============================================================================#
#              End of Calculation, Starting to write all data to file
#=============================================================================#
if myrank==0:
   print end
   for i in range(Generations):
      for j in range(mpi_y):
         for k in range(Num_Population):
            for w in range(mpi_z):

```

```
    f5.write('%2d\t%3d\t%4d\t%3d\t\t%f\t\t%f\t\t%f\t%f\t\t%f\t%f\t%f\t%f\t%f\t%6d'%(
459
    i+StartFrom,j,k,w,P_Ign[i][k][j][w][2],P_Ign[i][k][j][w][0],
460                             P_Ign[i][k][j][w][1],X_Ori[j][w][0],X_Ori[j][w][1],
461                             abs(P_Ign[i][k][j][w][0]-X_Ori[j][w][0]),
462                             abs(P_Ign[i][k][j][w][1]-X_Ori[j][w][1]),
463
    Fit_Ign[i][k][j][w][0],Fit_Ign[i][k][j][w][1],RReac[i][k])
464                             )
465                 f5.write('\n')
466 #=============================================================================#
467 #               End of GA
468 #=============================================================================#
```

Appendix D

290Rxn Mechanism

The mechanism provided here is the 290Rxn mechanism in Chemkin format.

```
!-------------------------------------------------------------------------------!
ELEMENTS
C H N O AR HE
END
!-------------------------------------------------------------------------------!
SPECIES
H               H2              O               O2
OH              OH*             H2O             N2
HO2             H2O2            AR              CO
CO2             HE              HCO             C
H2CC            HCCO            HOCH2O          HOCHO
HCOH            CH              CH2             CH2(S)
CH3             CH4             CH2O            CH2CHO
CH2CO           CH2OH           CH3CHO          CH3O
CH3OH           C3H5O           CH3O2H          CH3OCO
CH3OCH3         CH3OCH2         CH3CHCO         CH3COCH2
CH3O2           CH3CO           C2H             C2H2
C2H3            C2H4            C2H5            C2H6
C2H5O           C2H3OH          C2H5O2          C2H5OH
C2H3CHO         C2H3CO          C2H3O1-2        C2H4O1-2
C3H3            C3H4-A          C3H4-P          C3H5-A
C3H5-T          C3H6            IC3H7           NC3H7
C3H8            C4H2            C4H3-I          SC4H9
PC2H4OH         SC2H4OH         O2CHO           CH*
END
!-------------------------------------------------------------------------------!
REACTIONS

!REF:HONG ET AL., PROC. COMBUST.INST. 33(1) (2011) 309316.
H+O2<=>O+OH                           1.04E+14      0.00        15286
```

```
31
32 !REF:SUTHERLAND ET AL., 21ST SYMPOSIUM, P. 929 (1986)
33 O+H2<=>H+OH                            5.080E+04     2.67        6.292E+03
34
35 !REF:LAM ET AL. (STANFORD) SUBMITTED TO IJCK (2012)
36 OH+H2<=>H+H2O                          4.38E+13      0.0         6990.0
37
38 !REF:SUTHERLAND ET AL., 23RD SYMPOSIUM, P. 51 (1990)
39 O+H2O<=>OH+OH                          2.97E+06      2.02         1.340E+04
40
41 !REF:TSANG AND HAMPSON, J. PHYS. CHEM. REF. DATA, 15:1087 (1986)
42 H2+M<=>H+H+M                            4.577E+019    -1.400  104400.0
43 H2/ 2.50/ H2O/ 12.00/ CO/ 1.90/ CO2/ 3.80/ HE/ 0.83/ CH4/ 2.00/ C2H6/ 3.00/
44 O+O+M<=>O2+M                           6.165E+015    -0.500       0.0
45 H2/ 2.50/ H2O/ 12.00/ AR/ 0.83/ CO/ 1.90/ CO2/ 3.80/ HE/ 0.83/ CH4/ 2.00/ C2H6/
       3.00/
46 O+H+M<=>OH+M                           4.714E+018    -1.000       0.0
47 H2/ 2.50/ H2O/ 12.00/ AR/ 0.75/ CO/ 1.50/ CO2/ 2.00/ HE/ 0.75/ CH4/ 2.00/ C2H6/
       3.00/
48
49
50 !REF: LI INT. J. CHEM. KINET. 36(10) (2004) 566575.
51 H+OH+M<=>H2O+M                          3.5E+22      -2.000        0.000E+00
52 !REF:efficiencies: GRI 3.0
53 H2/ 0.73/ H2O/ 3.65/ CH4/ 2.00/ C2H6/ 3.00/ AR/ 0.38/
54
55 !--------------- H+O2(+M) = HO2 (+M)-----------------------------------
56 !REF: FERNANDES ET AL.,PHYS. CHEM. CHEM. PHYS. 10(29) (2008) 43134321
57 H+O2(+M)<=>HO2(+M)                      4.650E+12     0.440        0.000E+00
58 LOW / 1.737E+19    -1.23         0.000E+00 /
59 TROE / 0.67 1E-30 1E30 1E30 /
60 H2/ 1.30/ CO/ 1.90/ CO2/ 3.80/ HE/ 0.00/ H2O/ 10.00/ AR/ 0.00/ CH4/ 2.00/ C2H6/
       3.00/
61
62 H+O2(+HE)<=>HO2(+HE)                    4.650E+12    0.440        0.000E+00
63 LOW / 9.192E+18   -1.20         0.000E+00 /  ! FERNANDES X 1.5
64 TROE / 0.59 1E-30 1E30 1E30 /
65
66 H+O2(+AR)<=>HO2(+AR)                    4.650E+12    0.440        0.000E+00
67 !REF: BATES ET AL. PHYS. CHEM. CHEM. PHYS. 3(12) (2001) 23372342.
68 LOW / 6.810E+18    -1.200       0.0/
69 TROE /0.70 1.0E-30 1.0E+30 1.0E+30/
70 !-------------------------------------------------------------------------
71
72 !REF MUELLER ET AL., INT. J. CHEM. KINET. 31(10) (1999) 705724.
73 HO2+H<=>OH+OH                           7.079E+13    0.00          2.950E+02
74
75 !REF: MICHAEL ET AL., PROC. COMBUST. INST. 28(2) (2000) 14711478.
76 H2+O2<=>H+HO2                           5.176E+05    2.433          53502.0
77
78 !REF:BAULCH ET AL., J. PHYS. CHEM. REF DATA, 21(3) (1992) 411-734
```

```
79 HO2+O<=>OH+O2                          3.250E+13    0.000          0.000E+00
80
81 !REF:KEYSER, J. PHYS. CHEM. 92 (1988) 11931200. REDUCED BY 15%
82 HO2+OH<=>H2O+O2                        2.456E+13    0.000         -4.970E+02
83 !
84 !REF:HIPPLER ET AL., J. CHEM. PHYS. 93(3) (1990) 17551760.
85 HO2+HO2 = O2+H2O2                      1.300E+11    0.000          -1630.00
86 DUPLICATE
87 HO2+HO2 = O2+H2O2                      3.658E+14    0.000          12000.00
       !HIPPLER X 0.87
88 DUPLICATE
89
90 !--------------------- H2O2(+M) = OH+OH(+M)----------------------
91 !REF:troe, combust. flame, 158:594-601 (2011)
92 !REF:rate constant is for n2
93 H2O2(+H2O)<=>OH+OH(+H2O)                          2.000E+012     0.900   48749.0
94 LOW/                                             1.865E+025    -2.300   48749.0/
95 TROE/  5.100E-001  1.000E-030  1.000E+030/
96 H2O2(+M)<=>OH+OH(+M)                             2.000E+012     0.900   48749.0
97 LOW/                                             2.490E+024    -2.300   48749.0/
98 TROE/  4.300E-001  1.000E-030  1.000E+030/
99 H2O/ 0.00/ CO2/ 1.60/ N2/ 1.50/ O2/ 1.20/ HE/ 0.65/ H2O2/ 7.70/
100
101 !REF:efficiencies for h2 and co taken from li et al., int. j. chem. kinet.
       36:566-575 (2004)
102 H2/ 3.70/ CO/ 2.80/
103
104 !------------------------------------------------------------------------
105
106 !REF:TSANG AND HAMPSON, J. PHYS. CHEM. REF. DATA 15 (1986) 10871280.
107 H2O2+H<=>H2O+OH                          2.410E+13   0.000          3.970E+03
108
109 !REF: ELLINGSON ET AL., J. PHYS. CHEM. A 111(51) (2007) 1355413566. (FIT TO THE
       THEORETICAL RATE)
110 H2O2+H<=>H2+HO2                         2.150E+10   1.000          6.000E+03
111
112 !REF:TSANG AND HAMPSON, J. PHYS. CHEM. REF. DATA 15 (1986) 10871280.
113 H2O2+O<=>OH+HO2                         9.550E+06   2.000          3.970E+03
114
115 !REF: HONG ET AL., J. PHYS. CHEM. A 114(18) (2010) 57185727.
116 H2O2+OH<=>H2O+HO2                       1.74E+12    0.000          3.18E+02
117 DUPLICATE
118 H2O2+OH<=>H2O+HO2                       7.59E+13    0.000          7.269E+03
119 DUPLICATE
120
121 !------------------------------------------------------------------------
122 !-------------END OF H2 MECHANISM-----------------------------
123 !------------------------------------------------------------------------
124
125 !REF: TROE, J. PHYS. CHEM. 83 (1979) 114126. X 0.76
126 CO+O(+M)=CO2(+M)                         1.362E+10    0.000          2384.00
```

```
!REF: WESTMORELAND ET AL, AICHE JOURNAL 32(12) (1986) 19711979. X 0.87
LOW / 1.173E+24   -2.79           4191.   /
H2/ 2.00/ H2O/ 12.00/ CO/ 1.75/ CO2/ 3.60/ AR/ 0.70/ HE/ 0.70/

!REF:TSANG AND HAMPSON, J. PHYS. CHEM. REF. DATA 15 (1986) 10871280.
CO+O2 = CO2+O                          1.119E+12    0.000         47700.00

!REF: JOSHI AND WANG, INT. J. CHEM. KINET. 38(1) (2006) 5773.
CO+OH<=>CO2+H                          7.015E+04    2.053          -355.67
DUPLICATE
CO+OH<=>CO2+H                          5.757E+12   -0.664           331.83
DUPLICATE

!REF: YOU ET AL. J. PHYS. CHEM. A 111(19) (2007) 40314042.
CO+HO2<=>CO2+OH                        1.570E+05    2.180         1.794E+04

!REF: LI ET AL. INT. J. CHEM. KINET. 39(3) (2007) 109136.
HCO+M<=>H+CO+M                         4.750E+11    0.660         1.487E+04
H2/ 2.00/ H2O/ 12.00/ CO/ 1.50/ CO2/ 2.00/ CH4/ 2.00/ C2H6/ 3.00/

!REF: TIMONEN ET AL., J. PHYS. CHEM. 92(3) (1988) 651655.
HCO+O2<=>CO+HO2                        7.580E+12    0.000         4.100E+02

!REF: TIMONEN ET AL., J. PHYS. CHEM. 91(3) (1987) 692694.
HCO+H<=>CO+H2                          7.340E+13    0.000         0.000E+00

!REF:TSANG AND HAMPSON, J. PHYS. CHEM. REF. DATA 15 (1986) 10871280.
HCO+O<=>CO+OH                          3.020E+13    0.000         0.000E+00
HCO+O<=>CO2+H                          3.000E+13    0.000         0.000E+00

!REF: BAULCH ET AL., J. PHYS. CHEM. REF. DATA 21(3) (1992) 411734.
HCO+OH<=>CO+H2O 1.020E+14 0.000 0.000E+00

!REF:TSANG AND HAMPSON, J. PHYS. CHEM. REF. DATA 15 (1986) 10871280.
HCO+HO2=>CO2+H+OH                      3.000E+13    0.000         0.000E+00
!HCO+HCO=>H2+CO+CO                      3.000E+12    0.000         0.000E+00
!Reaction HCO + HCO => H2 + CO + CO was eliminated during the search process.

!-------------------------------------------------------------------------
!-------------END OF H2/CO MECHANISM-------------------------
!-------------------------------------------------------------------------


!-------------------------------OH* MECHANISM----------------------
!REF: KATHROTIA ET AL., COMBUST. FLAME 157(7) (2010) 12611273
H+O+M<=>M+OH*                          1.50E+13      0.0          5.975E3
H2/ 1.00/ H2O/ 6.50/ O2/ 0.40/ N2/ 0.40/ AR/ 0.35/

!REF: TAMURA ET AL., COMBUST. FLAME 114(3-4) (1998) 502514.
OH*+H2O<=>OH+H2O                      5.930E+12      0.5         -8.60E2
OH*+H2<=>OH+H2                        2.950E+12      0.5         -4.44E2
```

```
!OH*+N2<=>OH+N2                          1.080E+11      0.5         -1.242E3
OH*+OH<=>OH+OH                          6.010E+12      0.5        -7.64E2
OH*+H<=>OH+H                            1.310E+12      0.5         -1.67E2
OH*+O2<=>OH+O2                          2.100E+12      0.5         -4.78E2
OH*+CO2<=>OH+CO2                        2.750E+12      0.5         -9.68E2
OH*+CO<=>OH+CO                          3.230E+12      0.5         -7.87E2
OH*+CH4<=>OH+CH4                        3.360E+012     0.500    -635.0
CH+O2<=>CO+OH*                          4.040E+013     0.000       0.0
!REF: PAUL ET AL., J. CHEM. PHYS. 102(21) (1995) 83788384.
!OH*+AR<=>OH+AR                          1.690E+12      0.0          4.135E3

!REF: SMITH ET AL., COMBUST. FLAME 131(1-2) (2002) 5969.
!OH*<=>OH+HV                             1.450E+06      0.0           0.0

!----------------------------END OH* MECHANISM-----------------
C2H+O<=>CO+CH*                                        6.200E+012     0.000       0.0
C+H+M<=>CH*+M                                         6.000E+014     0.000    6940.0

!REF:devriendt, van look, ceursters, and peeters, chem phys lett. 261 (1996)
    450, c2h+o2
C2H+O2<=>CO2+CH*                                      2.170E+010     0.000       0.0

!REF:hwang, gardiner, frenklach, hidaka, comb. fl. 67, 65-75 (1987) ch*+m<=>ch+m
CH*+AR<=>CH+AR                                        4.000E+011     0.500       0.0
CH*+H2O<=>CH+H2O                                      5.300E+013     0.000       0.0
CH*+CO<=>CH+CO                                        2.440E+012     0.500       0.0
CH*+CO2<=>CH+CO2                                      2.410E-001     4.300   -1694.0
CH*+O2<=>CH+O2                                        2.480E+006     2.140   -1720.0
CH*+H2<=>CH+H2                                        1.470E+014     0.000    1361.0
CH*+CH4<=>CH+CH4                                      1.730E+013     0.000     167.0
CH*<=>CH                                              1.860E+006     0.000       0.0
CH*+N2<=>CH+N2                                        3.030E+002     3.400    -381.0
!----------------------------END CH* MECHANISM-----------------

!REF:laskin et al. ijck 32 589-614 2000
HCO+H(+M)<=>CH2O(+M)                                  1.090E+012     0.480    -260.0
LOW/                                                  1.350E+024    -2.570    1425.0/
TROE/  7.824E-001  2.710E+002  2.755E+003  6.570E+003/
H2/ 2.00/ H2O/ 6.00/ AR/ 0.70/ CO/ 1.50/ CO2/ 2.00/ CH4/ 2.00/ C2H6/ 3.00/ HE/
    0.70/

!REF:v. vasudevan et al. ijck. 37: 98--109 (2005).
CH2O+OH<=>HCO+H2O                                     7.820E+007     1.630   -1055.0

!REF:irdam et al., ijck 1993, 25, 285
CH2O+H<=>HCO+H2                                       5.740E+007     1.900    2740.0

!REF:curran fit to NIST database
CH2O+O<=>HCO+OH                                       6.260E+009     1.150    2260.0

!REF:baulch et al.
```

```
!REF:journal of physical and chemical reference data:
!REF:34, 3, 757-1397 2005
CH2O+CH3<=>HCO+CH4                                  3.830E+001     3.360    4312.0

!REF:J. Phys. Chem. A 109, 12027-12035, 2005
CH2O+HO2<=>HCO+H2O2                                 1.880E+004     2.700   11520.0

!REF:Phil Taylor ch3cho+oh x 1.5
!REF:26th Intl. Combustion Symp. p 497--504.
CH2O+OH<=>HOCH2O                                    4.500E+015    -1.100       0.0

!REF:curran estimate
HOCH2O<=>HOCHO+H                                    1.000E+014     0.000   14900.0

!REF:Mulenko, S.A. Rev. Roum. Phys. 32, 173 (1987)
HCO+CH3<=>CH4+CO                                    2.650E+013     0.000       0.0

!REF:N. K. Srinivasan et al.,J. Phys. Chem. A 109, 7902-7914 (2005)
CH2O+O2<=>HCO+HO2                                   8.070E+015     0.000   53420.0

C3H8+OH<=>IC3H7+H2O                                 4.670E+007     1.610     -35.0
C3H8+HO2<=>NC3H7+H2O2                               4.080E+001     3.590   17160.0

!REF:Blake et al. J. Chem. Soc. B: 10, 1923 (1971)
HOCHO<=>CO+H2O                                      2.450E+012     0.000   60470.0

!REF:marinov estimate
HOCHO+OH=>H2O+CO2+H                                 2.620E+006     2.060     916.0
HOCHO+H=>H2+CO2+H                                   4.240E+006     2.100    4868.0

!REF:marinov estimate
HOCHO+H=>H2+CO+OH                                   6.030E+013    -0.350    2988.0
HOCHO+CH3=>CH4+CO+OH                                3.900E-007     5.800    2200.0

!REF:marinov estimate
HOCHO+HO2=>H2O2+CO+OH                               1.000E+012     0.000   11920.0

!REF:Hippler et al. PCCP. 3: 3450--2458 (2001).
CH3O(+M)<=>CH2O+H(+M)                               6.800E+013     0.000   26170.0
LOW/                                                1.867E+025    -3.000   24307.0/
TROE/  9.000E-001  2.500E+003  1.300E+003  1.000E+099/
H2/ 2.00/ H2O/ 6.00/ CO/ 1.50/ CO2/ 2.00/ CH4/ 2.00/ C2H6/ 3.00/

!REF:Wantuck, P.J. e al. J. Phys. Chem. 91, 4653 (1987)
CH3O+O2<=>CH2O+HO2                                  4.380E-019     9.500   -5501.0

!REF:tsang and hampson, j. phys. chem. ref. data, 15:1087 (1986)
CH3+CH3OH<=>CH4+CH3O                                1.440E+001     3.100    6935.0

!REF:
CH3O+CH3<=>CH2O+CH4                                 1.200E+013     0.000       0.0
```

```
278
279 !REF:hoyermann et al., 18th symposium
280 CH3O+H<=>CH2O+H2                                    2.000E+013     0.000       0.0
281
282 !REF:laskin et al. ijck 32 589-614 2000
283 CH2O+H(+M)<=>CH2OH(+M)                             5.400E+011     0.454    3600.0
284 LOW/                                              1.270E+032    -4.820    6530.0/
285 TROE/  7.187E-001  1.030E+002  1.291E+003  4.160E+003/
286 H2/ 2.00/ H2O/ 6.00/ CO/ 1.50/ CO2/ 2.00/ CH4/ 2.00/ C2H6/ 3.00/
287
288 !REF:Grotheer, H. H. et al., J. Phys. Chem. 92: 4028 (1988).
289 CH2OH+O2<=>CH2O+HO2                               2.410E+014     0.000    5017.0
290 DUP
291
292 !REF:tsang, jpc ref. data, 16:471 (1987)
293 CH2OH+H<=>CH2O+H2                                  6.000E+012     0.000       0.0
294
295 !REF:tsang, jpc ref. data, 16:471 (1987)
296 OH+CH2OH<=>H2O+CH2O                               2.400E+013     0.000       0.0
297 O+CH2OH<=>OH+CH2O                                 4.200E+013     0.000       0.0
298
299 !REF:from jasper/ Klipp,j.phys.chem a 111,19,3932-3950
300 !REF:neglecting hcoh channels as they are not important
301 CH3OH(+M)<=>CH3+OH(+M)                             2.084E+018    -0.615   92540.6
302 LOW/                                              1.500E+043    -6.995   97992.2/
303 TROE/ -4.748E-001  3.558E+004  1.116E+003  9.023E+003/
304
305 !REF:J. Chem. Phys. 134, 094302 (2011)
306 CH3OH+H<=>CH2OH+H2                                3.070E+005     2.550    5440.0
307 CH3OH+H<=>CH3O+H2                                 1.990E+005     2.560   10300.0
308
309 !REF:tsang, jpc ref. data, 16:471 (1987)
310 CH3OH+O<=>CH2OH+OH                                3.880E+005     2.500    3080.0
311
312 !REF:xu et al. proc 31 2007 159-166
313 CH3OH+OH<=>CH2OH+H2O                              3.080E+004     2.650    -806.7
314 CH3OH+OH<=>CH3O+H2O                               1.500E+002     3.030    -763.0
315
316 !REF:walker, r. w., reaction kinetics, vol. 1, s. p. r. chemical society, 1975
317 CH3OH+O2<=>CH2OH+HO2                               2.050E+013     0.000   44900.0
318
319 !REF:curran estimate
320 CH3OH+HO2<=>CH2OH+H2O2                             1.080E+004     2.550   10530.0
321
322 !REF:tsang, jpc ref. data, 16:471 (1987)
323 CH3OH+CH3<=>CH2OH+CH4                               3.190E+001     3.170    7172.0
324
325 !REF:GRI
326 CH3+H(+M)<=>CH4(+M)                                 1.270E+016    -0.630     383.0
327 LOW/                                              2.477E+033    -4.760    2440.0/
328 TROE/  7.830E-001  7.400E+001  2.941E+003  6.964E+003/
```

```
H2/ 2.00/ H2O/ 6.00/ AR/ 0.70/ CO/ 1.50/ CO2/ 2.00/ CH4/ 2.00/ C2H6/ 3.00/ HE/
    0.70/

!REF:Baulch, D.L.; et al.,J. Phys. Chem. Ref. Data (2005)
CH4+H<=>CH3+H2                                      6.140E+005     2.500    9587.0

!REF:curran, fit to NIST database
CH4+OH<=>CH3+H2O                                    5.830E+004     2.600    2190.0

!REF:GRI 3.0
CH4+O<=>CH3+OH                                      1.020E+009     1.500    8600.0

!REF:J. Aguilera-Iparraguirre et al. J Phys Chem A (2008) 112(30): 7047-7054.
!REF:x1.5
CH4+HO2<=>CH3+H2O2                                  1.695E+001     3.740   21010.0

!REF:GRI 3.0
CH4+CH2<=>CH3+CH3                                   2.460E+006     2.000    8270.0

!REF:from jasper/ Klipp,j.phys.chem a 111,19,3932-3950
CH3+OH<=>CH2(S)+H2O                                 4.936E+014    -0.669    -445.8
PLOG/      0.0100     4.936E+014    -0.669      -445.8/
PLOG/      0.1000     1.207E+015    -0.778      -175.6/
PLOG/      1.0000     5.282E+017    -1.518      1772.0/
PLOG/     10.0000     4.788E+023    -3.155      7003.0/
PLOG/    100.0000     8.433E+019    -1.962      8244.0/
CH3+OH<=>CH2O+H2                                    3.502E+005     1.441   -3244.0
PLOG/      0.0100     3.502E+005     1.441     -3244.0/
PLOG/      0.1000     8.854E+005     1.327     -2975.0/
PLOG/      1.0000     1.650E+007     0.973     -2010.0/
PLOG/     10.0000     5.374E+009     0.287       280.0/
PLOG/    100.0000     9.494E+018    -2.199      9769.0/

!REF:increased by factor of 2 to improve agreement with Ch4 flamespeed
CH3+OH<=>CH2OH+H                                    1.621E+010     0.965    3210.0
PLOG/      0.0100     1.621E+010     0.965      3214.0/
PLOG/      0.1000     1.807E+010     0.950      3247.0/
PLOG/      1.0000     4.686E+010     0.833      3566.0/
PLOG/     10.0000     1.525E+013     0.134      5641.0/
PLOG/    100.0000     3.590E+014    -0.186      8601.0/

!REF:from jasper/ Klipp,j.phys.chem a 111,19,3932-3950
CH3+OH<=>H+CH3O                                     1.186E+009     1.016   11940.0
PLOG/      0.0100     1.186E+009     1.016     11940.0/
PLOG/      0.1000     1.188E+009     1.016     11940.0/
PLOG/      1.0000     1.230E+009     1.011     11950.0/
PLOG/     10.0000     1.798E+009     0.965     12060.0/
PLOG/    100.0000     5.242E+010     0.551     13070.0/

!REF: jasper/ klippenstein proc combust inst 32 (2009) 279286
CH3+HO2<=>CH3O+OH                                   1.000E+012     0.269    -687.5
```

```
CH3+HO2<=>CH4+O2                                  1.160E+005     2.230   -3022.0

!REF:Harding and Klippenstein 2B04, 30th Symp 2004.
CH3+O<=>CH2O+H                                    5.540E+013     0.050    -136.0

!REF:N. K. Srinivasan et al.,J. Phys. Chem. A 109, 7902-7914 (2005)
CH3+O2<=>CH3O+O                                   7.546E+012     0.000   28320.0

!REF: personal communication, Steve Klippenstein
CH3+O2<=>CH2O+OH                                  2.641E+000     3.283    8105.0

!REF:R.X. Fernandes et al.,J Phys. Chem. A, (2006) 110:4442-4449.
CH3+O2(+M)<=>CH3O2(+M)                            7.812E+009     0.900       0.0
LOW/                                              6.850E+024    -3.000       0.0/
TROE/  6.000E-001  1.000E+003  7.000E+001  1.700E+003/

!REF:tsang and hampson, j. phys. chem. ref. data, 15:1087 (1986)
CH3O2+CH2O<=>CH3O2H+HCO                           1.990E+012     0.000   11660.0

!REF:new fit from HJC
!REF:x1.5
CH4+CH3O2<=>CH3+CH3O2H                            9.600E-001     3.770   17810.0

!REF:Keiffer, M. et al.,J. Chem. Soc. Faraday Trans. 2: 84, 505 (1988)
CH3O2+CH3<=>CH3O+CH3O                             5.080E+012     0.000   -1411.0

!REF: Lightfoot,P.D. etal., Atmos. Environ. Part A: 26, 1805-1961 (1992)
CH3O2+HO2<=>CH3O2H+O2                             2.470E+011     0.000   -1570.0

!REF:Lightfoot et al. J. Chem. Soc. Fara Trans. 1991, 87(19), 3213--3220.
CH3O2+H<=>CH3O+OH                                 9.600E+013     0.000       0.0
CH3O2+O<=>CH3O+O2                                 3.600E+013     0.000       0.0
CH3O2+OH<=>CH3OH+O2                               6.000E+013     0.000       0.0
CH3O2H<=>CH3O+OH                                  6.310E+014     0.000   42300.0

!REF:laskin et al. ijck 32 589-614 2000
CH2+H(+M)<=>CH3(+M)                               2.500E+016    -0.800       0.0
LOW/                                              3.200E+027    -3.140    1230.0/
TROE/  6.800E-001  7.800E+001  1.995E+003  5.590E+003/
H2/ 2.00/ H2O/ 6.00/ AR/ 0.70/ CO/ 1.50/ CO2/ 2.00/ CH4/ 2.00/ C2H6/ 3.00/ HE/
    0.70/

!REF:gri 3.0
CH2+O2<=>HCO+OH                                   1.060E+013     0.000    1500.0
CH2+O2=>CO2+H+H                                   2.640E+012     0.000    1500.0
CH2+O=>CO+H+H                                     5.000E+013     0.000       0.0
CH2+H<=>CH+H2                                     1.000E+018    -1.560       0.0
DUP
CH2+OH<=>CH+H2O                                   1.130E+007     2.000    3000.0
CH+O2<=>HCO+O                                     3.300E+013     0.000       0.0

```

```
!REF: GRI
CH+H<=>C+H2                                          1.100E+014     0.000       0.0

!REF:messing et al.,j. chem. phys. 74, 3874 (1981)
CH+O<=>CO+H                                          5.700E+013     0.000       0.0

!REF:Smith et al., GRI Mech version 2.11
CH+H2O<=>H+CH2O                                      1.713E+013     0.000    -755.0

!REF:wang et al., jpc a 107:11414 (2003)
CH3+CH3(+M)<=>C2H6(+M)                               2.277E+015    -0.690     174.9
LOW/                                                 8.054E+031    -3.750     981.6/
TROE/  0.000E+000  5.700E+002  1.000E+030  1.000E+030/
H2O/ 5.00/ CO/ 2.00/ CO2/ 3.00/

!REF:GRI 3.0
C2H5+H(+M)<=>C2H6(+M)                                5.210E+017    -0.990    1580.0
LOW/                                                 1.990E+041    -7.080    6685.0/
TROE/  8.420E-001  1.250E+002  2.219E+003  6.882E+003/
H2/ 2.00/ H2O/ 6.00/ AR/ 0.70/ CO/ 1.50/ CO2/ 2.00/ CH4/ 2.00/ C2H6/ 3.00/ HE/
    0.70/

C2H6+H<=>C2H5+H2                                     1.150E+008     1.900    7530.0

!REF: *Miyoshi,A. et al., Chem. Phys. Lett. 204, 241-247 (1993)
C2H6+O<=>C2H5+OH                                     3.550E+006     2.400    5830.0

!REF:curran, fit to NIST database
C2H6+OH<=>C2H5+H2O                                   1.480E+007     1.900     950.0

!REF:baulch et al., j. phys. chem. ref data, 21:411 (1992)
C2H6+O2<=>C2H5+HO2                                   6.030E+013     0.000   51870.0

!REF:tsang and hampson, j. phys. chem. ref. data, 15:1087 (1986)
C2H6+CH3<=>C2H5+CH4                                  5.480E-001     4.000    8280.0

!REF:J. Aguilera-Iparraguirre et al. J Phys Chem A (2008) 112(30): 7047-7054.
C2H6+HO2<=>C2H5+H2O2                                 3.460E+001     3.610   16920.0

!REF:miller klippenstein pccp 2004, 6, 1192-1202
!REF:hp and lp limit*0.7
C2H4+H(+M)<=>C2H5(+M)                                9.569E+008     1.463    1355.0
LOW/                                                 1.419E+039    -6.642    5769.0/
TROE/ -5.690E-001  2.990E+002 -9.147E+003  1.524E+002/
H2/ 2.00/ H2O/ 6.00/ CH4/ 2.00/ CO/ 1.50/ CO2/ 2.00/ C2H6/ 3.00/ AR/ 0.70/

!REF:
H2+CH3O2<=>H+CH3O2H                                  1.500E+014     0.000   26030.0

!REF:Zhu, R.S. et al.,J. Chem. Phys. 120:6566:6573 (2004)
CH3+C2H5<=>CH4+C2H4                                  1.180E+004     2.450   -2921.0
```

```
479
480 !REF:stewart et al c&f 1989
481 CH3+CH3<=>H+C2H5                                    4.740E+012     0.105   10664.3
482 PLOG/      0.0100     4.740E+012     0.105     10664.3/
483 PLOG/      0.1000     2.570E+013    -0.096     11406.1/
484 PLOG/      1.0000     3.100E+014    -0.362     13372.5/
485 PLOG/     10.0000     2.150E+010     0.885     13532.5/
486 PLOG/    100.0000     1.032E+002     3.230     11236.1/
487
488 !REF:from jasper/ Klipp,j.phys.chem a 111,19,3932-3950
489 CH3+OH<=>HCOH+H2                                   8.674E+008     0.787   -3046.0
490 PLOG/      0.0100     8.674E+008     0.787     -3046.0/
491 PLOG/      0.1000     3.115E+009     0.630     -2669.0/
492 PLOG/      1.0000     1.557E+011     0.156     -1368.0/
493 PLOG/     10.0000     1.704E+021    -2.641      6412.0/
494 PLOG/    100.0000     7.250E+020    -2.402      9639.0/
495
496 !REF:marinov 1996
497 HCOH+O2=>CO2+H+OH                                  5.000E+012     0.000       0.0
498 HCOH+O2<=>CO2+H2O                                  3.000E+013     0.000       0.0
499 HCOH+H<=>CH2O+H                                    2.000E+014     0.000       0.0
500
501 !REF:Curran: fit to Pratt/ Wood 84 and Pratt/ Veldman 76
502 C2H5+H<=>C2H4+H2                                   2.000E+012     0.000       0.0
503
504 !REF:GRI 3.0
505 C2H5+O<=>CH3CHO+H                                  1.100E+014     0.000       0.0
506
507 !REF:Carstensen and Dean Proc Combust Inst 30 (2005) 9951003
508 C2H5+O2<=>C2H4+HO2                                 2.094E+009     0.490    -391.4
509 DUP
510 PLOG/      0.0400     2.094E+009     0.490      -391.4/
511 PLOG/      1.0000     1.843E+007     1.130      -720.6/
512 PLOG/     10.0000     7.561E+014    -1.010      4749.0/
513 C2H5+O2<=>C2H4+HO2                                   6.609E+000     3.510   14160.0
514 DUP
515 C2H5+O2<=>CH3CHO+OH                                  4.908E-006     4.760     254.3
516 PLOG/      0.0400     4.908E-006     4.760       254.3/
517 PLOG/      1.0000     6.803E-002     3.570      2643.0/
518 PLOG/     10.0000     8.265E+002     2.410      5285.0/
519 C2H5+O2<=>C2H4O1-2+OH                                1.303E+003     1.930    -502.7
520 PLOG/      0.0400     1.303E+003     1.930      -502.7/
521 PLOG/      1.0000     2.438E+002     2.180       -62.5/
522 PLOG/     10.0000     4.621E+009     0.150      5409.0/
523
524 !REF:Sivaramakrishnan J. Phys. Chem. A, Vol 114, No. 2, 2010
525 CH3CHO(+M)<=>CH3+HCO(+M)                            2.450E+022    -1.740   86355.0
526 LOW/                                               1.030E+059   -11.300   95912.5/
527 TROE/  2.490E-003  7.181E+002  6.089E+000  3.780E+003/
528
529 !REF:Harding J. Phys. Chem., Vol. 114, No. 2, 2010
```

```
CH3CHO+H<=>CH3CO+H2                                 1.310E+005     2.580    1220.0
CH3CHO+H<=>CH2CHO+H2                                2.720E+003     3.100    5210.0

!REF:Juan Lis PhD thesis
CH3CHO+OH<=>CH3CO+H2O                               3.370E+012     0.000    -619.0

!REF:baulch et al., j. phys. chem. ref data, 21:411 (1992)
CH3CHO+O2<=>CH3CO+HO2                               3.010E+013     0.000   39150.0

!REF:baulch et al., j. phys. chem. ref data, 21:411 (1992)
CH3CHO+HO2<=>CH3CO+H2O2                             3.010E+012     0.000   11920.0

!REF:Taylor et al. 1996
CH3CHO+OH<=>CH2CHO+H2O                              1.720E+005     2.400     815.0

!REF:J. Phys. Chem. A 2006, 110, 5772-5781
CH3CO(+M)<=>CH3+CO(+M)                              1.070E+012     0.630   16900.0
LOW/                                                5.650E+018    -0.970   14600.0/
TROE/  6.290E-001  8.730E+009  5.520E+000  7.600E+007/

!REF:J. Phys. Chem. A 2006, 110, 5772-5781
CH2CHO(+M)<=>CH2CO+H(+M)                            1.430E+015    -0.150   45600.0

!REF:lpl times 2
LOW/                                                6.000E+029    -3.800   43423.9/
TROE/  9.850E-001  3.930E+002  9.800E+009  5.000E+009/
!REF:J. Phys. Chem. A 2006, 110, 5772-5781
CH2CHO(+M)<=>CH3+CO(+M)                             2.930E+012     0.290   40300.0
LOW/                                                9.520E+033    -5.070   41300.0/
TROE/  7.130E-017  1.150E+003  4.990E+009  1.790E+009/

CH2CHO+O2=>CH2O+CO+OH                               2.680E+017    -1.840    6530.0
PLOG/      0.0100     2.680E+017    -1.840      6530.0/
PLOG/      0.1000     1.520E+020    -2.580      8980.0/
PLOG/      1.0000     1.650E+019    -2.220     10340.0/
PLOG/     10.0000     8.953E+013    -0.600     10120.0/

!REF:laskin et al. ijck 32 589-614 2000
CH2+CO(+M)<=>CH2CO(+M)                              8.100E+011     0.000       0.0
LOW/                                                2.690E+033    -5.110    7095.0/
TROE/  5.907E-001  2.750E+002  1.226E+003  5.185E+003/
H2/ 2.00/ H2O/ 6.00/ AR/ 0.70/ CO/ 1.50/ CO2/ 2.00/ CH4/ 2.00/ C2H6/ 3.00/ HE/
    0.70/

!REF:J. Phys. Chem. A 2006, 110, 5772-5781
!REF:defined in the reverse from SJK, P dependence from CHEMDIS
!REF:important for acetone flame speeds
CH3CO(+M)<=>CH2CO+H(+M)                             9.413E+007     1.917   44987.2
LOW/                                                1.516E+051   -10.270   55390.0/
TROE/  6.009E-001  8.103E+009  6.677E+002  5.000E+009/

```

```
!REF:wkm (see comments at beginning of file 15/ 09/ 2011
CH2CO+H<=>HCCO+H2                                 1.401E+015    -0.171    8783.2
CH2CO+H<=>CH3+CO                                  7.704E+013    -0.171    4183.2

!REF:Curran estimate
CH2CO+O<=>CH2+CO2                                 1.750E+012     0.000    1350.0

!REF:
CH2CO+O<=>HCCO+OH                                 1.000E+013     0.000    8000.0
CH2CO+OH<=>HCCO+H2O                               1.000E+013     0.000    2000.0

!REF:Brown et al. Chem. Phys. Lett. 1989, 161, 491.
CH2CO+OH<=>CH2OH+CO                               2.000E+012     0.000   -1010.0

!REF:WKM calculation, chemically activated, appears pressure independant
CH2CO+CH3<=>C2H5+CO                               4.769E+004     2.312    9468.0

!REF:WKM calculation, chemically activated, appears pressure independant
HCCO+OH=>H2+CO+CO                                 1.000E+014     0.000       0.0
HCCO+O=>H+CO+CO                                   8.000E+013     0.000       0.0

!REF:klippenstein 2002
HCCO+O2=>OH+CO+CO                                 1.910E+011    -0.020    1020.0
HCCO+O2=>CO2+CO+H                                 4.780E+012    -0.142    1150.0

!REF:Fulle, D.; Hippler, H.; Striebel, F.
!REF:J. Chem. Phys. 108: 6709-6716 1998
CH+CO+M<=>HCCO+M                                  7.570E+022    -1.900       0.0

!REF:GRI 3.0
C2H3+H(+M)<=>C2H4(+M)                             6.080E+012     0.270     280.0
LOW/                                              1.400E+030    -3.860    3320.0/
TROE/  7.820E-001  2.075E+002  2.663E+003  6.095E+003/
H2/ 2.00/ H2O/ 6.00/ AR/ 0.70/ CO/ 1.50/ CO2/ 2.00/ CH4/ 2.00/ C2H6/ 3.00/ HE/
    0.70/

!REF:GRI
C2H4(+M)<=>H2+H2CC(+M)                            8.000E+012     0.440   88770.0
LOW/                                              7.000E+050    -9.310   99860.0/
TROE/  7.345E-001  1.800E+002  1.035E+003  5.417E+003/
H2/ 2.00/ H2O/ 6.00/ CH4/ 2.00/ CO/ 1.50/ CO2/ 2.00/ C2H6/ 3.00/ AR/ 0.70/

!REF:Knyazev,V.D. et al.,J. Phys. Chem. 100, 11346-1135 (1996)
C2H4+H<=>C2H3+H2                                  5.070E+007     1.930   12950.0

!REF:baulch et al.
!REF:journal of physical and chemical reference data:
!REF:34, 3, 757-1397 2005
!REF:making branching ratio 55:45
C2H4+O<=>CH3+HCO                                  7.453E+006     1.880     183.0
C2H4+O<=>CH2CHO+H                                 6.098E+006     1.880     183.0
```

```
630
631 !REF:j. phys. chem 109 2005 7489-7499 (Peeters)
632 !REF: from stanford
633 C2H4+OH<=>C2H3+H2O                                  2.230E+004     2.745    2215.5
634
635 !REF:SJK, j phys chem 110 2006 6960-6970
636 C2H4+OH<=>CH3+CH2O                                  5.350E+000     2.920   -1732.7
637 PLOG/      0.0100     5.350E+000     2.920     -1732.7/
638 PLOG/      0.0250     3.190E+001     2.710     -1172.3/
639 PLOG/      0.1000     5.550E+002     2.360      -180.8/
640 PLOG/      1.0000     1.780E+005     1.680      2060.5/
641 PLOG/     10.0000     2.370E+009     0.560      6006.7/
642 PLOG/    100.0000     2.760E+013    -0.500     11455.1/
643 C2H4+OH<=>C2H3OH+H                                  1.040E+004     2.600    4121.0
644 PLOG/      0.0100     1.040E+004     2.600      4121.0/
645 PLOG/      0.0250     1.070E+004     2.600      4129.0/
646 PLOG/      0.1000     1.520E+004     2.560      4238.3/
647 PLOG/      1.0000     3.190E+005     2.190      5255.6/
648 PLOG/     10.0000     1.940E+008     1.430      7828.8/
649 PLOG/    100.0000     8.550E+010     0.750     11490.8/
650
651 !REF:tsang and hampson, j. phys. chem. ref. data, 15:1087 (1986)
652 C2H4+CH3<=>C2H3+CH4                                  6.620E+000     3.700    9500.0
653
654 !REF:wkm 19/ 04/ 2010
655 !REF:taken from san diego mech
656 !REF: marinov, 1995
657 !REF:check effect!!!!!
658 C2H4+O2<=>C2H3+HO2                                  4.220E+013     0.000   57623.1
659
660 !REF:butler, fleming, goss, lin, acs symp. ser. 134 (1980).
661 CH+CH4<=>C2H4+H                                     6.000E+013     0.000       0.0
662
663 !REF:miller klippenstein pccp 2004, 6, 1192-1202
664 C2H2+H(+M)<=>C2H3(+M)                               1.710E+010     1.266    2709.0
665 LOW/                                               6.346E+031    -4.664    3780.0/
666 TROE/  7.880E-001 -1.020E+004  1.000E-030/
667 H2/ 2.00/ H2O/ 6.00/ AR/ 0.70/ CO/ 1.50/ CO2/ 2.00/ CH4/ 2.00/ C2H6/ 3.00/ HE/
      0.70/
668
669 !REF:N.M Marinov et al., Combust. Flame 114 (1998) 192-213
670 !REF:Adopting Klippensteins products for one of the channels,
671 !REF:to combat over-production of c2h2 in ethylene JSR
672 C2H3+O2<=>CH2O+HCO                                   1.700E+029    -5.312    6503.1
673 C2H3+O2<=>CH2CHO+O                                  7.000E+014    -0.611    5262.4
674 C2H3+O2=>H+CO+CH2O                                  5.190E+015    -1.260    3312.6
675
676 !REF:
677 CH3+C2H3<=>CH4+C2H2                                 3.920E+011     0.000       0.0
678
679 !REF:86TSA/ HAM
```

```
C2H3+H<=>C2H2+H2                                  9.000E+013     0.000       0.0

!REF:USC estimate
C2H3+H<=>H2CC+H2                                  6.000E+013     0.000       0.0

!REF:tsang and hampson, j. phys. chem. ref. data, 15:1087 (1986)
C2H3+OH<=>C2H2+H2O                                3.011E+013     0.000       0.0

!REF:99 Las/ Wan
C2H2(+M)<=>H2CC(+M)                               8.000E+014    -0.520   50750.0
LOW/                                              2.450E+015    -0.640   49700.0/
H2/ 2.00/ H2O/ 6.00/ CH4/ 2.00/ CO/ 1.50/ CO2/ 2.00/ C2H6/ 3.00/ C2H2/ 2.50/
    C2H4/ 2.50/

!REF:Nguyen et al. j.phys.chem a 2006, 110, 6696-6706
C2H2+O<=>CH2+CO                                   7.395E+008     1.280    2472.0
C2H2+O<=>HCCO+H                                   2.958E+009     1.280    2472.0

!REF:GRI 3.0 and USC II
H2CC+O2<=>HCO+HCO                                 1.000E+013     0.000       0.0

!REF:WJP: based on ch3+c2h4 addition, Curran IJCK 2006
CH2CO+CH3<=>CH3COCH2                              1.760E+004     2.480    6130.0

!REF:Cook et al. j. phys. chem a 2009, 113, 9974-9980
CH3OCH3(+M)<=>CH3+CH3O(+M)                        4.380E+021    -1.570   83890.0
LOW/                                              7.520E+015     0.000   42790.0/
TROE/  4.540E-001  1.000E-030  2.510E+003/

!REF:curran, fit to NIST database
CH3OCH3+H<=>CH3OCH2+H2                            7.721E+006     2.090    3384.0

!REF:Pierre Glaudes rates
CH3+CO2<=>CH3OCO                                  4.760E+007     1.540   34700.0
CH3O+CO<=>CH3OCO                                  1.550E+006     2.020    5730.0

!REF:GRI
CH2(S)+N2<=>CH2+N2                                1.500E+013     0.000     600.0
CH2(S)+AR<=>CH2+AR                                9.000E+012     0.000     600.0
CH2(S)+H<=>CH+H2                                  3.000E+013     0.000       0.0
CH2(S)+H2<=>CH3+H                                 7.000E+013     0.000       0.0
CH2(S)+O2=>H+OH+CO                                2.800E+013     0.000       0.0
CH2(S)+O2<=>CO+H2O                                1.200E+013     0.000       0.0
CH2(S)+CO2<=>CH2O+CO                              1.400E+013     0.000       0.0
CH2(S)+H2O<=>CH2+H2O                              3.000E+013     0.000       0.0

!REF:miller, j.a. and bowman, c.t.,
!REF:mechanism and modeling of nitrogen chemistry in combustion, wss/ ci, autumn
    1988
CH2(S)+C2H6<=>CH3+C2H5                            1.200E+014     0.000       0.0

```

```
!REF:GRI
HCCO+H<=>CH2(S)+CO                                  1.000E+014     0.000       0.0

!REF:from jasper/ Klipp,j.phys.chem a 111,19,3932-3950
!REF:neglecting hcoh channels as they are not important
CH3OH(+M)<=>CH2(S)+H2O(+M)                          3.121E+018    -1.017   91712.0
LOW/                                                1.430E+047    -8.227   99417.1/
TROE/  2.545E+000  3.290E+003  4.732E+004  4.711E+004/

!REF:Oehschlaeger et al., Proc Comb Inst 30 (2005) 1119-1127
C3H8(+M)<=>CH3+C2H5(+M)                             1.290E+037    -5.840   97380.0
LOW/                                                5.640E+074   -15.740   98714.0/
TROE/  3.100E-001  5.000E+001  3.000E+003  9.000E+003/
H2/ 2.00/ H2O/ 6.00/ AR/ 0.70/ CO/ 1.50/ CO2/ 2.00/ CH4/ 2.00/ C2H6/ 3.00/ HE/
    0.70/

!REF:laskin et al. ijck 32 589-614 2000
C2H3+CH3(+M)<=>C3H6(+M)                             2.500E+013     0.000       0.0
LOW/                                                4.270E+058   -11.940    9769.8/
TROE/  1.750E-001  1.341E+003  6.000E+004  1.014E+004/

!REF:GRI 3.0 and USC II
C2H2+CH2<=>C3H3+H                                   1.200E+013     0.000    6620.0

!REF:laskin et al ijck 32 589-614 2000
C3H6+H<=>C3H5-A+H2                                  1.730E+005     2.500    2492.0
C3H5-A+H(+M)<=>C3H6(+M)                             2.000E+014     0.000       0.0
LOW/                                                1.330E+060   -12.000    5967.8/
TROE/  2.000E-002  1.097E+003  1.097E+003  6.860E+003/
C3H4-P+H<=>C3H3+H2                                  1.300E+006     2.000    5500.0
C3H3+H<=>C3H4-P                                     1.500E+013     0.000       0.0
C3H4-A+OH<=>C3H3+H2O                                5.300E+006     2.000    2000.0
C2H3+CH3<=>C3H5-A+H                                 1.500E+024    -2.830   18618.0
C3H4-P+CH3<=>C3H3+CH4                               1.800E+012     0.000    7700.0
C3H4-P+OH<=>C3H3+H2O                                1.000E+006     2.000     100.0
C3H6+H<=>C3H5-T+H2                                  4.050E+005     2.500    9794.0
C3H3+O<=>CH2O+C2H                                   2.000E+013     0.000       0.0
C3H4-A+H<=>C3H3+H2                                  1.300E+006     2.000    5500.0

!REF:SJK j. phys. chem a 2005, 109, 6045-6055
C2H2+OH<=>CH2CO+H                                   1.578E+003     2.560    -844.5
PLOG/      0.0100     1.578E+003     2.560      -844.5/
PLOG/      0.0250     1.518E+004     2.280      -292.1/
PLOG/      0.1000     3.017E+005     1.920       598.1/
PLOG/      1.0000     7.528E+006     1.550      2106.0/
PLOG/     10.0000     5.101E+006     1.650      3400.0/
PLOG/    100.0000     1.457E+004     2.450      4477.0/
C2H2+OH<=>CH3+CO                                    4.757E+005     1.680    -329.8
PLOG/      0.0100     4.757E+005     1.680      -329.8/
PLOG/      0.0250     4.372E+006     1.400       226.5/
PLOG/      0.1000     7.648E+007     1.050      1115.0/
```

```
PLOG/      1.0000     1.277E+009     0.730      2579.0/
PLOG/     10.0000     4.312E+008     0.920      3736.0/
PLOG/    100.0000     8.250E+005     1.770      4697.0/


!REF:Updated based on Hansons total rate
C3H6+OH<=>C3H5-A+H2O                                 1.970E+006     2.200     540.0

!REF:pitz estimate
C2H+CH3<=>C3H4-P                                     8.000E+013     0.000       0.0

!REF:Davis and Law J. Phys. Chem. A 1999, 103, 5889-589
C3H4-A+H<=>C3H5-A                                    9.600E+061   -14.670   26000.0
PLOG/      0.1000     9.600E+061   -14.670     26000.0/
PLOG/      1.0000     1.520E+059   -13.540     26949.0/
PLOG/      2.0000     3.780E+057   -12.980     26785.0/
PLOG/      5.0000     7.340E+054   -12.090     26187.0/
PLOG/     10.0000     2.400E+052   -11.300     25400.0/
PLOG/    100.0000     6.900E+041    -8.060     21300.0/

!REF:GRI
C2H+O2<=>HCO+CO                                      5.000E+013     0.000    1500.0

!REF:baldwin et al., j. chem. soc. faraday trans. 1, 80, 435 (1984)
C2H3O1-2<=>CH2CHO                                    1.000E+014     0.000   14000.0

!REF:laskin et al. ijck 32 589-614 2000
C3H3+O2<=>CH2CO+HCO                                  3.000E+010     0.000    2868.0

!REF:!From Koert et al. energy & fuels Vol 6: 485-493 1992
C3H6+O=>CH3CHCO+H+H                                  2.500E+007     1.760      76.0
C3H6+O<=>C2H5+HCO                                    1.580E+007     1.760   -1216.0
C3H6+O<=>C3H5-A+OH                                   5.240E+011     0.700    5884.0
C3H6+O=>CH2CO+CH3+H                                  2.500E+007     1.760      76.0

!REF:
H+C3H8<=>H2+IC3H7                                    1.300E+006     2.400    4471.0
C3H8+O<=>IC3H7+OH                                    5.490E+005     2.500    3140.0

!REF:J. Aguilera-Iparraguirre et al. J Phys Chem A (2008) 112(30): 7047-7054.
C3H8+HO2<=>IC3H7+H2O2                                6.320E+001     3.370   13720.0

!REF:Curran Inc. Int J Chem Kinet 38: 250275, 2006
H+C3H6<=>IC3H7                                       4.240E+011     0.510    1230.0



C4H3-I+H<=>C4H2+H2                                   6.000E+013     0.000       0.0

!REF:Davis and Law J. Phys. Chem. A 1999, 103, 5889-589
C2H2+CH3<=>C3H4-P+H                                  4.500E+006     1.860   11600.0
```

```
PLOG/      0.1000     4.500E+006     1.860     11600.0/
PLOG/      1.0000     2.560E+009     1.100     13644.0/
PLOG/      2.0000     2.070E+010     0.850     14415.0/
PLOG/      5.0000     2.510E+011     0.560     15453.0/
PLOG/     10.0000     1.100E+012     0.390     16200.0/
PLOG/    100.0000     2.100E+012     0.370     18100.0/

!REF: GRI 3.0
C2H+H(+M)<=>C2H2(+M)                                  1.000E+017     0.000       0.0
LOW/                                                  3.750E+033    -4.800    1900.0/
TROE/  6.460E-001  1.320E+002  1.315E+003  5.566E+003/
H2/ 2.00/ H2O/ 6.00/ AR/ 0.70/ CO/ 1.50/ CO2/ 2.00/ CH4/ 2.00/ C2H6/ 3.00/ HE/
    0.70/

!REF:laskin et al ijck 32 589-614 2000
!REF:original:Tsang, W. J.Phys.Chem.Ref.Data 1991, 20, 221.
C3H6+H<=>C2H4+CH3                                     8.800E+016    -1.050    6461.0
PLOG/      0.1000     8.800E+016    -1.050     6461.0/
PLOG/      1.0000     8.000E+021    -2.390    11180.0/
PLOG/     10.0000     3.300E+024    -3.040    15610.0/

!REF:Updated based on Hansons total rate
C3H6+OH<=>C3H5-T+H2O                                  1.110E+006     2.000    1451.0

!REF:Glaude,P.A. et al,Proc. combust. inst
C3H5-A+HO2<=>C3H5O+OH                                 7.000E+012     0.000   -1000.0
C3H5-T+O2<=>CH3COCH2+O                                3.810E+017    -1.360    5580.0
C3H5-A+CH3O2<=>C3H5O+CH3O                             7.000E+012     0.000   -1000.0

!REF:Davis and Law J. Phys. Chem. A 1999, 103, 5889-589
C3H4-P+H<=>C3H4-A+H                                   2.300E+015    -0.260    7600.0
PLOG/      0.1000     2.300E+015    -0.260     7600.0/
PLOG/      1.0000     6.270E+017    -0.910    10079.0/
PLOG/      2.0000     1.500E+018    -1.000    10756.0/
PLOG/      5.0000     1.930E+018    -1.010    11523.0/
PLOG/     10.0000     3.100E+022    -2.180    14800.0/
PLOG/    100.0000     6.400E+027    -3.580    21200.0/

!REF:Davis and Law J. Phys. Chem. A 1999, 103, 5889-589
C3H4-P+H<=>C3H5-T                                     4.600E+044   -10.210   10200.0
PLOG/      0.1000     4.600E+044   -10.210    10200.0/
PLOG/      1.0000     1.660E+047   -10.580    13690.0/
PLOG/      2.0000     5.040E+047   -10.610    14707.0/
PLOG/      5.0000     9.620E+047   -10.550    15910.0/
PLOG/     10.0000     7.000E+047   -10.400    16600.0/
PLOG/    100.0000     3.200E+044    -9.110    17400.0/

!REF:baldwin et al., j. chem. soc. faraday trans. 1, 80, 435 (1984)
C2H3O1-2<=>CH3CO                                      8.500E+014     0.000   14000.0

!REF:Ju-Xiang Shao Theor Chem Acc (2011) 128:341-348
```

```
!REF:changed products from ch3+hco
C2H3OH<=>CH3CHO                                   7.420E+046   -10.560   67420.0
PLOG/      0.1000     7.420E+046   -10.560     67420.0/
PLOG/      1.0000     4.420E+042    -9.090     67069.2/
PLOG/    100.0000     2.900E+027    -4.350     61612.9/

!REF:ethenol chemistry from Curran/ yasunaga
C2H3OH+OH<=>CH2CHO+H2O                            3.330E+009     1.100     540.5
C2H3OH+CH3<=>CH2CHO+CH4                           2.030E-008     5.900    1052.0

!REF:
C3H5O<=>C2H3CHO+H                                 1.000E+014     0.000   29100.0

!REF:Tsang, W. J.Phys.Chem.Ref.Data 1991, 20, 221.
C3H5-A+O<=>C2H3CHO+H                              6.000E+013     0.000       0.0

!REF:Based on ch3cho+ho2
C2H3CHO+CH3<=>C2H3CO+CH4                          2.608E+006     1.780    5911.0

!REF:tsang and hampson, j. phys. chem. ref. data, 15:1087 (1986)
C2H3+CO<=>C2H3CO                                  1.510E+011     0.000    4810.0

!REF:baldwin et al., j. chem. soc. faraday trans. 1, 80, 435 (1984)
C2H4O1-2+H<=>C2H3O1-2+H2                          8.000E+013     0.000    9680.0

!REF:Lifshitz et al. 1983
C2H4O1-2<=>CH3+HCO                                3.630E+013     0.000   57200.0

!REF:curran, fit to NIST database
C2H4O1-2<=>CH3CHO                                 7.407E+012     0.000   53800.0

!REF: Curran estimate
CH3+CH2O<=>C2H5O                                  3.000E+011     0.000    6336.0

!REF:Harding J. Phys. Chem., Vol. 114, No. 2, 2010
CH3CHO+H<=>C2H5O                                  4.610E+007     1.710    7090.0

!REF:Curran. Based on ch3+ho2<=>products
C2H5+HO2<=>C2H5O+OH                               1.100E+013     0.000       0.0

!REF:Curran. Based on ch3+ho2<=>products
CH3O2+C2H5<=>CH3O+C2H5O                           8.000E+012     0.000   -1000.0

C2H5O2<=>C2H4+HO2                                 1.782E+032    -7.100   32840.0
PLOG/      0.0400     1.782E+032    -7.100     32840.0/
PLOG/      1.0000     2.701E+037    -8.470     35840.0/
PLOG/     10.0000     1.980E+038    -8.460     37900.0/

!REF:Carstensen and Dean Proc Combust Inst 30 (2005) 9951003
C2H5+O2<=>C2H5O2                                  3.398E+053   -13.900    9279.0
PLOG/      0.0400     3.398E+053   -13.900     9279.0/
```

```
PLOG/      1.0000     9.362E+059   -15.280     14240.0/
PLOG/     10.0000     1.262E+060   -14.910     16240.0/

!REF:sivaramakrishnan J. Phys. Chem. A, Vol. 114, No. 35, 2010
C2H5OH<=>C2H5+OH                                  8.100E+046   -11.300  111053.4
PLOG/      0.0010     8.100E+046   -11.300    111053.4/
PLOG/      0.0100     1.860E+056   -13.500    107238.4/
PLOG/      0.1000     4.650E+063   -15.000    109622.8/
PLOG/      1.0000     4.460E+065   -14.900    112345.0/
PLOG/     10.0000     2.790E+061   -13.400    113080.2/
PLOG/    100.0000     6.170E+051   -10.300    109940.7/

!REF:ref:Curran Inc. Int J Chem Kinet 38: 250275, 2006
CH3+C2H4<=>NC3H7                                  1.760E+004     2.480    6130.0
H+C3H6<=>NC3H7                                    2.500E+011     0.510    2620.0

!REF:
C3H8+O<=>NC3H7+OH                                 3.710E+006     2.400    5505.0
C3H8+OH<=>NC3H7+H2O                               1.054E+010     0.970    1586.0
H+C3H8<=>H2+NC3H7                                 3.490E+005     2.690    6450.0

!REF:
HCO+O2<=>O2CHO                                    1.200E+011     0.000   -1100.0

!REF:Enol+h Rao |J. Phys. Chem. A 2011, 115, 1602-1608,
!REF:Except for sc2h4oh channel kept WKM calculation
C2H3OH+H<=>PC2H4OH                                3.010E+008     1.577    3670.0

!REF:SJK, j phys chem 110 2006 6960-6970
C2H4+OH<=>PC2H4OH                                 1.740E+043   -10.461    7698.7
PLOG/      0.0100     1.740E+043   -10.461     7698.7/
PLOG/      0.0250     3.250E+037    -8.629     5214.7/
PLOG/      0.1000     1.840E+035    -7.750     4908.9/
PLOG/      1.0000     2.560E+036    -7.752     6946.1/
PLOG/     10.0000     3.700E+033    -6.573     7605.9/
PLOG/    100.0000     1.120E+026    -4.101     5757.0/

!REF:da silva J. Phys. Chem. A 2009, 113, 8923-8933
SC2H4OH+O2<=>CH3CHO+HO2                           5.260E+017    -1.638     869.0
PLOG/      0.0100     5.260E+017    -1.637      838.0/
PLOG/      0.1000     5.260E+017    -1.637      838.0/
PLOG/      1.0000     5.280E+017    -1.638      839.0/
PLOG/     10.0000     1.540E+018    -1.771     1120.0/
PLOG/    100.0000     3.780E+020    -2.429     3090.0/

!REF:curran, fit to NIST database
!REF:WKM calculation.
SC2H4OH<=>CH3CHO+H                                5.690E+052   -13.380   45049.0
PLOG/      0.0010     5.690E+052   -13.380    45049.0/
PLOG/      0.0100     3.290E+056   -14.120    48129.0/
PLOG/      0.1000     8.580E+057   -14.160    50743.0/
```

```
PLOG/      1.0000     5.360E+055   -13.150     51886.0/
PLOG/     10.0000     1.660E+048   -10.640     50297.0/
PLOG/     20.0000     8.260E+044    -9.590     49218.0/
PLOG/     50.0000     1.010E+040    -8.060     47439.0/
PLOG/    100.0000     1.100E+036    -6.840     45899.0/

!REF:sivaramakrishnan J. Phys. Chem. A, Vol. 114, No. 35, 2010
C2H5OH+H<=>SC2H4OH+H2                              8.790E+004     2.680    2910.0
C2H5OH+OH<=>SC2H4OH+H2O                            7.170E+004     2.540   -1534.0

!REF:
C3H6+CH3<=>SC4H9                                   1.760E+004     2.480    6130.0

!REF:fit to Nist database
CH3+C3H8<=>CH4+IC3H7                               6.400E+004     2.170    7520.0

!REF:Scott and Walker C&F 129(4) 365--377 2002
C3H6+HO2<=>C3H5-A+H2O2                             2.700E+004     2.500   12340.0

!REF:J. Aguilera-Iparraguirre et al. J Phys Chem A (2008) 112(30): 7047-7054.
!REF:Scaled as per carstensen et al
CH3O2+C3H8<=>CH3O2H+IC3H7                          1.019E+001     3.580   14810.0

!REF:Carstensen and Dean Proc Combust Inst 30 (2005) 9951003
C2H6+CH3O2<=>C2H5+CH3O2H                           1.940E+001     3.640   17100.0

END
```

Bibliography

[1] W Felder and S Madronich. High temperature photochemistry (HTP): kinetics and mechanism studies of elementary combustion reactions over 300-1700 K. *Combustion Science and Technology*, 50(1-3):135–150, 1986.

[2] NK Srinivasan, M-C Su, JW Sutherland, and JV Michael. Reflected shock tube studies of high-temperature rate constants for $\mathrm{OH} + \mathrm{CH_4} \rightarrow \mathrm{CH_3} + \mathrm{H_2O}$ and $\mathrm{CH_3} + \mathrm{NO_2} \rightarrow \mathrm{CH_3O}$ + NO. *The Journal of Physical Chemistry A*, 109(9):1857–1863, 2005.

[3] Zekai Hong, David Frank Davidson, King-Yiu Lam, and Ronald Kenneth Hanson. A shock tube study of the rate constants of $\mathrm{HO_2}$ and $\mathrm{CH_3}$ reactions. *Combustion and Flame*, 159(10):3007–3013, 2012.

[4] JWHG Ernst, H Gg Wagner, and R Zellner. A combined flash photolysis/shock-tube study of the absolute rate constants for reactions of the hydroxyl radical with $\mathrm{CH_4}$ and $\mathrm{CF_3H}$ around 1300 K. *Berichte der Bunsengesellschaft für physikalische Chemie*, 82(4):409–414, 1978.

[5] Ghanshyam L Vaghjiani and AR Ravishankara. New measurement of the rate coefficient for the reaction of OH with methane. *Nature*, 350(6317):406–409, 1991.

[6] Tomasz Gierczak, Ranajit K Talukdar, Scott C Herndon, Ghanshyam L Vaghjiani, and AR Ravishankara. Rate coefficients for the reactions of hydroxyl radicals with methane and deuterated methanes. *The Journal of Physical Chemistry A*, 101(17):3125–3134, 1997.

[7] BJ Finlayson-Pitts, MJ Ezell, TM Jayaweera, HN Berko, and CC Lai. Kinetics of the reactions of OH with methyl chloroform and methane: implications for global tropospheric OH and the methane budget. *Geophysical Research Letters*, 19(13), 1992.

[8] James R Dunlop and Frank P Tully. A kinetic study of hydroxyl radical reactions with methane and perdeuterated methane. *The Journal of Physical Chemistry*, 97(43):11148–11150, 1993.

[9] A Mellouki, S Tton, G Laverdet, A Quilgars, and G Le Bras. Kinetic studies of OH reactions with H_2O_2, C_3H_8 and CH_4 using the pulsed laser photolysis-laser induced fluorescence method. *Journal de Chimie Physique*, 91(5):473–487, 1994.

[10] Amlie Bonard, Vronique Dale, Jean-Louis Delfau, and Christian Vovelle. Kinetics of OH radical reactions with methane in the temperature range 295-660 k and with dimethyl ether and methyl-tert-butyl ether in the temperature range 295-618 k. *The Journal of Physical Chemistry A*, 106(17):4384–4389, 2002.

[11] Mikhail G Bryukov, Vadim D Knyazev, Slawomir M Lomnicki, Cheri A McFerrin, and Barry Dellinger. Temperature-dependent kinetics of the gas-phase reactions of OH with Cl_2, CH_4, and C_3H_8. *The Journal of Physical Chemistry A*, 108(47):10464–10472, 2004.

[12] Hong Du, Jan P Hessler, and Paul J Ogren. Recombination of methyl radicals. 1. New data between 1175 and 1750 k in the falloff region. *The Journal of Physical Chemistry*, 100(3):974–983, 1996.

[13] SM Hwang, HGG Wagner, and Th Wolff. Recombination of CH_3 radicals at elevated pressures and temperatures. In *Symposium (International) on Combustion*, volume 23, pages 99–105. Elsevier, 1991.

[14] DF Davidson, RK Hanson, and CT Bowman. Revised values for the rate coefficients of ethane and methane decomposition. *International Journal of Chemical Kinetics*, 27(3):305–

308, 1995.

[15] Matthew A Oehlschlaeger, David F Davidson, and Ronald K Hanson. High-temperature ethane and propane decomposition. *Proceedings of the Combustion Institute*, 30(1):1119–1127, 2005.

[16] Ahren W Jasper, Stephen J Klippenstein, and Lawrence B Harding. Theoretical rate coefficients for the reaction of methyl radical with hydroperoxyl radical and for methylhydroperoxide decomposition. *Proceedings of the Combustion Institute*, 32(1):279–286, 2009.

[17] Rongshun Zhu and C Lin. The $CH_3 + HO_2$ reaction: First-principles prediction of its rate constant and product branching probabilities. *The Journal of Physical Chemistry A*, 105(25):6243–6248, 2001.

[18] O Mathieu, MM Kopp, and EL Petersen. Shock-tube study of the ignition of multi-component syngas mixtures with and without ammonia impurities. *Proceedings of the Combustion Institute*, 34(2):3211–3218, 2013.

[19] S Subith Vasu, F David Davidson, and K Ronald Hanson. Shock tube study of syngas ignition in rich CO_2 mixtures and determination of the rate of $H+O_2+CO_2 \rightarrow HO_2+CO_2$. *Energy & Fuels*, 25(3):990–997, 2011.

[20] Ying Jia Zhang, Zuo Hua Huang, Liang Jie Wei, Jia Xiang Zhang, and Chung K. Law. Experimental and modeling study on ignition delays of lean mixtures of methane, hydrogen, oxygen, and argon at elevated pressures. *Combustion and Flame*, 159:918–931, 2012.

[21] Assa Lifshitz, Karl Scheller, Alexander Burcat, and Gordon B Skinner. Shock-tube investigation of ignition in methane-oxygen-argon mixtures. *Combustion and Flame*, 16(3):311–321, 1971.

[22] Daniel J Seery and Craig T Bowman. An experimental and analytical study of methane oxidation behind shock waves. *Combustion and Flame*, 14(1):37–47, 1970.

[23] Nicola Donohoe, Karl A Heufer, Christopher J Aul, Eric L Petersen, Gilles Bourque, Robert Gordon, and Henry J Curran. Influence of steam dilution on the ignition of hydrogen, syngas and natural gas blends at elevated pressures. *Combustion and Flame*, 162(4):1126–1135, 2015.

[24] J Herzler and C Naumann. Shock-tube study of the ignition of methane/ethane/hydrogen mixtures with hydrogen contents from 0 % to 100 % at different pressures. *Proceedings of the Combustion Institute*, 32(1):213–220, 2009.

[25] Michael Frenklach and David E Bornside. Shock-initiated ignition in methane-propane mixtures. *Combustion and Flame*, 56(1):1–27, 1984.

[26] Eric L Petersen, Danielle M Kalitan, Stefanie Simmons, Gilles Bourque, Henry J Curran, and John M Simmie. Methane/propane oxidation at high pressures: Experimental and detailed chemical kinetic modeling. *Proceedings of the Combustion Institute*, 31(1):447–454, 2007.

[27] D Healy, HJ Curran, JM Simmie, DM Kalitan, CM Zinner, AB Barrett, EL Petersen, and G Bourque. Methane/ethane/propane mixture oxidation at high pressures and at high, intermediate and low temperatures. *Combustion and Flame*, 155(3):441–448, 2008.

[28] Hongyan Sun, SI Yang, G Jomaas, and CK Law. High-pressure laminar flame speeds and kinetic modeling of carbon monoxide/hydrogen combustion. *Proceedings of the Combustion Institute*, 31(1):439–446, 2007.

[29] Nicolas Bouvet, Christian Chauveau, Iskender Gökalp, and Fabien Halter. Experimental studies of the fundamental flame speeds of syngas (H_2/CO/air mixtures). *Proceedings of the Combustion Institute*, 33(1):913–920, 2011.

[30] MI Hassan, KT Aung, and GM Faeth. Properties of laminar premixed CO/H/air flames at various pressures. *Journal of Propulsion and Power*, 13(2):239–245, 1997.

[31] Ian C McLean, David B Smith, and Simon C Taylor. The use of carbon monoxide/hydrogen

burning velocities to examine the rate of the $CO + OH$ reaction. In *Symposium (International) on Combustion*, volume 25, pages 749–757. Elsevier, 1994.

[32] C Prathap, Anjan Ray, and MR Ravi. Investigation of nitrogen dilution effects on the laminar burning velocity and flame stability of syngas fuel at atmospheric condition. *Combustion and Flame*, 155(1):145–160, 2008.

[33] Alan Kéromnès, Wayne K Metcalfe, Karl A Heufer, Nicola Donohoe, Apurba K Das, Chih-Jen Sung, Jürgen Herzler, Clemens Naumann, Peter Griebel, Olivier Mathieu, et al. An experimental and detailed chemical kinetic modeling study of hydrogen and syngas mixture oxidation at elevated pressures. *Combustion and Flame*, 160(6):995–1011, 2013.

[34] Michael C Krejci, Olivier Mathieu, Andrew J Vissotski, Sankaranarayanan Ravi, Travis G Sikes, Eric L Petersen, KÃ Alan, Wayne Metcalfe, Henry J Curran, et al. Laminar flame speed and ignition delay time data for the kinetic modeling of hydrogen and syngas fuel blends. *Journal of Engineering for Gas Turbines and Power*, 135(2):021503, 2013.

[35] J Natarajan, T Lieuwen, and J Seitzman. Laminar flame speeds of H_2/CO mixtures: Effect of CO_2, dilution, preheat temperature, and pressure. *Combustion and Flame*, 151(1):104–119, 2007.

[36] Erjiang Hu, Jin Fu, Lun Pan, Xue Jiang, Zuohua Huang, and Yang Zhang. Experimental and numerical study on the effect of composition on laminar burning velocities of H_2/CO/N_2/CO_2/air mixtures. *International Journal of Hydrogen Energy*, 37(23):18509–18519, 2012.

[37] V Ratna Kishore, Ringkhang Muchahary, Anjan Ray, and MR Ravi. Adiabatic burning velocity of mixtures diluted with CO_2/N_2/Ar. *International Journal of Hydrogen Energy*, 34(19):8378–8388, 2009.

[38] Jinhua Wang, Zuohua Huang, Hideaki Kobayashi, and Yasuhiro Ogami. Laminar burning

velocities and flame characteristics of CO–H_2–CO_2–O_2 mixtures. *International Journal of Hydrogen Energy*, 37(24):19158–19167, 2012.

[39] Apurba K Das, Kamal Kumar, and Chih-Jen Sung. Laminar flame speeds of moist syngas mixtures. *Combustion and Flame*, 158(2):345–353, 2011.

[40] Deepti Singh, Takayuki Nishiie, Saad Tanvir, and Li Qiao. An experimental and kinetic study of syngas/air combustion at elevated temperatures and the effect of water addition. *Fuel*, 94:448–456, 2012.

[41] G Yu, CK Law, and CK Wu. Laminar flame speeds of hydrocarbon + air mixtures with hydrogen addition. *Combustion and Flame*, 63(3):339–347, 1986.

[42] Nicola Donohoe, Alexander Heufer, Wayne K Metcalfe, Henry J Curran, Marissa L Davis, Olivier Mathieu, Drew Plichta, Anibal Morones, Eric L Petersen, and Felix Güthe. Ignition delay times, laminar flame speeds, and mechanism validation for natural gas/hydrogen blends at elevated pressures. *Combustion and Flame*, 161(6):1432–1443, 2014.

[43] CK Law and OC Kwon. Effects of hydrocarbon substitution on atmospheric hydrogen–air flame propagation. *International Journal of Hydrogen Energy*, 29(8):867–879, 2004.

[44] Patricia Dirrenberger, Hervé Le Gall, Roda Bounaceur, Olivier Herbinet, Pierre-Alexandre Glaude, Alexander Konnov, and Frédérique Battin-Leclerc. Measurements of laminar flame velocity for components of natural gas. *Energy & Fuels*, 25(9):3875–3884, 2011.

[45] F Halter, C Chauveau, N Djebaili-Chaumeix, and I Gökalp. Characterization of the effects of pressure and hydrogen concentration on laminar burning velocities of methane–hydrogen–air mixtures. *Proceedings of the Combustion Institute*, 30(1):201–208, 2005.

[46] RTE Hermanns, AA Konnov, RJM Bastiaans, LPH De Goey, K Lucka, and H Köhne. Effects of temperature and composition on the laminar burning velocity of CH_4 + H_2 + O_2 + N_2 flames. *Fuel*, 89(1):114–121, 2010.

[47] Graeme MG Watson, Jeffrey D Munzar, and Jeffrey M Bergthorson. NO formation in model syngas and biogas blends. *Fuel*, 124:113–124, 2014.

[48] FN Egolfopoulos, P Cho, and CK Law. Laminar flame speeds of methane-air mixtures under reduced and elevated pressures. *Combustion and Flame*, 76(3):375–391, 1989.

[49] Th. Just. *Personal Communication*, 1994.

[50] Christine M Vagelopoulos and Fokion N Egolfopoulos. Direct experimental determination of laminar flame speeds. In *Symposium (International) on Combustion*, volume 27, pages 513–519. Elsevier, 1998.

[51] A Van Maaren, DS Thung, and L. P. H. de Goey. Measurement of flame temperature and adiabatic burning velocity of methane/air mixtures. *Combustion Science and Technology*, 96(4-6):327–344, 1994.

Copyright Clearance Center RightsLink®

Home | Account Info | Help | Live Chat

ACS Publications Most Trusted. Most Cited. Most Read.

Title: Comprehensive Comparison of Chemical Kinetics Mechanisms for Syngas/Biogas Mixtures

Author: H. C. Lee, A. A. Mohamad, L. Y. Jiang

Publication: Energy & Fuels

Publisher: American Chemical Society

Date: Sep 1, 2015

Copyright © 2015, American Chemical Society

Logged in as:
Hsu Chew Lee
Account #:
3000678254

LOGOUT

PERMISSION/LICENSE IS GRANTED FOR YOUR ORDER AT NO CHARGE

This type of permission/license, instead of the standard Terms & Conditions, is sent to you because no fee is being charged for your order. Please note the following:

- Permission is granted for your request in both print and electronic formats, and translations.
- If figures and/or tables were requested, they may be adapted or used in part.
- Please print this page for your records and send a copy of it to your publisher/graduate school.
- Appropriate credit for the requested material should be given as follows: "Reprinted (adapted) with permission from (COMPLETE REFERENCE CITATION). Copyright (YEAR) American Chemical Society." Insert appropriate information in place of the capitalized words.
- One-time permission is granted only for the use specified in your request. No additional uses are granted (such as derivative works or other editions). For any other uses, please submit a new request.

BACK | CLOSE WINDOW

Copyright © 2016 Copyright Clearance Center, Inc. All Rights Reserved. Privacy statement. Terms and Conditions.
Comments? We would like to hear from you. E-mail us at customercare@copyright.com